

# Statistical Properties of a Randomly Excited Granular Fluid.

*David Jonathan Bray, MSci.*

Thesis submitted to the University of Nottingham for the degree  
of Doctor of Philosophy

September 2009

# Abstract

In this thesis we describe numerical simulations performed in one- and two-dimensions to decipher the structural and velocity properties of a theoretical granular model called the Random Force Model. We are interested in this model because the dynamical and structural properties of non-equilibrium steady state granular media are still hotly debated amongst the current literature despite there being several developed granular kinetic theories.

Our study begins by an introduction to this field of granular materials and non-equilibrium steady states. We report on the current state of affairs into the Random Force Model: by defining the model; describing the wealth of previous research; outlining the disagreements that exist into the structural and velocity properties of the systems. Next the methodology of performing Molecular Dynamic simulations is discussed which leads us to demonstrate that the Random Force Model settles into a steady state whereupon the average kinetic energy per particle remains fixed.

The research of the thesis is commenced by observing that the one-dimensional Random Force Model manifest multi-scaling behaviour brought on by the clustering of particles within the system. This has not previously been observed. For high dissipation we find that the distribution of nearest neighbour distances are approximately renormalisable, such that a larger populated system has structural properties similar to that of a smaller one, and devise a geometrical method of breaking the system into spatial parts that accounts for some of the structural features seen in these systems.

We next study the structural and velocity behaviour of the two dimensional Random Force Model. In previous literature it has been observed that the structure factor exhibits fractal characteristics. It varies, for small  $k$ , as a power-law with an exponent  $D_f$ , referred to as the fractal dimension, but currently there is no consensus into what form this might take. We conclusively show that the decay is unchanged with respect to both dissipation and particle density. Furthermore we suggest that the power-law decay has an exponent different from that given in any previous study. These structural

features are subsequently suggested to be the hallmarks of anomalous behaviour found in the locally dilute regions of the system. Ultimately these regions influences the long distance behaviour of individual particles by affecting the distances travelled by particles between consecutive collision.

The velocity distribution is known to strongly deviate away from Maxwell-Boltzmann statistics, but again there is no consensus into the shape of the asymptotic high velocity tail. In this thesis we advocate that it is likely that the velocity distributions have asymptotic shape which is universal over a range of dissipation and particle densities.

This invariance in behaviour of the large-scale structure and velocity properties of the two-dimensional Random Force Model leads us to develop a new self-consistent model based around the motion of single high velocity particles. The background mass of low velocity particles are considered to be arrange as a fractal whereby the high velocity particles move independently in ballistic trajectories between collisions. We use this description to construct the overall velocity distribution which we expect to correctly describe high velocity particles in the Random Force Model. We demonstrate that the new model numerically describes the high velocity tail of the velocity distribution and calculate the asymptotic shape to be approximately exponential. This new theory incorporates the fractal nature of the structure of the system as well as the dynamics of particles between collision.

Finally we propose a method of structure formation for these systems. We adopt a previously suggested idea in which these systems are the result of grains self-organising into a state of criticality and put forward another geometrical process that builds self-similarity into the system by consecutively fracturing the system into smaller parts. The resultant system has structural properties similar to the two-dimensional Random Force Model.

# Acknowledgement

I would like to take this opportunity to dedicate this thesis to the many people I have known during my PhD who without which it would not have been possible to complete this thesis. Over these past four years they have given up so much of their time to provide guidance, support or simply friendship.

First, I would like to sincerely thank my supervisors Prof. Mike Swift, Prof. Roger Bowley and Prof. Peter King for their dedication, guidance and vision over these past four years. I am deeply gratified for all their hard work. Subsequently, I would like to acknowledge my good friends Tom and Adam who I have been fortunate to share a house with and whose friendship has been invaluable. I would also like to thank those I knew from the Lower Court halls of residents, at Broadgate Park, who made my first year so enjoyable. Further, I would like to show my appreciation to those on my course Helen, Hector, Daphne, Christian, Kathryn and Lui. The office has always been lively with them around. Lastly, I would like to thank my parents and brother, Andrew, who have shown me nothing but loving support and motivation during my PhD. I only hope that this thesis does them all justice.

# Publication

The material of this thesis is based primarily on work that has been presented to the academic community. We have presented one talk at a conference:

D. J. Bray, (July 2006). Velocity Statistics in Dense Granular Beds. Dygram2006 - Granular Dynamics, Jamming, Rheology and Instabilities conference, University of Rennes, France.

Also there has been a poster presentation for a conference:

D. J. Bray, M. R. Swift and P. J. King (July 2007). Velocity Statistics in Dissipative, Dense Granular Media. Statics and dynamics of granular media and colloidal suspensions, Satellite conference of StatPhys 23, Napoli, Italy.

The material of the poster was published in the letter:

D. J. Bray, M. R. Swift and P. J. King (2007). Velocity Statistics in Dissipative, Dense Granular Media Phys. Review E. *75*, 062301

We are currently in the process of writing a paper based on chapter four and five:

D. J. Bray, M. R. Swift and R. M. Bowley (2009). Structure and Statistics of 2D Randomly Excited Granular Gas. In preparation.

# Reference of Notation

Within this thesis we often replace quantities with symbolic representation. It is important to use a set of notation which is both clearly distinguishable (to prevent confusion or misinterpretation) and logical. As far as possible we use commonly accepted notation (such as  $t$  for time,  $G$  for gravitational field strength) or alternative symbol when a single notation is multiply defined (by different fields of physics). Below provides tables of reference defining all common symbols used within the thesis:

Quantity	Symbol
<b>Particle Properties</b>	
$i^{th}$ Particle's Position	$\mathbf{r}_i$
$i^{th}$ Particle's Velocity	$\mathbf{v}_i$
A component of Particle Velocity	$v$
Particle Mass	$M$
Particle Radius	$r$
Particle Diameter	$d$
Free Path	$l$
Mean free path	$l_0$
<b>Collision Properties</b>	
A Force	$F$
Normal Vector	$\hat{\mathbf{n}}$
Tangential Vector	$\hat{\mathbf{t}}$
Normal Coefficient of Restitution	$\varepsilon, \varepsilon_n$
Tangential Coefficient of Restitution	$\varepsilon_t$
Sliding Friction coefficient	$\mu$
Spring Constant	$k_s$
Dissipation Coefficients	$\gamma_n, \gamma_t$

Quantity	Symbol
<b>System Properties</b>	
Time	$t$
Time-step	$\Delta t$
General Distance	$x$
System Size	$L$
Reduced Distance	$L', x'$
Distance Between Particles	$R$
Phase Space	$k$
Number of Particles	$N$
Packing Fraction	$\phi$
Granular Temperature	$T$
The Random Force	$\eta$
Gaussian Noise Strength	$D$
<b>Probability Distributions</b>	
General Probability Distribution	$P(..), Q(..), R(..)$
Velocity Distribution	$P(v)$
Distribution of Free Path	$P_l(l)$
1 <sup>st</sup> Nearest Neighbour Distribution	$G_1(R; N)$
$h^{\text{th}}$ Nearest Neighbour Distribution	$G_h(R; N)$
Spatial Correlation Function	$g(R)$
Number of Particles around a Point	$C(R), n(R)$
Structure Factor	$S(k)$
Fractal Dimension	$D_f$
$m^{\text{th}}$ moment of $x$	$\langle x^m \rangle$
Number Dependence Exponents	$\xi_m, \zeta_m$
Crossover Velocity-scale	$v_c$
Other Velocity-scales	$v_0, v_A, v_r$
$n^{\text{th}}$ Level Distribution of Partition Lengths	$P_n(x_n)$
<b>General Constants</b>	
An Integer	$i, j, g, h$
Constants	$A, B, C, E, H$
Exponents	$\alpha, \beta, \gamma$
A Random Number	$a, a_i, a_{i,j}$

# Contents

<b>Abstract</b>	<b>i</b>
<b>Acknowledgement</b>	<b>iii</b>
<b>Publication</b>	<b>iv</b>
<b>Reference of Notation</b>	<b>v</b>
<b>1 Introduction to Granular Systems</b>	<b>1</b>
1.1 What are Granular Materials? . . . . .	1
1.2 Non-Equilibrium States and Granular Cooling . . . . .	2
1.3 Steady State and Shaken Beds . . . . .	3
1.4 Granular Hydrodynamic Equations . . . . .	5
1.4.1 Some Specific Granular Kinetic Theories . . . . .	6
1.4.2 Applying Hydrodynamic Theories . . . . .	7
1.5 The Random Force Model . . . . .	8
1.5.1 Mean Field Temperature of One-dimensional Systems . . . . .	9
1.5.2 Structural Properties of a Two-dimensional System . . . . .	10
1.5.3 Velocity Properties of Multi-dimensional Systems . . . . .	11
1.6 Thesis outline . . . . .	13
<b>2 Modelling Granular Systems</b>	<b>16</b>
2.1 Molecular Dynamics Technique . . . . .	16
2.1.1 Selecting a Method . . . . .	16
2.1.2 General Methods for running the Simulation . . . . .	18
2.1.3 Boundary Conditions . . . . .	23
2.1.4 Initial Conditions . . . . .	24
2.1.5 Energy Dissipation during Collision . . . . .	25
2.2 The One-dimensional Random Force Model . . . . .	27

2.2.1	Computation of a Random Force . . . . .	27
2.2.2	Simulation Details . . . . .	28
2.2.3	Steady States . . . . .	29
2.3	The Two-dimensional Random Force Model . . . . .	32
2.3.1	Computation of a Random Force . . . . .	32
2.3.2	Simulation Details . . . . .	33
2.3.3	Steady States . . . . .	36
2.4	Summary . . . . .	36
<b>3</b>	<b>Multi-Scaling Properties of a One-dimensional Random Force Model</b>	<b>39</b>
3.1	The Second Moment of Velocity . . . . .	40
3.1.1	Deriving a Scaling Relation . . . . .	41
3.1.2	The Simulations . . . . .	42
3.1.3	Dependence on Population Size . . . . .	44
3.2	Higher order Moments of Velocity . . . . .	46
3.2.1	A Study of Two Extreme Cases . . . . .	48
3.2.2	General Dependence on Population Size . . . . .	48
3.2.3	Can Multi-Scaling be Observed through the Velocity Distribution? . . . . .	50
3.3	The Structure of the System . . . . .	52
3.3.1	The Separation Distances between Neighbouring Particles . . . . .	54
3.3.2	The Nearest Neighbour Distribution . . . . .	56
3.3.3	Renormalisation and Self-Similarity of the Structure . . . . .	60
3.4	Multiplicative Fracture Process . . . . .	62
3.4.1	Multiplicative Bisection Process . . . . .	65
3.4.2	A Simple Case . . . . .	66
3.4.3	Comparison with data from the Random Force Model . . . . .	68
3.5	Summary . . . . .	72
<b>4</b>	<b>Fractal Properties of a Two-dimensional Random Force Model</b>	<b>75</b>
4.1	Structure Factor . . . . .	76
4.1.1	Large-scale Structure and the Dissipative Regime . . . . .	77
4.1.2	Increasing the Size of the System, $L$ . . . . .	79
4.1.3	Stability with Respect to Dissipation . . . . .	83
4.1.4	Stability with Respect to Packing Fraction . . . . .	88
4.1.5	Brief Summary on Structure . . . . .	90

4.2	Implications on Real Space Structure . . . . .	90
4.3	The Distribution of Free Paths . . . . .	94
4.3.1	Finite Size Effects . . . . .	95
4.3.2	Estimating the long distance tail of $P_l(l)$ . . . . .	96
4.3.3	Comparison with data from the Random Force Model . . . . .	98
4.4	Summary . . . . .	99
<b>5</b>	<b>Velocity Properties of a Two-dimensional Random Force Model</b>	<b>101</b>
5.1	Observations using Standard Methods . . . . .	102
5.1.1	The Velocity Distribution for a Fixed System Size . . . . .	105
5.1.2	System Size Dependence and Stability with Respect to Packing Fraction . . . . .	111
5.1.3	A Crossover in Particle Behaviour and Stability with Respect to Dissipation . . . . .	114
5.1.4	Brief Summary on the Velocity Distribution . . . . .	119
5.2	A Single Particle Model . . . . .	120
5.2.1	A Physical Basis . . . . .	120
5.2.2	SPM Integral Identity . . . . .	125
5.2.3	Performing Numerical Simulations . . . . .	125
5.3	Self-Consistent Calculation of the Asymptotic Behaviour of the Velocity Distribution . . . . .	127
5.3.1	A Single Particle in a Circular System of Fixed Radius $l$ . . . . .	128
5.3.2	Solving the SPM Integral Identity . . . . .	128
5.3.3	Comparison with data from the Random Force Model . . . . .	134
5.3.4	Implications for lower Dissipation Systems . . . . .	136
5.4	Summary . . . . .	139
<b>6</b>	<b>Multiplicative Cascade Process and Fractal Structure</b>	<b>142</b>
6.1	Self-Similarity . . . . .	142
6.2	The Multiplicative Cascade Process . . . . .	144
6.2.1	Outline of the Method . . . . .	144
6.2.2	Comparison with data from the Random Force Model . . . . .	147
6.3	Summary . . . . .	149
<b>7</b>	<b>Concluding Remarks</b>	<b>152</b>
7.1	Chapter Review . . . . .	152

7.2	Future Work . . . . .	156
<b>A</b>	<b>Velocity Properties a One-dimensional Random Force Model</b>	<b>159</b>
A.1	Details of Technique used for Generating Velocity Distribution . . . . .	159
A.2	The Variation of Shape with Respect to Dissipation . . . . .	162
A.3	Measuring the Observable High Velocity Behaviour . . . . .	164
<b>B</b>	<b>A Single Particle in a One-dimensional Interval</b>	<b>168</b>
B.1	Solving the Fokker-Planck Equation . . . . .	168
B.2	What is the form of $Q(v, l)$ ? . . . . .	175
	<b>Bibliography</b>	<b>177</b>

# Chapter 1

# Introduction to Granular Systems

Granular media is often underestimated because of its superficial similarity to classical media of solid, liquid or gas but its attributes can be dramatic, unpredictable and dangerous in real world environments. For example, avalanches in stable granular media occur as a result of minute changes in conditions. One of the difficulties in studying granular media is that despite its closeness to classical media we cannot describe it by standard theories.

In this chapter we introduce dry granular dynamics and discuss the pitfalls and successes of current attempts to describe its kinetic behaviour. This culminates in the exposition of the Random Force Model and we discuss critically the associated published literature. At the end of the chapter we outline the work contained in the thesis.

## 1.1 What are Granular Materials?

Granular materials are found in many environments, from industrial processes such as hoppers, grain silos and mixing vats; to domestic washing powders and salt pots. Although individually the grains have solid properties, the collection of grains can display properties of solid (stress chains, arching), fluid (flow, convection) or both (piling). The vast variation in physical behaviour can lead to unexpected problems when handling granular media: for example the flow of grains through a narrow pipe can become blocked when a group of grains form a bridge across the cross-section of the pipe strong enough to support the weight of grains above. To avoid undesirable

results when using granular materials it is important to understand how collections of granules behave.

Granular materials have long been of interest to scientists: for example, early clock makers exploited sands ability to flow at a constant rate, regardless of the bulk weight above, to manufacture sand timers that accurately measured the passage of time. The nature of granular materials prevented description by simple general theories of solid, liquid and gas. Instead properties of granular materials can change depending on the quantity of grains and scale of the system. Until the advent of high performance computing granular materials were difficult to model at sufficient sized systems. In recent times the advances in computing have allowed detailed simulation studies to be performed and several puzzling behaviours have been described which includes segregation (Kudrolli 2004), pattern formation (Aranson and Tsimring 2006), ‘Brazil nut’ effect (Williams 1976) and clustering (Jaeger, Nagel, and Behringer 1996). It is now understood that the position, orientation and dissipation of individual grains play major roles in causing these effects.

## 1.2 Non-Equilibrium States and Granular Cooling

Granular Systems are simple examples of non-equilibrium systems. When grains collide they dissipate kinetic energy. They constantly require absorption of energy to keep them in motion. The dissipation of the grain is quantified by a term called the coefficient of restitution ( $\varepsilon$ ) which determines the remaining centre of mass velocity, normal to a collision, between a pair of grains after collision,

$$v'_2 - v'_1 = \varepsilon(v_1 - v_2), \quad (1.1)$$

where  $v_i, v'_i$  are the normal velocity components before and afterwards of the  $i^{\text{th}}$  particle.

### Haff’s Law

The granular temperature of the system is defined to be the average kinetic energy of a grain. When a collection of grains is left ‘unheated’, with no kinetic energy injected into the system, it will cool as the granular temperature reduces each time a collision occurs. If a granular gas (which we define to be energetic grains under no gravity or other long-ranged force) is left unheated it will cool. Haff’s law predicts how the granular temperature of granular gas decays with time. A cooling granular gas of energetic grains under no gravity or other long-ranged force, is expected to have a

granular temperature,  $T$ , that obeys Haff's law as time progresses (Brilliantov and Pöschel 2004):

$$T_t = T_0 \left[ 1 + \frac{4}{\sqrt{\pi}} (1 - \varepsilon) \frac{\phi T_0^{1/2}}{s^*(\phi) d} t \right]^{-2}, \quad (1.2)$$

where  $\phi$  is the packing fraction (a measure of the density of the gas of grains) and  $s^*(\phi) = (1 - \phi)^2 / (1 - 7\phi/16)$ . Here  $t$  is the time and  $T_0$  is the starting granular temperature at  $t = 0$ .

When the grains are weakly dissipative and each collision removes only a small fraction of the grain's energy, Haff's law provides a good prediction for the cooling. In contrast, when the grains are highly dissipative, each collision removes large fractions of the grain's energy and the grains cluster together which consequently means that Haff's law breaks down.

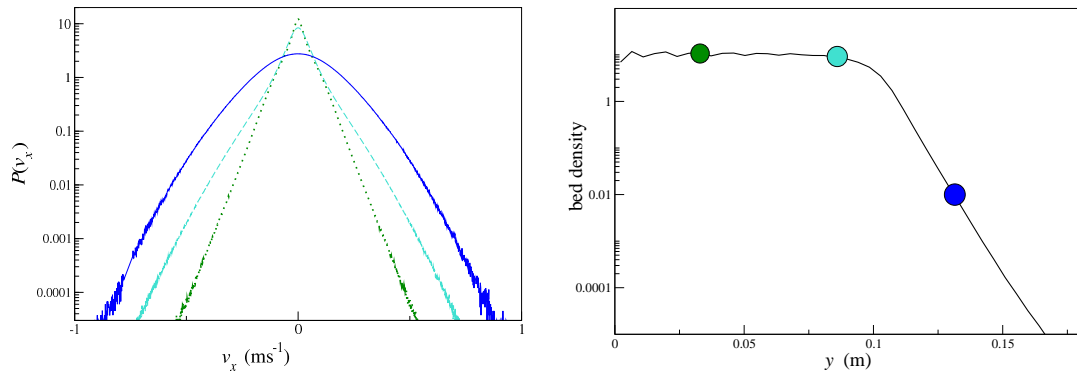
In the case of a one-dimensional system, its pathological nature ultimately leads to chains of particles forming and the system collapses to a singularity by an effect called Inelastic Collapse, as noted in the papers of McNamara and Young (1992) and McNamara and Young (1994). Inelastic collapse does not occur in higher dimension systems and is otherwise prevented, through the use of a slight randomisation of velocity just after collision, by treating the particle's surface as rough.

Haff's law is an example of applying hydrodynamical theory to granular media. The failure of Haff's law at moderate to high dissipations demonstrates that mean theory and the principle of treating the distribution of grains as homogeneous is wrong and instead the spatial structure of the system must be considered.

### 1.3 Steady State and Shaken Beds

Granular cooling can be prevented by the injection of kinetic energy into the system. When a granular system settles into a state with a steady granular temperature it is said to be in a steady state. Here the rate of energy dissipation through collision equals the rate of energy injected. Many types of granular systems form steady states, these include: grains contained within a vertically vibrated box (Warr, Huntley, and Jacques 1995; Olafsen and Urbach 1998; Losert, Cooper, Delour, Kudrolli, and Gollub 1999; Rouyer and Menon 2000; Blair and Kudrolli 2001; Baxter and Olafsen 2003; Blair and Kudrolli 2003; Huan, Yang, Candela, Mair, and Walsworth 2004); rotating drums of grains where a shear force is applied to grains at the boundaries (Schöllmann 1999; Lätzel, Luding, Herrmann, Howell, and Behringer 2003); electro-statically driven

Fig. 1.1: The statistical behaviour of a simulated granular bed of shaken vertically by sinusoidal vibration.



(a) The distribution of horizontal velocity measured at the highly fluidised top of the bed (solid line), the densely packed bottom (dotted line) and the intermediate region (dashed line). (b) The bed density, on log-linear scale, as a function of height. The circles show the approximate positions of the three regions in the bed sampled.

systems (Kohlstedt, Snezhko, Sapozhnikov, Aranson, Olafsen, and Ben-Naim 2005) and inclined planes of grains (Moka and Nott 2005).

In all of the above granular systems, the direction of travel for a particle perpendicular to the driving mechanism is unbiased. However the statistical behaviour of the grains cannot be described by equilibrium theories. Particularly, the velocity distributions of grains are not described by the Maxwell-Boltzmann distribution of velocities (Herrmann, Luding, and Cafiero 2001; Barrat, Trizac, and Ernst 2005), except in dilute, highly energetic and low dissipative granular gases.

One of the clearest demonstrations of the above point is the behaviour of granular systems that are vertically vibrated. A granular bed, many grains in depth and with low dissipation, is vertically excited under gravity through sinusoidal shaking of the base of the container. The grains in the system cycle through: expansion, as the grains are launched into the air; reorder; and collapse, as the grains fall under gravity back into the container. Figure 1.1 shows an example of the statistical properties of simulations of a shaken bed where 3000 spherical particles, with diameter 3mm and density of  $2500\text{kgm}^{-3}$ , are contained in a box, of horizontal dimensions  $0.25\text{m} \times 4.5\text{mm}$  and height 0.36m, such that the average depth of the bed is about 36 grains. The base of the box vibrates sinusoidally at a frequency 30Hz such that there is a maximum acceleration of three times the gravitational field strength.

The horizontal velocity of the grain is strongly dependent on the height within the bed where the grain is found (Kawarada and Hayakawa 2004). The vertical velocity of

grains is strongly dependent on the mechanism of shaking. At the top of the bed the density quickly decays with increasing height as the particles become more energetic and gaseous-like. No distinct boundary can be seen between the top of the bed and the air. The distribution of horizontal velocities of grains approximates Gaussian as expected for an equilibrium system.

The bulk of the bed behaves (on average over a cycle) liquid-like with constant density profile independent of height. If walls are present convection cells can form where grains circulate around in a vertical loop. The distribution of horizontal velocities of grains are anomalous and distinctly non-Gaussian.

## 1.4 Granular Hydrodynamic Equations

One of the main reasons why the equilibrium theories, such as Maxwell-Boltzmann statistics, fail is that these theories do not account for the dissipation and injection of kinetic energy that occurs in granular systems. One method to characterise the perturbations of the velocity distribution away from Gaussian involves measuring the Sonine polynomial expansion of the velocity distribution (Brilliantov and Pöschel 2004) in which the distribution is treated as a product of a Gaussian multiplied by a polynomial. A drawback of this approach is that, as we move away from the central peak of the distribution, more polynomial terms have to be included to remain accurate and hence it becomes difficult to predict asymptotic high velocity behaviour. Alternatively physicists would like to modify existing theories to incorporate collisional dissipation and energy injection. These modified theories would then be solved to obtain new solutions. The difficulty arises in how to include these additional energy terms.

Kinetic theories are mostly derived from the Boltzmann equation of motion. The Boltzmann equation assumes that the state of a particle is separable from the system's other particles. In which case molecular chaos applies, such that there exists no correlation between grain velocities. For a steady state of fluidised inelastic hard spheres the Boltzmann equation is written as:

$$\mathbf{v} \cdot \frac{\partial f}{\partial \mathbf{r}} + \frac{\mathbf{F}}{M} \cdot \frac{\partial f}{\partial \mathbf{v}} = C(f) - E(f), \quad (1.3)$$

where  $f$  is the distribution function that describes a grain in terms of position  $\mathbf{r}$ , velocity  $\mathbf{v}$  and time  $t$ . The other terms comprise the forces acting on the particles between collision  $\mathbf{F}$ ; the mass of a grain  $M$ ; the rate of change of  $f$  due to collisions  $C(f)$ ; and the rate of change of  $f$  due to energy injection  $E(f)$ .

Frequently an assumption to the Boltzmann equation is that the system is spatially homogeneous. Two criticisms can be made of these assumptions: first, many granular systems are spatially homogeneous *only* on time average and not at any moment of time; second, the dissipation of energy during collision in granular media leads to notable correlation in particle velocity even at reasonably low dissipation. Despite these drawbacks several granular kinetic theories have been developed the most notable of which are now briefly outlined.

### 1.4.1 Some Specific Granular Kinetic Theories

One of the easiest methods to inject energy into a system is to uniformly thermalise particles with a random force, to be described in more detail in section 1.5. The Boltzmann equation can then be solved to obtain the distribution of velocity. In practice it is very difficult to describe the complete velocity distribution and instead researchers have opted to calculate the high velocity tail of the distributions. This has resulted in a variety of solutions for the asymptotic behaviour of the velocity distribution  $P(v)$ , where  $v$  is a component of the velocity  $\mathbf{v}$ .

The most commonly quoted approach was that taken in the paper of van Noije and Ernst (1998). The system was assumed to be thermally heated by uncorrelated Gaussian white noise. The Boltzmann equation was approximated as the Enskog-Boltzmann equation for a uniform heated system. The high velocity tail of the distribution of velocity was calculated as a stretched-exponential of the form  $P(v) = A \exp(-B|v|^{3/2})$ . Later it was suggested by Barrat, Biben, Rácz, Trizac, and van Wijland (2002) that the velocity distribution is more complicated with  $P(v)$  crossing over from  $A \exp(-B|v|^{3/2})$  to  $A' \exp(-B'|v|^3)$  such that for systems with near-elastic collisions the cubic behaviour was dominant over observable statistics.

An alternative approach is to use the Maxwell Model as an approximation for the Boltzmann equation as was done by Ben-Naim and Krapivsky (2000). In this case the collision rate is independent of the particle's velocity. The collision integral,  $C(f)$ , is derived by just considering a collision between a pair of grains such that  $C(f)$  contains both a single gain and a single loss term that deal with a grain achieving a speed  $v$  after collision and a grain starting with a speed  $v$  respectively. The Maxwell Model is solved by ignoring the gain term, which provides only minor corrections, and the high velocity tail of the velocity distribution is calculated to be approximately exponential of the form  $P(v) = A \exp(-Bv)$ .

A third approach to solving the Boltzmann equation was published in the paper of Ben-Naim, Machta, and Machta (2005). The Boltzmann equation is linearised by studying only the fastest particles. The collision rate is chosen to be a power of the relative difference in velocity between colliding grains. As the fastest grains are very rare, they effectively see all other inbound grains as stationary and the collisions of the system leads to a cascade (of one collision causing two further collisions which in turn leads to four further collisions and so on) such that the energy contained per grain, in the form of the velocities, reduces in value. The theory assumes the condition that the energetic grains are uncorrelated to the slow grains and so the Boltzmann equation can be linearised by taking the second grain's velocity to be zero. Solving the equation produces a power-law approximation for the high velocity tail of the distribution of velocities.

In all these above theories the system is treated as homogeneous. One theory that does include spatial variation was proposed by Puglisi, Loreto, Marconi, and Vulpiani (1999). A system is broken up into a number of boxes with fixed width containing a variable number of particles. Particles can move between boxes but the overall number remains the same. The kinetic energy of the box is dependent on the number of particles held within and the distribution of velocity for each box is assumed to be Gaussian with standard deviation governed by the box's kinetic energy. The total velocity distribution of the system is thus equal to the sum of all boxes distribution of velocity and thereby incorporates the structure of the system.

### 1.4.2 Applying Hydrodynamic Theories

In most granular systems the energy injection is both time and position dependent. For example in shaken beds kinetic energy is only given to those grains that are both in contact with the base and at the point in the cycle when the base is moving upwards. The remainder of grains exchange energy through subsequent collision. For this reason it is difficult to represent these systems by granular kinetic theories. Instead the granular kinetic theories are tested against simpler systems where the driving energy injection can be considered to act at all times over all grains. One such theoretical granular system was proposed in Williams and MacKintosh (1996) and is known as the Random Force Model.

## 1.5 The Random Force Model

The Random force model is defined as a set of confined identical grains, from now on referred to as particles, where kinetic energy is injected into the system by individually applying a random force, statistically distributed as a Gaussian, to each particle. The random force represents the overall effect of particles picking up successive packets of energy, identically distributed, over an infinitesimal period of time such that the Central Limit Theory applies.

These models are of particular relevance currently as several experiments have been performed that form near approximations to the two-dimensional case. In the papers of Reis, Ingale, and Shattuck (2006), Reis, Ingale, and Shattuck (2007a) and Reis, Ingale, and Shattuck (2007b) a layer of identical spheres are trapped between two glass plates, the lower of which is roughened. The plates are separated by just over a particle diameter to create a quasi-two dimensional system. During experiment the system is vertically vibrated and the roughened base acts as a source of random force for the particles. Of particular interest, these researchers have measured the velocity statistics of particles and compared the results against the granular kinetic theory of van Noije and Ernst (1998). While most recently these researchers have claimed that these experimental granular systems broadly mimic equilibrium systems as a result of all spatial gradients being removed (Shattuck, Ingale, and Reis 2009).

Considering the simplicity of the Random Force Model and the level of study available in the literature it is surprising to find that unresolved conflicts remain about the specific nature of these systems. For example, disagreement exists in both velocity and structural properties of the two-dimensional case and arise from whether or not a hydrodynamical description is believed to be applicable in these systems.

In these systems the slight correlation of particle velocity with its neighbour after collision leads to clustering. The random force prevents the system from undergoing Inelastic collapse by decorrelating the particles over time. This tendency of particles to cluster puts into question any theories that suggest the system is homogeneous. However much of the previous analysis of the Random Force Model assumes just that. For example, Williams and MacKintosh (1996) states that the granular temperature can be derived from mean field approach.

We now review the previous literature on the Random Force Model. We emphasise three topics that are of particular interest us: can the granular temperature be described by mean field theory, what are the structural features of these systems and what is the

behaviour of the velocity statistics? In all the described papers energy is dissipated through a reduction of velocity normal to the collision whilst tangentially the collision is elastic. It is not clear whether ignoring tangential dissipation significantly affects the dynamics or structure of these systems and is a question that will also be discussed later.

### 1.5.1 Mean Field Temperature of One-dimensional Systems

One of the most influential studies into the properties of the one-dimensional Random Force Model was performed by Williams and MacKintosh (1996). A system of  $N$  point-like particles are contained within a interval of length  $L$ . The random force provides the energy for the particles to move along the interval and energy is dissipated at collision, such that there is a coefficient of restitution  $\varepsilon$  with value between zero and one. The kinetic energy per particle,  $K$ , of the system in the steady state was calculated using mean field theory and expressed in the following form:

$$K^{\frac{3}{2}}(1 - \varepsilon^2)N = CL\Omega, \quad (1.4)$$

where  $C$  is a numerical constant and the rate of energy input is given by  $\Omega N$ . A key assumption used for the equation is that the average distance between collision is equal to the average density of particles  $L/N$ .

However, mean field theory ignores the spatial clustering that occurs in the system for moderate/high dissipations. A clear indication that clustering is occurring in the Random Force Model is given by Williams and MacKintosh with the two-particle correlation function, defined as the density of particles a distance  $x$  away from a test particle. For low coefficient of restitution, the two-particle correlation function has small  $x$  behaviour that is a power-law decay of exponent  $-1/2$ . In an uncorrelated system the correlation function would be a constant.

The explanation of the correlation was provided in the paper of Swift, Boamfá, Cornell, and Maritan (1998) which explains, using the analogy to a single particle trapped between dissipative walls, that clustered particles act as boundary walls to free particles. The complete system is dominated by the breaking up of clusters of particles where the dissipation of the cluster is near-inelastic.

### 1.5.2 Structural Properties of a Two-dimensional System

The structure of a bed of particles can be quantified by a probability distribution called the structure factor,  $S(k)$ , which measures the Fourier transform of the correlations in positions between pairs of particles. A specific definition of  $S(k)$  is given later in chapter four of the thesis. The parameter  $k$  is inversely proportional to distance such that large scale structure is described by small scale  $k$ -space. There is a general consensus amongst the literature that the structure factor of the two-dimensional Random Force Model varies as a power-law for small  $k$  of the form  $k^{-D_f}$ , but disagreement exists into the exact value of the exponent  $D_f$ . The earliest studies into the structure factor of the Random Force Model were performed in the papers of Peng and Ohta (1998a) and Peng and Ohta (1998b). The small scale power-law correlations of  $S(k)$  were measured to be  $Ak^{-1.42}$  such that  $D_f = 1.42$ . To this it was added that the observed exponent  $D_f$  does not change with coefficient of restitution but instead the scaling region reduces in length with decreasing dissipation. The suggested explanation for the power-law decay was that the system self-organising into critical state such that there were no characteristic spatial- or temporal-scales in the correlations.

A year later a theoretical paper was written by van Noije, Ernst, Trizac, and Pagonabarraga (1999) to explain the power-law decay of  $S(k)$  using theory based on Hydrodynamical approach to a randomly driven inelastic hard sphere fluid. Their theory predicted that the system would exhibit three spatial regimes: dissipative; standard; and elastic, that determine the behaviour of spatial features at specific scales. The dissipative regime was stated to be dominated by the dissipation effects and represented features in  $S(k)$  when  $k \lesssim (1 - \varepsilon^2)/4l_0$  (where  $l_0$  was the mean free path of a particle between collision). Whereas the elastic regime was dominated by heat conduction and described  $S(k)$  for  $k \gtrsim \sqrt{1 - \varepsilon^2}/2l_0$ . The standard regime described the remainder of  $S(k)$ . Importantly the authors discussed whether or not these regimes could be seen in a system of a given size and concluded that the power-law decay of  $S(k)$  was only appreciable when the system has lengths of  $L > 4l_0/(1 - \varepsilon^2)$ . Within the dissipative regime the structure factor was derived to obey  $S(k) \propto k^{-2}$ . This relation was compared with simulation data but accurate evaluation was not possible due to the data quality. It was finally acknowledged that molecular chaos was violated for high inelasticity due to short range velocity-velocity correlations which were not predicted by their theory.

Another set of values for  $D_f$  can be derived from a third set of papers, those of Puglisi, Loreto, Marconi, Petri, and Vulpiani (1998), Puglisi, Loreto, Marconi, and

Vulpiani (1999) and Puglisi, Baldassarri, and Loreto (2002). In these papers a more complicated model than the Random Force Model was used in which the particles were acted on by both the random force and a drag term characterised by a relaxation time  $\tau$ . When  $\tau$  was large compared to mean collision time the Random Force Model was regained. Whereupon the structural measure of the integral of the pair correlation function,  $C(R)$ , was calculated to be a power-law with exponent  $d_2$ . We calculate that  $D_f = d_2 + 1$  and therefore find that Puglisi *et al.* determine that  $1.4 < D_f < 1.9$  such that  $D_f$  increases as the dissipation of the system reduces. As  $\tau$  is made increasingly large, such that the Puglisi *et al.* model approaches the Random Force Model, the rise in value of  $D_f$  with coefficient of restitution becomes steeper suggesting that it might plateau at low values of coefficient of restitution but unfortunately these were not measured.

The selection of papers described above highlight the variation of views held on the form of the structural properties of the two-dimensional Random Force Model. Although all papers agree that there are power-law correlations in the structure factor for small  $k$ -space, they disagree on whether the power-law's exponent is independent of the coefficient of restitution and the exact value for the exponent of the power-law decay which lies somewhere between  $1.4 \leq D_f \leq 2.0$ .

### 1.5.3 Velocity Properties of Multi-dimensional Systems

In many granular steady states there lacks a consensus among research groups about the nature of the distribution of velocity. Even in the relatively simple Random Force Model the exact determination of the high velocity tail of the distribution has not been achieved. In early work on the two-dimensional Random Force Model the velocity distribution was said to be Gaussian for all cases (Peng and Ohta 1998a; Peng and Ohta 1998b). However, on inspection of the data presented, it could be argued that these distributions show some evidence of deviation away from Gaussian for large velocity. This view was supported by the work done by Puglisi, Loreto, Marconi, and Vulpiani (1999) where the system is said to exhibit strong spatial clustering and the velocity distribution deviates away from Gaussian.

These velocity distributions were next thought of as functions with two regions of behaviour such that the distribution crossed over from Gaussian for low velocity to anomalous for high velocity. One of the most popular granular kinetic theories to be tested against these systems was that derived by van Noije and Ernst (1998)

whereby the high velocity tails of the velocity distribution is deduced to be stretched-exponential of the form  $P(v) = A \exp(-B|v|^{3/2})$ . However the credibility of fitting this distribution to data was more recently put into doubt by the papers of Barrat, Trizac, and Ernst (2005) and Barrat and Trizac (2003) who stated that the asymptotic limit of the theory is of an order of magnitude for  $P(v)$  well beyond that which can be measured in experiment or simulation. Nonetheless this theory was used by Moon, Shattuck, and Swift (2001) in a study of the three dimensional Random Force Model. They argue that the velocity distributions crossed over from  $A' \exp(-B'v^2)$ , for low velocities, to  $A \exp(-B|v|^{3/2})$ , for large velocities. On examination of the data presented only the last points of the velocity distribution, representing highest velocities, can be fitted with the trend lines of  $A \exp(-B|v|^{3/2})$ . By our judgement it can equally be argued that the asymptotic behaviour of the velocity distribution is described by a stretched-exponential with some other valued exponent.

The Moon *et al.* paper made two more observations of relevance to our study. First, they proposed that these distribution might have universal asymptotic behaviour stating that ‘the crossover behaviour may occur at higher velocities as’ the coefficient of restitution ‘approaches to 1.0’, and was based on the evidence that the crossover point between Gaussian and anomalous statistics shifts as coefficient of restitution varies. Second, they implied that mean field approximation, used by many kinetic theories, is not valid in these systems, even at near-elastic and dilute cases, and hence deviations in velocity statistics away from the predicted behaviour are caused by the spatial correlation.

In contrast more recent studies of the Random Force Model contest the use of  $A \exp(-B|v|^{3/2})$ . For example, the papers of van Zon and MacKintosh (2004) and van Zon and MacKintosh (2005) state that the velocity distribution do not cross over to  $A \exp(-B|v|^{3/2})$  but rather may have a range of apparent exponents. Curiously it is also claimed that spatial correlations play a minor or no role in the form of the velocity distribution, contrary to that suggested by Puglisi, Loreto, Marconi, Petri, and Vulpiani (1998).

These papers highlight the current state of play amongst the literature on the two-dimensional Random Force Model’s distribution of velocity. Although it is known that these distributions deviate away from being Gaussian there is no consensus into the shape of the asymptotic velocity distribution, whether it can be described by a universal curve or even if structure plays an important role in determining the shapes.

## 1.6 Thesis outline

The purpose of this thesis is to show how structural features give rise to velocity properties. We show evidence that it is the structure of the Random Force Model that influence the motion of the high velocity particles. Consequently this thesis re-examines many previous topics on the Random Force Model but provides a new interpretation into what is occurring. Firstly, we ask: can the current hydrodynamical kinetic theories describe these systems? Secondly, we resolve some of the confusion concerning the structure and velocity statistics of these systems, that is contained within current literature. Thirdly, we describe an alternative theory, for the velocity statistics, to those already proposed which incorporates the structure of the system. We use this new theory to model the correct behaviour of high velocity particles. Lastly, we propose a mechanism for structure formation in these systems, based around an idea previously mentioned but seemingly unexplored, whereby the particles self-organise into a critical state. We now progress, in the remaining text, to briefly outline the layout of the material contained within the main part of the thesis.

**In Chapter Two** we describe how to perform computer simulations of granular media. We discuss the simulation of the one- and two-dimensional Random Force Model and show that these systems form steady states where particles temporarily arrange into clusters, before breaking, at moderate to high dissipations.

**In Chapter Three** we study the one-dimensional Random Force Model and ask the question: is hydrodynamic mean theory sufficient to describe the moments of velocity and structure? The moments of velocity are found to show weak multi-scaling behaviour that deviates away from that predicted by mean field theory. As a result these systems do not have a well-defined thermodynamic limit in which the statistics of the system are dependent only on the average linear density of particles in the system and not on its size. We next study the structure of the system and observe strong multi-scaling behaviour. It is proposed that, for systems of high dissipation, the structure is caused by the system self-organising into a state of criticality. We finally describe a geometrical method of fracturing the system into small regions that produces self-similar structure and conclude that the structure produced by this method incorporates the correct kind of structural features seen in the Random Force Model.

**In Chapter Four** we investigate the structural properties of the two-dimensional Random Force Model. Currently in the literature there remains two outstanding questions about these models: what is the large-scale structure of the system? how do the velocity distributions behave at asymptotically large velocity? Previously it has been shown that these models have structure factors that exhibit power-law correlations, but the exact form is in dispute. This suggests that the structure factor exhibits a fractal behaviour with a fractal dimension,  $D_f$ , given by the exponent of the power-law decay. We study the structure factor for a wide range of dissipation and densities, beyond that of any previous work, and accurately determine the shape of the power-law decay. We calculate that  $D_f$  has a value different to that described in previous works. By introducing a coefficient of tangential restitution we can increase the dissipation of the system beyond that obtained through normal dissipation alone. It is found that these power-law decays remain unchanged with any variation of density or dissipation. We now ask: how does this fractal behaviour affect the dynamics of individual particles? The behaviour of  $S(k)$  is related back to the real-space arrangement of particles and we assert that although the bulk behaviour of the system is nominal it is the fluctuations away in the regions that are locally dilute that particles fractally arrange. We measure the distribution of distance travelled between collision and find the large distance tail is influenced by the fractal structure present in the system.

**In Chapter Five** we study the velocity distributions of these systems and calculate the shape of the high velocity tail. Importantly we show that the asymptotic behaviour of the velocity distribution is of one shape given by a stretched-exponential. Again this implies that the asymptotic limit of the distribution is unchanged with density of particles and dissipation. Significantly we find that none of the previously described granular kinetic theories can describe these velocity distributions and we conclude that this is because the theories do not include any of the structural clustering present in the system. We next create a new self-consistent theory for the Random Force Model based around the behaviour of individual high velocity particles. The motion of each particle is thought of as an accelerated walk between two collisions. This forms the basis for a new model which we call the Single Particle Model. We derive an expression for the velocity distribution by using the behaviour of a particle during a walk and the probability of a particle travelling a distance  $l$  between collision. The structure of the Random Force Model is incorporated into the calculation by imagining that fast particles move through a fractal environment consisting of the remaining particles.

The resultant shape of the asymptotic tail of the velocity distribution is a stretched-exponential whereby the exponent is dependent only on the fractal dimension of the Random Force Model's structure and is consistent with that found in chapter four.

**In Chapter Six** we present a geometrical method for generating the type of large-scale structural features seen in the two-dimensional Random Force Model. We determine a fractal dimension comparable to that measured in chapter four. The significance of this work is that it allows us to perform the Single Particle Model without using any measured data from simulated Random Force Models. Therefore for two-dimensional systems we can predict features of both the structural behaviour and the high velocity tail of the velocity distribution before performing simulation.

**In Chapter Seven** we provide some concluding remarks on the work provided by this thesis. Each chapter is summarised and then general statements are made about the Random Force Model as a whole. We finally discuss the relevance of this thesis to the wider granular field and suggest some directions for further research based on the material described here.

## Chapter 2

# Modelling Granular Systems

In chapter two we explain the computational methods used for modelling dry granular media. We describe in detail the computational technique of molecular dynamics and conclude the chapter by performing molecular dynamics simulation of the one- and two-dimensional Random Force Model. These simulations represent systems that stabilize into a steady state where the time average kinetic energy of particles remains constant.

### 2.1 Molecular Dynamics Technique

To run simulations successfully requires programmers to go through three stages: selecting a method; implementation of the method; testing the method.

#### 2.1.1 Selecting a Method

In computer simulations, granular systems are treated as a collection of particles in a one or more dimensional space and time that continually interact with long-ranged external forces, such as gravity, whilst instantaneously responding to any contacting boundary conditions or colliding particles. The grains are often assumed to be a non-rotating single sphere with spatial extent or a composite collection of spheres; such a configuration is a simplification of true geometry and is made to optimize the method of collision detection between grains.

During a collision between a pair of granular particles two important axioms hold: first, the momentum of the collision is conserved:

$$\mathbf{v}'_1 + \mathbf{v}'_2 = \mathbf{v}_1 + \mathbf{v}_2, \quad (2.1)$$

where  $\mathbf{v}_1, \mathbf{v}_2$  are the pairs incoming velocity before collision and  $\mathbf{v}'_1, \mathbf{v}'_2$  are the pairs outgoing velocity after collision.

second, the energy of the collision is dissipated (through deformation, heating) such that:

$$(\mathbf{v}'_2 - \mathbf{v}'_1) \cdot \hat{\mathbf{n}} = \varepsilon(\mathbf{v}_1 - \mathbf{v}_2) \cdot \hat{\mathbf{n}}, \quad (2.2)$$

where  $\hat{\mathbf{n}}$  is the unit normal vector to the collision. The decay constant  $\varepsilon$  is called the coefficient of restitution and takes values from zero to one. If the coefficient of restitution is one then the two particles conserve energy during collision and the collision is considered to be elastic. If the coefficient of restitution is zero then the two particles after collision move as one and the collision is considered to be totally inelastic.

In simulation it is not possible to model the true deformation that occurs as particles collide and so simpler models must be used where the collisions are modelled such that the above two axioms are satisfied. Two common methods used in simulations are: Event Driven (ED) (Lubachevsky 1991) and Molecular Dynamics (MD) (Herrmann and Luding 1998).

In Event Driven simulation each collision is resolved at the moment of time it occurs. The system of particles evolve in time using long-ranged forces until a pair of particles come into surface contact. The collision is resolved by satisfying the two axioms and the pair of particles are assumed to have finished colliding. The system then continues to evolve in time until another collision is reached. Treating collisions as instantaneous can be problematic as if a collision results in prolonged contact or multiple contacts then the ED code will not progress the system beyond the point of contact and the system experiences granular collapse where several particles cluster together.

In Molecular Dynamics particles evolve numerically using discrete time steps and force equations. The collisions between soft particles [that dissipate energy through temporary deforming during a collision] are treated as occurring over a finite time rather than being instantaneous where a pair of colliding particles exert a repulsive contact force on the other during the duration of contact. Using a discrete time step allows the simulated particles to become partially overlapped and the extent of the overlap represents the severity of the particle's deformation (a situation which is not possible with ED). MD induces larger errors than ED as we are approximating the forces over the time step.

Which of the two methods is appropriate depends on the granular system being modelled. ED is effective for dilute granular gases but breaks down when dealing with large numbers of collisions such as occurs in dense granular beds. Hence it is sensible

to use MD code in this research as many of the systems that are investigated involve dense regions of grains.

Having chosen the appropriate simulation technique it is now time to construct the algorithm that will model the time evolution of the system. All programs are constructed in three stages: The bulk of the program consists of general methods that deal with the physics of the collection of particles and non-system specific external forces such as gravity; the program is tailored by applying system specific boundary conditions such as vibrating walls; the program is initialised with physical properties given to the collection of grains.

### 2.1.2 General Methods for running the Simulation

Molecular Dynamic modelling evolves the simulated spherical particles by a time step  $\Delta t$ , using a numerical method such as the Verlet algorithm (Verlet 1967);

$$\mathbf{r}(t + \Delta t) = 2\mathbf{r}(t) - \mathbf{r}(t - \Delta t) + \mathbf{a}(t)\Delta t^2, \quad (2.3)$$

where  $\mathbf{r}(t)$  is the particle's position and  $\mathbf{a}(t)$  is the particle's acceleration at time  $t$ . As the system is not relativistic, Newton's second law is sufficient to relate the acceleration of a particle to the force exerted on it,  $\mathbf{F}$ , such that  $\mathbf{a}(t) = \mathbf{F}/M$  with  $M$  is the particle mass. Allowing particle rotation requires further equations and shall be ignored.

The short ranged repulsive contact force of particles in collision can be represented as the sum of forces that are normal and tangential to the surface of contact. Any forces tangential to the surface of contact can be considered to result from the rubbing together of the two particles. In the simplest model we can assume the spherical particles are smooth and so we can ignore the tangential forces completely. The normal component of the repulsive force can be considered to have an elastic and a dissipative component.

#### The Normal Elastic Force

In this thesis the normal elastic force of collision between particles is taken to obey Hook's law and the spring constant,  $k_s$ , is chosen such that particles packed and at rest, under gravity, satisfy  $Mg \simeq k_s \delta r$ , where  $\delta r$  is the maximum overlap between particles in contact and describes the softness/extent of deformity of the particle and  $g$  is the gravitational field strength. The linear spring is used in preference to more realistic collision force approximations, such as Hertzian contacts, because the calculations are computationally less intensive and measured properties of the system are insensitive

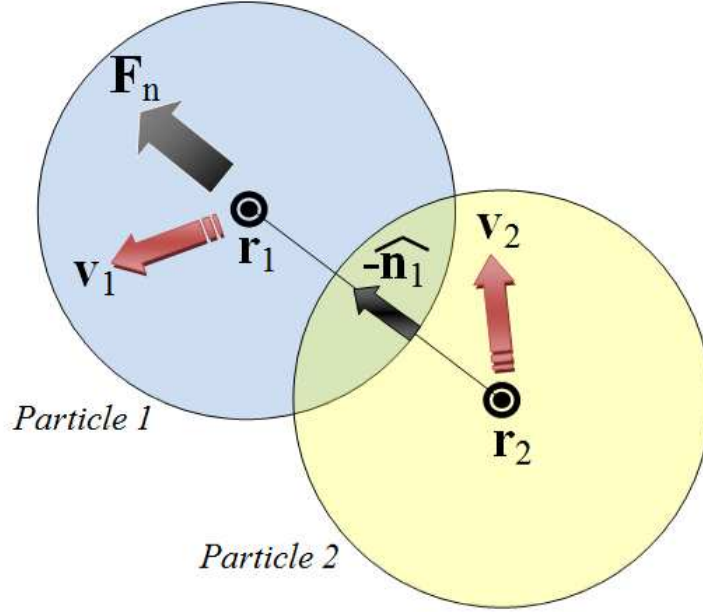


Fig. 2.1: Model of layout of contact between two particles that leads to a normal dissipative force,  $\mathbf{F}_n = \mathbf{F}_{elast} + \mathbf{F}_{dis}$ . For clarity the overlap of the particles is exaggerated.

to internal changes of the collision as long as the resultant outcome of the collision remains the same.

Such an arrangement means that for a pair of colliding particles the elastic force acting on particle 1, as shown in figure 2.1, can be described as;

$$\mathbf{F}_{elast} = \begin{cases} -k_s(d - |\mathbf{r}_1 - \mathbf{r}_2|)\hat{\mathbf{n}}_1 & |\mathbf{r}_1 - \mathbf{r}_2| < d, \\ 0 & \text{otherwise.} \end{cases} \quad (2.4)$$

where  $\mathbf{r}_i$  is the position of the centre of the  $i^{\text{th}}$  particle and  $\hat{\mathbf{n}}_1$  is the unit vector normal to the collision orientated *out of* the surface of particle 1. For spherical particles  $\hat{\mathbf{n}}_1$  is calculated as  $\hat{\mathbf{n}}_1 = -\frac{\mathbf{r}_1 - \mathbf{r}_2}{|\mathbf{r}_1 - \mathbf{r}_2|}$ . Collisional forces only occur whilst particles are in contact and thus the elastic force is zero once the separation between particles exceeds the diameter of a particle,  $d$  (assuming all particles have identical radii).

### The Normal Dissipative Force

Real granular systems contain particles that dissipate energy as particles collide. The loss of energy can be modelled through a dissipative force which acts against the relative motion in a collision (Herrmann and Luding 1998), ensuring that whilst kinetic energy is lost the total momentum is preserved.

During collision the extent of energy lost is determined by a fixed coefficient of

restitution  $\varepsilon$ , as defined in equation 2.2. The dissipative force,  $F_{dis}$ , is the dash-pot force normal to the collision (see figure 2.1);

$$\mathbf{F}_{dis} = \begin{cases} -\gamma_n [(\mathbf{v}_1 - \mathbf{v}_2) \cdot \widehat{\mathbf{n}}_1] \widehat{\mathbf{n}}_1 & |\mathbf{r}_1 - \mathbf{r}_2| < d, \\ 0 & \text{otherwise.} \end{cases} \quad (2.5)$$

Here we consider that there are two particles colliding with velocities  $\mathbf{v}_1$  and  $\mathbf{v}_2$ . The dissipative force described is acting on particle 1 and  $\widehat{\mathbf{n}}_1$  is the unit vector normal to the collision out of the surface of particle 1. The dissipation coefficient  $\gamma_n$  can be shown to be related to  $\varepsilon$  by:

$$\gamma_n^2 = \left( \frac{\ln(\varepsilon)}{\pi} \right)^2 \frac{4m_{12}k_s}{1 + \left( \frac{\ln(\varepsilon)}{\pi} \right)^2}, \quad (2.6)$$

where  $m_{12} = m_1 m_2 / (m_1 + m_2)$  and  $m_1, m_2$  are the masses of the two particles. The second particle experiences an equal but oppositely directed dissipative force to that of the first (Newton's third law).

### The Tangential Dissipative Force

In more complicated models we allow the particle's surface to have microscopic roughness, which does not affect the geometry of the particle but introduces tangential dissipative forces.

Two possible methods for producing a tangential dissipative force during collision are outlined below and are either sliding friction or tangential dash-pot force.

Friction between the particles affects the flow of the system by resisting the motion of the particles. To simulate such systems a frictional constraint is added, but particle rotation ignored. As materials collide, the roughness of their surfaces leads to a tangential frictional force against the relative motion. Friction comes in two forms: static and sliding. For the purposes of simplicity we shall assume that all friction is sliding. The error produced by ignoring static friction should be small as most particles are moving faster than the crossover limit. Thus we can describe the frictional force as  $F_{fric} = -\mu |F_{elast} + F_{dis}|$ , where  $\mu$  is the frictional coefficient and the total collision force on particle 1,  $\mathbf{F}_c$ , is given as;

$$\mathbf{F}_c = (F_{elast} + F_{dis}) \widehat{\mathbf{n}}_1 + \frac{(\mathbf{v}_1 - \mathbf{v}_2) \cdot \widehat{\mathbf{t}}_1}{|(\mathbf{v}_1 - \mathbf{v}_2) \cdot \widehat{\mathbf{t}}_1|} F_{fric} \widehat{\mathbf{t}}_1, \quad (2.7)$$

where  $\widehat{\mathbf{n}}_1$  and  $\widehat{\mathbf{t}}_1$  are the normal and tangential unit vectors for the surface of contact of particle 1 (figure 2.2). The tangential unit vector is defined from the normal unit

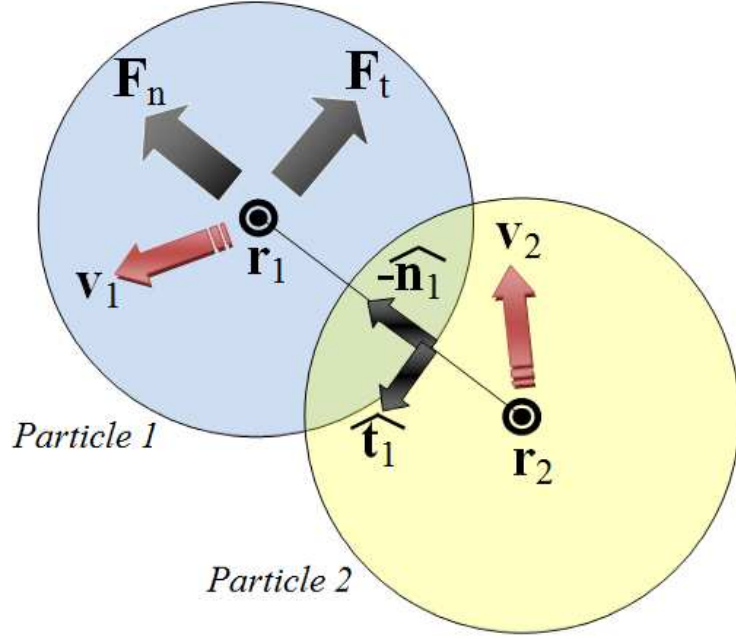


Fig. 2.2: Model of layout of collision between particles that results in both a normal dissipative force,  $\mathbf{F}_n$ , and a tangential dissipative force,  $\mathbf{F}_t$ .

vector by use of a 90 degrees rotation matrix, such that:

$$\hat{\mathbf{t}}_1 = \begin{bmatrix} 0 & 1 \\ -1 & 0 \end{bmatrix} \hat{\mathbf{n}}_1. \quad (2.8)$$

### Tangential Coefficient of Restitution

An alternative method of tangential dissipation is to introduce a tangential dash-pot force  $\mathbf{F}_{\text{diss},t}$  to the collision.  $\mathbf{F}_{\text{diss},t}$  is defined by an associated tangential dissipation coefficient  $\gamma_t$  such that:

$$\mathbf{F}_{\text{dis},t} = \begin{cases} -\gamma_t [(\mathbf{v}_1 - \mathbf{v}_2) \cdot \hat{\mathbf{t}}_1] \hat{\mathbf{t}}_1 & |\mathbf{r}_1 - \mathbf{r}_2| < d, \\ 0 & \text{otherwise.} \end{cases} \quad (2.9)$$

The tangential dissipation coefficient is determined by considering a fixed tangential coefficient of restitution  $\varepsilon_t$  which characterises the energy lost in collision by the correlation of particle momentum tangential to collision:

$$(\mathbf{v}'_1 - \mathbf{v}'_2) \cdot \hat{\mathbf{t}} = \varepsilon_t (\mathbf{v}_1 - \mathbf{v}_2) \cdot \hat{\mathbf{t}}, \quad (2.10)$$

where  $\mathbf{v}'_1, \mathbf{v}'_2$  are post collision velocity of the pair of particles and  $\mathbf{v}_1, \mathbf{v}_2$  the initial velocities. The equation 2.10 is analogous to equation 2.2. The time scale of collision

is related to the spring constant by  $t = \pi\sqrt{m_{12}/k_s}$ . Thus the tangential coefficient of restitution can be replaced by:

$$\varepsilon_t = \exp\left(\frac{-\gamma_t\pi}{\sqrt{km_{12}}}\right). \quad (2.11)$$

By rearrangement we obtain  $\gamma_t$  as:

$$\gamma_t = -\frac{\sqrt{km_{12}}}{\pi} \ln(\varepsilon_t). \quad (2.12)$$

To avoid confusion when using this form of dissipation we denote the normal coefficient of restitution with  $\varepsilon_n$ .

### Choosing a Time-step

For the Verlet algorithm to remain an accurate numerical method, we must ensure that the time-step is sufficiently small. This is maintained by choosing a  $\Delta t$  that is 10 times smaller than the collision time, for example  $\Delta t \leq 2\pi\sqrt{\frac{M}{k_s}}$  (derived from Newton's Second law).

When too large a time-step is used, for a given spring constant, the particles move too far each iteration resulting in some collisions being ignored and incorrect amounts of energy being dissipated during collision.

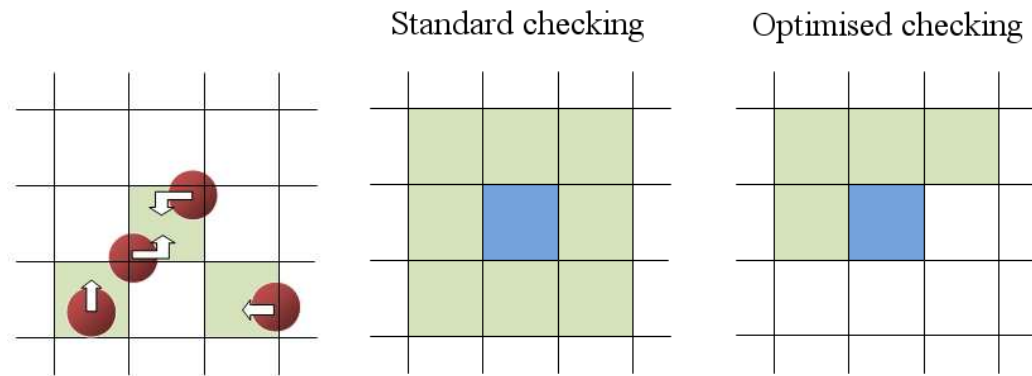
A compromise must be reached between size of time-step and spring constant. Choosing a larger spring constant increases the hardness of the particle and reduces the time constant of the collision, but requires a smaller time-step and hence increases the computational time of the computer simulation.

### Method for Efficient Collision Handling

Each advance of the system by a time step requires the calculation of all collisions between particles; when using a computer each particle's current position can be checked against all other particles to see if there is an overlap in their positions and hence a collision. Such a method is both inefficient and unnecessary. The collisions between particles are a result of short range forces and so only other particles that are near (with centres less than a diameter away from the centre of the first particle) need to be checked. The near particles are determined by using a grid which reduces the required number of calculations a computer must run before all occurring collisions are checked (Allen and Tildesley 1987).

The grid is created by splitting the system into an array of identical rectangular boxes [the boxes must have dimensions larger than the diameter of the largest grain

Fig. 2.3: Overlaying a grid of boxes onto the system allows collisions between neighbouring particles to be identified using an efficient computational algorithm.



(a) A visual demonstration of particles being assigned boxes where each particle belongs to the box in which their centre lies. (b) The nine neighbouring grid boxes, shown as shaded boxes in the left-hand diagram, required for checking collisions on particles contained within the central box. The right-hand diagrams show the equivalent reduced number of boxes used in an efficient code.

and are most efficient if they have dimensions less than two grain diameters]. Each particle is assigned to the box corresponding to its position (see figure 2.3(a)). For a two dimensional system the computer only checks for collisions between a particle contained within each box and particles within the same box [other particles may be contained within the same box and might be in collision with the particle] and 8 neighbouring boxes (see left-hand side of figure 2.3(b)). An efficient code will only require the checking of four neighbouring boxes and the box the particle is contained within (see right-hand side of figure 2.3(b)), as the contact forces on both colliding particles are simultaneously stored.

### 2.1.3 Boundary Conditions

Every system simulated must be bounded to prevent dilution of the granular medium when the particles spread out. There are two types of boundary conditions that are used in simulations called physical, or periodic: the former are computational representations of container walls used in real experimental systems, the latter are used to enable a small collection of simulated grains to appear to be a subset of a much larger group.

Physical barriers deflect the particle as if they are unmovable grains and can be set to be dissipative or elastic. They can also provide a source of energy injection for the system by vibrating or increasing the kinetic energy of particles that are in contact with the barrier.

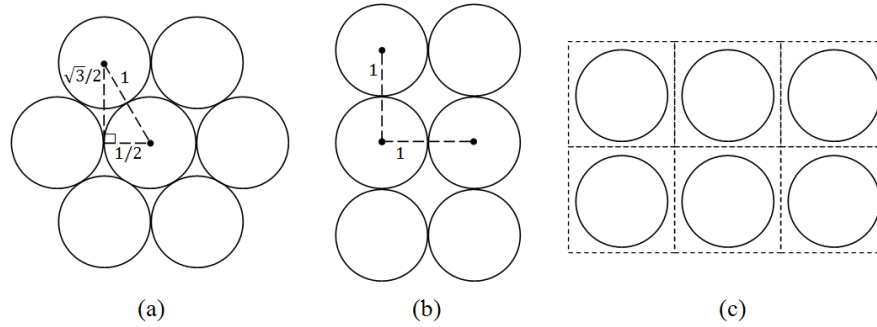


Fig. 2.4: The arrangement of particles in order to achieve (a) hexagonal packing (b) square packing and (c) uniform spread of particles. All lengths are measured in units of particle diameter.

Periodic boundaries require careful handling as a particle moving through the boundary translates to the other side of the container. Therefore particles near a periodic boundary must be able to interact with particles on the opposite boundary as they are effectively neighbouring one-another.

Consideration is required before choosing the type of barriers to bound the system. Physical boundaries are necessary for using vibration to drive the system and to model the effects generated by the geometry of the box such as convection and arching. Periodic boundaries increase the apparent size/number of grains of the system but can lead to net drifts of particles and cannot be used in non-tessellating boxes.

#### 2.1.4 Initial Conditions

For a program to be initialised, sensible values must be provided to a set of parameters: system parameters include length scales, gravitational field strengths and vibration constraints such as frequency and amplitude; grain parameters include size, mass, initial velocity and coefficients for friction and dissipation.

Most importantly the grains must be placed inside the system: inappropriate positioning could lead to a cascade of momentum as a particle inside another or wall receives an extreme collisional force and explodes into other particles.

Three suitable techniques for placing particles are outlined. Hexagonal packing minimises the occupied volume of the bed of grains, is a stable arrangement which allows the maximum number of particles to fit in a volume such that for a rectangular system  $N_{max} = \frac{2}{\sqrt{3}} \frac{L_1 L_2}{d^2}$  where  $L_1, L_2$  are the systems dimensions (figure 2.4(a)). Square packing provides a simple method for starting all particles at one end of the system (figure 2.4(b)), but is an unstable arrangement that easily collapses into the more stable hexagonal packing or becomes disordered. A uniform spread of particles allocates each

particle an equal volume of the system such that the sum of volumes assigned to each particle equals that of the system (figure 2.4(c)).

The first two techniques provide bed-like situations and are best used when the grains of a system are likely to condense out into a crystalline structure. An example is a bed of grains under gravity. The third technique is useful for its ability to quickly reach a steady state where the particles are evenly spread out over the whole box. In most systems the initial arrangements of particles does not affect the final outcome.

### 2.1.5 Energy Dissipation during Collision

When a pair of particle collides the centre of mass velocity decreases as energy is dissipated. The fractional energy loss of the pair, for a one-dimensional collision, is governed by:

$$\frac{\Delta T}{T} = 1 - \varepsilon^2. \quad (2.13)$$

Similarly for a two-dimensional collision, in which we remove the angular dependence of the energy loss by choosing the normal coefficient of restitution and the tangential coefficient of restitution to be equal,  $\varepsilon_n = \varepsilon_t$ , the fractional energy loss is governed by:

$$\frac{\Delta T}{T} = 1 - \frac{\varepsilon_n^2 + \varepsilon_t^2}{2}. \quad (2.14)$$

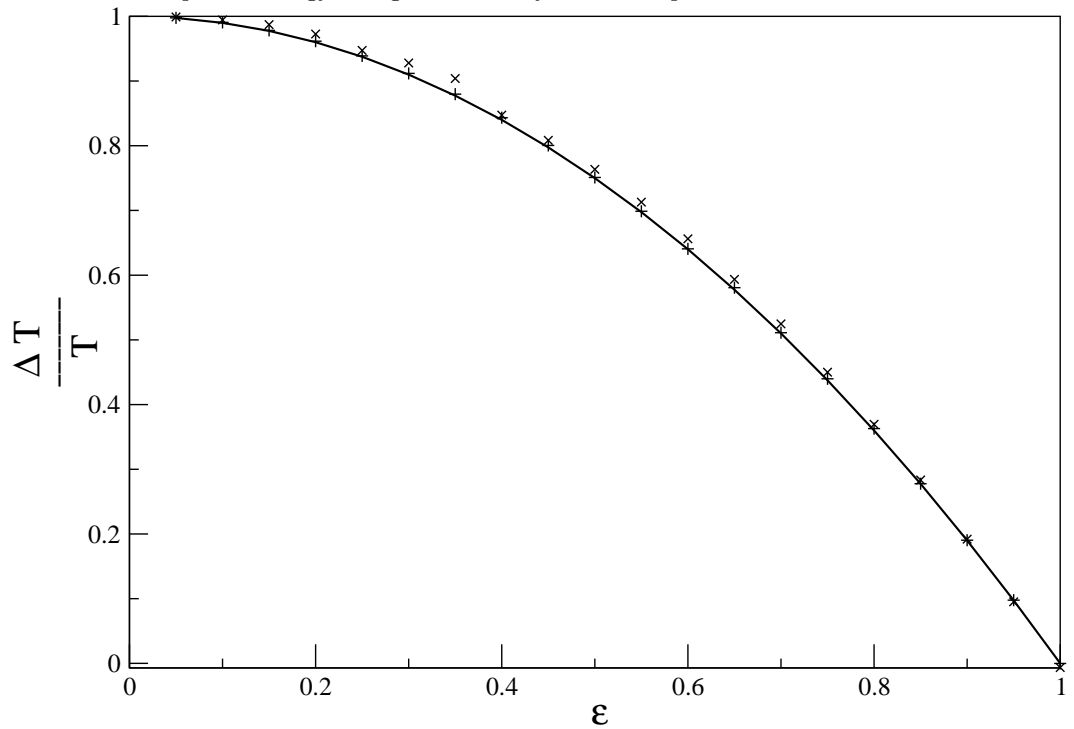
To demonstrate that our computer code does indeed obey the above collision properties, we simulate the collision of two particles. The table below shows four possible collisions, inside the brackets are the value of the  $x$ - and  $y$ - components of the initial position  $\mathbf{x}_i$  and velocity  $\mathbf{v}_i$ ,  $r$  is the radius of the particle.

Simulation number	$\mathbf{x}_1$	$\mathbf{v}_1$	$\mathbf{x}_2$	$\mathbf{v}_2$
1	(0,0)	(1,0)	(1,0)	(0,0)
2	(0,0)	(1,1)	(1,1)	(0,0)
3	(0,0)	(0,1)	( $r$ , 1)	(0,0)
4	(0,0)	( $1 + r$ , 1)	(1,1)	(0,0)

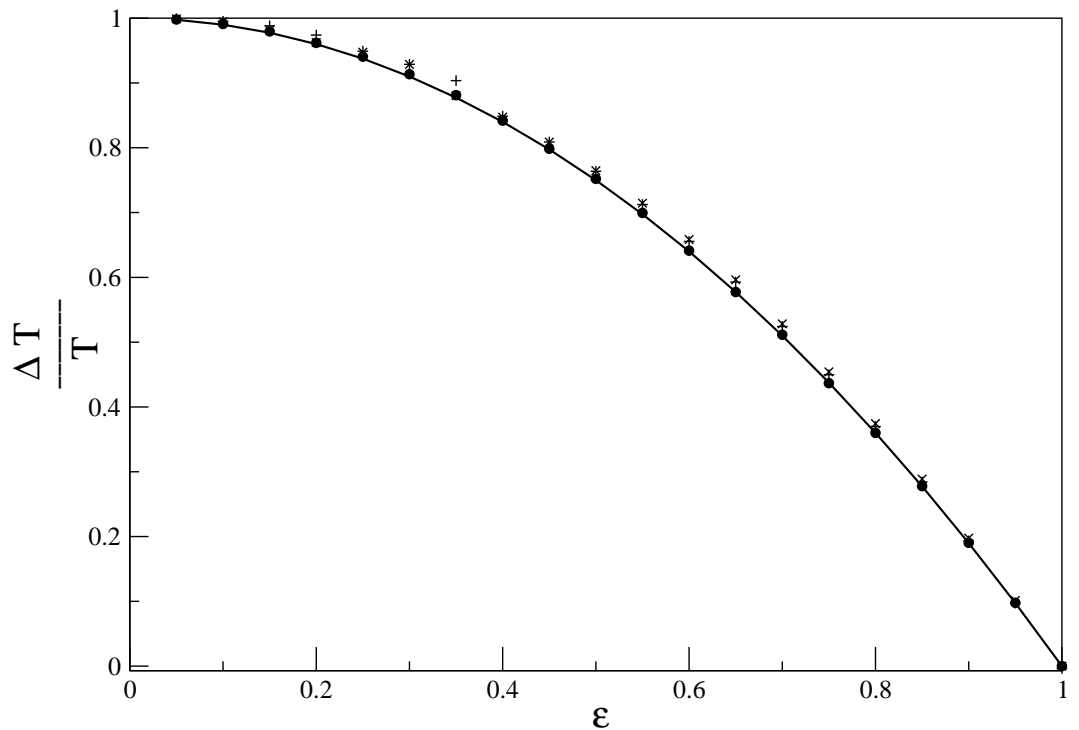
Table 2.1: The vector components of the initial position and velocity of two particles that are about to undergo a collision. For simplicity the mass of each particle is 1kg.

Simulation 1 is a one-dimensional collision. Simulation 2 to 4 provides a sample of possible two-dimensional collisions. In all the above simulations a frame of reference is chosen such that the second particle is initially motionless. The fractional energy loss

Fig. 2.5: The fractional energy lost per pair collision as a function of coefficient of restitution. The solid line is the expected energy change from theory whilst the points are simulation data.



(a) Simulation 1 with a time-step of  $\Delta t = 1 \times 10^{-5}$  and spring constant of  $k_s = 5000\text{kgs}^{-2}$  (cross) or  $\Delta t = 1 \times 10^{-6}$  and  $k_s = 500000\text{kgs}^{-2}$  (plus).



(b) Simulation 2 (cross), Simulation 3 (plus) and Simulation 4 (circle), where a time-step of  $\Delta t = 1 \times 10^{-6}$  and spring constant  $k_s = 500000\text{kgs}^{-2}$  is used.

of these collisions are shown in figures 2.5(a), 2.5(b) and the simulation data agrees reasonably with the predicted theory of equations 2.13 and 2.14.

## 2.2 The One-dimensional Random Force Model

We now briefly outline the routines required to run simulations of the one-dimensional Random Force Model.

### 2.2.1 Computation of a Random Force

We develop routines for performing simulation of the one-dimensional Random Force Model by calculating a discrete approximation for the random force and then deriving the Newtonian equation of motion of each particle.

The random force acts continuously on all particles in the system, feeding in kinetic energy to the system through the acceleration of the particles. The force exerted on a particle  $i$  through the interaction with the random force is denoted by  $\eta_i(t)$  and statistically behaves as Gaussian *white* noise, with magnitude controlled by the noise strength,  $D$ . The interaction of the random force and particles is uncorrelated in respect to time and different particles such that the correlator can be expressed as:

$$\langle \eta_i(t) \eta_j(t') \rangle = 2D \delta(t - t') \delta_{i,j}. \quad (2.15)$$

In the simulation we use a discrete approximation for the random force, increasing the particles momentum by  $\eta_i(t) \Delta t$  each time we evolve the system by a single time-step,  $\Delta t$ . We select values for the random force during simulation by using the Box Muller Transformation Method (Abramowitz and Stegun 1965) in which  $\eta_i$  is calculated from two generated random numbers using

$$\eta_i = \sqrt{-2 \ln(a_1)} \sqrt{\frac{2D}{\Delta t}} \cos(2\pi a_2), \quad (2.16)$$

where  $a_1, a_2$  are random numbers generated from a uniform probability distribution such that  $a_1, a_2$  lies in the range 0 to 1. In this way the average increase of kinetic energy per second of each particle due to the random force is kept fixed at  $D/M$  regardless of the time-step used in simulation.

Particles of a one dimensional Random Force Model have a Newtonian equation of motion given by:

$$M \frac{dv_i(t)}{dt} = F_{i,i+1} + F_{i,i-1} + \eta_i(t), \quad (2.17)$$

where  $F_{i,j}$  is the interaction force between particle  $i$  and its nearest neighbour  $j$ . Collapse of the system is avoided because the random force continues to be exerted onto the particles during particle collision.

Finite sampling of the Gaussian random force has one draw back: the time average of the sum of the sampled random force does not equal 0. As a consequence, over time the system will develop a net drift as the centre of mass of the system diffuses due to the small net preference in direction of the sum of the random forces at any one time.

To ensure that no net drift of particles occurs we symmetrise the random force such that at any given time all generated measurements of the random force are mapped to:

$$\eta_i(t) \rightarrow \left( \eta_i(t) - \frac{1}{N} \sum_{j=1}^N \eta_j(t) \right). \quad (2.18)$$

As the number of particles in the system increases the adjustment reduces towards zero signifying that the sampled random force is approaching that of the true random force.

Alternatively, instead of symmetrising the random force, we could periodically translate the system to the centre of mass frame (as was done by Williams and MacKintosh (1996)) by subtracting the centre of mass velocity from the velocity of each particle.

### 2.2.2 Simulation Details

The one-dimensional system is ideal for a preliminary study of the Random Force Model because the dynamics of the particles are much simpler than for higher dimensional systems due to the reduced number of the degrees of freedom. In the Model particles cannot reorder and consequently collide only with those directly neighbouring. This means that the particles can be treated as point-like objects without exhibiting loss in behaviour. The dissipation of the system is maximised as the centre of mass velocity of a pair of colliding particles is parallel to the normal of collision.

In simulation, the one-dimensional system consists of a line of particles with periodic boundaries separated by a distance  $L$ . Each particle can be imagined to be a disk, constrained to move along the one-dimensional line, such that the particle's width is two times the radius,  $r$ . The  $N$  particles are initially placed uniformly along a horizontal line with spacing  $L/N$  and given a small initial random velocity of  $v_i(0) = 0.1 \times a$ , where  $a$  is a value picked at random from a uniform probability distribution  $U(a)$  such that  $-0.5 \leq a \leq 0.5$  and  $U(a) = 1$ . The inclusion of a small initial velocity increases the rate of randomisation of the system but is quickly overwhelmed by the momentum increase

generated by subsequent injections of energy by the random force. The table below defines the following properties for the particles:

Particle Parameters	Symbol	Value
Radius	$r$	1.5 mm
Mass	$M$	$3.53 \times 10^{-5}$ kg
Spring constant	$k_s$	$500,000 \text{kg s}^{-2}$
Noise strength	$D$	$1 \times 10^{-8} \text{N}^2 \text{s}$

Table 2.2: List of fixed system properties for the Random Force Model.

These values are selected to be comparable with experiments such that particles travel at realistic velocities but other choices can be made without changing the type of behaviour seen. In chapter three we study the one-dimensional Random Force Model for a range of systems containing between 100 and 10000 particles and the complete spectrum of coefficient of restitution between 0.01 and 0.999.

Figure 2.6 show some of the possible arrangements of particles that occur during simulation of the Random Force Model in which 600 particles are contained in an interval of  $L = 0.8\text{m}$ . Each line of particles represents a snap-shot in time and particles contained in a small section of the system are shown. Two dissipation states are shown. In figure 2.6(a) particles have a high coefficient of restitution ( $\varepsilon = 0.9$ ) and are distributed nearly homogeneously, small fluctuations of density occur predominantly through chance but also through the slight correlation of velocity of particles after collision. The velocity of the particles are close to being uncorrelated with the position of the particles.

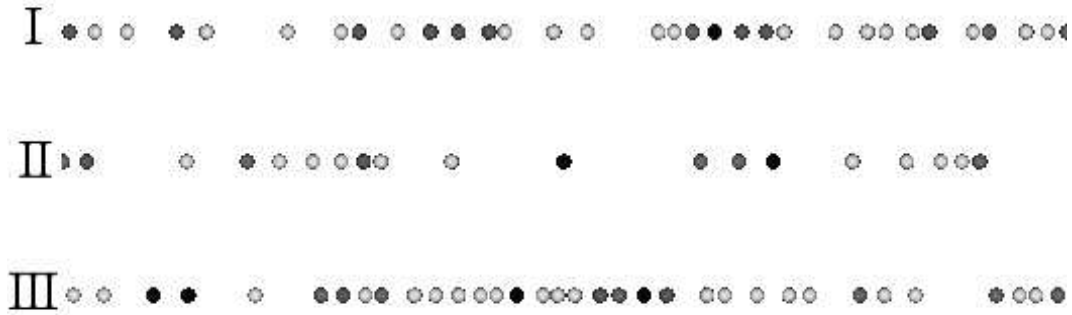
In figure 2.6(b) particles have a low coefficient of restitution ( $\varepsilon = 0.1$ ) and particles have a stronger tendency to cluster with other particles. These clusters occur due to the strong correlation in velocity between neighbours after collision and hence the fastest particles are in general those found away from clustered regions.

### 2.2.3 Steady States

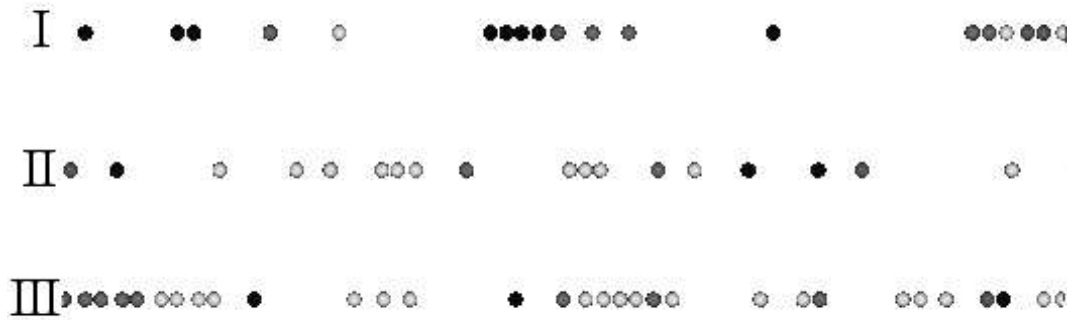
We wish to ensure that measurements are made once the system is in a steady state, where the rate of energy gained by driving forces equals the rate of energy loss through dissipation. In the steady state the exact nature of the initial conditions are ‘forgotten’.

The granular temperature,  $T$ , of the system is defined to be proportional to the

Fig. 2.6: Three snapshots of the position of particles in a small region of the system. The system contains 100 particles with a system size of 0.8m. The different colours give an estimate of the particle momentum, where darker shaded particles are faster.



(a) Low dissipation,  $\varepsilon = 0.9$



(b) High dissipation,  $\varepsilon = 0.1$

average kinetic energy of the system:

$$T = \frac{1}{N} \sum_{i=1}^N |\mathbf{v}_i(t) - \langle v \rangle|^2, \quad (2.19)$$

where  $\langle v \rangle$  is the mean velocity. In the steady state the system has a granular temperature that is constant over large time scales.

Figure 2.7 shows the granular temperature for the first six seconds of a system containing 1000 particles and system size of  $L = 4\text{m}$ . Two different coefficients of restitution are used. The solid line represents a system with low dissipation of  $\varepsilon = 0.9$ . The particles are initially spread uniformly across the system. Within a very short time (less than one second) the granular temperature becomes roughly constant (although this is difficult to see from the figure, due to strong fluctuations in value of  $T$ , it will be shown later that the time average behaviour of  $T$  is constant) and the system can be considered to be in a steady state. The remaining two lines shown in the figure represent

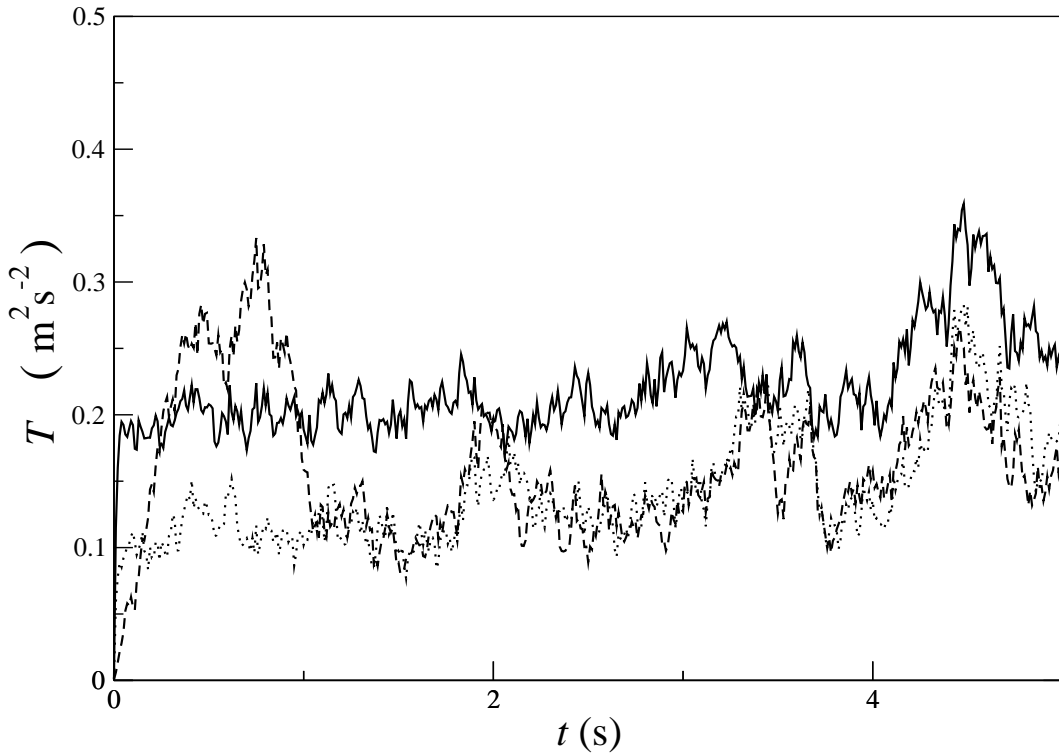


Fig. 2.7: A temperature verses time plot of the Random Force Model of 1000 particles in a 4m long system progressing to steady state. The dissipation is  $\varepsilon = 0.9$ (solid line) or  $\varepsilon = 0.1$ (dashed and dotted lines).

a system with high dissipation of  $\varepsilon = 0.1$ . Initially the particles are either uniformly spread across the system (dotted line) or formed into a single cluster (dashed line). Notice that the increase in granular temperature is finished after about one second of simulation.

Three points on the granular temperature in the steady state can be made: first, the initial condition of the system does not affect the outcome once the steady state has been reached; second, the steady state granular temperature increases with increase in coefficient of restitution; third, strong fluctuations in the granular temperature occur due to clustering – in a cluster there are many more collisions, leading to a lowering of the granular temperature.

The fluctuations in granular temperature can be smoothed out by using the time average granular temperature,  $\langle T \rangle$ , calculated in the simulation by the formula:

$$\langle T \rangle = \frac{1}{NN_t} \sum_{\tau=1}^{N_t} \sum_{i=0}^N |v_i(t_\tau) - \langle v \rangle|^2, \quad (2.20)$$

where  $N_t$  is the number of samples. Figure 2.8 shows the time average granular temperature for a system containing 1585 particles and coefficient of restitution 0.1. It requires a period of approximately 200 seconds to elapse in the simulation before the

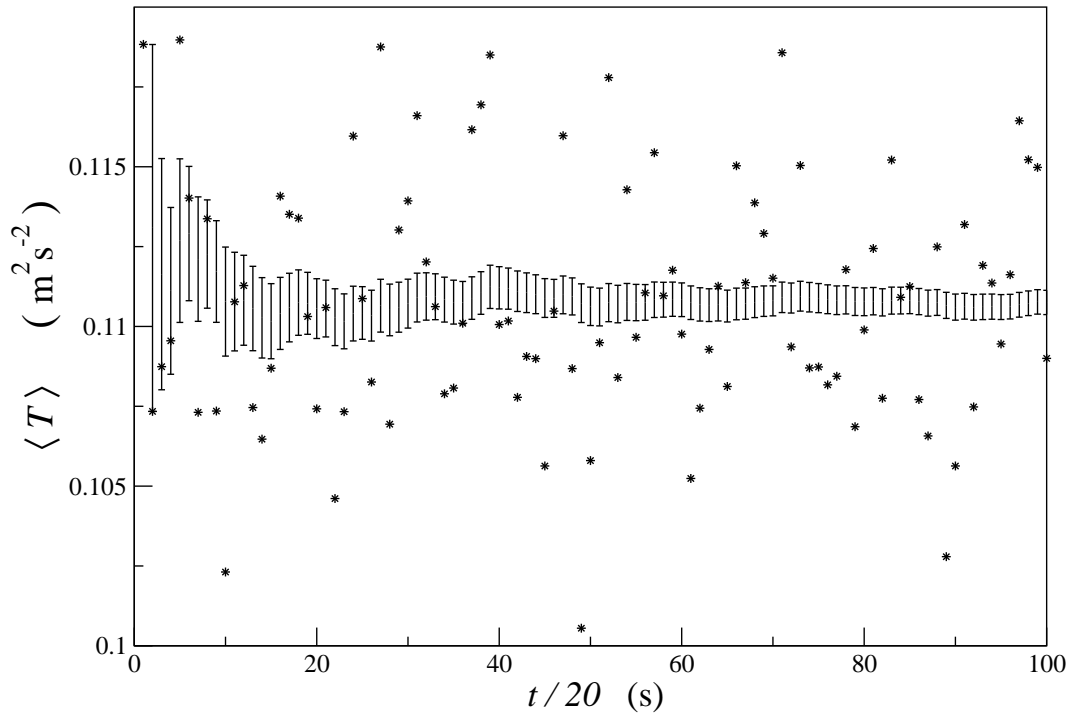


Fig. 2.8: The time average value of granular temperature when estimated over 20 second periods (points) and a running average sampled over  $t$  seconds (error bars). The system contains 1585 particles with coefficient of restitution of 0.1.

fluctuations in granular temperature have been reduced sufficiently.

## 2.3 The Two-dimensional Random Force Model

We next describe the methods required to simulate the two-dimensional Random Force Model, which is studied in chapter four. We describe the general routines used to represent the random force that acts on each particles in a two-dimensional system, define the set-up of the various systems studies and discuss their geometrical properties. We conclude by demonstrating that these systems form steady states.

### 2.3.1 Computation of a Random Force

Particles of a two-dimensional Random Force Model have a Newtonian equation of motion given by:

$$M \frac{d\mathbf{v}_i(t)}{dt} = \sum_{i \neq j} \mathbf{F}_{i,j} + \boldsymbol{\eta}_i(t), \quad (2.21)$$

where  $\mathbf{F}_{i,j}$  is the particle-particle interaction term and  $\boldsymbol{\eta}_i(t)$  is the random force. The random force is assumed to have orthogonal components,  $\eta_{x,i}, \eta_{y,i}$ , that are independent of one another and whose strength is controlled by a common noise strength  $D$ . The

interaction of the random force and particles is uncorrelated with respects to time, different particles and direction such that the correlator can be expressed as:

$$\langle \eta_{z',i}(t) \eta_{z'',j}(t') \rangle = 2D \delta(t - t') \delta_{i,j} \delta_{z',z''}. \quad (2.22)$$

We select values for the random force during simulation using the Box Muller transformation Method (Abramowitz and Stegun 1965) in which  $\boldsymbol{\eta}_i$  is calculated from two random numbers using:

$$\boldsymbol{\eta}_i = \begin{bmatrix} \eta_{x,i} \\ \eta_{y,i} \end{bmatrix} = \sqrt{-2 \ln(a_1)} \sqrt{\frac{2D}{\Delta t}} \begin{bmatrix} \cos(2\pi a_2) \\ \sin(2\pi a_2) \end{bmatrix}, \quad (2.23)$$

where  $a_1, a_2$  are random numbers generated from a uniform probability distribution such that  $a_1, a_2$  lie in the range 0 to 1 while the vector component randomly orientates the force ensuring independence of the orthogonal components.

To ensure that the simulation does not develop a net drift of particles we periodically translate the system to the centre of mass frame by subtracting the centre of mass velocity from the velocity of each particle.

### 2.3.2 Simulation Details

We describe the method of dissipation and geometric properties of the systems under study and discuss the added complexity that develops in two-dimensional systems as opposed to those of one dimensions. These consideration equally apply to higher dimensional systems.

#### Particle Properties, Boundary Conditions and Method of Dissipation

In the two-dimensional Random Force Model particles are placed in a square system with periodic boundaries of separation  $L$ . The noise strength remains fixed at  $D = 1 \times 10^{-8} \text{N}^2\text{s}$ . The particles are circular, with radius 1.5mm, each has a mass of  $3.53 \times 10^5 \text{kg}$  and their collisions are assumed to behave as if the particles are repelled by springs with spring constant of  $500\,000 \text{kgs}^{-2}$  that are damped so as to mimic dissipation. The particles dissipate via a normal coefficient of restitution  $\varepsilon_n$  and a tangential coefficient of restitution  $\varepsilon_t$ .

The simulation is initiated by distributing the collection of particles either with square or hexagonal packing. Again each particle in the system is given a small non-zero initial velocity which has orthogonal components  $(v_{x,i}(0), v_{y,i}(0))$  that are picked

from an uncorrelated random uniform distribution, as already described for one dimensions. For every simulation the system is allowed to evolve for one second from initial conditions before measurements are taken. Doing so allows sufficient time for the system to reach the steady state.

### Added Complexity

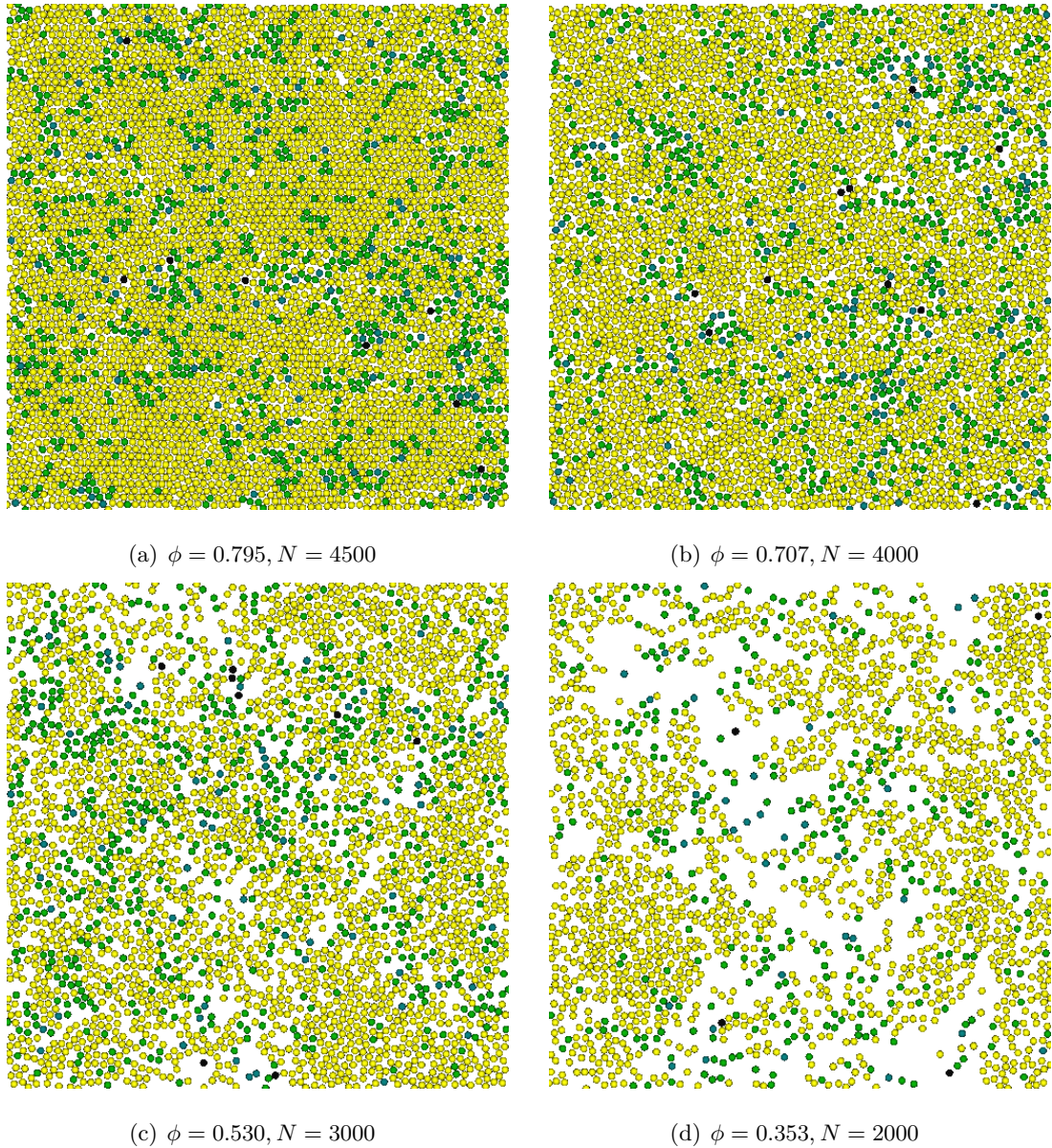
In the one-dimensional Random Force Model three simplifications were present: particles can not reorder; particles must collide with neighbouring particles; particles collide along the normal of collision maximising dissipation. However, in the two dimensional random force model none of the above applies. In addition, particles cannot be treated as point-like objects, because the chance in a two-dimensional system that two particles have a centre of mass velocity that is parallel to the vector of the displacement between the two is zero. Instead the collision needs to occur over the finite cross section of the particle. Thus a second length scale, the particle's diameter is introduced to the system, independent to the system size.

For particles of radius  $r$ , the particle occupation of the system is given by the packing fraction, defined as:

$$\phi = \frac{N\pi r^2}{L^2} \quad (2.24)$$

A high packing fraction corresponds to a dense system where collisions are frequent and a low packing fraction represents a dilute system where collisions are rare. The maximum packing fraction occurs when all particles pack to minimise the volume of the bed and the resulting lattices spans the complete area of the system. Geometrically particles occupy the minimum amount of space when they are all hexagonally packed with a packing fraction of  $\phi_{max} = \frac{\pi}{2\sqrt{3}} \simeq 0.907$ . As the packing fraction of the system is reduced from 0.907 the particles become less jammed with fewer locked into regular-crystals. Overall the system remains crystalline until the packing fraction is sufficiently reduced that there is ample unoccupied space and particles can avoid being in contact. At this point the system undergoes a phase transition from crystalline to granular liquid. The packing fraction at which this occurs is known as the point of crystallisation which is stated to occur for  $\phi_c \simeq 0.719$  in the paper of Reis, Ingale, and Shattuck (2006). Decreasing the packing fraction beneath  $\phi_c$  leads to increasingly dilute systems where interaction between particles becomes less dominant and the particle's motion is less dependent on the behaviour of surrounding particles. In all cases the system cannot be treated as uniform.

Fig. 2.9: Snapshots of particle positions at a moment in time for a system in steady state.



### Phase States

What are the physical changes that occur with decreasing packing fraction? Figure 2.9 shows a snap-shot of particle configuration for a simulation of the two-dimensional Random Force Model where the system size is  $L = 0.2m$ . The coefficients of restitution are kept fixed at  $\varepsilon_n = \varepsilon_t = 0.2$ . The particles in the figures are highlighted in three shades of colour corresponding to the speed of the particle relative to the root mean square velocity. The fastest particles are black-shaded whereas the majority slow moving particles are lightly-shaded.

The maximum number of particles that can be placed in the system without overlap is 5132 whereas the point of regular crystallisation occurs at 4068 particles. Figure 2.9

demonstrates the changes in state of the system as the number of particles are varied. Figure (a) shows a system, with packing fraction above  $\phi_c$ , where the population of particles are crystallised. The extremely fast particles (compared to the bulk) are constrained to small imperfections in the crystal. When the packing fraction is just less than  $\phi_c$ , see figure (b), some particles are detached from the rest, but the majority remain in contact. As the packing factor further decreases, figures (c) and (d), more of the particles becomes separate, with large distance (compared to diameter) between them and clustered particles. These systems become increasingly dominated, as the population of particles declines, by particle-particle interactions rather than particle-cluster interaction. Eventually the packing fraction drops sufficiently that the system is so dilute that particle interaction is rare and no durable clusters are seen.

### 2.3.3 Steady States

We demonstrate that away from the dense limit the simulation of the two-dimensional Random Force Model settles, after a short time, into a steady state where the granular temperature, as defined in equation 2.20, becomes constant. We simulate a system with packing fraction of 0.353 such that the system size is  $L = 0.2\text{m}$  and there are 2000 particles. A moderate dissipation is used with coefficients of restitution equalling  $\varepsilon_n = \varepsilon_t = 0.6$ .

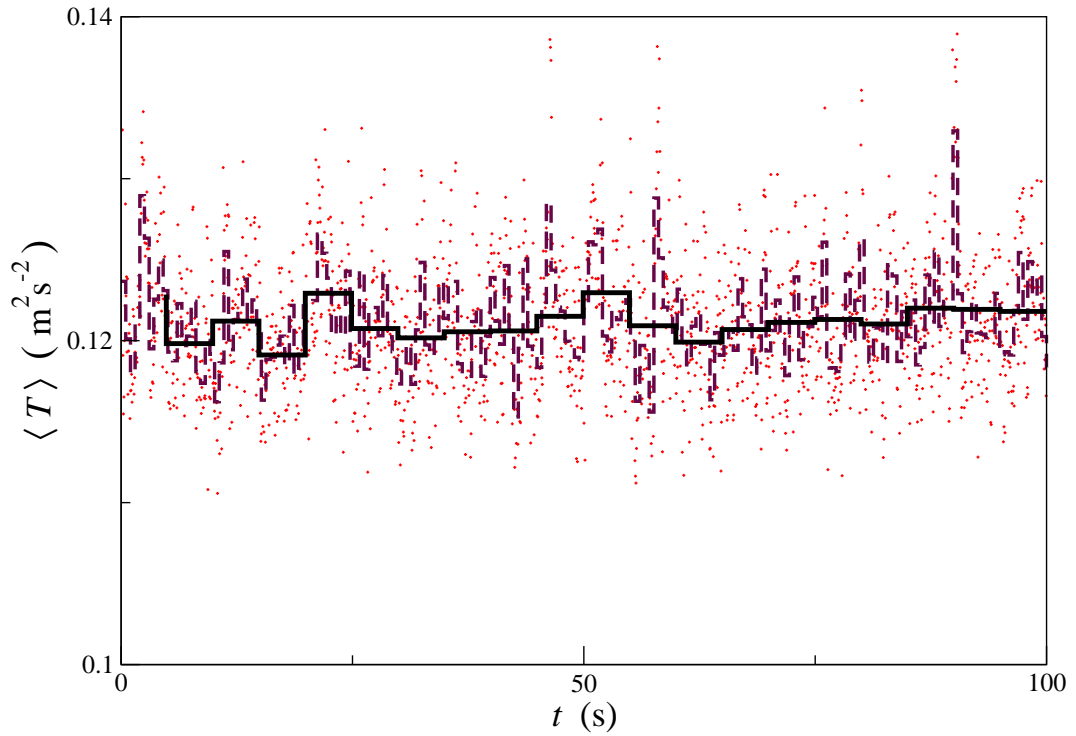
Figure 2.10(a) plots mean averages of the granular temperature for the first 100 seconds. The system reaches a steady state within the first second of the simulation. The measured value of granular temperature at any moment of time can fluctuate in a range comparable to its mean temperature. As the mean granular temperature is calculated for longer times the fluctuation in value becomes smaller.

Figure 2.10(b) plots the mean granular temperature of the system where the particles are initially arranged either in hexagonal packing; square packing; or uniformly spread. In each case the granular temperature in the steady state is approximately equal to  $12\text{m}^2\text{s}^{-2}$  and demonstrates that the initial conditions of the system do not affect the two-dimensional Random Force Model.

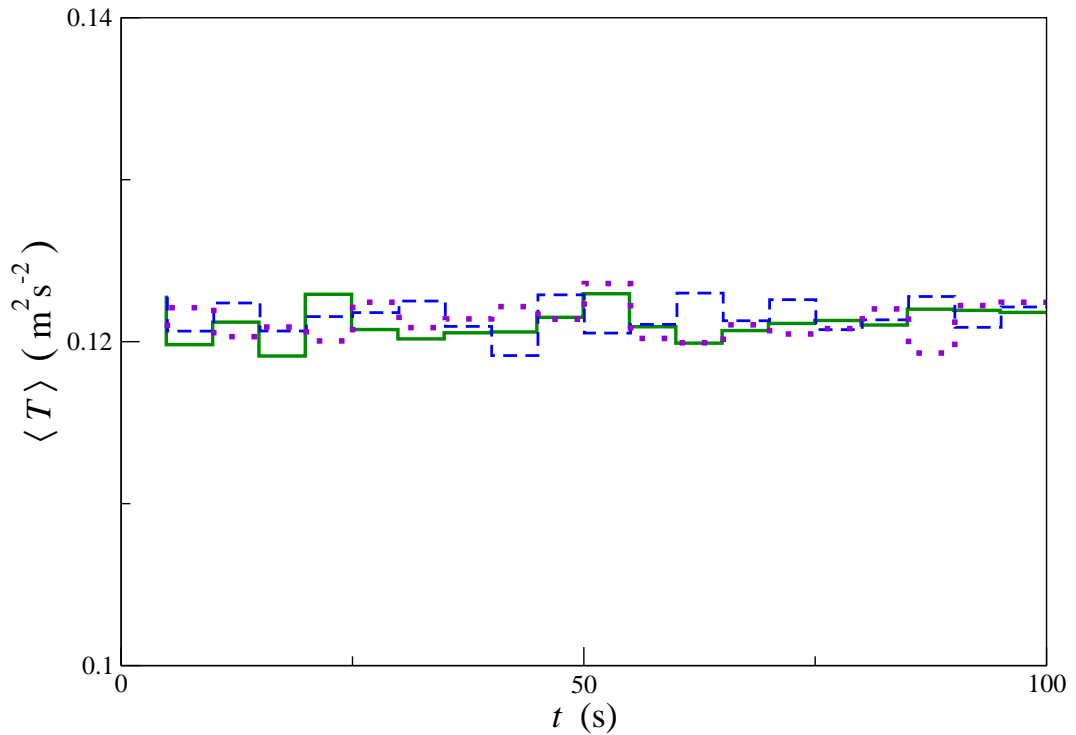
## 2.4 Summary

In chapter two we explained how to simulate granular media in computers using the technique of Molecular Dynamics. A system of grains are modelled as particles that evolve independently in space until collision. During collision normal and tangential

Fig. 2.10: A temperature verses time plot of a typical system moving to steady state.



(a) The system has an initial state of hexagonal packing. The data shows averages over 0.05 seconds (points); 0.5 seconds (dashed line) and 5 seconds (solid line).



(b) The system has an initial state of either hexagonal packing (solid line), square packing (dashed line) or uniform spreads (dotted line). The data sets are averages over 5 seconds.

forces are calculated and used to modify the trajectory of the particle. These adjustments of particle momentum represent the particle responding to a collision over a finite time and preserve the two axioms of granular collision: momentum conservation and energy dissipation. Energy dissipation is characterised by a coefficient of restitution which takes values between zero and one. We demonstrate that Molecular Dynamic simulations correctly model collisions by showing that the energy lost during a single collision is equal to that expected from theory.

Finally we simulate the one- and two-dimensional Random Force Model. These Models settle into a steady state where the granular temperature becomes constant. Clustering of particles causes strong fluctuations to be present in the granular temperature.

In the next chapter we study the one-dimensional Random Force Model. We are interested in characterising the effects that spatial clustering has on properties of these models. Particularly we show that these systems have multi-scaling velocity and structural features that are caused by clustering.

## Chapter 3

# Multi-Scaling Properties of a One-dimensional Random Force Model

In 1996 Williams and MacKintosh proposed, through mean field arguments, that the average kinetic energy,  $K$ , of a point-like particle within a one-dimensional Random Force Model, of length  $L'$ , was related to the total number of particles,  $N$ , by:

$$K^{\frac{3}{2}} = C\Omega(L'/N)/(1 - \varepsilon^2), \quad (3.1)$$

where  $C$  was a numerical constant,  $\Omega N$  was the rate of energy input,  $\varepsilon$  was the coefficient of restitution and  $L'/N$  was the average linear density of particles. Ever since then it was thought that this relation was valid. However, upon testing we found from our simulations of the one-dimensional Random Force Model that the measured kinetic energy per particle deviates notably away from this relation, with the deviation becoming stronger as the coefficient of restitution is reduced.

This new observation provided the motivation for this chapter. We begin by studying the second moment of the velocity distribution,  $\langle v^2 \rangle$ , which is directly related to  $K$ . The second moment of velocity has scaling that is dependent on the coupling between coefficient of restitution and particle number which has not been commented on before. It is then contemplated that if the second moment of velocity shows anomalous scaling then it is very likely that higher order moments of the velocity distribution will do as well. We observe that each higher order moment of velocity has a different scaling behaviour. This is a significant new observation because it implies that no single velocity-scale can characterise all the moments of velocity. Instead there is a multi-

scaling behaviour of the velocity distribution not described by any previous granular kinetic theory.

This naturally leads us to ask: what is driving this multi-scaling behaviour? We begin by examining which assumptions used in the arguments of Williams and MacKintosh (1996) might break-down in these systems. One prominent assumption is that the one-dimensional Random Force Model can be described as structurally homogeneous. We show this to be invalid by illustrating that the moments of the distributions of nearest neighbours exhibit strong multi-scaling behaviour with respect to  $N$  for a range of coefficients of restitution. We shall have to understand what process might cause the system to exhibit these behaviours. Through considering higher neighbour separation distances we show that the highly dissipative one-dimensional Random Force Model is approximately renormalisable and motivates us to use a mathematical multiplicative bisection process to perform the reverse process of renormalisation. The multiplicative bisection process captures similar hierarchical structure seen in the Random Force Model and so merits further study.

### 3.1 The Second Moment of Velocity

This section is all about whether the arguments of Williams and MacKintosh (1996) can really be applied to the one-dimensional Random Force Model. Since the work of Williams and MacKintosh, the performance of computers has greatly improved and we are now able to obtain better statistics, for a larger range of systems, than was previously described. In this section we discuss the the derivation of Williams and MacKintosh (1996) arguments for the second moment of velocity. We provide details of the simulations performed and then examine the results obtained for the second moment of velocity for a variety of coefficients of restitution. Importantly, we show that the exact dependence on the number of particles of the second moment of velocity is controlled by the extent of the dissipation, something that has not previously been suggested.

The second moment of velocity, denoted by  $\langle v^2 \rangle$ , in the centre of mass frame of the system is related to the velocity probability distribution,  $P(v)$ , by the relation:

$$\langle v^2 \rangle = \int_{-\infty}^{\infty} v^2 P(v) dv. \quad (3.2)$$

It is closely related to the granular temperature of the system,  $T$ , and the kinetic energy,  $K$ , through the relation  $K = M \langle v^2 \rangle / 2$ . During simulation the second moment

is calculated by the expression:

$$\langle v^2 \rangle = \frac{1}{NN_t} \sum_{\tau=1}^{N_t} \sum_{i=1}^N |v_i(t_\tau)|^2, \quad (3.3)$$

where  $N_t$  is the number of samples taken.

### 3.1.1 Deriving a Scaling Relation

The moments of velocity are affected by several properties of the one dimensional Random Force Model, which can be classified into three categories: noise strength; unoccupied space; extent of dissipation. Let us now briefly describe each in turn.

The strength of the random force sets the energy-scale of the system. Changing the value of the noise strength,  $D$ , or the particle mass,  $M$ , will effectively rescale time for all the particles contained within the system. Systems that keep  $2D/M^2$  fixed (with all other parameters fixed) maintain identical dynamics where the average rate of increase in momentum of a particle remains unchanged.

In one dimension a particle's physical size is irrelevant to the dynamics of the system as particles cannot go through one another, nor can they reorder. Thus all particles can be treated as point-like. Only the unoccupied *free volume* of the system is available for particles to move through. The total unoccupied length of the system is simply given by

$$L' = L - Nd. \quad (3.4)$$

Hence systems which keep  $L'$  fixed, regardless of particle radius, (whilst keeping all other parameters, such as  $N$  and  $\varepsilon$  fixed) will have identical dynamical behaviour. Consequently  $L'$  is the only natural length-scale associated with a one-dimensional system. We are now in a position to derive velocity-scale,  $v_0$ , for the second moment of velocity based on dimensional analysis and obtain that:

$$v_0^3 \sim \frac{DL'}{M^2}. \quad (3.5)$$

The remaining quantities of the system, that of coefficient of restitution and particle number, are dimensionless and cannot be pinned down using dimensional analysis. We must therefore rely on physical theory to derive how these affect  $\langle v^2 \rangle$ . One method is to use mean field theory as was used by Williams and MacKintosh (1996) and their arguments are as follows.

When a system of the one-dimensional Random Force Model is in a steady state the rate of energy injection equals the rate of energy loss through dissipation during

collision. The rate of energy injection,  $\Delta E_{in}$ , is determined by the random force and is proportional to the number of particles such that  $\Delta E_{in} = ND/M$ . The rate of energy loss through dissipation,  $\Delta E_{out}$ , is equal to the average loss of energy during a collision, given in equation 2.13 last chapter, multiplied by the rate of having a collision,  $\tau$ . The collision rate  $\tau$  is determined by the total number of possible particle pairs that can collide, which is  $N/2$ , divided by the time taken for a collision to occur,  $t_c$ . It is at this point that mean field theory is applied in order to determine  $t_c$ . It is argued that the distance a particle moves between collision is equal to the average distance a particle is separated from a neighbour, which is  $L'/N$ . Therefore, given that the mean speed of the particle between collision is  $\langle |v| \rangle$  then  $t_c$  is given by the distance between collision divided by  $\langle |v| \rangle$  and the collision rate  $\tau$  is derived as  $\tau = (N/2) \times \langle |v| \rangle \times (N/L')$ . Thus the rate of energy loss is the average energy lost per collision, which is  $(1 - \varepsilon^2) \times M \langle v^2 \rangle / 2$ , multiplied by the collision rate, which gives:

$$\Delta E_{out} = \left(\frac{N}{2}\right) \times \left(\frac{N}{L'} \langle |v| \rangle\right) \times \left(\frac{1}{2} M \langle v^2 \rangle (1 - \varepsilon^2)\right). \quad (3.6)$$

The equation of state can then be written as:

$$\langle v^2 \rangle^{\frac{3}{2}} = \frac{4C}{N} \frac{DL'}{M^2(1 - \varepsilon^2)}, \quad (3.7)$$

where we have applied a simple assumption: that the mean speed of a particle is proportional to the root mean square velocity,  $\langle v^2 \rangle^{\frac{1}{2}}$ , such that  $C$  is a numerical compensation constant.

Thus we have arrived at scaling relation of Williams and MacKintosh for the second moment of velocity. In the next section we proceed to test this relation by fitting the the second moment of velocity to a power-law in  $N$  of the form:

$$\langle v^2 \rangle = \left(\frac{DL'}{M^2}\right)^{\frac{2}{3}} \times \lambda(\varepsilon) N^{-\xi_2(\varepsilon)}, \quad (3.8)$$

where  $\lambda(\varepsilon)$  and  $\xi_2(\varepsilon)$  are dimensionless numbers dependent only on the coefficient of restitution. If the arguments of Williams and MacKintosh are correct then  $\xi_2$  will equal  $2/3$ . The implication of such a result would be that the system can be increased by doubling particle number and system size without affecting the overall kinetic energy-per-particle.

### 3.1.2 The Simulations

The systems we have studied have a population of particles ranging from 100 to 10000 and coefficients of restitution which lie between 0.1 and 0.99. For all simulation we keep

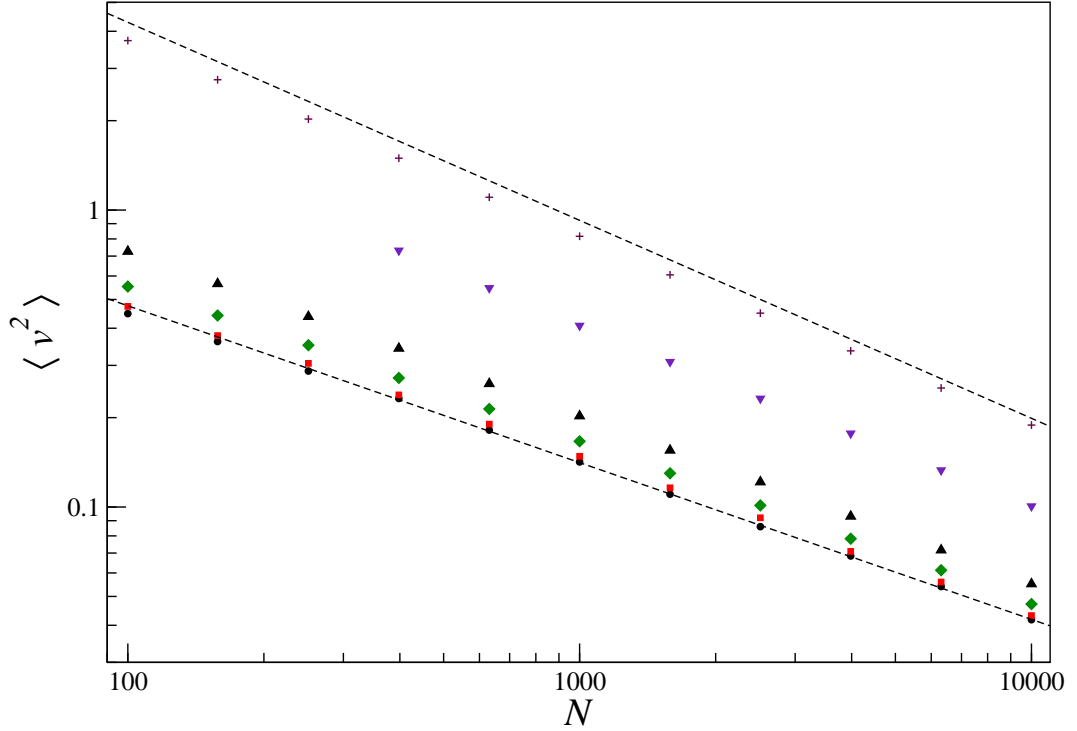


Fig. 3.1: The average value of the second moment of velocity with respect to the number of particles ( $N$ ) with a fixed size system of reduced system size of  $L' = 1$ . The data sets represent mean values and are for (bottom set upwards) coefficients of restitution of 0.1, 0.5, 0.75, 0.87, 0.97 and 0.99 respectively. The line fits are corresponding power laws defined by  $\langle v^2 \rangle \propto N^{-0.528}$  (lower line) and  $\langle v^2 \rangle \propto N^{-\frac{2}{3}}$  (upper line).

the reduced system length fixed at  $L' = 1$  and so remove the dependence on system size.

The population is chosen to be either 100; 158; 251; 398; 631; 1000; 1585; 2512; 3981; 6310; or 10000, such that the increase in population is logarithmic. The range of particles used is sufficient to demonstrate that the variations we find are not due to the finite size or number of particles of the system but are present as the system becomes large (both in system size and numbers of particles). The coefficient of restitution has values of: 0.10; 0.21; 0.37; 0.50; 0.60; 0.68; 0.75; 0.80; 0.84; 0.87; 0.90; 0.94; 0.97; or 0.99.

The simulations are performed by allowing 20 simulated seconds to elapse (for the system to relax from initial conditions) before calculating the second moment of velocity. We estimate the value of the second moment of velocity from 20 seconds of data and sample either a total of fifty times for systems where  $N < 1000$ , or ten times for the remaining larger systems. Only a single configuration is considered in this study but the sample size is considered to be sufficient that the error is small.

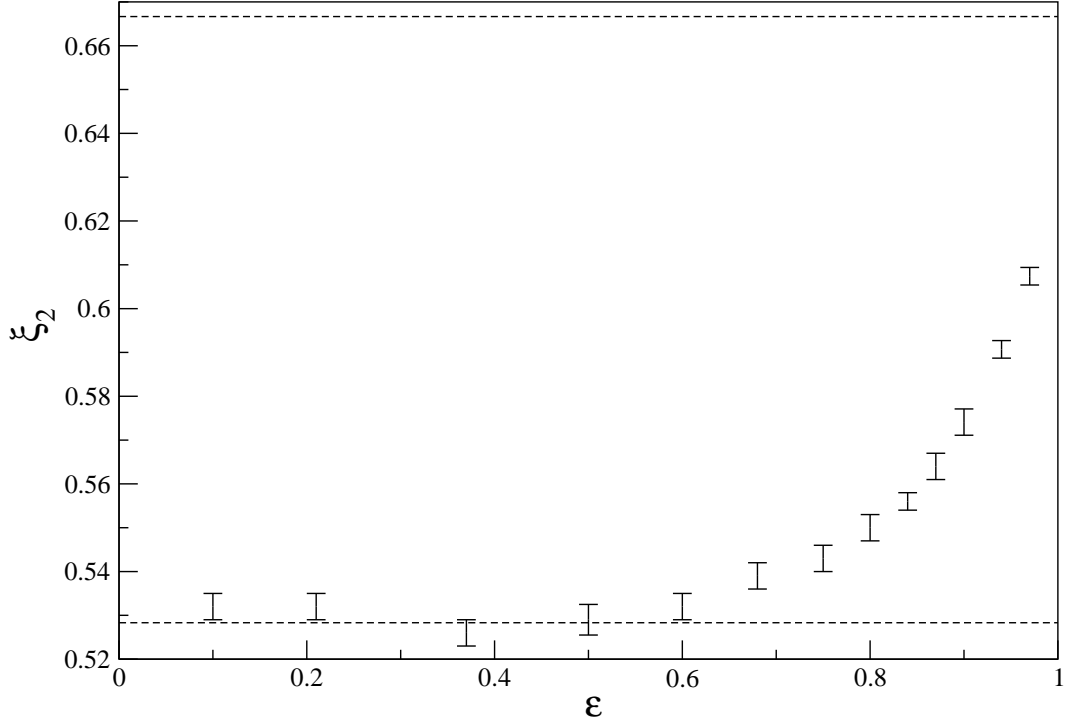


Fig. 3.2: The value of  $\xi_2$  for different coefficients of restitution. The dashed lines are constant fits of 0.528 and  $2/3$ .

### 3.1.3 Dependence on Population Size

The measurements of the second moment of velocity are analysed in the following way. First, we compare our measurements against that predicted from Williams and MacKintosh theory. Second, we demonstrate that the measurements of all systems can be collapsed onto a curve which depends only on the coefficient of restitution.

Figure 3.1 shows, for a selection of coefficients of restitution (that span over the entire spectrum of dissipations), the measured results for the second moment of velocity when compared against the number of particles. We attempt to fit power-law relations of the form given in equation 3.7 over the available data sets. By inspection we can observe that the near elastic data set, represented by a coefficient of restitution of 0.99, fits a power-law close to (but less than) the homogeneous prediction of  $\xi_2 = 2/3$ . As the extent of dissipation of the system increases, the exponent  $\xi_2$  rapidly decreases towards a value of  $\simeq 0.53$ . For any system, the value of the exponent  $\xi_2$  is found to lie within the range:

$$0.53 \lesssim \xi_2 < \frac{2}{3}. \quad (3.9)$$

The data sets of figure 3.1 are fitted to equation 3.7 via a  $\chi^2$  fitting program. Figure 3.2 shows the estimated value of  $\xi_2$  obtained from the power law fits as a

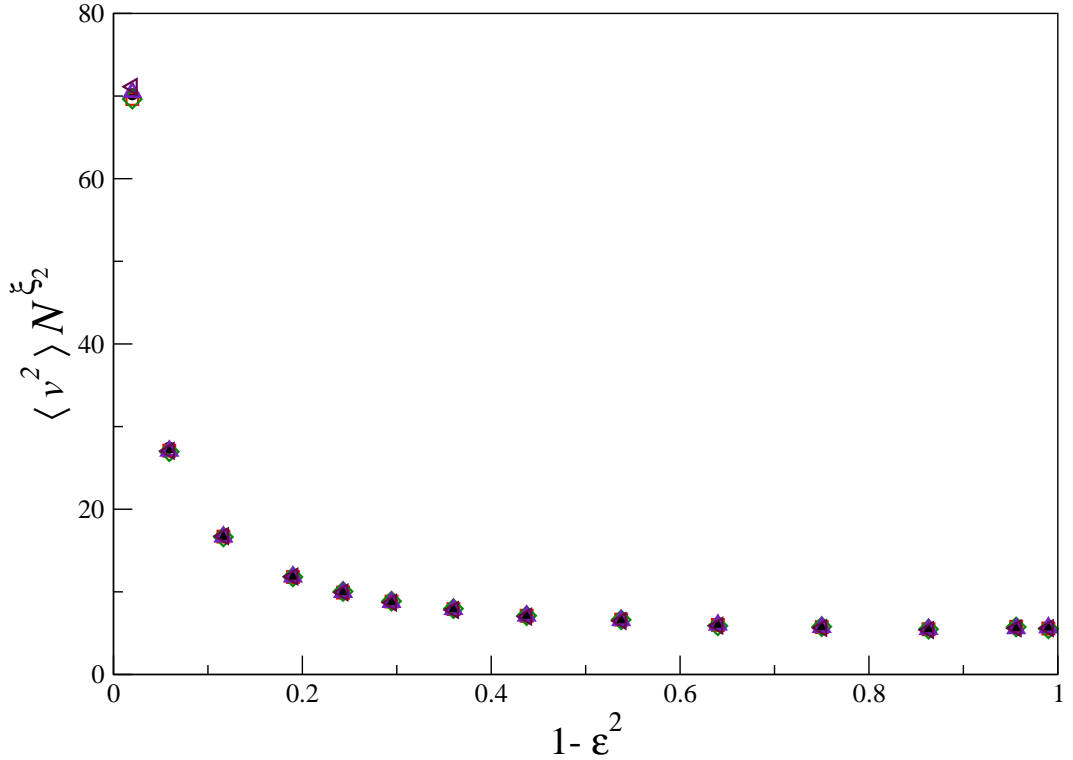


Fig. 3.3: A demonstration that the kinetic energy can be collapsed onto a universal curve (with respect to restitution) via a compensation for the number of particles in the system. Plots for five systems are shown, containing either 631 (circle); 1585 (square); 2512 (diamond); 6310 (up-triangle) or 10000 (left-triangle) particles.

function of coefficient of restitution. The decrease in value of exponent  $\xi_2$  with respect to dissipation is more clearly represented in figure 3.2 where closer examination shows that the dependence of the second moment of velocity is such that  $\xi_2$  is always distinctly less than  $\frac{2}{3}$ .

We have ignored data for systems containing 100, 158 or 251 particles (the three most dilute systems show significant difference in trend to the others). These dilute systems are affected by large fluctuations of long duration that arise due to the small number of particles and large average separation distance between neighbouring particles (with respect to particle size, typically of an order of diameter or more). Ignoring these three allows a good fit to equation 3.7 to be achieved over the remaining systems.

We make two observations from figure 3.2: first, that the relation  $\langle v^2 \rangle \sim N^{-\frac{2}{3}}$  does not hold in these models, when particles dissipate such that  $\epsilon < 1$ ; second, there exists a range of dissipations, in the range  $0 \leq \epsilon \lesssim 0.5$ , where  $\xi_2$  can be considered to be approximately constant at a value of  $\simeq 0.53$ .

The first observation is strong evidence that these systems are inhomogeneous. As a consequence the system behaviour does not remain unchanged as  $L'$  is increased

whilst  $L'/N$  remains fixed. In contrast the latter observation suggests that there is an extensive range of coefficients of restitution where collisions are near-inelastic and further dissipation has little effect on the dynamics. A similar observation was made for a granular cooling gas (Ben-Naim, Chen, Doolen, and Redner 1999), where once a cluster of particles reached a certain size a particle subsequently colliding behaved as if the coefficient of restitution was effectively zero.

Finally, we demonstrate in figure 3.3 that the values of  $\xi_2$ , given in figure 3.2, can be used to collapse the second moments as a function of  $1 - \varepsilon^2$ , onto a single curve for all systems.

### 3.2 Higher order Moments of Velocity

We have so far discovered that the second moment of velocity does not scale with linear density  $L'/N$ . Consequently this means that Williams and MacKintosh were wrong to use mean field theory to suggest that  $L'/N$  was the average distance travelled by a particle between collision. We are now interested in testing another assumption made by Williams and MacKintosh: that the mean velocity scaled equivalently to the root mean square velocity. We generalise this to mean that different order moments of velocity exhibit similar scaling behaviour and so we ask the question: does the system have simple scaling or multi-scaling?

The  $m^{\text{th}}$  order moment of velocity, denoted by  $\langle |v|^m \rangle$ , in the centre of mass frame of the system, characterises the velocity probability distribution,  $P(v)$ . The moments are defined by the following relation:

$$\langle |v|^m \rangle = \int_{-\infty}^{\infty} |v|^m P(v) dv. \quad (3.10)$$

The moments of velocity are calculated in simulation by the expression:

$$\langle |v|^m \rangle = \frac{1}{NN_t} \sum_{\tau=1}^{N_t} \sum_{i=1}^N |v_i(t_\tau)|^m, \quad (3.11)$$

where  $N_t$  is the number of samples taken. If the velocity distribution  $P(v)$  scales with the use of single velocity-scale then so do all the orders of the moment of velocity, such that:

$$\langle |v| \rangle \sim \langle |v|^2 \rangle^{\frac{1}{2}} \sim \dots \sim \langle |v|^m \rangle^{\frac{1}{m}} \text{ where } m = 1, 2, 3, \dots \quad (3.12)$$

Let us suppose that the  $m^{\text{th}}$  moment of velocity is related to the number of particles contained in a system by a simple power law:

$$\langle |v|^m \rangle \sim \left( \frac{DL'}{M^2} \right)^{\frac{m}{3}} N^{-\xi_m(\varepsilon)}, \quad (3.13)$$

where  $\xi_m$  is a dimensionless number associated with the moment that is dependent only on the coefficient of restitution and the moment's order,  $m$ .

We find that equation 3.12 is only satisfied when

$$\frac{\xi_m(\varepsilon)}{m} \equiv \kappa(\varepsilon) \quad \text{where } m = 1, 2, 3, \dots \quad (3.14)$$

Here  $\kappa(\varepsilon)$  is a constant with respect to  $m$ , dependent only on the value of the coefficient of restitution. Thus in this section we will calculate the values of  $\xi_m/m$  for the one-dimensional Random Force Model to test the validity of relation 3.14. If  $\xi_m/m$  is a constant with respect to  $m$  then simple scaling exist; if not then the system exhibits multi-scaling behaviour.

We discuss the details of the simulations performed and then examine the results obtained for the 9 lowest moments of velocity for two extreme cases before generalising to include a variety of coefficients of restitution.

## The Simulations

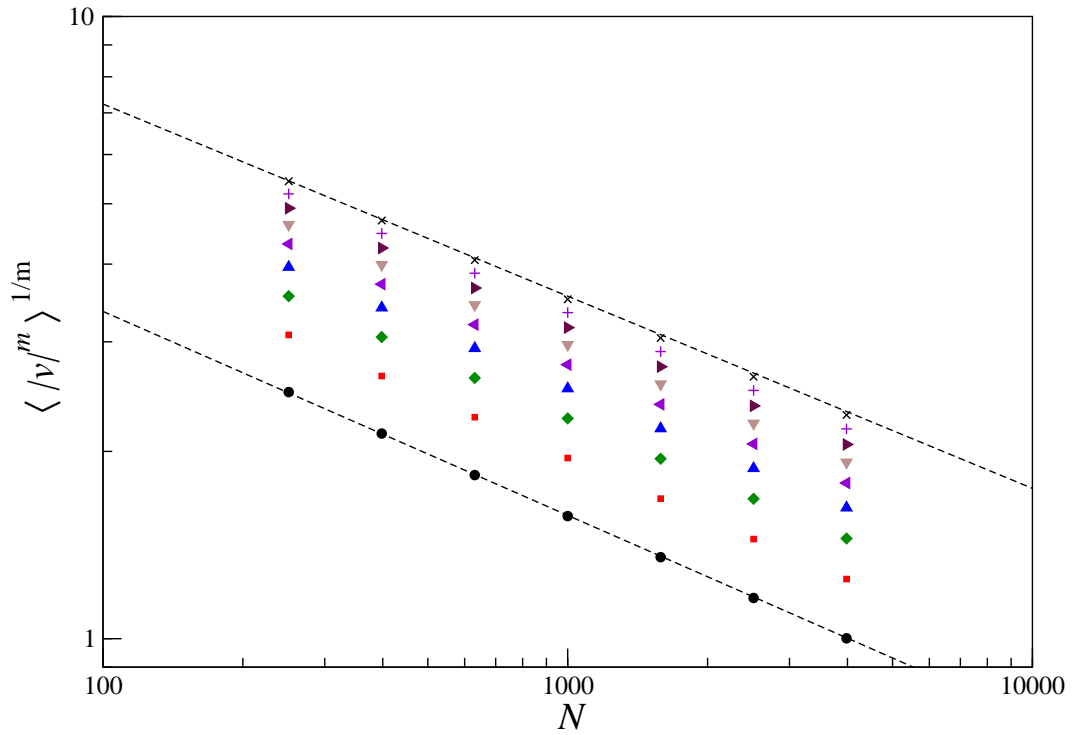
We run simulations for 7 different systems containing 251, 398, 1000, 1585, 2512 or 3981 particles and measure the lowest nine moments of velocity. Systems containing the two highest numbers of particles in the studied range (that of 6310 and 10000) are avoided because the real computing time required to achieve sufficient output becomes unacceptably large.

The simulation of each system is ran once from a single initial configuration. The first 20 seconds of simulation goes without sampling to allow the system to reach the steady state. The mean value of the  $m^{th}$  moment of velocity is calculated 50 times from 20 seconds of simulation data by the method described in equation 3.11. The total time the system evolves (from initial conditions to end) is thus equal to  $20 + 50 \times 20 = 1020$  seconds. These simulations are repeated for six coefficients of restitution representing a cross-section of dissipations, namely  $\varepsilon = 0.001, 0.37, 0.68, 0.84, 0.94$  and  $0.999$ .

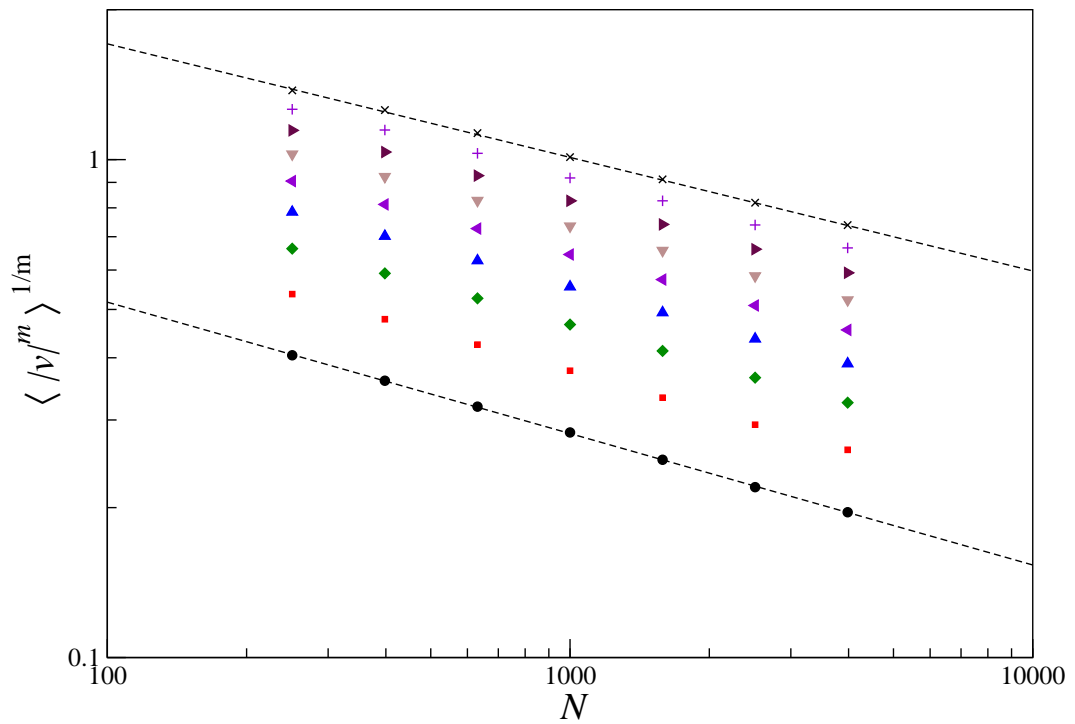
### 3.2.1 A Study of Two Extreme Cases

We first consider the two extreme cases: the near-elastic or the near-inelastic system. The systems with  $\varepsilon = 0.999$  are examples of a near-elastic system. Figure 3.4(a) shows the value of the different moments of velocity. For each order of the moment of velocity the obtained value of  $\xi_m/m$  is found to be nearly one-third. As the order of the moment is increased each measured value of  $\xi_m/m$  is slightly different from the previous

Fig. 3.4: The behaviour of higher moments for a fixed coefficient of restitution as a function of number of particles. The sets of data represent progressively larger order of velocity moments as we move vertically up the graph from the 1<sup>st</sup>( $\circ$ ) through to the 9<sup>th</sup>( $\times$ ) moment of velocity.



(a) For a high coefficient of restitution. The dashed lines are power-law fits of  $\propto N^{-0.328}$  (lower line) and  $\propto N^{-0.309}$  (upper line).



(b) For a low coefficient of restitution. The dashed lines are power-law fits of  $\propto N^{-0.264}$  (lower line) and  $\propto N^{-0.228}$  (upper line).

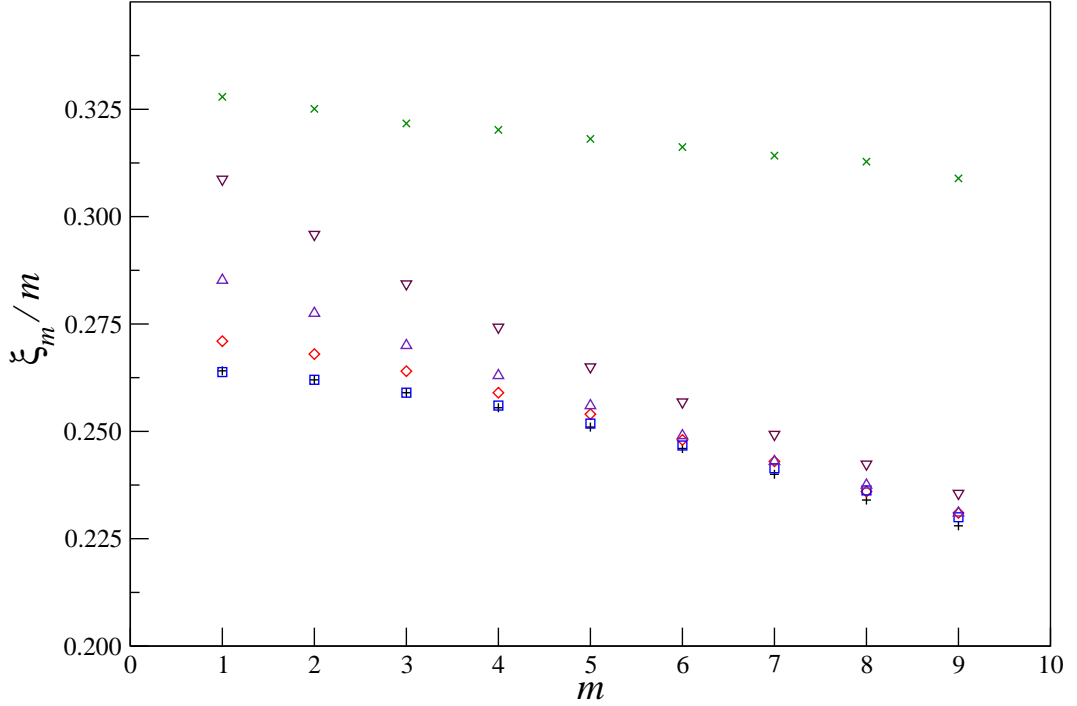


Fig. 3.5: The change in behaviour of  $\xi_m/m$  with higher moment for the coefficients of restitution: 0.001 (plus); 0.37 (square); 0.68 (diamond); 0.84 (up-arrow); 0.94 (down-arrow) and 0.999 (cross).

and decreases away from one third. Hence the moments of velocity do not exhibit a common scaling behaviour which suggests that the system violates the conditions for homogeneity. Instead the particles have a slight tendency to cluster (even at near elasticity) because of the loss of energy and slight correlation in velocity of pairs of particles after collision.

The near-inelastic limit describes systems that dissipate sufficiently such that the granular temperature is effectively independent of the coefficient of restitution. Systems that behave this way were found to have coefficients of restitution less than 0.5. The described results are for a selection of systems with a coefficient of restitution of 0.001. The values of the different moments of velocity are displayed in figure 3.4(b).

What is immediately obvious from the figure is that there is only a weak variation in behaviour of  $\langle |v|^m \rangle^{\frac{1}{m}}$  with respect to  $N$  as we move between the different orders of the moment of velocity. The exponent  $\xi_m$  decreases from  $\xi_m/m \simeq 0.26$  towards  $\simeq 0.225$ . It is clear that the velocity moments of highly dissipative systems are significantly different in behaviour from that predicted in previous works where  $\xi_m/m = 0.333$ .

### 3.2.2 General Dependence on Population Size

Can we strengthen these observations to extend to the whole range of possible dissipation? From the estimates of the  $m^{\text{th}}$  moment of velocity we determine more rigorously the values of the power exponent  $\xi_m$  using equation 3.13 and a chi-square fitting program. Figure 3.5 shows the values of the exponent  $\xi_m$  for the six coefficients of restitution and illustrates three important points. First, the measured values of  $\xi_m/m$  becomes closer to 0.333 as the system's coefficient of restitution increases. Second, the value of  $\xi_m/m$  becomes smaller with increasing  $m$  indicating that the velocity probability distribution does not have a single scaling behaviour (with respect to  $N$ ) that will allow the velocity axis to be rescaled such that the distribution collapses onto a single 'standard/ universal' curve, but rather exhibits multi-scaling which prevents data collapse. Third, for a variety of coefficients of restitution (see the data sets of  $\varepsilon = 0.001, 0.37, 0.68, 0.84$  in figure 3.5) as  $m$  becomes large  $\xi_m/m$  converges to the same value such that:

$$\xi_m/m \rightarrow k(m), \quad (3.15)$$

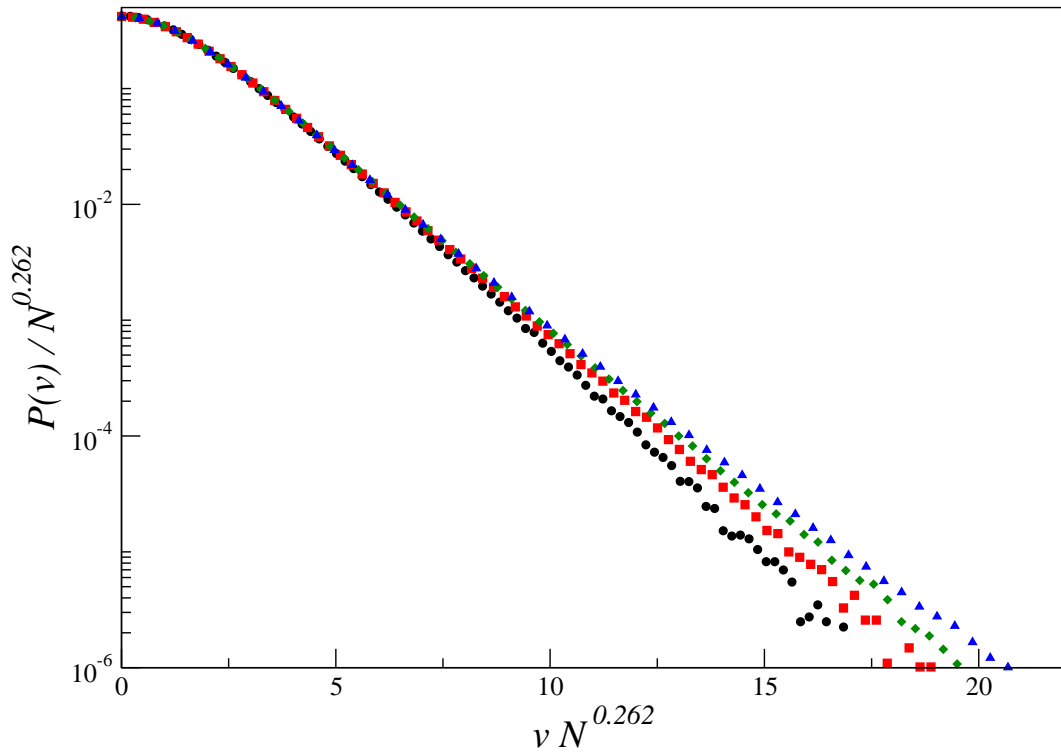
where  $k(m)$  is a set of values determined by  $m$  but independent of coefficient of restitution. For example, we previously found that the second moment of velocity had  $\xi_2/2 \simeq 0.264$  when the coefficient of restitution was less than 0.5. We find similar relations for higher order moments of velocity, for example, the fifth moment of velocity has  $\xi_5/5 \simeq 0.252$  when  $\varepsilon \lesssim 0.68$  and the sixth moment of velocity has  $\xi_6/6 \simeq 0.247$  when  $\varepsilon \lesssim 0.84$ . Moreover we can use figure 3.5 to project further and predict that by the twelfth moment of velocity the data set of  $\varepsilon = 0.94$  will have converged with that of  $\varepsilon = 0.01$ , implying that the  $\xi_{12}/12$  has a fixed value for coefficients of restitution less than 0.94. It can then be conjectured that as the order of the moment of velocity is increased then  $\xi_m/m$  takes a fixed value for coefficients of restitution near to one.

### 3.2.3 Can Multi-Scaling be Observed through the Velocity Distribution?

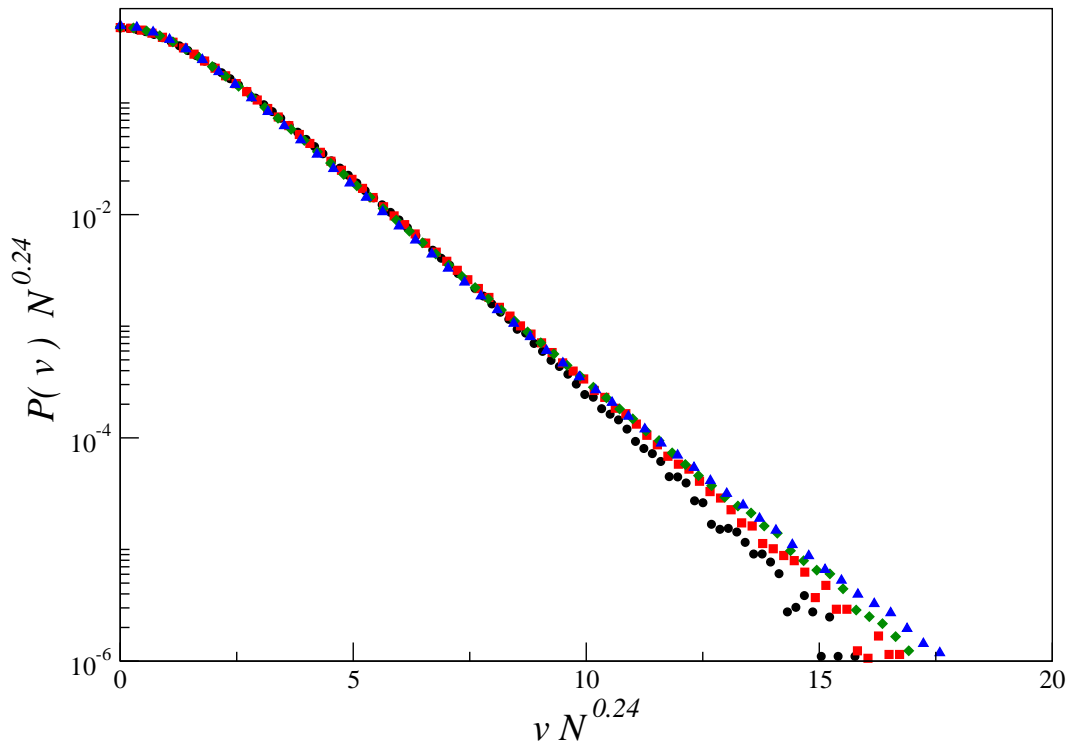
We attempt to collapse the velocity distribution, for fixed coefficient of restitution, by removing the dependence on particle number. We choose two extreme cases: the near-inelastic ( $\varepsilon = 0.1$ ) or the near-elastic ( $\varepsilon = 0.99$ ) system. All other dissipating systems are expected to have behaviour that falls in between these two cases.

Figures 3.6 and 3.7 show attempted collapses for the velocity distribution of systems containing between 100 and 1585 particle. These distributions are distinctly

Fig. 3.6: The scaled velocity statistics of a high dissipative systems with  $\varepsilon = 0.1$ . Data sets are for systems with particle populations of 100 (circle); 251(square); 631(diamond); 1585(up-triangle),



(a) The velocity axis is scaled using the second moment



(b) The velocity axis is scaled using the seventh moment

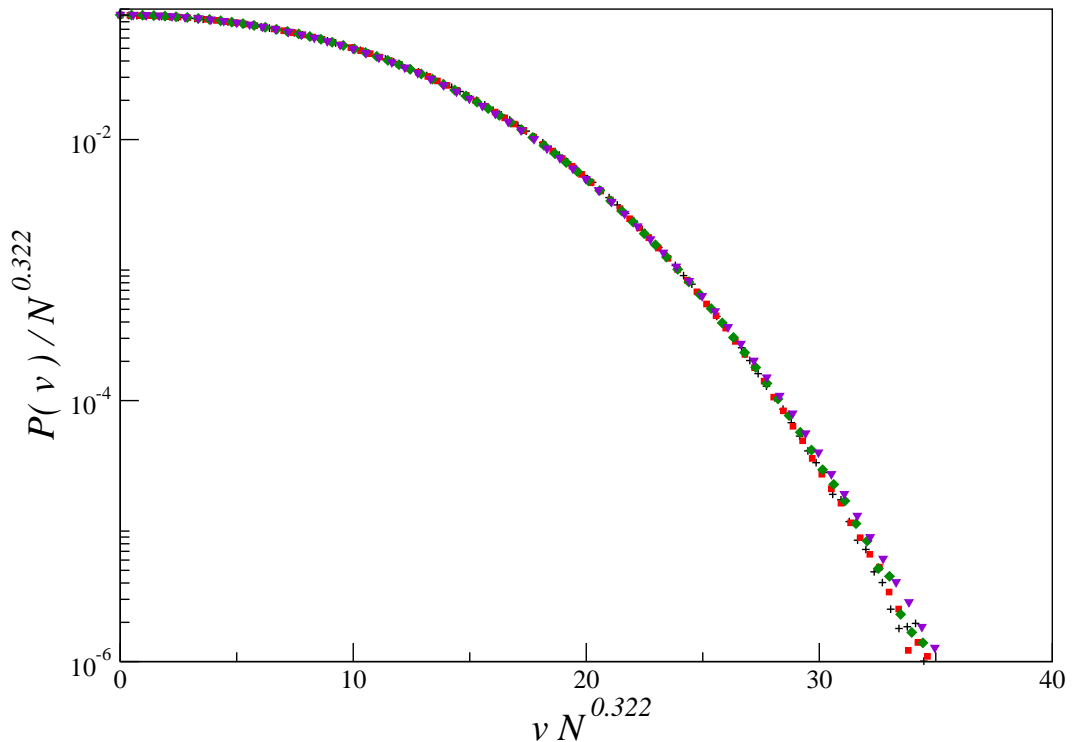


Fig. 3.7: The scaled velocity statistics of a high dissipative systems with  $\varepsilon = 0.99$ . Data sets are for systems with particle populations of 251 (cross); 398 (square); 631 (diamond); 1000 (down-triangle),

non-Gaussian. Figures 3.6(a) and (b) show that for the highest dissipations the velocity distributions cannot be collapsed by rescaling the velocity axis using a measured moment of velocity. For low dissipation, figure 3.7, the velocity distribution collapses much better with only slight divergence at large velocity.

These figures demonstrate that as the coefficient of restitution decreases the behaviour of different order moments becomes dissimilar, resulting in less of the velocity distribution collapsing onto a single curve when rescaling the velocity axis by  $v \mapsto v / \langle |v|^m \rangle^{1/m}$ .

### 3.3 The Structure of the System

The previous sections have demonstrated that the velocity distribution exhibits weak multi-scaling behaviour. The remainder of the chapter is concerned with discussing how multi-scaling arises.

We describe the structure of the systems by calculating the separation distance between neighbouring particles. We study the moments of separation distances and find that they obey similar power-law relations with respect to particle number as was found for the velocity statistics. Next we study the full distributions of separation

distance between nearest neighbour and describe the changes that occur with respect to particle number and coefficient of restitution.

The latter part of the section is concentrated on the little understood near-inelastic limit of the one dimensional Random Force Model. We show that these systems have structural features that are self-similar.

### A System of Point-like Particles

In one-dimensional geometry, particles can be treated as point-like. A system of  $N$  particles with diameter  $d$  contained in a length  $L$  are equivalent to  $N$  point-like particles contained in a reduced length  $L'$ . The space occupied by the particles has no effect on the dynamics of the system. Each particle's position has an equivalent *reduced position* in the point-like particle system. The positions of particles ( $r_i$ ) are mapped to the reduced particle positions ( $r'_i$ ) by a simple transformation. A single particle is used as a reference and indexed as particle 1. The remaining particles are indexed as 2 to  $N$  by consecutively labelling particles when travelling positively along the system in a loop from the position of particle 1 until return. The position of every particle can be translated by  $-r_1$  without effect, such that the position of particle 1 moves to the origin. These new positions are then mapped onto the reduced coordinate system by removing the space occupied by all particles that lie between the origin and the particle in question, so that:

$$r'_i = \begin{cases} r_i - r_1 - (i - 1)d & r_i - r_1 > 0, \\ r_i - r_1 + L - (i - 1)d & \text{otherwise.} \end{cases} \quad (3.16)$$

The transformation results in particle 1 remaining at the origin,  $r'_1 = 0$ , and the other particles are position between 0 and  $L'$  inclusively.

An important feature of the reduced coordinate system is that contacting particles occupy the same reduced position. Hence a chain of particles all in contact collapse onto a single point, in the reduced coordinates, whilst the cluster's length is contracted to zero.

#### 3.3.1 The Separation Distances between Neighbouring Particles

The separation distance between neighbouring particles,  $R_{i,i+1}$ , is defined as the effective difference in positions between particle  $i$  and  $i + 1$  at a given sample time  $t$ :

$$R_{i,i+1} = |r'_{i+1}(t) - r'_i(t)|, \quad (3.17)$$

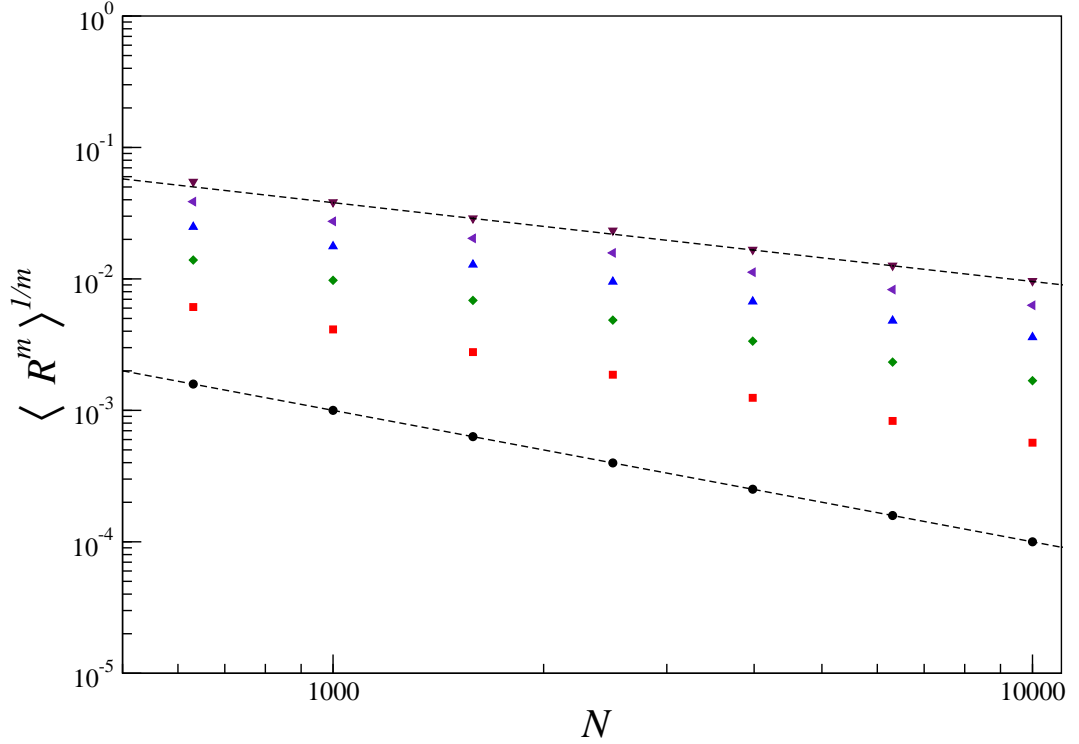


Fig. 3.8: The behaviour of higher moments of  $R$  for a coefficient of restitution of 0.1 as a function of number of particles. The sets of data represent progressively larger order of velocity moments as we move vertically up the graph from the 1<sup>st</sup> ( $\circ$ ) through to the 6<sup>th</sup> ( $\nabla$ ) moment of separation distance. The dashed lines represent power law fits of  $1/N$  (lower line) and  $2.4/N^{-0.6}$  (upper line).

the periodic nature of the system is accounted for through the relation  $r'_{j+N} = r'_j + L'$ .

The  $m^{\text{th}}$  moment of the separation distance between neighbouring particles,  $\langle R^m \rangle$ , is defined as the arithmetic average of the  $m^{\text{th}}$  power of the separation distance between consecutively neighbouring particles:

$$\langle R^m \rangle = \frac{1}{NN_t} \sum_{\tau=1}^{N_t} \sum_{i=1}^N (R_{i,i+1}(t_\tau))^m, \quad (3.18)$$

where  $N_t$  is the number of times sampled. It is calculated in simulations by the same method described for the moments of velocity. The zeroth and first moment are determined on physical grounds: the zeroth moment of  $R$  equals one and the first moment of  $R$  is determined to be:

$$\langle R \rangle = \frac{1}{N} \sum_{j=1}^N |r'_{j+1} - r'_j| = \frac{1}{N} ((r'_1 + L') - r'_1) = \frac{L'}{N}. \quad (3.19)$$

### The Number Dependence of the Moments

We repeat for these moments the type of measurements that were made for the  $m^{\text{th}}$  order moment of velocity using the same range of systems.

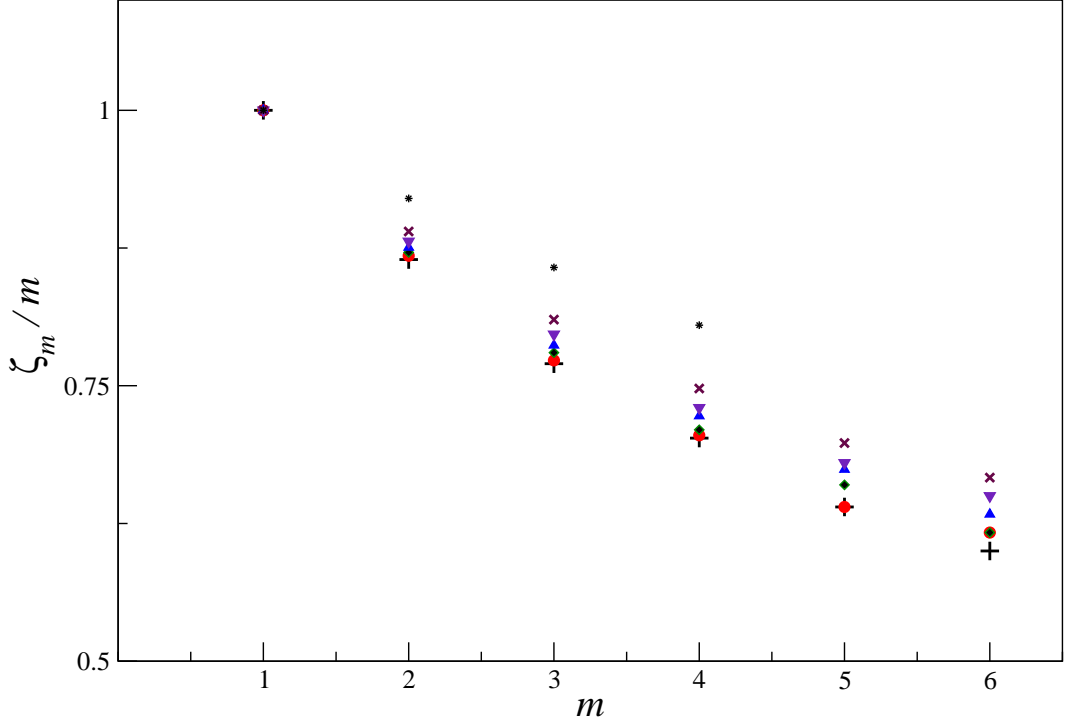


Fig. 3.9: The behaviour of higher moments of separation distance with respect to number of particles shown for coefficients of restitution of 0.1(plus), 0.37 (circle), 0.60 (up-triangle), 0.75 (down-triangle), 0.90 (cross) and 0.97 (star).

We hypothesise that the moment of separation distances is related to the number of particles by a power-law of the form:

$$\langle R^m \rangle \propto (L')^m N^{-\zeta_m}. \quad (3.20)$$

Here  $\zeta_m$  is an exponent that is dependent on the order of the moment and the extent of dissipation. If the structure of the system exhibits multi-scaling behaviour then  $\zeta_m/m$  is not a constant with respect to  $m$ .

We first explore the near-inelastic regime. Figure 3.8 shows the data obtained for the lowest 6 orders of the moment of separation, for a range of systems with fixed coefficient of restitution of 0.1. The data sets obey the power-law hypothesis shown in equation 3.20. The 1<sup>st</sup> moment of separation obeys the equation 3.19 with exponent  $\zeta_1$  constrained to be 1. As the order of the moment increases the exponent  $\zeta_m$  changes value such that  $\zeta_m/m$  decreases from 1 towards  $\simeq 0.6$ . This implies that near-inelastic systems have a structure that exhibit multi-scaling behaviour over the observable orders of moments.

The next question we ask is this: does the multi-scaling behaviour continue to be prominent as the dissipation of the system decreases? From the estimates of the  $m^{\text{th}}$

moment of separation we determine more rigorously the values of the power exponent  $\zeta_m$  using the equation 3.20 and a chi-square fitting program. Figure 3.9 shows the value of  $\zeta_m/m$  for the 6 lowest orders of moments of separation distance and six coefficients of restitution ranging between 0.10 and 0.97.

For each set of data, corresponding to a particular coefficient of restitution, a distinct drop in value for  $\zeta_m/m$  is observed as the value  $m$  increases. Significant decreases in the value of  $\zeta_m/m$  are still observed for a high coefficient of restitution, such as  $\varepsilon = 0.97$ . In contrast the related *velocity* multi-scaling was much weaker.

The absolute value of  $\langle R^m \rangle$ , where  $m > 1$ , drops several orders of magnitude with increasing coefficient of restitution corresponding to a reduced chance for a large separation distance occurring. This can be thought of as particles having a reduced tendency to cluster near one another and hence more particles occupy the voids between dense clumps. The measurements of moments of separations suggests that there exists strong multi-scaling in the structure of the system over a large range of dissipations from near elastic to highly inelastic systems. To understand further the significance of the moments of separation we next study the complete distribution of nearest neighbour separation distances.

### 3.3.2 The Nearest Neighbour Distribution

In a one-dimensional system, a particle can only collide with a particle that lies directly either side of it. These two bounding particles are defined to be the particles nearest neighbours, such that for the  $i^{th}$  particle the nearest neighbours are the particles indexed  $i - 1$  or  $i + 1$ . The distribution of the nearest neighbour describes the time-average probability that a consecutive neighbouring particle will be a distance  $R$  from the current particle's position:

$$G_1(R; N) = \frac{1}{N} \left\langle \sum_{i=1}^N \delta(R - R_{i,i+1}) \right\rangle. \quad (3.21)$$

The distribution is defined between  $R = 0$  and  $R = L'$  and is measured in simulation uniformly in time via the same method described for the velocity statistics in Appendix A.

The distribution of nearest neighbours provides a good method to study the structure of the system. Three features provide information about the systems structure. The distribution must cut-off at  $R = L'$ , no particle can be separated from another by more than the system size. If a distribution has a singularity at the zero separation

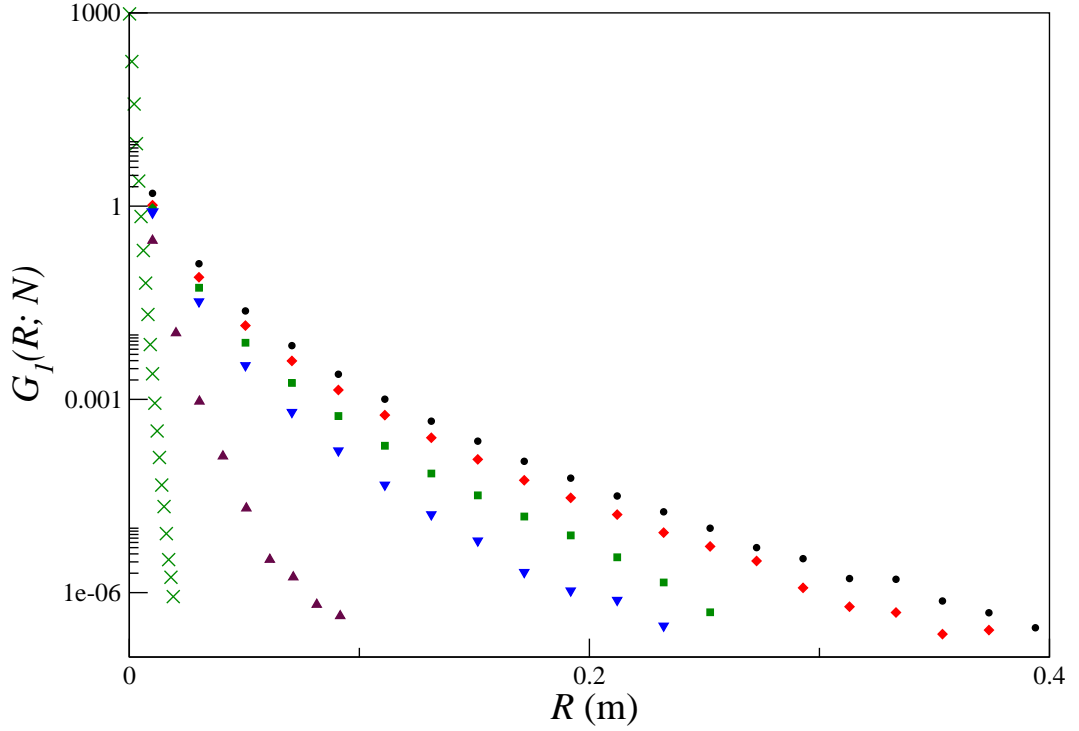


Fig. 3.10: The nearest neighbour distribution for various systems containing 1585 particles and fixed reduced system length of  $L' = 1$ . The distributions are for systems of different coefficients of restitution: 0.1(circle); 0.37(diamond); 0.68(square); 0.8(triangle down); 0.94(triangle up); and 0.99(cross).

distance then particles are clustering. There is no single length-scale to the distribution if the moment of separations exhibits multi-scaling.

We now describe characteristics of the nearest neighbour distributions as either the extent of dissipation or population of particles is changed.

### General Characteristics with Respect to Restitution of the System

First we consider the effect of the extent of dissipation on the structure of the system. Figure 3.10 shows the distribution of nearest neighbour distances for systems containing 1585 particles for a variety of coefficients of restitution.

For systems of near-elastic particles, shown by the data set of  $\varepsilon = 0.99$ , the nearest neighbour distribution exhibits a decay with respect to distance that is approximately exponential. The observation is consistent with the idea that the system of particles can be considered to be homogeneous as is the case for a gas of non-dissipating particles.

As the coefficient of restitution is decreased the distribution of nearest neighbours quickly moves away from exponential, developing an effective singularity at zero separation whilst particles achieving a large separation become increasingly likely.

Once the system's dissipation is sufficiently large, notable variation in the large

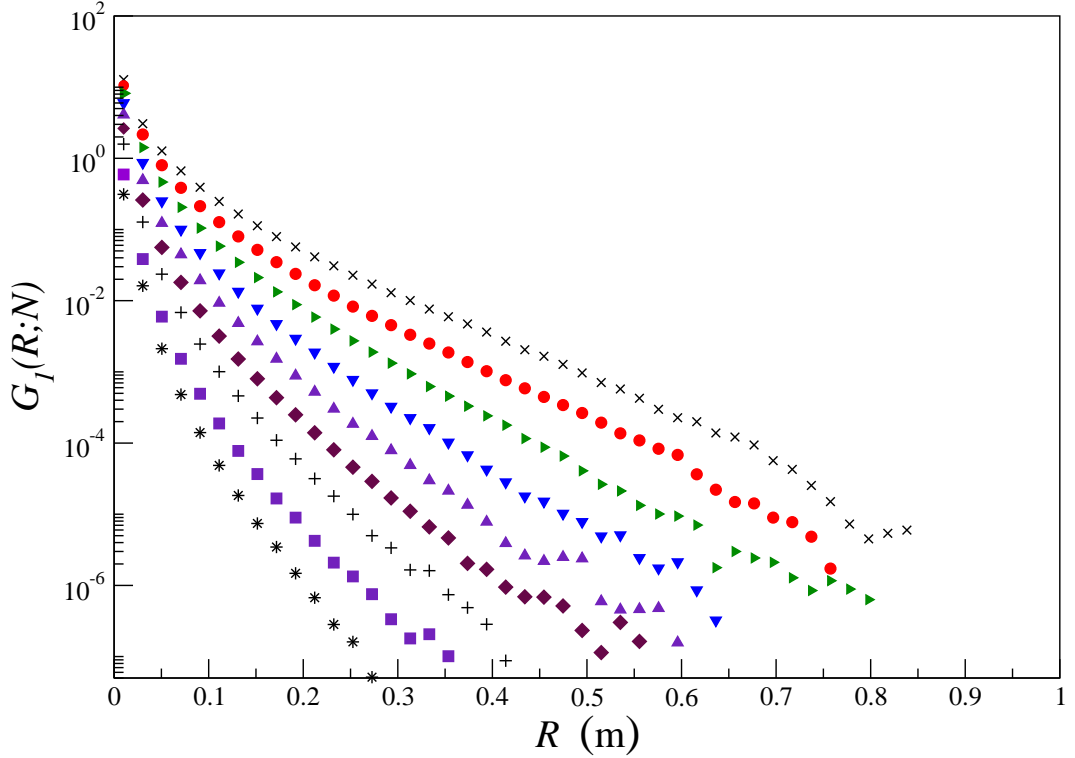


Fig. 3.11: The nearest neighbour distribution for various systems with low dissipation of  $\varepsilon = 0.1$  and fixed reduced system length of  $L' = 1$ . The distributions are for systems containing the following number of particles: 100(cross) 158(circle); 251(right triangle); 398(triangle down); 631(triangle up); 1000 (diamond); 1585(plus); 2512(square) and 3981(star).

scale shape of the distribution, with respect to coefficient of restitution, ceases and the distribution of nearest neighbours becomes effectively independent of coefficient of restitution. This happens for  $\varepsilon < 0.5$ . Only the small scale behaviour of the distribution, where  $R \simeq d$ , remains strongly influenced by the dissipation which results from particles multiply colliding over a finite time during collision.

### General Characteristics with respect to Number of Particles

We now study the effect of varying the number of particles contained in a system with near-inelastic dissipation, although observations are valid for other dissipations. Figure 3.11 shows the distribution of nearest neighbours for systems with a coefficient of restitution of 0.1.

As the number of particles in the system drops it becomes more likely for large separations to occur. This is in line with the increase in value of the average distance between particles, given by the first moment of separation, as the number of particles decreases. The distributions cannot be collapsed onto a single curve by any rescaling of

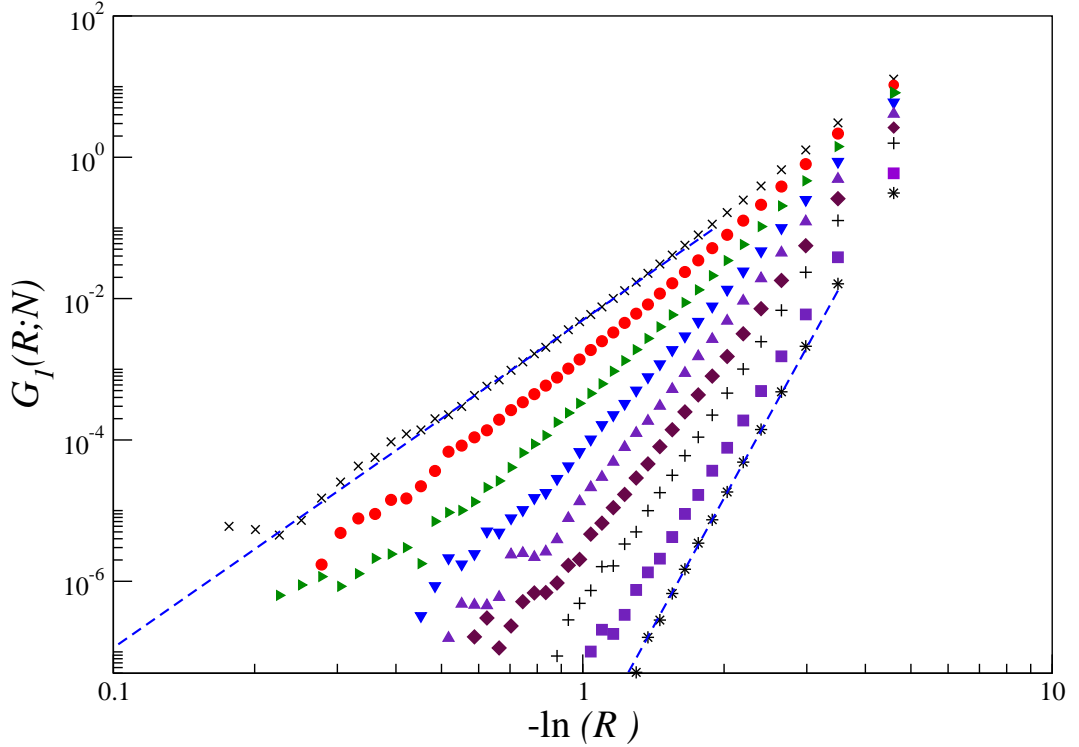


Fig. 3.12: The nearest neighbour distribution for various systems with low dissipation of  $\varepsilon = 0.1$  and fixed reduced system length of  $L' = 1$  plotted as a function of  $-\ln R$ . The distributions are for systems containing the following number of particles: 100(cross) 158(circle); 251(right triangle); 398(triangle down); 631(triangle up); 1000 (diamond); 1585(plus); 2512(square) and 3981(star). The dashed lines demonstrate fits of the form  $(-\ln(R))^{n_N - 1}$  where  $n_N$  is a number dependent on  $N$ .

the axis  $R$ . For a small number of particles such as for  $N = 100$ ,  $N = 158$  or  $N = 251$ , a point of inflection can be seen in the data. The inflection is present in all distributions and represents the distance after which the nearest neighbour distribution must decay, increasing more rapidly, until  $R = 1$  and the probability is zero.

### Logarithmic Behaviour in Highly Dissipative Systems

For the remainder of the chapter we are concerned with describing the behaviour of near-inelastic systems. Specifically we study systems where the coefficient of restitution equals 0.1. We ask the question: are the distributions of nearest neighbours of highly dissipative systems described by a simple function?

The distributions of highly inelastic systems have two important properties: first, they have no length scale that characterises the complete distribution; second, the probability density of a particle being separated by a distance  $R$  from a neighbour drops to 0 at the distance of the system size  $L'$  and gets very large at  $R = 0$ . The

simplest mathematical function that has both these properties is  $-\ln(R)$  and hence we ask the question: Can these distributions be related to  $-\ln(R)$  in any way?

Figure 3.12 plots the distributions of nearest neighbours, shown in figure 3.11, as a function of  $-\ln(R)$  on a log-log graph. If the distributions appear straight then they can be considered to satisfy a function of the form:

$$G_1(R; N) \propto (-\ln(R))^{n_N-1}, \quad (3.22)$$

where  $n_N$  is a power index determined by  $N$ .

The figure demonstrates that the nearest neighbour distribution can be considered to behave as the logarithmic function, described above, for large  $R$  where  $G_1(R; N)$  is less than  $10^{-2}$ . At small  $R$  (typically of order of a particle diameter) the distributions bend away from the suggested form. The deviation is partly due to finite bin-width of the measured distribution where the binning method is insufficient to compensate for the sharp increase in gradient of the distribution as  $R \rightarrow 0$ . More importantly at these small length scales particles are still strongly influenced by the aftermath of collision.

The key to understanding the structure of the system is to find a mechanism to account for these logarithmic distributions.

### 3.3.3 Renormalisation and Self-Similarity of the Structure

The logarithmic characteristics of the nearest neighbour distribution of these highly dissipative systems is the leading cause of the multi-scaling behaviour seen in the moments of the distribution.

A well known example, that also shows anomalous scaling, are equilibrium systems that are tuned into a state of criticality. These systems are known to exhibit structural self-similarity, whereby large-scale features are statistically similar to small-scale features, and as such the system can be renormalised without loss in detail (Yeomans 1992). For example, in the Ising model of a critical  $2N$  spin lattice it is possible to renormalise the system through a process called decimation. This involves removing every other site to leave  $N$  sites and subsequently rescaling all system lengths, by a factor of one half. The resultant new system has the same structural characteristics as the original and implies that the structure of every second site in the  $2N$  spin lattice has the same characteristics as the structure of every site in the  $N$  spin lattice.

Is it possible that the one-dimensional Random Force Model also has self-similar features that would allow these system to be renormalised without changing its behaviour?

To test this idea we would like to perform the equivalent process of decimation on these systems.

Let us imagine that we perform two simulations of equivalent systems except for particle number where one system contains  $N$  particles and the other  $2N$  particles. The larger populated system has more degrees of freedom than the smaller populated system and these can be separated within the larger system by ignoring every other particle such that we obtain a modified system with only  $N$  particles. This modified system now appears to approximately mimic the look of the  $N$  particle system, except for an increased energy-scale generated by the ignored particles acting as sources of additional random noise. The increased energy-scale does not modify the behaviour of the system, compared to the  $N$  particle system, and its effect can be removed by adjusting the value of the random force's noise strength  $D$ . If the properties of the system were the same then it would be expected that the nearest neighbour distribution of both systems should be similar. This would translate to comparing the distribution of nearest neighbour distance in the  $N$  particle system to the distribution of second nearest neighbours in the unaltered  $2N$  particle system. We hence would conclude that a particle within the  $2N$  particle system perceives the second further particle as if it was the adjacent particle within a  $N$  particle system and the ignored in-between particles play the role of an additional sources of random force.

In this view we assumed that the ignored particles simply act as uncorrelated noise. In reality the collision with these particles will bias the next collision due to memory effects. These memory effects become weaker the longer time a particle has between collisions due to the random force.

This simple hypothetical experiment motivates us to study higher order separation distances as a way of judging if these systems can be renormalised such that large-scale structure is self-similar to small-scale structure. The separation distance between particle  $i$  and  $j$  is given as the absolute difference in the particle's positions:

$$R_{i,j} = |r'_j - r'_i|. \quad (3.23)$$

The  $h^{th}$  nearest neighbour distribution, denoted  $G_h(R; N)$ , describes the time averaged probability that the  $i^{th}$  particle is separated from particle  $i + h$  by a distance  $R$ . The distribution is calculated by

$$G_h(R; N) = \frac{1}{N} \left\langle \sum_{i=1}^N \delta(R - R_{i,i+h}) \right\rangle, \quad (3.24)$$

such that when  $h$  equals one we obtain the nearest (or first) neighbour distribution.

We hypothesise that the  $h^{th}$  neighbour distributions have the scaling property:

$$G_h(R; hN) = G_1(R; N), \quad (3.25)$$

where the reduced system length is fixed at  $L' = 1$ . If this is the case a system of  $hN$  particles can be renormalised to a system of  $N$  by picking every  $h^{th}$  particle and removing all others.

We test the above hypothesis by modelling systems containing number of particles that are powers of two. The dissipation of all studied systems is equal to  $\varepsilon = 0.1$ . Initially we simulate a system containing 512 particles and measure the nearest neighbour distribution. Next we simulate systems containing 1024, 2048 and 4096 particles. These systems are renormalisable with one another if: the  $2^{nd}$  nearest neighbour, for the system  $N = 1024$ ; the  $4^{th}$  nearest neighbour, for the system  $N = 2048$ ; and the  $8^{th}$  nearest neighbour distribution, for the system  $N = 4096$ ; are identical to that of the nearest neighbour distribution, for the system  $N = 512$ .

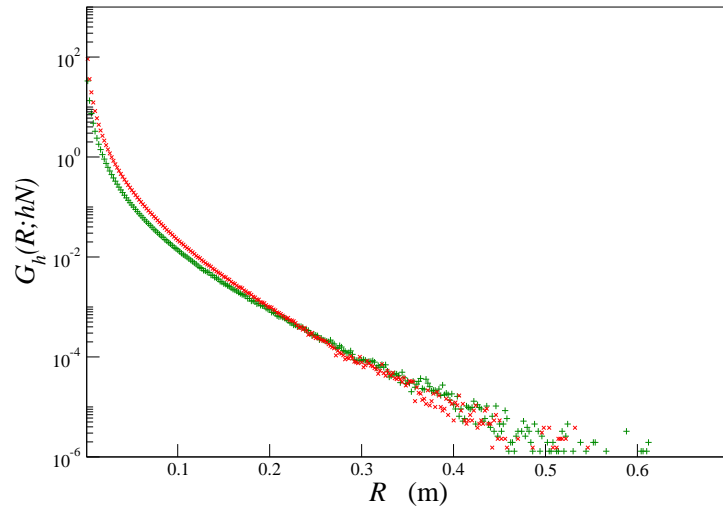
Figure 3.13 shows comparisons of pairs of  $h^{th}$  neighbour distributions, for the described systems. The  $2h^{th}$  neighbour distributions, corresponding to particle populations of  $2N_0$ , are vertically scaled onto the  $h^{th}$  neighbour distribution, of systems with particle populations of  $N_0$ . The high distance tails of the distributions approximately converge and demonstrates that to a certain extent large-scale structural features of systems with large particle populations can be renormalised onto the smaller populated systems. It is the correlations between neighbouring particles that prevent the system being treated as completely renormalisable.

### 3.4 Multiplicative Fracture Process

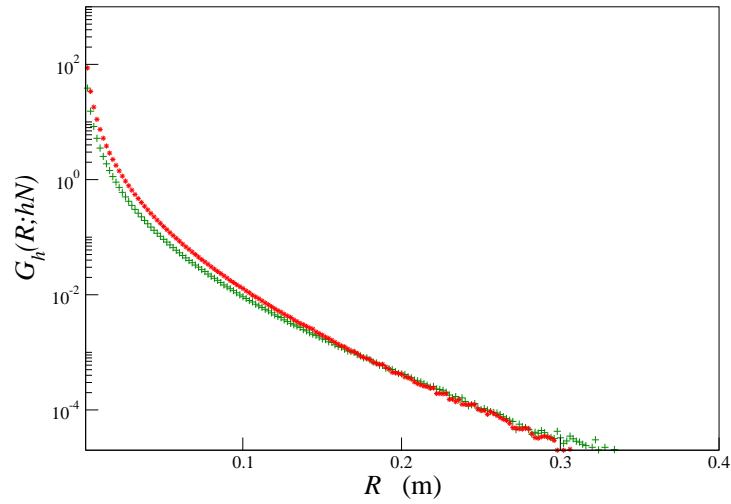
In the previous section it was suggested that the Random Force Model of highly dissipative systems can be spatially renormalised. The implication is that systems containing larger numbers of particles are structurally self-similar to lower occupied systems once excess particles are ignored. This leads us to postulate a reverse process to renormalisation, whereby additional particles are placed into an system in order to generate the structure of a system with more particles.

In this section we use a mathematical process for partitioning an interval into regions to represent populating a system with particles that incorporates similar hierarchical

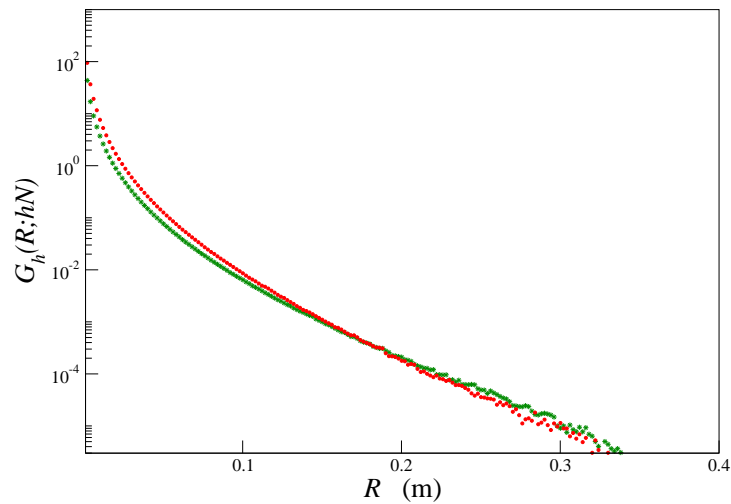
Fig. 3.13: Comparison of neighbour distributions for various systems with low dissipation of  $\varepsilon = 0.1$  and fixed reduced system length of  $L' = 1$ .



(a) The first neighbour of  $N = 512$ (plus) compared to the vertically scaled Second Neighbour of  $N = 1024$ (cross)



(b) The second neighbour of  $N = 1024$ (cross) compared to the vertically scaled fourth neighbour of  $N = 2048$ (star)



(c) The fourth neighbour of  $N = 2048$ (star) compared to the vertically scaled eighth neighbour of  $N = 4096$ (circle)

structure to that expected for a critical system. We compare it against the Random Force Model and find reasonable agreement.

### **Physical Interpretation**

The idea that a system with a large number of particles can be renormalised to become a system with a smaller number of particles motivates us to pursue the notion that we can do the process of renormalisation in reverse. If we can renormalise a system by removing half the particles then maybe we can generate a more populated system by placing the same number of additional particles into the system.

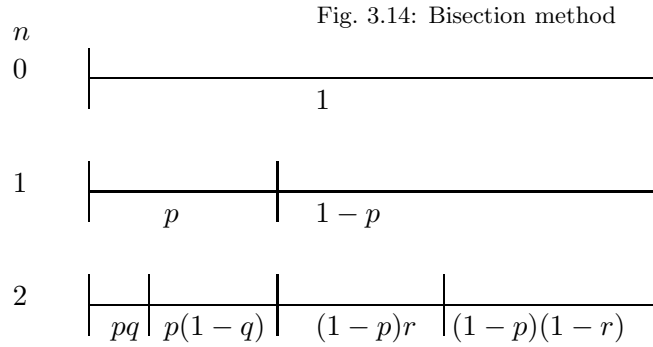
Imagine that a more populated system is constructed from one containing fewer point-particles by placing a new point-particle between all possible pairs of point-particles. The simplest case would start with a system containing one point-particle placed at a boundary. We obtain a system containing two particles by placing another point-particle in the interval between the first particle and the opposing boundary (the first particle itself) and then a system with 4 particles by placing 2 point-particles in the two intervals bounded by the already placed two particles. By continuing the process of placing particles in all available intervals (gaps between placed particles) we can build up any system that contains  $2^n$  particles.

In the reduced coordinate system particles have no size and the system length can be rescaled such that  $L' \mapsto 1$ . Consequently the position of particles represents the boundaries of unoccupied intervals and the distance between neighbouring particles the lengths of these intervals. In effect the system has been broken into  $N$  partitions.

By this interpretation we find that the distance between nearest neighbours can equally be viewed as a partition length and the distribution of nearest neighbour distance can therefore be thought of as the distribution of partition lengths. We further assume that the time average of the Random Force Model can be represented equivalently by a configuration average of placing particles into the system.

#### **3.4.1 Multiplicative Bisection Process**

A class of models that can be used to perform the placing of particles into a system are known as the multiplicative fracture process. A system of partitions is built up by consecutively breaking an interval into parts. The simplest case uses an interval of length 1 that is then repetitively bisected. Processes of this sort are known as multiplicative bisection process (Krapivsky and Majumdar 2000; Sibuya and Itoh 1987). They in-



volve breaking an interval into  $2^n$  parts such that the sum of all partition lengths totals the length of the original interval. The routine of creating partitions is as follows.

The interval is broken up through  $n$  levels. Each level involves the process of bisecting all available partitions. The boundaries of the two new partitions are assigned to be the boundaries of the replaced partition and a randomly placed boundary that lies between the previous two.

At the  $n^{th}$  level there exists  $2^n$  partitions. The  $i^{th}$  partition (where  $i = 1, 2, \dots, 2^n$ ) has boundaries denoted by  $r_{i,n}$  and  $r_{i+1,n}$  such that  $r_{i,n} < r_{i+1,n}$ . The interval is bounded by  $r_{1,n} = 0$  and  $r_{2^n,n} = 1$ . We progress to the  $n + 1^{th}$  level by bisecting all partitions. The position of each new boundary is determined probabilistically by picking a value  $0 \leq a_i \leq 1$ , selected from a probability distribution  $U_0(a_i)$  and placing boundaries as follows:

$$r_{2i,n+1} = r_{i,n}, \tag{3.26}$$

$$r_{2i+1,n+1} = r_{i,n} + a_i(r_{i+1,n} - r_{i,n}). \tag{3.27}$$

The distribution  $U_0(a_i)$  is identical for all partitions regardless of width. The above routine is repeated until the desired level is reached.

Figure 3.14 shows a pictorial representation of the process of partition formation for the first two levels. At  $n = 0$  only one partition exists and spans the whole interval with a length 1. The symbols  $p$ ,  $q$  and  $r$  are independent probabilities representing particular measurements of probability  $a_i$ . The length of each partition are stated as the product of the probabilities.

From the diagram it is clear that the length of any partition at the  $n^{th}$  level,  $x_n$ , is simply the product of  $n$  independent values picked from the same probability distribution  $U_0(a_i)$ . Hence the length of a partition is given by (Redner 1990):

$$x_n = \prod_{i=1}^n a_i. \tag{3.28}$$

### Obtaining the Probability Distribution of Partition Lengths

How do we obtain the distribution of partition lengths? One method is to numerically simulate, repeatedly, the breaking of an interval into  $2^n$  partitions, following the routine of the process outline previously and measure the average distribution of partitions lengths. Alternatively at each level the probability that a partition is of a length  $x_n$ , denoted as  $P_n(x_n)$  (the suffix  $n$  distinguishes the level the process is at), can be represented by the recursion relation described in the paper of Sornette (1998). The probability of getting  $x_{n+1}$  at the next level is simply the probability of starting at a value  $x_n$  multiplied by the probability of receiving a value  $a$  that allows the product( $a x_n$ ) to equal  $x_{n+1}$ , integrated over the complete set of allowed  $x_n$ :

$$P_{n+1}(x_{n+1}) = \int_{x_{n+1}}^1 dx_n \int_0^1 da P_n(x_n) U_0(a) \delta(x_{n+1} - ax_n). \quad (3.29)$$

A key element of the recursion relation is the partition probability  $U_0(a)$ . The multiplicative bisection method puts no constraint on the form of the  $U_0(a)$  except that:

$$U_0(a) = U_0(1 - a) \text{ where } 0 \leq a \leq 1. \quad (3.30)$$

The distribution of partition lengths are progressively calculated from the zeroth to the  $n^{\text{th}}$ , using equation 3.29.

#### 3.4.2 A Simple Case

In the simplest case, which we shall call the uniform bisection process, the partition probability is assumed to be the uniform distribution,  $U_0(a) = 1$ . No preference is made in the placing of partition boundaries and the distance away from other boundaries is neither minimised nor maximised.

The distribution of partition length,  $P_n(x_n)$ , is calculated using the relation 3.29, which simplifies to:

$$P_{n+1}(x_{n+1}) = \int_{x_{n+1}}^1 \frac{dx_n}{x_n} P_n(x_n). \quad (3.31)$$

At level zero (the unbroken interval) the probability distribution of partition lengths is defined as:

$$P_0(x_0) = \delta(x_0 - 1). \quad (3.32)$$

The delta function signifies that a single partition spans the complete interval.  $P_n(x_n)$  is calculated for the next three lowest levels as: level one,

$$P_1(x_1) = \int_{x_1}^1 \frac{dx_0}{x_0} \delta(x_0 - 1) = 1; \quad (3.33)$$

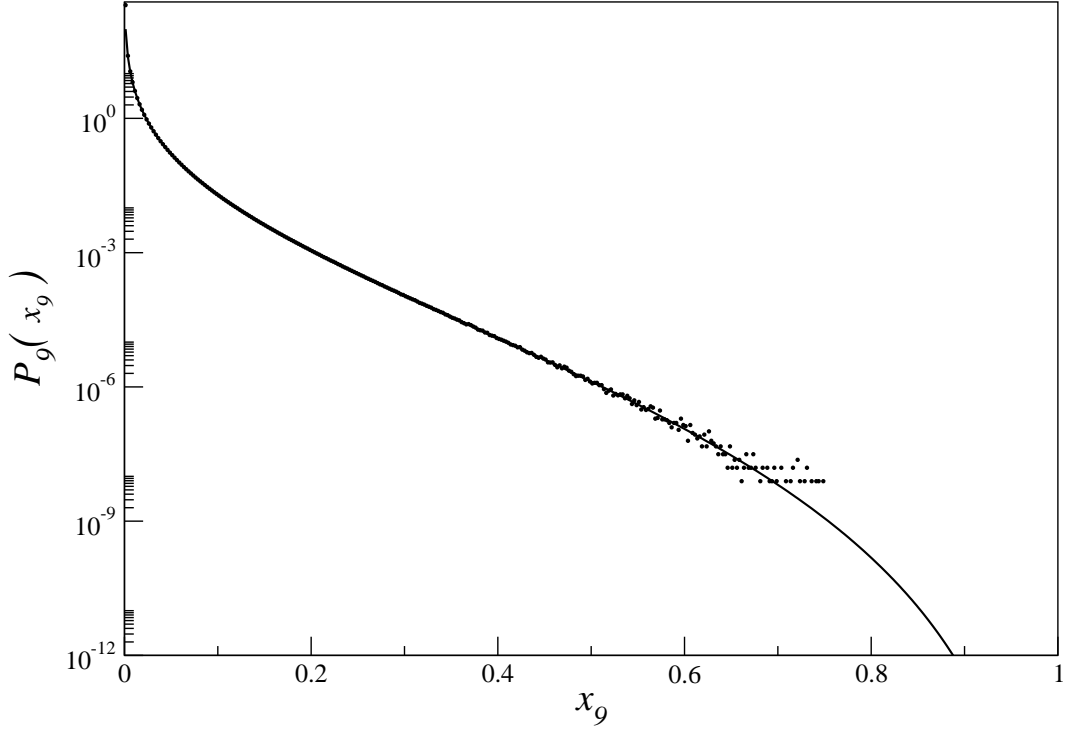


Fig. 3.15: Comparison of the solution for the bisection process obtained from equation 3.36(line) and by numerical partition breaking process (circles).

level two,

$$P_2(x_2) = \int_{x_2}^1 \frac{dx_1}{x_1} = -\ln(x_2); \quad (3.34)$$

level three,

$$P_3(x_3) = -\int_{x_3}^1 \frac{dx_2}{x_2} \ln(x_2) = \ln(x_3)^2 + \int_{x_3}^1 dx_2 \ln(x_2) \frac{1}{x_2} = \frac{(-\ln(x_3))^2}{2}. \quad (3.35)$$

Through induction we find that in general the distribution of partition lengths is of the form:

$$P_n(x_n) = \frac{(-\ln(x_n))^{n-1}}{(n-1)!}. \quad (3.36)$$

As the number of levels tend to infinity the distribution limits to log-Gaussian (by the Central Limit Theorem, as shown by Redner (1990)). However, in our study only small values for  $n$  are used such that the Central Limit Theorem is not applicable and equation 3.36 is sufficient.

We demonstrate that the above relation is correct in figure 3.15. An interval is partitioned, by applying the bisection method nine times to obtain  $2^9$  partitions. We repeat the process many times and measure the distribution of partition lengths. Equation 3.36 agrees well with the data obtained.

In general the uniform bisection process produces a distribution of partition lengths that is a function of logarithmic distance. This feature is also present in the nearest

neighbour distribution of the near-inelastic Random Force Model. A second feature that gives us optimism that a process such as this is applicable to the highly dissipative Random Force Model is the behaviour of the moments of partition length. The  $m^{\text{th}}$  moments of the partition length is calculated by the following expression:

$$\begin{aligned} \langle x_n^m \rangle &= \int_0^1 x_n^m P_n(x_n) dx_n \\ &= \frac{1}{(1+m)^n} \frac{1}{(n-1)!} \int_0^\infty z^{(n-1)} \exp(-z) dz \\ &= \frac{1}{(1+m)^n}. \end{aligned} \tag{3.37}$$

The predicted moment of partition length is transformed into a function of the number of partitions  $N$  by inserting  $N = 2^n$  into equation 3.37 such that:

$$\langle x_n^m \rangle = \exp\left(-\frac{\ln(N)}{\ln(2)} \ln(1+m)\right) = N^{-\frac{\ln(1+m)}{\ln(2)}}. \tag{3.38}$$

The described form of the moments behaves as a power-law of  $N$  in the same fashion as that already seen for the Random Force Model. Our task next is to ascertain whether the Random Force Model quantitatively matches these two features of the partition model: logarithmic function and power-law moments.

### 3.4.3 Comparison with data from the Random Force Model

The purpose of the following material is to investigate how well the fracture process describes the structural behaviour of the one-dimensional Random Force Model. We compare the distribution of partition lengths generated from the uniform bisection process to the nearest neighbour distribution of the Random Force Model. We first consider a system containing 1024 particles and then generalise over the range of studied systems.

#### Comparison with a specific system

A simulation of the random force model for 1024 particles is performed to generate the distribution of nearest neighbour distance. We next simulate the corresponding uniform bisection process by the partitioning of an interval through nine stages such that  $2^9$  partitions are achieved and calculate the distribution of partition lengths. Figure 3.16 shows the comparison between the two distributions and demonstrates that good agreement, without the use of fitting parameters, is seen between the random force model's distribution of nearest neighbours and the uniform bisection process's distribution of partition lengths.

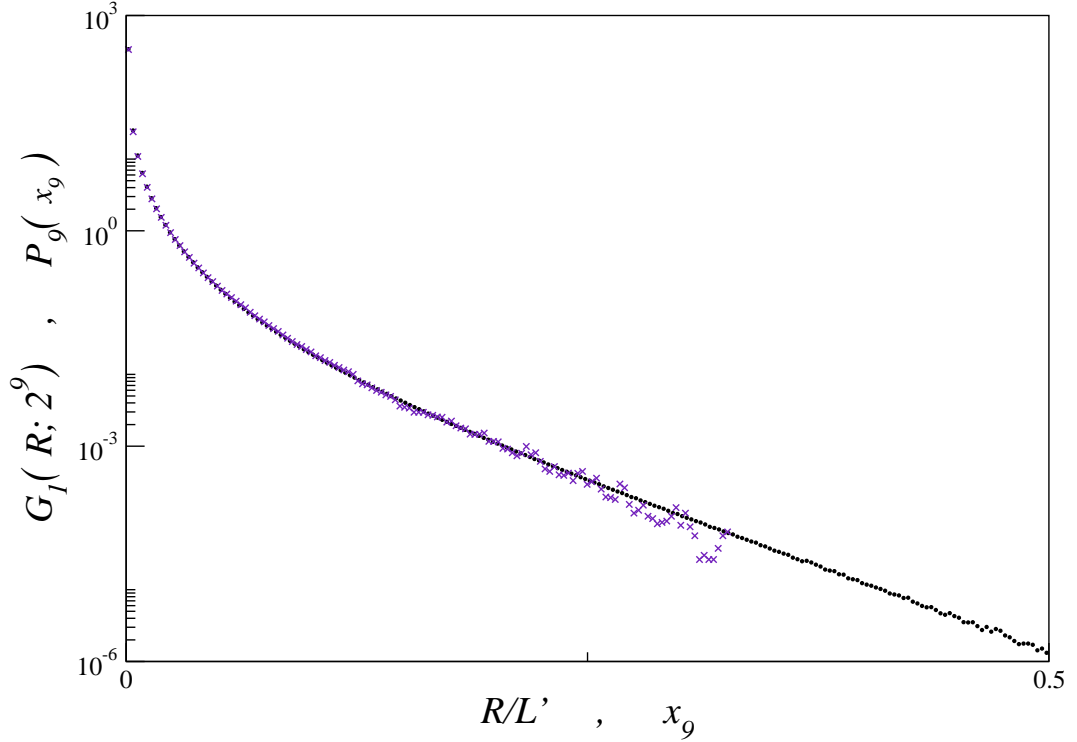


Fig. 3.16: Comparison of the bisection process (circles) with first nearest neighbour distribution of 1D Random Force Model (cross) when using  $N = 2^9$  particles which is equivalent to  $n = 9$  repetitions of partition breaking.

### Comparison with a range of systems

We now make comparisons over a range of systems containing between 100 and 3981 particles. Direct comparison between the multiplicative bisection process and the random force system is not possible in most systems as the multiplicative bisection process can only generate systems that contain integer powers of 2 particles. Instead we attempt to collapse nearest neighbour distributions using the scaling relation suggested by the fracture process.

If the Random Force Model has structure of the form determined by the multiplicative bisection process then the nearest neighbour distribution collapses onto one curve by the map:

$$G_1(R; N) \mapsto A_N [G_1(R; N)]^{\frac{1}{n-1}}, \quad (3.39)$$

where  $n$  is related to  $N$  by  $N = 2^n$  and  $A_N$  is a numerical factor used to renormalise the distributions. We choose  $A_N$  to be:

$$A_N = -\ln(0.7) [G_1(0.7; N)]^{-\frac{1}{n-1}}, \quad (3.40)$$

such that when  $R = 0.7$  the collapsed distributions all have magnitude  $-\ln(0.7)$ . Figure 3.17 shows the nearest neighbour distributions of the Random Force Model transformed

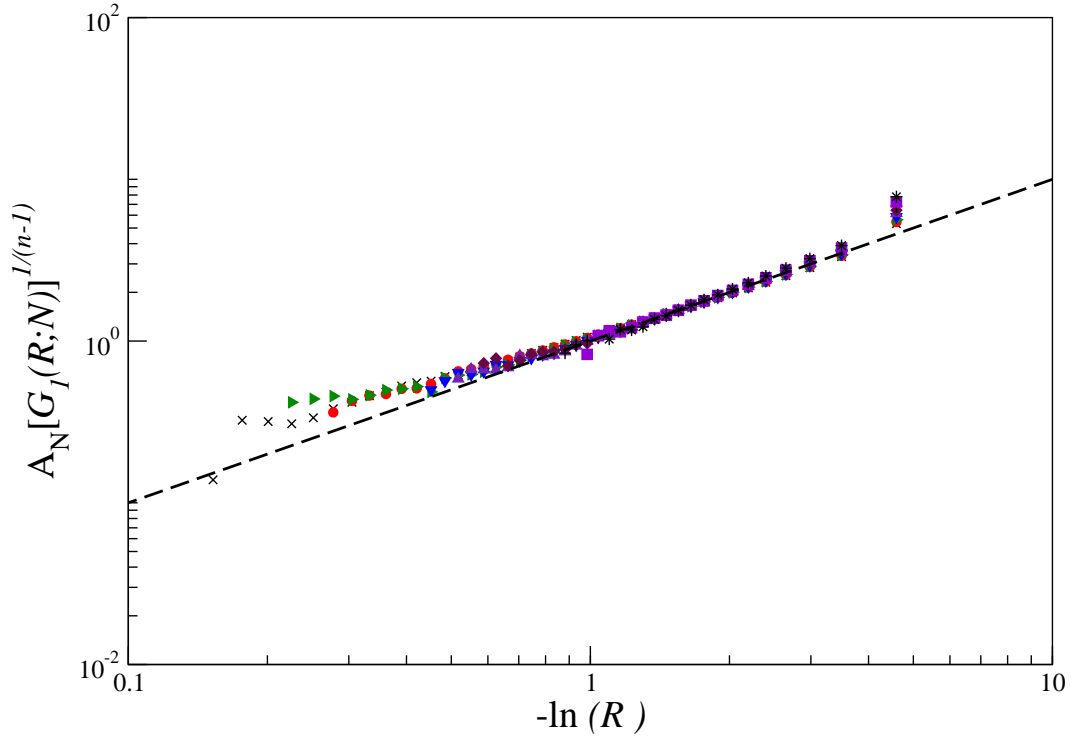


Fig. 3.17: The nearest neighbour distribution for various systems with low dissipation of  $\varepsilon = 0.1$  and fixed reduced system length of  $L' = 1$  plotted as a function of  $-\ln R$ . The distributions are for systems containing the following number of particles: 100(cross) 158(circle); 251(right triangle); 398(triangle down); 631(triangle up); 1000 (diamond); 1585(plus); 2512(square) and 3981(star). The dashed line is the function  $-\ln(R)$  and  $n = 2^N$ .

using the map 3.39. The data sets collapse onto one curve which suggests that in general a multiplicative bisection process does describe the structure of the Random Force Model.

Next we ask can we use a specific version of the multiplicative bisection process such as the uniform bisection process? If the uniform bisection process describes the structure of Random Force Model, then the collapsed curves will be parallel to the function  $-\ln(R)$ , for all separation distances  $R$  (which we arrive at from equation 3.36). In figure 3.17 the dashed line represents the prediction of the uniform bisection process.

For large values of  $-\ln(R)$ , corresponding to small/moderate separation distances between particles, the slope of the multiplicative prediction and the collapsed data are approximately the same.

As  $-\ln(R)$  becomes smaller, corresponding to the larger separation distances, the collapsed data of the nearest neighbour deviates away from the multiplicative prediction. The most likely explanation is that the deviation occurs because particle interac-

tion cannot be ignored and there is an increased tendency for the particles to be close to each other that is not accounted for in the uniform bisection process. The resultant effect on the distribution of nearest neighbours is that the singular peak of the distribution becomes steeper and the tail of the distribution for large distances become shallower than predicted by the uniform bisection process.

**Behaviour of the Moments**

We now quantify the differences between Random Force Model and uniform bisection process by comparing the moments of separation distance of the two. It is not expected that the moments of separation between theoretical and model will agree. Indeed this is seen in the table below where the predicted (Process) and measured (Model) exponent  $\zeta_m$  is given for the first five moments:

$m^{th}$ Moment	$\zeta_m$ (Predicted)	$\zeta_m$ (Measured)
1	$\frac{\ln(2)}{\ln(2)} = 1$	1
2	$\frac{\ln(3)}{\ln(2)} \approx 1.58$	$1.729 \pm 0.008$
3	$\frac{\ln(4)}{\ln(2)} \approx 2$	$2.31 \pm 0.03$
4	$\frac{\ln(5)}{\ln(2)} \approx 2.32$	$2.81 \pm 0.06$
5	$\frac{\ln(6)}{\ln(2)} \approx 2.58$	$3.2 \pm 0.1$

Table 3.1: The comparison of the particle number behaviour of the  $m^{th}$  moments of separation, where  $\langle R^m \rangle = AN^{-\zeta_m}$ , between that predicted from the uniform bisection process and that measured from data of the Random Force Model.

As the order of the moment increases the discrepancy between the predicted value of  $\zeta_m$ , given by equation 3.38, and the measured value, obtained from simulation of the Random Force Model becomes more significant.

In conclusion the multiplicative bisection process captures the essence of the structure observed in the highly dissipative Random Force Model. The process treats every region of the interval as a scaled down version of the original interval and thus introduces self-similarity to the system. No preference is placed on the attraction between particles and hence the process maximises randomness within the hierarchical structure. Clustered regions are represented by a collection of boundaries placed inside successively smaller regions.

We compared one of the simplest multiplicative bisection process with data from

the one-dimensional Random Force Model. Overall approximate agreement is found in the shape of the nearest neighbour distribution between the process and the Model, confirming the relevance of these processes as descriptions for the Model's structure. However, significant divergence occurs between the two solutions, for larger separation distances, which advocates that the tendency of particles to be near each other is greater than that suggested by the simplest process. Improvement to the multiplicative process can be achieved by instead using a partition probability,  $U_0(a)$ , with a concave profile such that there is an increased likelihood for  $a$  to take value near either zero or one. For example using a profile of  $U_0(a) \sim a^{-A} + (1 - a)^{-A}$ , where  $A$  is a small constant, produces  $P_n(x_n)$  with similar qualitative characteristics upon collapse as the Random Force Model. Unfortunately there is no clear indication as to what the exact profile of  $U_0(a)$  should be.

### 3.5 Summary

In this chapter we demonstrated that the one-dimensional Random Force Model had multi-scaling properties through which the velocity distribution had a shape that was non-universal with respect to system population.

The moments of a particle velocity exhibited a scaling behaviour, with respect to particle number, that was not invariant to linear density,  $L'/N$ , nor preserve a common scaling behaviour for the different orders of moment such that  $\langle |v| \rangle \propto \langle |v|^m \rangle^{1/m}$ . Instead we observed that the the moments of velocity could be described by a power-law in  $N$  of the form:

$$\langle |v|^m \rangle \propto N^{-\xi_m}.$$

For the second moment of velocity we found that  $\xi_2$  took a value which lied in the range 0.53 to 0.666. Furthermore, in general  $\xi_m/m$  was fixed in value over a range of coefficients of restitution. For example,  $\xi_2/2 \simeq 0.264$  when  $\varepsilon < 0.5$ .

We next wanted to gain further insight into the cause of the multi-scaling behaviour and postulated that the system's structure played an important role. Thus the distribution of nearest neighbours was measured and found to have moments of separation between neighbouring particles that also showed strong multi-scaling behaviour.

The combination of these observations implied that these systems have no well-defined thermodynamic limit but instead become more clustered as further particles are placed in the interval of the system.

For systems that exist in a near-inelastic state ( $\varepsilon \rightarrow 0$ ) the nearest neighbour distributions were shown to be power-law functions of the logarithmic separation distance which only deviate at small separation distances where correlations between particles become important. In these systems approximate renormalisation characteristics are seen for large separation distances and implied that when particles were separated far enough apart the intermediate particles could be ignored without loss of generality. The ignored particles effectively became extra sources of random noise.

The renormalisation of the system provided motivation for a multiplicative bisection process. The simplest case was described as the uniform bisection process. The process had two features of relevance: firstly the distribution of partition lengths was a power-law of  $-\log(R)$ ; secondly the moments of the partition length were related to the number of partitions by a power-law. We compared the process to the Random Force Model by collapsing the nearest neighbour distributions. The time-average structure of these systems was found to be sufficiently described by a multiplicative bisection process. We speculate that it may also be possible to use other partition processes to describe the structure of the Random Force Model for high coefficients of restitution.

### **Implications for Higher Dimensions**

An intriguing feature of this chapter is that, when all other parameters are fixed, the value of the  $m^{\text{th}}$  moment of velocity converges for nearly all coefficients of restitution. When studying the second moment of velocity we found that if the coefficient of restitution was  $\varepsilon < 0.5$  then the moments power-law dependence on  $N$  becomes fixed with  $\xi_2 \simeq 0.53$ . Similarly when we study the higher moments of velocity we find that for coefficients of restitution  $\varepsilon < \epsilon_m$ , where  $\epsilon_m$  is a number that lies between 0 and 1, that  $\xi_m$  is a fixed number independent of  $\varepsilon$ . Significantly the value of  $\epsilon_m$  increases towards one as the order of the moment,  $m$ , increases. We speculate that this means that for a range of low to moderate dissipations the shape of the high velocity tail of these distributions is independent of coefficient of restitution, which is suggestive from the simple analysis of Appendix A. The physical grounding for this speculation is that the system's fast particles move the furthest and have forgotten the previous collision as momentum gained through a particles interaction with the random force washes out any remaining memory of the previous collision. In contrast, it is the low velocity particles that are strongly dependent on the level of dissipation.

This property of the fast particle's behaviour being independent of the extent of

dissipation continues to be exhibited in higher dimensional Random Force Model. In the next chapters we study the two-dimensional Random Force Model and show that large-scale structural features and the shape of the high-velocity tails of the velocity distribution are independent of coefficient of restitution and of particle numbers.

The dependence on particle numbers in the one-dimensional Model is in some sense due to it being pathological: particles must collide and cannot reorder. In the two-dimensional Model the moments of velocity only exhibit simple scaling.

## Chapter 4

# Fractal Properties of a Two-dimensional Random Force Model

We showed, in chapter one, that there exist two prominent questions in the literature associated with the two-dimensional Random Force Model with inconsistent answers. These are: what form does the large-scale structure take given that it exhibits fractal properties? and what is the asymptotic form of the velocity distribution? In this chapter we describe the structural properties of the two-dimensional Random Force Model to determine the fractal properties of the system. To do this we reduce the dissipation in a collision further than in previous work, using a tangential coefficient of restitution, which has the effect of enhancing the fractal structure.

The first section of this chapter discusses the structure obtained by using Random Force Model, specifically a distribution called the structure factor. We demonstrate that the large-scale structure of systems, of sufficient size, have common fractal behaviour irrespective of the systems dissipation, size and packing fraction.

The second section is concerned with understanding how the overall fractal structure of the system affects the behaviour of individual particles. We study the distance travelled by particles between consecutive collisions and find that those particles which travel a long distance are influenced by the fractal background of particles.

## 4.1 Structure Factor

The two-dimensional Random Force Model is thought to exhibit fractal structure, as was demonstrated by Peng and Ohta (1998a). As a consequence the system is self-similar on long length-scales. The structure of the system is quantified by a distribution called the structure factor,  $S(k)$ , which varies at small  $k$  as a power-law,  $Ak^{-D_f}$ . It is the power-law which gives rise to the notion of fractal-like structure.

In chapter one we reviewed the current literature and found that disagreements exist as to whether  $S(k)$  decays as  $k^{-2}$  (van Noije, Ernst, Trizac, and Pagonabarraga 1999) or as  $k^{-1.4}$  (Peng and Ohta 1998a). Puglisi, Loreto, Marconi, and Vulpiani (1999) found that  $S(k)$  varied as  $k^{-1.4}$  to  $k^{-1.9}$  depending on the choice of coefficient of restitution.

In this section we attempt to unearth the small  $k$  behaviour of the structure factor. We demonstrate that, as long as the system is of sufficient size, the large-scale structure, as characterised by the exponent  $D_f$ , is to a large extent unchanged, with only very weak and unsystematic variation seen as the dissipation or density is varied. Instead the variation of density and dissipation only affects the amplitude ( $A$ ) of these structures (and not the form) when we change the relative rate of dissipation compared to the rate of energy injection.

### Definition of the Structure Factor

The spatial correlation function,  $g(\mathbf{R})$ , measures the probability that any two particles are separated by a displacement  $\mathbf{R}$  at any given moment in time. The vector structure factor,  $S(\mathbf{k})$ , is defined as the Fourier transform of the spatial correlation function  $g(\mathbf{R})$  (Chaikin and Lubensky 1995):

$$S(\mathbf{k}) = 1 + \frac{N}{L^2} \int \int (g(\mathbf{R}) - 1) \exp(-i\mathbf{k} \cdot \mathbf{R}) d^2\mathbf{R}. \quad (4.1)$$

Using our simulations, the vector structure factor is calculated by taking the time average of the sum of the Fourier transforms of the separation distance over all possible pairs of particles (including self-correlated pairs):

$$S(\mathbf{k}) = \frac{1}{N} \left\langle \sum_{i=1}^N \sum_{j=1}^N \exp(i\mathbf{k} \cdot (\mathbf{r}_i(t) - \mathbf{r}_j(t))) \right\rangle. \quad (4.2)$$

We determine  $S(\mathbf{k})$  at discrete values of  $\mathbf{k}$  such as:

$$\mathbf{k} = \frac{2\pi k_i}{L} \hat{\mathbf{i}} + \frac{2\pi k_j}{L} \hat{\mathbf{j}}, \quad (4.3)$$

giving a magnitude  $k = \frac{2\pi}{L}(k_i^2 + k_j^2)^{\frac{1}{2}}$ , where  $k_i, k_j$  are integers. We can readily calculate the circular averaged  $S(k)$  from these points by taking the angular average of  $S(\mathbf{k})$ .

The  $k$ -space coordinates are inversely proportional to the distance within the system. Thus small  $k$ -space behaviour of  $S(k)$  corresponds to large-scale structural features of the system and similarly large  $k$ -space behaviour corresponds to small scale structural features.

For large  $k$ , the structure factor exhibits oscillations. The first peak occur at distances corresponding to the length scale of touching neighbouring particles, where  $k \simeq 2\pi/d$  with  $d$  the diameter of the particles. Subsequent peaks occur periodically at  $k \simeq 4\pi/d$ ,  $k \simeq 6\pi/d$  and so on. The strength of the peaks gives an indication of the extent of small-scale clustering occurring in the system.

For small  $k$ , the structure factor may exhibit one of several forms as  $k$  tends towards 0. Either  $S(k) - 1$  tends to 0 (as in fluid) suggesting that the system appears homogeneous at large-scale; or it tends to a non-zero plateau (sticky colloids as described by Zaccarelli, Saika-Voivod, Buldyrev, Moreno, Tartaglia, and Sciortino (2006)) suggesting particles form clusters with characteristic size; or it tends to infinity as a power-law, which suggests the system has fractal-like behaviour.

#### 4.1.1 Large-scale Structure and the Dissipative Regime

We have carried out simulations to determine  $S(k)$  for larger systems than previously studied so as to explore the small  $k$  region. The structure factor is found to have small  $k$  behaviour that obeys a power-law of the form:

$$\lim_{k \rightarrow 0} S(k) = Ak^{-D_f}, \quad (4.4)$$

where  $D_f$  is called the fractal dimension of the systems large-scale structure. Such a law has no associated characteristic length scale and hence is a fractal property. The power-law decay holds true over a range of small  $k$ , which we will call the dissipative regime in accordance with the naming convention of van Noije, Ernst, Trizac, and Pagonabarraga (1999). We find that a useful upper-bound,  $k'$ , to the range of  $k$  is given by  $k' = k_D$  where:

$$k_D = \frac{2 - \varepsilon_n^2 - \varepsilon_t^2}{8l_0}, \quad (4.5)$$

with  $l_0$  the mean free path of a particle between collision,  $\varepsilon_n$  is the normal coefficient of restitution and  $\varepsilon_t$  is the tangential coefficient of restitution. This is a generalisation of

the ideas of van Noije *et al.* for inelasticity in which collisions are allowed to have tangential dissipation (where one such method involves using  $\varepsilon_t$ , as shown in chapter two). Including tangential dissipation allows us to simulate systems of higher dissipation than normal dissipation alone.

### Predicting the System Size at which the Dissipative Regime is Observable

The largest structural features of the system occur at length scales of the order of the system size and as such the structure factor has a the minimum measurable value of  $k$  given by  $k_{min} = 2\pi/L$ . When  $k_{min}$  is greater than  $k_D$  the dissipative regime cannot be observed and the system exhibits finite size effects. In these cases the limited system size impedes the formation of large structure and prevents fractal structural behaviour being exhibited. Therefore to study the dissipative regime of the structure factor a sufficient system size of  $L > L_{min}$  must be used, where  $L_{min}$  is derived using equation 4.5 such that:

$$L_{min} \simeq \frac{2\pi}{k_D} \simeq \frac{16\pi l_0}{(2 - \varepsilon_n^2 - \varepsilon_t^2)}. \quad (4.6)$$

The mean free path  $l_0$  incorporates the systems packing fraction and can be estimated using mean field theory as

$$l_0 = \frac{L^2}{2dN} = \frac{\pi d}{8\phi}, \quad (4.7)$$

where  $\phi$  is the packing fraction of the system, defined as  $\phi = N\pi r^2/L^2$ . We can explicitly express  $L_{min}$  in terms of the packing fraction as

$$L_{min} \simeq \frac{2\pi}{k_D} \simeq \frac{2\pi^2}{(2 - \varepsilon_n^2 - \varepsilon_t^2)} \frac{d}{\phi}. \quad (4.8)$$

In practice we require more than one measurable  $k$  value to lie inside the dissipative regime before any measurement of the power-law decay can be made. Hence the system needs to have a size much larger than  $L_{min}$  and the minimum effective system size is given by

$$L_{Eff} = 2\sqrt{2}L_{min}, \quad (4.9)$$

such that the five lowest measurable values of  $k$ , that of:  $\frac{2\pi}{L}$ ;  $\frac{2\sqrt{2}\pi}{L}$ ;  $\frac{4\pi}{L}$ ;  $\frac{2\sqrt{5}\pi}{L}$  and  $\frac{4\sqrt{2}\pi}{L}$ , lie within the dissipative regime,  $k < k_D$ .

### Results

In our studies we measure the fractal dimension  $D_f$  of the power-law decay of  $S(k)$ , given in equation 4.4. The study into the structure factor is performed by varying three types of quantities: system size; dissipation and density. First, the size of the

system is changed for a given packing fraction. We show that reliable measurements of the power-law decay are only made for system sizes and scales where structural features are present of the order of the dissipative regime. We find that a power-law of  $S(k) = Ak^{-1.4}$  is recovered at conditions described by (Peng and Ohta 1998a) but later show that this is an artefact of using an insufficiently large system. Second, we change the effective dissipation of the system, keeping the packing fraction fixed and using a sufficiently large system. We vary both tangential and normal coefficients of restitution and show that the behaviour of the structure factor is invariant to the extent of dissipation. Third, the packing fraction of the system is changed by varying the population of particles per unit area.

#### 4.1.2 Increasing the Size of the System, $L$

We perform simulations where the packing fraction of the system is fixed and both the size of the system,  $L$ , and the population of the particle,  $N$ , are increased so that  $N/L^2$  is constant. We scale up the system by first simulating a system of size  $L = 0.1$  and population  $N$ , then choosing integer multiples,  $j = 2, 4, 6, 8, 10$  such that the new system size is  $L' = jL$  and particle population is  $N' = j^2N$ . We simulate four packing fractions, that of  $\phi = 0.088; 0.177; 0.353$  and  $0.530$ . The particles are made extremely dissipative with coefficients of restitution given as  $\varepsilon_n = 0.1$  and  $\varepsilon_t = 0.1$  such that all collisions dissipate the same proportion of energy regardless of orientation. Such a large dissipation maximises the range of  $k$  considered to be within the dissipative regime.

#### Observed effect on Large and Small Scale Features

Figures 4.1 and 4.2 overlay data on the structure factor of successively larger sized systems of two packing fractions  $\phi = 0.088$  and  $0.353$ . The minimum measured value of  $k$  occurs when  $k = 2\pi/L$ . By increasing the system size we are able to extend the form of  $S(k)$  further back towards a  $k$  of zero and study features of smaller  $k$ -order.

The large  $k$  behaviour of  $S(k)$  remains unchanged with increased size. The peaks of the oscillations occur at  $k$  corresponding to the particle diameter which indicates that the tendency for particles to cluster is not affected by the system size.

When the packing fraction of the system is sufficiently high the size of the system does not have to be particularly large before the power-law decay of  $S(k)$  is visible, as demonstrated in figure 4.2. As the packing fraction of the system becomes more dilute it becomes difficult to simulate a system of sufficient size that the power-law decay can

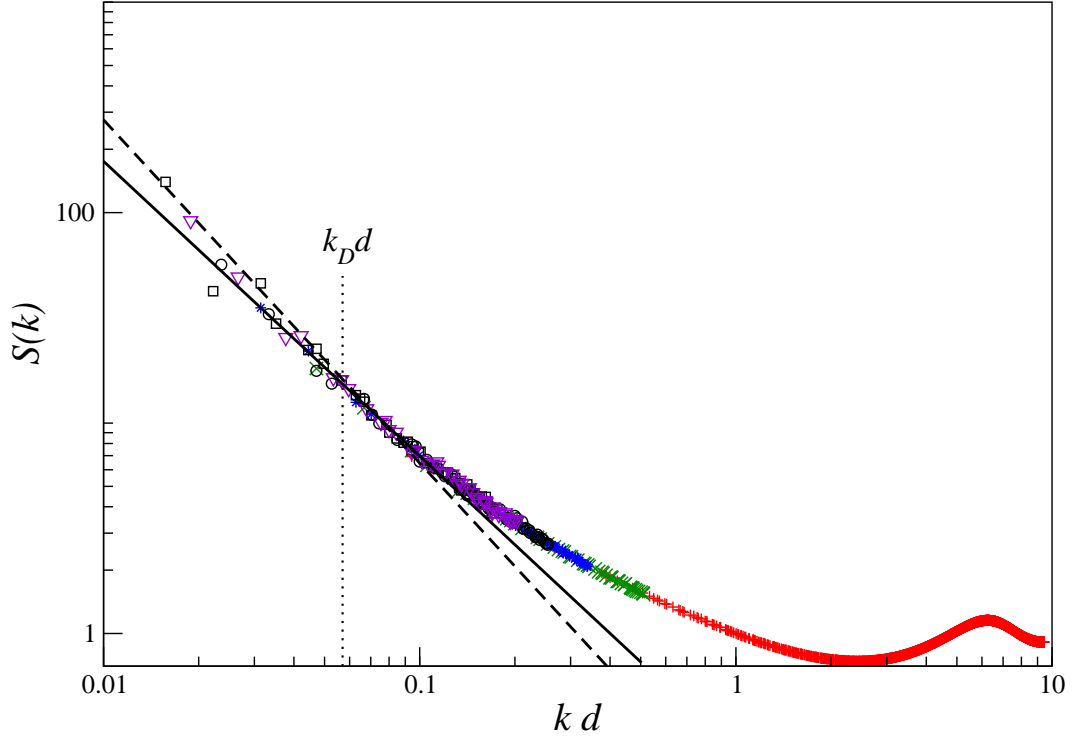


Fig. 4.1: The structure factor for a system with fixed density of 0.088 and dissipation of  $\varepsilon_n = \varepsilon_t = 0.1$ . The data sets are for combinations of particle number and system size such that  $N = 500, L = 0.2\text{m}$  (plus);  $N = 2000, L = 0.4\text{m}$  (cross);  $N = 4500, L = 0.6\text{m}$  (star);  $N = 8000, L = 0.8\text{m}$  (circle);  $N = 12500, L = 1.0\text{m}$  (down-triangle) and  $N = 18000, L = 1.2\text{m}$  (square). The lines are power-law fits of  $S(k) = Ak^{-1.63}$  (dashed) and  $S(k) = Ak^{-1.4}$  (solid).

be seen, as demonstrated by figure 4.1.

### Estimating the System Size at which the Dissipative Regime is Present

An estimate for the system size at which the dissipative regime can be observed is obtained using the approach of van Noije *et al.* (1999). Their theory suggests that when  $k < k_D$  the structure factor can be considered to be in the dissipative regime. For the packing fractions  $\phi = 0.088$  and  $\phi = 0.353$  we calculate  $k_D$  to have values  $0.057/d$  and  $0.223/d$  respectively, where  $d$  is the particle diameter. The vertically dotted lines on figures 4.1 and 4.2 mark the predicted value of  $k_D$  at which the structure factor behaves as a power-law for  $k < k_D$ . The figures show that  $k_D$  provides a reasonable estimate to the upper limit of the dissipative regime.

For the packing fractions  $\phi = 0.088$  and  $\phi = 0.353$  we predict that the dissipative regime is only visible in data of the structure factor when system size is greater than  $L_{min} \simeq \frac{2\pi}{k_D} \simeq 0.330\text{m}$  or  $0.084\text{m}$  respectively. The data is only usable, with at least five points of  $S(k)$  lying inside the dissipative regime, if the system is larger than

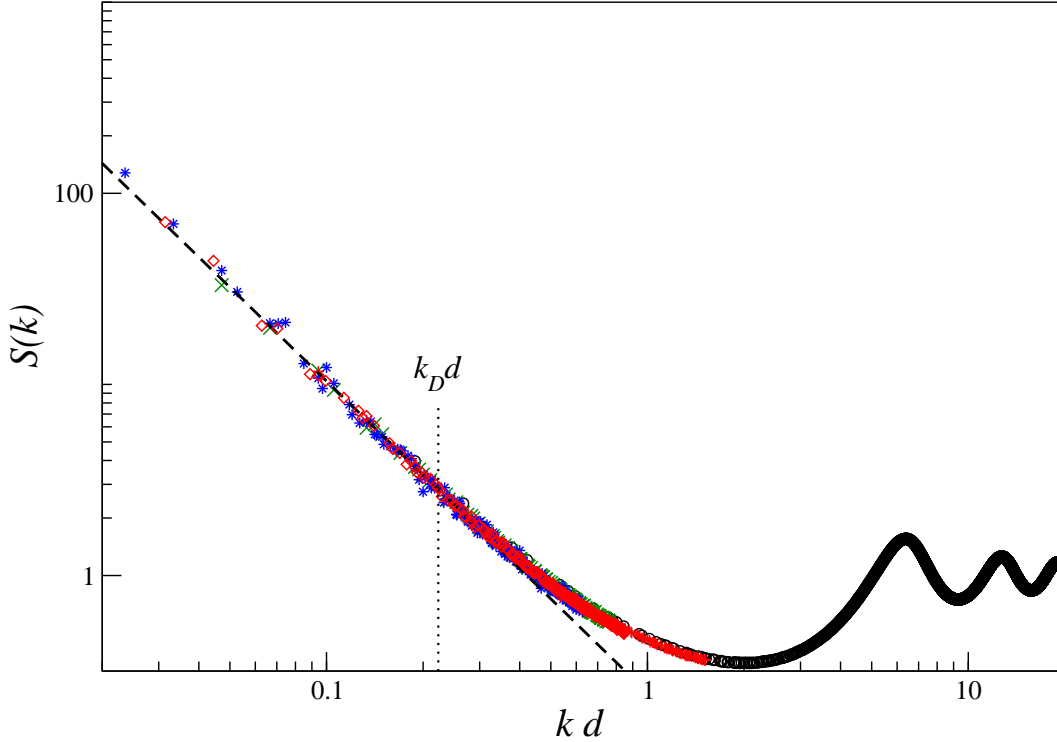


Fig. 4.2: The structure factor for a system with fixed density of 0.353 and dissipation of  $\varepsilon_n = \varepsilon_t = 0.1$ . The data sets are for combinations of particle number and system size such that  $N = 500, L = 0.1\text{m}$  (circle);  $N = 2000, L = 0.2\text{m}$  (plus);  $N = 8000, L = 0.4\text{m}$  (cross);  $N = 18000, L = 0.6\text{m}$  (diamond) and  $N = 32000, L = 0.8\text{m}$  (star). The dashed line is a power-law fit of  $S(k) = Ak^{-1.63}$ .

$L_{Eff} \simeq 0.934\text{m}$  or  $\simeq 0.240\text{m}$ , respectively.

### Measurement of the Power-Law Decay

We now attempt to estimate the fractal dimension of the structure factor for these systems by fitting power-law functions (of the form described in equation 4.4) to the dissipative regime of the structure factor across the range  $k < k'$  where the constant  $k'$  is an estimated upper limit to the dissipative regime. Three system scales are chosen, corresponding to system sizes of  $L = 0.2\text{m}$ ,  $0.4\text{m}$  and  $0.8\text{m}$ . Simulation of larger systems are avoided as the measurement of small  $k$  behaviour of the structure factor becomes significantly less reliable and more scattered since the huge population of particles degrades computer performance. For example, transient effects take much longer time to die away in the computing.

The following table shows the estimated fractal dimension of the structure for systems of fixed packing fraction and various system sizes. The lowest considered packing fractions are difficult to simulate with a system at a sufficient scale in which power-law decay is observable. In contrast the higher packing fractions require only a small sys-

tem size before power-law behaviour is seen. The upper limit  $k'$  is chosen to be equal to  $k_D$  if the system size satisfies  $L_{Eff} < L$  or  $2k_D$  else.

$\phi$	$k_D d$	$L_{Eff}$	$D_f(L = 0.2)$	$D_f(L = 0.4)$	$D_f(L = 0.8)$
0.177	0.112	0.48	$1.30 \pm 0.1$	$1.48 \pm 0.02$	<b><math>1.55 \pm 0.10</math></b>
0.353	0.223	0.24	$1.50 \pm 0.04$	<b><math>1.60 \pm 0.08</math></b>	<b><math>1.66 \pm 0.09</math></b>
0.530	0.334	0.16	<b><math>1.63 \pm 0.03</math></b>	<b><math>1.65 \pm 0.02</math></b>	<b><math>1.60 \pm 0.03</math></b>

Table 4.1: The measured values of  $D_f$  obtained for three packing fractions and three system sizes of highly dissipative systems.

For system sizes smaller than  $L_{Eff}$  we find that the estimate of the fractal dimension is consistently under-predicted. We obtained a estimated value for  $D_f$  consistent with the results Peng and Ohta (1998a) (where their system parameters are equivalent to  $\phi = 0.16$ ,  $L = 0.21$ ,  $\varepsilon_n = 0.1$ ,  $\varepsilon_t = 1.0$  and  $D_f = 1.4$ ) when the packing fraction is  $\phi = 0.177$  and system size is  $L = 0.2$ . We also find a similar value when using Peng and Ohta actual parameters. This suggests that Peng and Ohta considered a set of parameters which the dissipative regime is not sufficiently visible. Hence data outside the power-law decay was fitted and lead to the under-estimate in the value of  $D_f$ . In figure 4.1 we demonstrate that the structure factor agrees with a power-law fit of  $k^{-1.4}$  (shown as a solid line) only over the finite range of  $kd$  bounded between  $2k_D d - 0.05$  to  $2k_D d$ .

For system sizes greater than  $L_{Eff}$  the fractal dimension  $D_f$  settles into the range 1.60 to 1.66. Variation in value between subsequent system sizes lies well inside the reported error tolerance of any single measurement. Hence the value of  $D_f$  can be considered to be reliable and approximately constant with any variation due to packing fraction being very weak and masked by the fitting uncertainty. Even in the most dilute system, shown in the table as  $\phi = 0.177$  at  $L = 0.8m$ , the measurement of exponent  $D_f$  improves to  $1.64 \pm 0.26$  if the upper-bound  $k'$  is decreased to  $2k_D/3$  and demonstrates how sensitive the measurement of  $D_f$  is with respect to fluctuations in data quality.

In figures 4.1 and 4.2 we demonstrate that these constant values of  $D_f$ , achieved when  $L > L_{Eff}$ , are sufficient to describe the complete range of the power-law decay from  $k$  of zero to  $k'$  by drawing dashed-line power-law fits of exponent -1.63 through the distributions.

The results from the table suggest that, for systems of high dissipation and system size that satisfies  $L > L_{Eff}$ , the fractal dimension  $D_f$  is approximately constant over the packing fractions considered. In the next section we investigate how far the fractal dimension changes when either the dissipation of the collision or the packing fraction of the system is varied.

### 4.1.3 Stability with Respect to Dissipation

In the previous section we discovered that the fractal dimension  $D_f$  took a value around  $1.63 \pm 0.03$  for a variety of packing fractions where the system had a very high dissipation and a system size that was sufficiently large that  $2\pi/L < k_D$ . In these systems the particles dissipate both normally and tangentially to the collision. We are now interested in determining if  $D_f$  remains fixed for all dissipation, as previously found by Peng and Ohta. We test the hypothesis that the fractal dimension  $D_f$  has one common value for the complete spectrum of dissipations by considering three cases:

**Case I**, No tangential dissipation,  $\varepsilon_t = 1$  ;

**Case II**, Maximum Tangential dissipation,  $\varepsilon_t = 0.1$ ;

**Case III**, Minimal normal dissipation,  $\varepsilon_n = 0.9$ .

If the dissipative regime of the structure factor has common valued fractal dimension for all three cases then we expect the same to hold true for all other combinations of dissipation.

In all cases we simulate systems of a moderate density such that the packing fraction is chosen to be  $\phi = 0.530$ . The system size is chosen such that it is either  $L = 0.2m$ ,  $0.4m$  or  $0.8m$  and the corresponding particle populations are either 3000, 12000 or 48000 respectively. For most coefficients of restitution the choice of size is sufficient that the dissipative regime of  $S(k)$  is visible for at least one size of  $L$ .

We now discuss the different dissipation cases in more detail. Case I produces systems where the dissipation extent is comparable with previous published works. Colliding particles dissipate energy due to their velocity becoming slightly correlated normally to the direction of collision. The quantity of energy that can be lost by the collision is restricted because the collision does not affect the magnitude of the velocities tangential to the collision. As a result a pair of colliding particles can never become totally correlated. We can introduce further energy loss by allowing tangential dissipation during collision, as is done in Case II and III. Case II maximises tangential dissipation by using a very low coefficient of tangential restitution of fixed value 0.1

whilst the normal coefficient of restitution is allowed to vary. When both normal and tangential coefficients of restitution are set to zero, maximum dissipation is achieved and pairs of particles become totally correlated (in velocity) at collision. Inelastic collapse is prevented by the random force de-correlating the particles. An alternative approach is given by Case III. Here the normal dissipation is kept to a minimum by using a high coefficient of normal restitution of fixed value 0.9 and instead the tangential coefficient of restitution is allowed vary. Again these colliding particles cannot become totally correlated as the little momentum is lost normal to collision.

In the following sections we calculate the fractal dimension  $D_f$  for the three dissipation cases.

### Case I, Systems where Dissipation is Normal to the Collision

In Case I, we simulate systems with a coefficient of normal restitution chosen in the range 0.9 to 0.1, whilst the coefficient of tangential restitution is kept at 1. The system scale is chosen such that  $L = 0.2\text{m}$ ,  $0.4\text{m}$  or  $0.8\text{m}$ . We measure the structure factor and best fit the dissipative regime to a power-law decay of equation 4.4 over the range of  $k < k'$ . The exponent of the power-law determines the fractal dimension  $D_f$ . The limit  $k'$  is chosen to be equal to  $k_D$ , when the system satisfies  $L_{Eff} < L$  or  $2k_D$  else. The following table tabulates the results, entries for systems where  $2\pi/L < 2k_D$  are omitted.

$\varepsilon_n$	$k_{Dd}$	$L_{Eff}$	$D_f(L = 0.2)$	$D_f(L = 0.4)$	$D_f(L = 0.8)$
0.2	0.162	0.32	$1.56 \pm 0.05$	<b><math>1.62 \pm 0.06</math></b>	<b><math>1.57 \pm 0.06</math></b>
0.3	0.154	0.34	$1.59 \pm 0.03$	<b><math>1.63 \pm 0.10</math></b>	<b><math>1.58 \pm 0.06</math></b>
0.4	0.142	0.37	$1.58 \pm 0.03$	<b><math>1.64 \pm 0.09</math></b>	<b><math>1.66 \pm 0.07</math></b>
0.5	0.127	0.42	N/A	$1.61 \pm 0.09$	<b><math>1.66 \pm 0.07</math></b>
0.6	0.108	0.49	N/A	N/A	<b><math>1.66 \pm 0.05</math></b>

Table 4.2: The measured values for  $D_f$  for systems with a fixed packing fraction of 0.530 and various dissipations in which  $\varepsilon_t$  is fixed at 1.0.

When the systems is too small in size, such that  $L < L_{Eff}$ , the estimated value of  $D_f$  is much too small resulting from the fitting over data points of  $S(k)$  that lie outside the dissipative regime and with  $k$  of  $k > k_D$ . By contrast, in sufficiently large systems (bold data values), where  $L > L_{Eff}$ , the measured value for the fractal dimension,  $D_f$ , is found to be in the range 1.57 to 1.66. We suggest that  $D_f$  may be considered

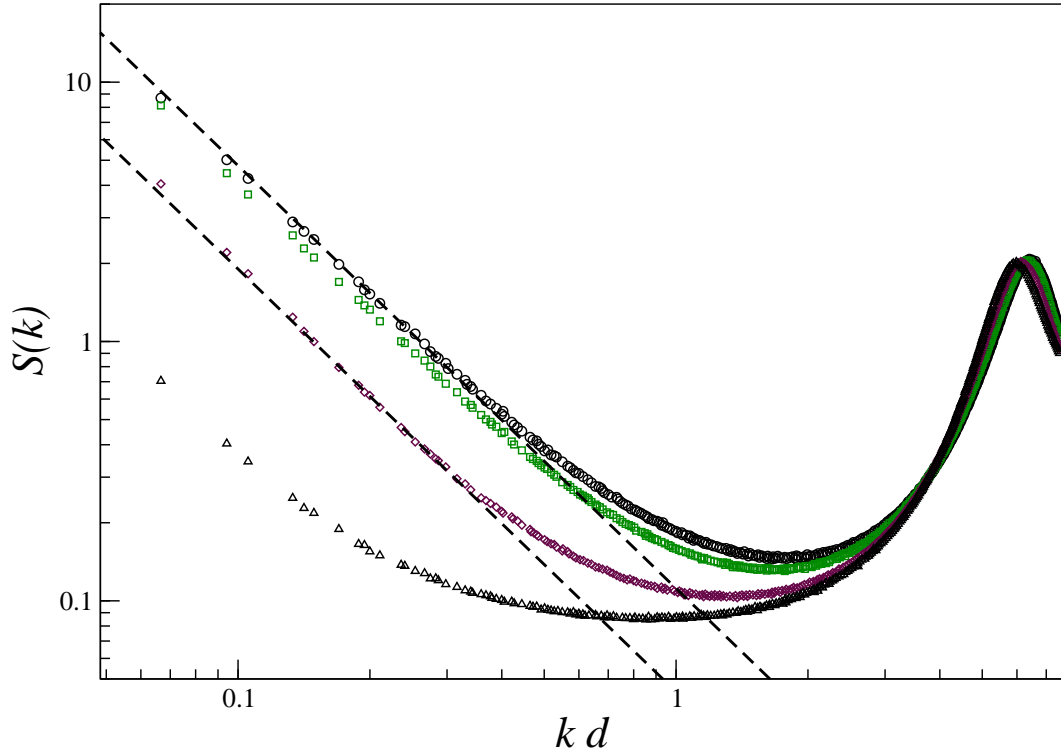


Fig. 4.3: Variation of structure factor for a system with fixed packing fraction and tangential coefficient of restitution 1. The four data sets represent different extents of normal dissipation such that  $\varepsilon_n = 0.2$  (circle);  $\varepsilon_n = 0.4$  (square);  $\varepsilon_n = 0.6$  (diamond);  $\varepsilon_n = 0.8$  (up-triangle). The dashed lines are power-law fits of  $Ak^{-1.63}$ .

approximately constant within the level of accuracy achieved here for two reasons: one, no systematic trend in values is seen with respect to coefficient of normal restitution or size of system (when  $L > L_{Eff}$ ); two, the variation in value of  $D_f$  is of order, or less than, that of any tolerance error of an individual measurement so cannot be distinguished from fitting limitations.

The measurement of  $D_f$  becomes increasingly difficult as higher coefficients of normal restitution are considered. For systems of packing fraction 0.530 measurement of  $D_f$  for lower dissipations than  $\varepsilon_n = 0.6$  can not be made without using a system size larger than  $L = 0.8$ . It is beyond the scope of this thesis to measure such systems as increasing the system size further, to even say  $L = 1.0m$ , requires simulation of at least 75,000 particles which is computationally very demanding. We are left to conjecture that the estimated value for  $D_f$  will continue to remain within the range 1.57 to 1.66 for higher coefficients of restitution, beyond that accurately measured here, as long as  $L > L_{Eff}$ .

We now demonstrate for a system of length 0.4m and particle population is 12000 that the dissipative regime of the structure factor is indeed described by power-laws

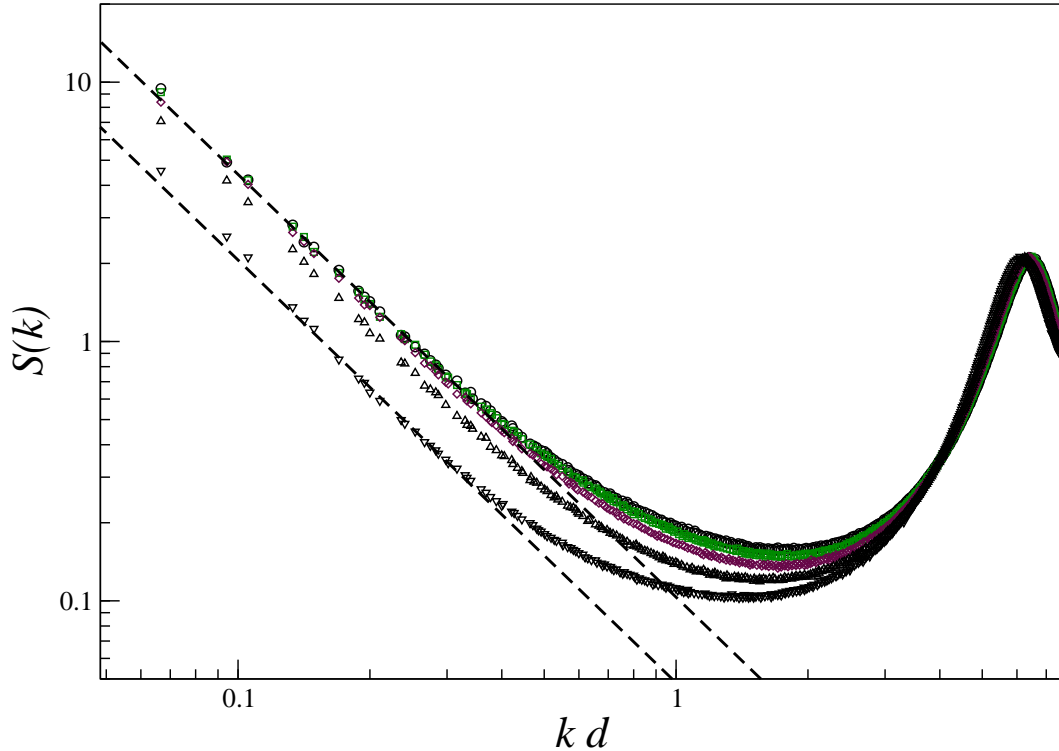


Fig. 4.4: Variation of structure factor for a system with fixed packing fraction and tangential coefficient of restitution 0.1. The five data sets represent different extents of normal dissipation such that  $\varepsilon_n = 0.1$  (circle);  $\varepsilon_n = 0.3$  (square);  $\varepsilon_n = 0.5$  (diamond);  $\varepsilon_n = 0.7$  (up-triangle) and  $\varepsilon_n = 0.9$  (down-triangle). The dashed lines are power-law fits of  $Ak^{-1.63}$ .

of fixed fractal dimension  $D_f$ . Figure 4.3 shows the structure factor for a range of coefficients of normal restitutions. As the coefficient of normal restitution increases the region of  $S(k)$  considered to be within the dissipative regime and approximately a power-law decay reduces in correspondence with the reduction of value of  $k_D$ .  $S(k)$  exhibits no observable power-law decay for the system where  $\varepsilon_n = 0.8$ . For the remaining systems (where  $\varepsilon_n$  is 0.6, 0.4 or 0.2) the dissipative regime of the structure factor can be fitted by power-law decays of  $Ak^{-1.63}$ , shown on figure as dashed lines, which demonstrates that good agreement is achieved between power-law and  $S(k)$  when a constant value for the fractal dimension is chosen.

### Case II and III, Systems with Dissipation in both Directions

We now allow colliding particles to dissipate energy tangentially to the collision. Such particles are contained in systems that obey dissipation of Case II or III. We demonstrate that the dissipative regime of the structure factor are consistent with there being a single value for the fractal dimension  $D_f$ . No detailed determination of  $D_f$  are carried out. Instead data of the structure factor is fitted to by a power-law decay using the

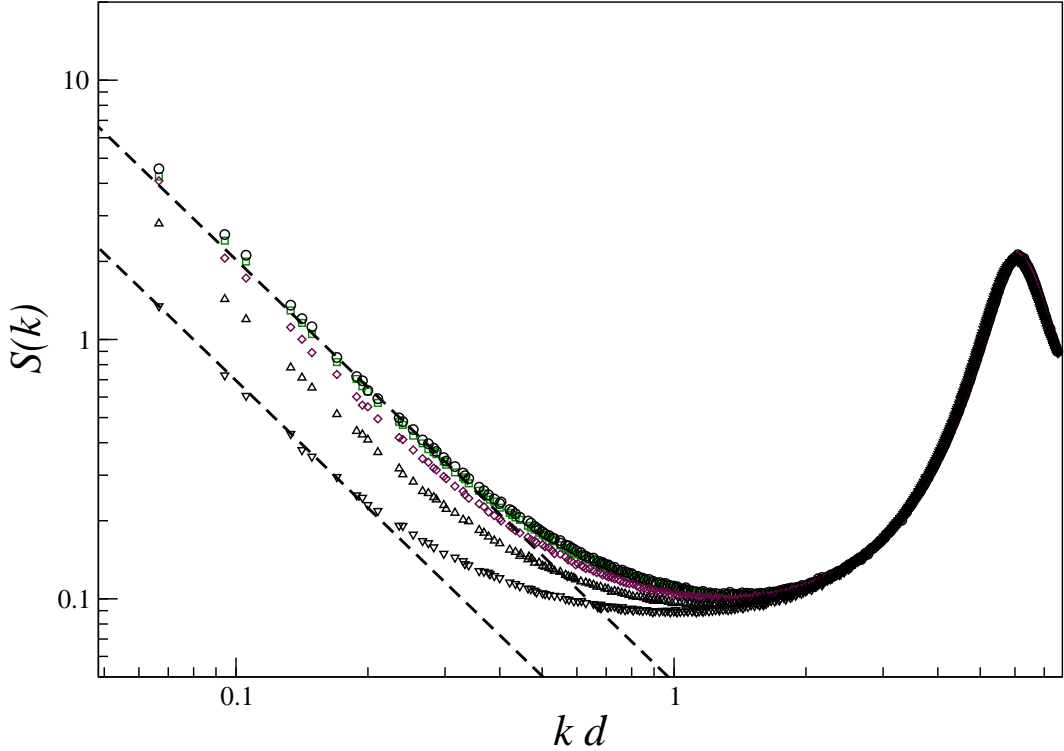


Fig. 4.5: Variation of structure factor for a system with fixed packing fraction and normal coefficient of restitution 0.9. The five data sets represent different extents of tangential dissipation such that  $\varepsilon_t = 0.1$  (circle);  $\varepsilon_t = 0.3$  (square);  $\varepsilon_t = 0.5$  (diamond);  $\varepsilon_t = 0.7$  (up-triangle) and  $\varepsilon_t = 0.9$  (down-triangle). The dashed lines are power-law fits of  $Ak^{-1.63}$ .

same value for  $D_f$  as previously determined from data of Case I. We use systems of a fixed size containing 12000 particles and width  $L = 0.4m$ .

We first study Case II dissipating systems. The systems are chosen to dissipate with a coefficient of normal restitution picked from the range 0.9 to 0.1 whilst the coefficient of tangential restitution is kept fixed at 0.1. In these systems particles in collision separate normally to the collision with little tangential motion relative to one another. The chance of re-collision is high for moderate to high dissipation values of  $\varepsilon_n$ .

Figure 4.4 shows the structure factor for a range of coefficients of normal restitution. The size of the system is sufficient that the dissipative regime can always be observed whereas the upper limit of  $k$  (given by approximately  $k_D$ ) obeys  $k_D d > 0.167$  (determined when  $\varepsilon_n = 1$ ). We find that within the dissipative regime these structure factors are well approximated by power-law functions of  $D_f \simeq 1.63$ , which we show in the figure as dashed lines.

Remarkably these power-law fits are as good an approximation for the dissipative regime of  $S(k)$  in moderate dissipation systems represented by  $\varepsilon_n = 0.9$  as for highly

dissipative systems represented by  $\varepsilon_n = 0.1$ . The statement adds weight to the conjecture that  $D_f$  is approximately independent of dissipation.

We now study Case III dissipating systems and find that the the same picture emerges. Here the systems have coefficients of normal dissipation fixed at  $\varepsilon_n = 0.9$  whilst tangential dissipation is chosen from  $\varepsilon_t = 0.9$  to  $\varepsilon_t = 0.1$ .

Figure 4.5 shows the structure factor for a range of tangential restitutions. Again we find that the dissipative regime of  $S(k)$  can be well described by power-law functions where  $D_f \simeq 1.63$ . Examples are shown by dashed-lines in the figure.

Thus we make the following conclusions about the effect of dissipation on the structure factor: one, the fractal dimension which characterises the dissipative regime of the structure factor has a constant value independent of extent of dissipation; two, the range of  $k$  that lies within the dissipative regime increases as the coefficients of restitution become smaller.

#### 4.1.4 Stability with Respect to Packing Fraction

Finally, we consider the effect of the packing fraction on the fractal dimension,  $D_f$ . We choose systems of moderate dissipation  $\varepsilon_n = 0.4$  and no tangential dissipation. We ensure that the dissipative regime of  $S(k)$  is observable at systems sizes that can be practically simulated by choosing packing fractions that avoid being very dilute. Instead we study packing fraction from  $\phi = 0.353$  to just above the crystalline limit with  $\phi = 0.795$ . The range of packing fractions is sufficiently broad and we believe that no additional effects are seen for lower packing fractions as no structural change in phase is known for packing fractions below 0.353. Instead only the range of  $k$  which  $S(k)$  can be considered to be in the dissipative regime changes as the mean free path of particles increases inversely with packing fraction.

Figure 4.6 shows the obtained structure factors for systems with a packing fraction in the range 0.353 to 0.795 and system size of  $L = 0.4m$ . As the packing fraction increases the large  $k$  oscillations of  $S(k)$  increases in amplitude corresponding to tighter clustering between neighbouring particle as the unoccupied area of the system reduces. When the packing fraction is beneath the crystallisation packing fraction  $\phi_c = 0.719$ , the range of  $k$  that lies within the dissipative regime of  $S(k)$  proportionally increases with packing fraction. These structure factors have dissipative regimes that can be fitted with a power-law decays of fixed exponent  $D_f$  consistent with that shown in

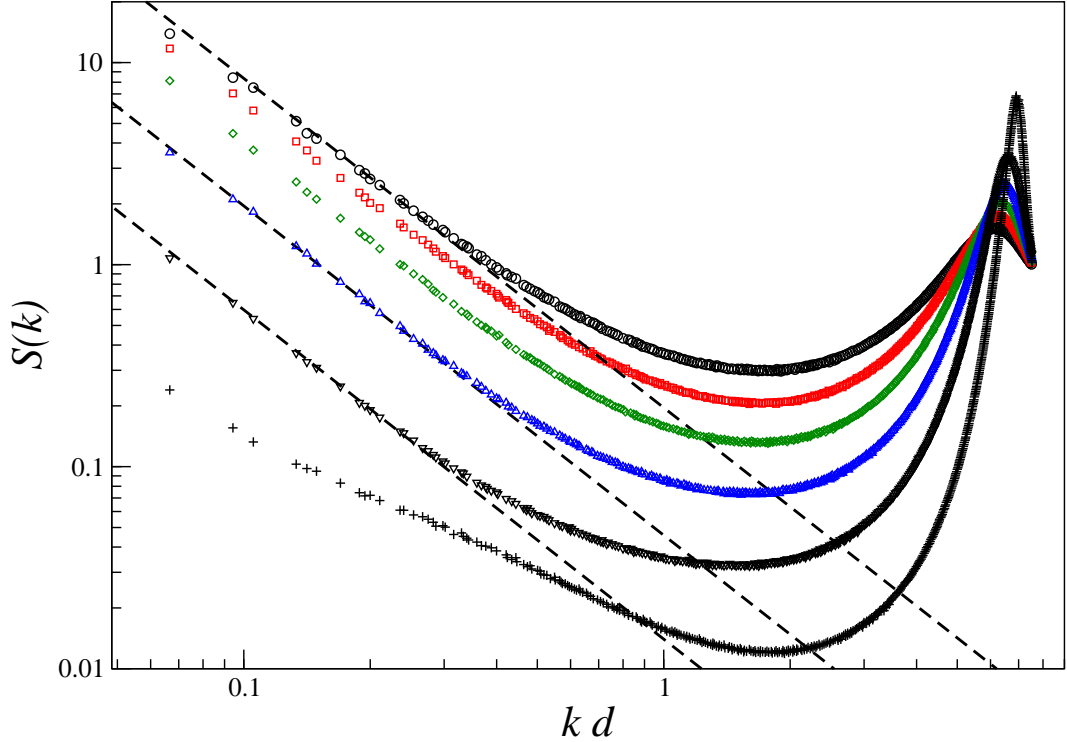


Fig. 4.6: Variation of structure factor for a system with fixed dissipation,  $\varepsilon_n = 0.4$  and  $\varepsilon_t = 1.0$  but varying packing fraction such that  $\phi = 0.353$  (circle);  $\phi = 0.442$  (square);  $\phi = 0.530$  (diamond);  $\phi = 0.619$  (up-triangle);  $\phi = 0.707$  (down-triangle) and  $\phi = 0.795$  (cross). The dashed lines are power-law fits of  $\sim k^{-1.63}$ .

previous sections, examples of which are shown by the dashed lines in figure 4.6.

The behaviour of the structure factor changes once the packing fraction exceeds the liquid-crystalline phase transition ( $\phi_c = 0.719$ ) as seen by the data for  $\phi = 0.795$ . Here the large-scale oscillations spike, signifying that large numbers of particles are packed as crystals. Similarly the small  $k$  behaviour of the structure factor changes and power-law decay does not seem to occur.

We next calculate estimates for the fractal dimension,  $D_f$ , for the range packing fractions shown in the figure 4.6 and three system sizes,  $L = 0.2m, 0.4m$  or  $0.8m$ . The upper limit for the dissipative regime,  $k'$ , is chosen to be equal to  $k_D$ , when the system size is such that  $L > L_{Eff}$  or  $2k_D$  else. The table tabulates the measured values of  $D_f$ :

When the system has both a packing fraction beneath crystallisation and a system size where  $L > L_{Eff}$  then the fractal dimension  $D_f$  is measured to lie in the range 1.60-1.66. The value of  $D_f$  is sufficiently similar (to within fitting error) across a range of packing fractions that it can be considered to be approximately constant with any variation weak beyond the accuracy of the data.

$\phi$	$k_D d$	$L_{Eff}$	$D_f(L = 0.2)$	$D_f(L = 0.4)$	$D_f(L = 0.8)$
0.353	0.095	0.56	N/A	$1.53 \pm 0.11$	<b><math>1.54 \pm 0.27</math></b>
0.442	0.118	0.45	$1.54 \pm 0.24$	$1.57 \pm 0.08$	<b><math>1.56 \pm 0.14</math></b>
0.530	0.142	0.38	$1.58 \pm 0.03$	<b><math>1.64 \pm 0.09</math></b>	<b><math>1.66 \pm 0.07</math></b>
0.619	0.166	0.32	$1.57 \pm 0.04$	<b><math>1.62 \pm 0.05</math></b>	<b><math>1.66 \pm 0.07</math></b>
0.707	0.189	0.29	$1.44 \pm 0.09$	<b><math>1.64 \pm 0.04</math></b>	<b><math>1.65 \pm 0.03</math></b>
0.795	0.213	0.25	$0.97 \pm 0.04$	$1.04 \pm 0.07$	$1.05 \pm 0.05$

Table 4.3: The measure values of  $D_f$  for systems with a moderate fixed dissipation in which  $\varepsilon_n = 0.4$  and  $\varepsilon_t = 1.0$  and various packing fractions.

When the packing fraction exceeds the point of crystallisation, such as shown by  $\phi = 0.795$ , the structure of the system changes and the measured  $D_f$  drops to 1. However it is uncertain if structure factors in the crystal limit have a power-law dissipative region as particle mobility is severely restricted.

#### 4.1.5 Brief Summary on Structure

We now give a brief summary of the structural properties of the two dimensional Random Force Model. The structure factor has small  $k$  behaviour, called the dissipative regime, that is described by a power-law decay. By choosing values of  $k$  less than  $k_D$  we ensure that we consider only  $S(k)$  that lies within the dissipative regime. Consequently systems must be of size  $L > L_{min}$  before the dissipative regime can be observed and systems that are smaller can be considered to show strong finite size effects. The fractal dimension,  $D_f$ , determines the exponent of the power-law decay through equation 4.4. We conclude, over the range of systems seen, that the fractal dimension of the large-scale structure is both largely invariant to the extent of dissipation and the extent of density when the packing fraction is below the point of crystallisation. We conjecture that it continues to hold true for packing fractions below 0.353. We conclude that in general  $D_f$  takes a value in the range  $1.63 \pm 0.03$ . Any variation seen in the value of  $D_f$  is very weak and is masked by the fitting uncertainty.

## 4.2 Implications on Real Space Structure

It is now clear, from our studies describing the structure factor, that the Random Force Model has  $k$ -space structural properties that are statistically fractal for small  $k$ .

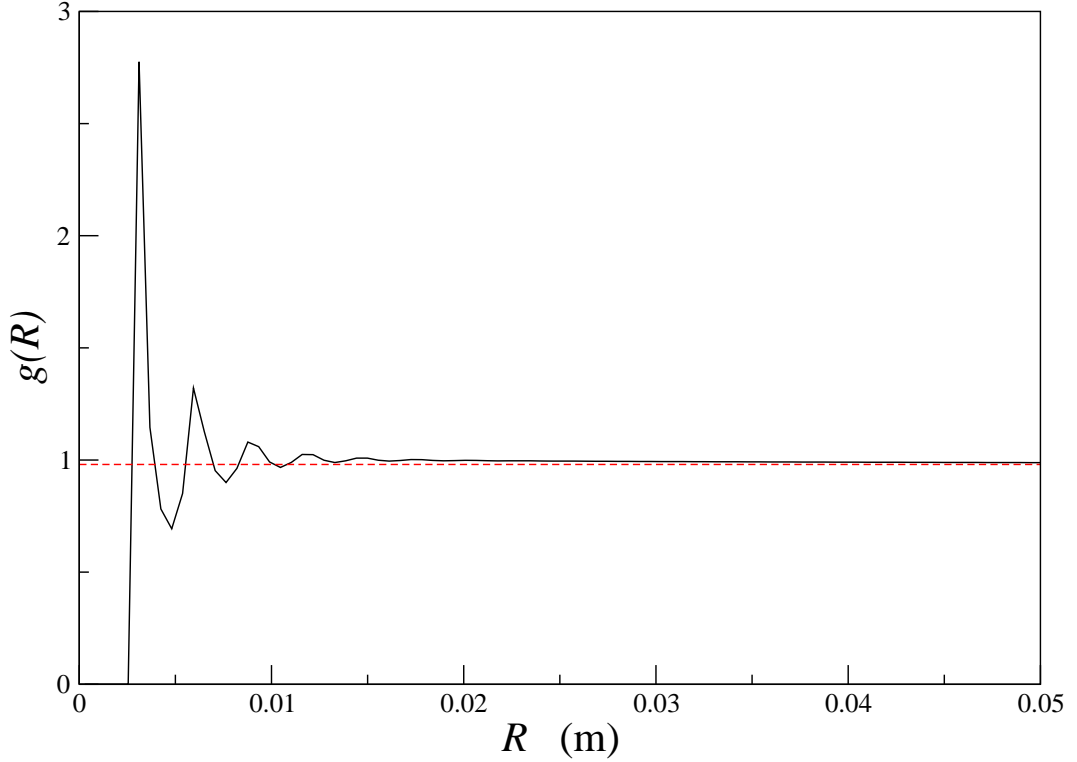


Fig. 4.7: The spatial correlation function for a system with a packing fraction of 0.530, system size  $L = 0.4\text{m}$  and dissipation  $\varepsilon_n = \varepsilon_t = 0.1$ . The dashed line is a constant fit of 0.98.

Nonetheless, it is not trivial how this relates back to the real-space occupied by the particles. From the fractal nature of  $S(k)$  we can infer that the system is inhomogeneous. Consequently we would like to know: what this tells us about the arrangement of the particles within the system?

Another standard measure of a systems structural behaviour is given by the angular average spatial correlation function,  $g(R)$ . It describes the time-average probability of finding a particle a distance  $R$  away from another other particle. During simulation  $g(R)$  is calculated using the following:

$$g(R) = \frac{2L^2}{2\pi RN^2} \left\langle \sum_{i=1}^N \sum_{j=i+1}^N \delta(R - R_{ij}) \right\rangle, \quad (4.10)$$

where  $R_{ij}$  is the separation distance between particle  $i$  and  $j$  at time  $t$  given by

$$R_{ij} = |\mathbf{r}_i(t) - \mathbf{r}_j(t)|.$$

Figure 4.7 shows the typical form of  $g(R)$  obtained from simulation. For small distance the spatial correlation oscillates with sharp peaks occurring at distances corresponding to particles in contact. The exact values of these peaks infer the extent of clustering occurring within the system.

The large distance behaviour of  $g(R)$  tells us about how homogeneous the system

is: a system that is truly homogeneous has a spatial correlation function that is flat and constant, equal to one; a system that is inhomogeneous has a spatial correlation function that decays towards a constant. The distributions of  $S(k)$  suggest the two-dimensional Random Force Model is inhomogeneous but, as figure 4.7 demonstrates, this is difficult to distinguish from the form of  $g(R)$  which weakly decays, for large distance  $R$  such that  $g(R)$  appears nearly constant when compared to either the peak value or the asymptotic value. Furthermore, the range of  $R$  is limited to  $R < L/2$  as larger  $R$  is strongly influenced by the periodic nature of the system boundaries. This all means that it is very difficult to reliably measure the decay in  $g(R)$ . We cannot be sure of the value that  $g(R)$  tends to for large  $R$  as it need not be one and appears to be affected by the finite size of the system.

Instead we use the behaviour of the structure factor to infer the large  $R$  behaviour of  $g(R)$ . Let us begin by making the simple hypothesis that  $g(R)$  approximately decays towards one, for large  $R$ , by the simple form:

$$g(R) = 1 + AR^{-\gamma}, \quad (4.11)$$

where  $\gamma$  is a fixed undetermined exponent and  $A$  a fixed constant specific to the system.

The angular average spatial correlation function is related to the angular average structure factor,  $S(k)$ , by the relation (Chaikin and Lubensky 1995):

$$\begin{aligned} S(k) &= 1 + \frac{N}{L^2} \int (g(R) - 1) \int_0^{2\pi} \exp(-ikR \cos(\theta)) d\theta R dR \\ &= 1 + 2\pi \frac{N}{L^2} \int (g(R) - 1) J_0(kR) r dR, \end{aligned} \quad (4.12)$$

where the lower expression of identity 4.12 is obtained by using a zero-order Hankel transform such that  $J_0(x)$  is a Bessel function.  $k$ -space is related to real-space by  $k = 2\pi/R$  and thus the large  $r$  behaviour of  $g(R)$  corresponds with the small  $k$  behaviour of  $S(k)$ . If for large distance  $g(R)$  obeys the hypothesis of relation 4.11 then, using identity 4.12, we can determine the implication this has on the small  $k$  behaviour of the structure factor. Thus for small  $k$  the structure factor is given by the integral:

$$\begin{aligned} S(k) - 1 &\approx \frac{2\pi N}{L^2} \int AR^{-\gamma} J_0(kR) R dR \\ &\approx \frac{2\pi N}{L^2} \int A \frac{z^{-\gamma}}{k^{-\gamma}} J_0(z) \frac{z dz}{k^2} \\ &\approx A' k^{\gamma-2}, \end{aligned} \quad (4.13)$$

where  $z$  is used as a substitution variable defined as  $z = kR$  and  $A'$  is a constant of the system. At small  $k$  the structure factor has a value much bigger than one and so  $S(k)$

is predicted to behave approximately as a power-law. This of course is only consistent if  $\gamma$  is related to the fractal dimensional  $D_f$  by  $\gamma = 2 - D_f$ . Therefore the large  $R$  behaviour of  $g(R)$  is approximately given by:

$$g(R) = 1 + AR^{D_f-2}. \quad (4.14)$$

It should be noted that the  $g(R)$  dependence on  $R$  is not affected by choosing  $g(R)$  to tend to some other value. In such case  $S(k)$  of equation 4.13 is described with an additional delta function term that contribute only for  $k = 0$  where  $S(k)$  is singular.

We are now interested in studying the local environment around a particle as it is this that most affects a particles behaviour.

The average number of particles found within a distance  $R$  from a particular particle,  $C(R)$ , is given by :

$$C(R) \propto 2\pi \int_0^R g(R') R' dR'. \quad (4.15)$$

The relation above implies that for large distance  $C(R)$  is given by:

$$C(R) \sim \frac{2\pi A'}{D_f} R^{D_f} + \pi R^2. \quad (4.16)$$

Hence the average number of particles found within a distance  $R$  scales normally with distance, for large  $R$  (as the  $R^2$  term of  $C(R)$  dominates), and not as a fractal. Nonetheless it is not the average particle that leads to the anomalous properties of the system but rather those particles that find themselves in locally dilute regions of the system. It is the number of particles found within a distance  $R$  around these anomalous particles,  $n(R)$ , that can be shown to be fractal.

We can obtain the anomalous behaviour of the system by subtracting off the mean field behaviour, such that  $n(R)$  is given by:

$$n(R) = C(R) - \bar{n} \sim A'' R^{D_f}, \quad (4.17)$$

where  $\bar{n}$  is the expected mean field behaviour if the system was homogeneous, which goes as  $\bar{n} \sim R^2$ , and  $A''$  a constant of the system. This anomalous behaviour can be thought to be associated with particles found in dilute regions as the local density can drop many orders beneath that suggested by the system's packing fraction. In comparison, the local density cannot increase as much above the average density and particles within these regions are near-uniformly distributed.

Thus we arrive at the conclusion that the large-scale structure around particles in low dense regions is fractal. With this new measure we are now open to discuss the effect that the fractal structure has on the motion of an individual particle.

### 4.3 The Distribution of Free Paths

We are now interested in understanding how these structural behaviours affect the motion of the individual particles in the system. We ask the question: what influence does the fractal structure have on the behaviour of individual particles? In the system each particle is surrounded by a local environment consisting of other particles and unoccupied *free* volume. If the particles are arranged in a fractal structure then it is natural to invert this idea and suggest that the unoccupied regions of the system are also fractally sized. Between collision particles move through the unoccupied space and temporarily behave independently of the other particles. The larger the unoccupied space around each particle the further it will travel before collision and hence the more uncorrelated its motion becomes with respect to other particles. This in turn would be expected to strongly affect the behaviour of the velocity properties of the system. Therefore we propose to study the overall distance travelled by particles between collision as a first step to understanding the behaviour of other properties of individual particles in the system. This is different to the approach taken in one dimensions where we were able to measure the separation distance between nearest neighbours.

The free path of a particle,  $l_i$ , is defined as the effective change in the position of the particle between two consecutive collisions:

$$l_i = |\mathbf{r}_i(\tau + t_0) - \mathbf{r}_i(t_0)|, \quad (4.18)$$

where  $\mathbf{r}_i(t)$  is the  $i^{\text{th}}$  particle's position at time  $t$ ,  $t_0$  is the initial time just after the previous collision and  $\tau$  is the time between successive collisions.

The distribution of free paths,  $P_l(l)$ , is defined to be the probability that a particle has travelled a free path  $l$  upon arrival at the next collision. We measure the free path distribution for a range of systems sizes. For simplicity we choose only highly dissipative systems, where  $\varepsilon_n = \varepsilon_t = 0.1$ , in order to maximise the length of the long distance tail which is characterised by particles whose motion is dominated by the random noise. We expect similar shaped long distance tails to be present in lower dissipative systems, but these will begin at progressively longer length scales as the dissipation decreases. The free path distribution, as with the structure factor, is also affected by the finite size of the system. We measure the free path distribution and find that for all systems, once the system is of sufficient size that finite size effects become irrelevant, the long distance tail is describes by the same shape. This shape can be predicted by the theory of Isliker and Vlahos (2003), using solely the fact that the large-scale structure of the

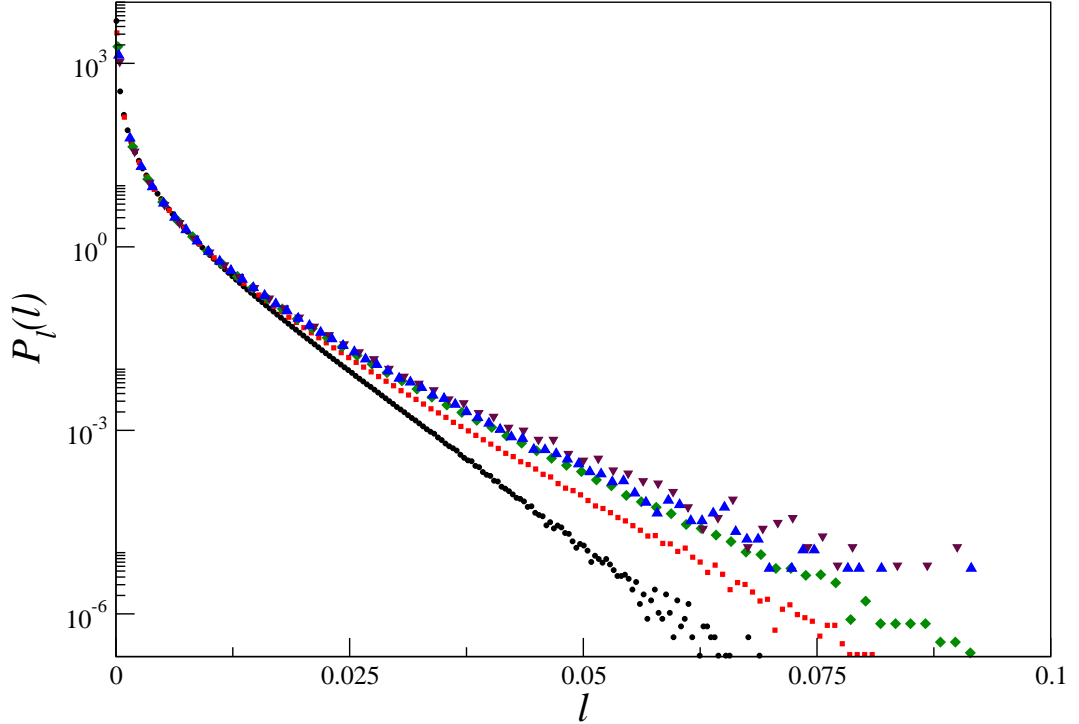


Fig. 4.8: The free path distribution for a system with fixed density of 0.353. The data sets are for combinations of particle number and system size such that  $N = 500, L = 0.1\text{m}$  (circle);  $N = 2000, L = 0.2\text{m}$  (square);  $N = 8000, L = 0.4\text{m}$  (diamond);  $N = 18000, L = 0.6\text{m}$  (up-triangle) and  $N = 32000, L = 0.8\text{m}$  (down-triangle).

system is fractal. We find that this prediction matches the data over a large number of decades and we determine the same value for  $D_f$  by fitting the free path distribution as was measured directly for the structure factor.

### 4.3.1 Finite Size Effects

Before we progress to predicting the shape of the free path distribution we must ensure that the systems we study are sufficiently large that they do not exhibit any strong finite size effects that might impeded the formation of true long distance behaviour. In this section we determine the minimum system size in which the free path distribution stops exhibiting large finite size effects and find that the system must be much larger than that required to see the power-law decay in the structure factor. The system is expected to exhibit strong finite size effect when the system is either of insufficient size that fractal structure is not observed or comparable in size to the length-scale,  $2\pi/k_D$ , which defines when structural features can be treated as fractal.

We simulate the two-dimensional Random Force Model for a system with packing fraction of 0.353 and dissipation  $\varepsilon_n = \varepsilon_t = 0.1$ . The size of the system is varied from

$L = 0.1\text{m}$  to  $L = 0.8\text{m}$  and we plot the free path distributions in figure 4.8. As the size of the system increases it becomes more likely that a particle will travel a long distance before colliding and is exhibited in the free path distribution by the long distance tail becoming shallower. For this example packing fraction, we find that once the system is larger than  $L_c \approx 0.4\text{m}$  notable change in shape of  $P_l(l)$  ceases and implies that finite size effects play only a minor role in larger systems. Significantly, we find that the minimum system size at which finite size effects become irrelevant,  $L_c$ , is much larger than that required to observe the power-law decay in the structure factor, where  $L_{min}$  is calculated to be only  $0.085\text{m}$ . Hence we should ensure that we use only systems where  $L \geq L_c \gg L_{min}$ , say  $L_c \approx 5L_{min}$ , to avoid large deviation in the form of  $P_l(l)$  due to finite size effects.

### 4.3.2 Estimating the long distance tail of $P_l(l)$

We are now ready to attempt to describe the free path distribution using theory. We begin with knowledge of two properties of these systems: the large-scale environment of particles is distributed as a fractal; on average a particle increases its velocity with distance from collision. We based our approach of determining the free path distribution on the methods employed in the paper of Isliker and Vlahos (2003). In this paper the system is made up of background particles arranged in a static three-dimensional fractal of dimension  $d_f$ . Particles detach from the fractal background and move ballistically until collision with another particle within the fractal.

It requires a little thought to understand the relevance of Isliker and Vlahos work to the two-dimensional Random Force Model. Statistically it is those particles which achieve the highest velocity during a walk between collision that move the furthest. In comparison, the remaining particles in the system act as background, where their velocity is so low, compared to the fast particles, that the change in position of these particles is insignificant compared to the free path of the fast particle. Thus, the high velocity particles effectively see their environment as a static fractal background.

It should be noted that these arguments only apply to the extremely high velocity particles that consequently travel a large distance. Therefore it is expected that only the high distance tail of the free path distribution of the Random Force Model will converge with that obtained for a particle undergoing a random walk through a fractal environment.

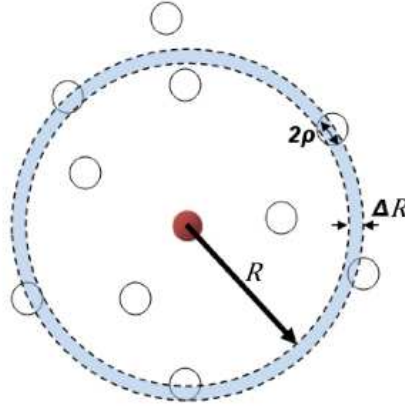


Fig. 4.9: Pictorial representation of a fast particle moving a radial distance  $r$  and colliding within the highlighted circular shell

We now sketch out the derivation of the free path distribution in two dimensions following the arguments laid out by Isliker and Vlahos. The system has a background of particles arranged in a fractal with dimension  $D_f$ . The fractal dimension  $D_f$  is the same as that found for the small  $k$  power-law decay of the structure factor. The number of particles found within a circle of radius  $R$ , around a point  $x$ , is expected to be:

$$n(R) = A \left( \frac{R}{\delta_*} \right)^{D_f}, \quad (4.19)$$

where  $\delta_*$  is the most probable value of the nearest neighbour distance. The number of particles found in a circular shell,  $m(R) \Delta R$ , of radial thickness  $\Delta R$  around point  $x$  is given as:

$$m(R) \Delta R = \frac{d}{dR} n(R) \Delta R = A \frac{D_f}{\delta_*} \left( \frac{R}{\delta_*} \right)^{D_f-1} \Delta R. \quad (4.20)$$

A fast particle starts at position  $x$  and travels radially a distance  $R$  in a random direction. A pictorial representation is shown in figure 4.9. In the Random Force Model high velocity particles approximately travel ballistically, with the random force providing only minor alterations to the course. The probability of the particle,  $q_R \Delta R$ , hitting a background particle in the circular shell  $R$  to  $R + \Delta R$  is given by the ratio of the total occupied length of the shell divided by the circumference of the shell:

$$q_R \Delta R = m(R) \Delta R \frac{2\rho}{2\pi R} = A \frac{D_f \rho}{\pi \delta_*^2} \left( \frac{R}{\delta_*} \right)^{D_f-2} \Delta R, \quad (4.21)$$

where  $\rho$  is the cross-sectional radius of an interaction between fast particle and background particle.

The probability of a particle,  $p_R \Delta R$ , moving freely for a distance  $R$  and then colliding with a background particle is given by the product of the probability of going

through  $n - 1$  shells, successively without colliding, multiplied by the probability of colliding in the  $n^{\text{th}}$  shell:

$$p_R \Delta R = \underbrace{\prod_{i=0}^{n-1} (1 - q_{R_i} \delta R)}_{\pi_R} q_R \delta R. \quad (4.22)$$

Each shell has a radial width  $\delta R$  and boundaries at radial distances  $R_i = i \delta R$  and  $R_{i+1} = (i + 1) \delta R$ . The product  $\pi_R$  can be re-written as:

$$\ln(\pi_R) \approx \int_0^R -q_{R'} dR', \quad (4.23)$$

using the identity  $\ln(1 + x) \approx x$  for  $x \ll 1$ . We solve the above integral and finally arrive at the solution for  $p_R \Delta R$ :

$$p_R \Delta R = \exp\left(-A \frac{D_f \rho}{(D_f - 1) \pi \delta_*^{D_f}} R^{D_f - 1}\right) \times A \frac{D_f \rho}{\pi \delta_*^2} \left(\frac{R}{\delta_*}\right)^{D_f - 2} \Delta R. \quad (4.24)$$

The distribution  $p_R$  is the distribution of free paths,  $P_l(l)$ , (where  $R$  is relabelled as  $l$ ) and we conclude that  $P_l(l)$  is of the form:

$$P_l(l) \simeq A_0 \exp(-Cl^{D_f - 1}) l^{D_f - 2}. \quad (4.25)$$

### 4.3.3 Comparison with data from the Random Force Model

In the last section we derived that the long distance tail of the free path distribution of the Random Force Model is described by the expression 4.25. We will now put this to the test and demonstrate that the proposed long distance shape of  $P_l(l)$  provides a suitable solution over a large number of decades to simulated data of the Random Force Model. Simulations are performed and the free path distribution calculated for two systems of size  $L = 0.6$ , high dissipation where coefficients of restitution are  $\varepsilon_n = \varepsilon_t = 0.1$  and packing fraction either of 0.353 or of 0.530. The exact choice of system parameters is irrelevant as long as: one, the system size is sufficient that the measured structure factor,  $S(k)$ , has an observable power-law decay; two, the statistics of the free path distribution are sufficiently accurate and precise that an asymptotically large free path can be seen. The above statements imply that decreasing either density or dissipation of the system means that both the size of the system and the precision of the free path distribution must increase.

We fit the expected free path distribution (equation 4.25) to the lowest decades of data from the Random Force Model, where  $P(v) < 1$ , and determine that the best fit is given when  $D_f$  has the value  $1.64 \pm 0.07$ , for packing fraction of 0.363 (fitted over four

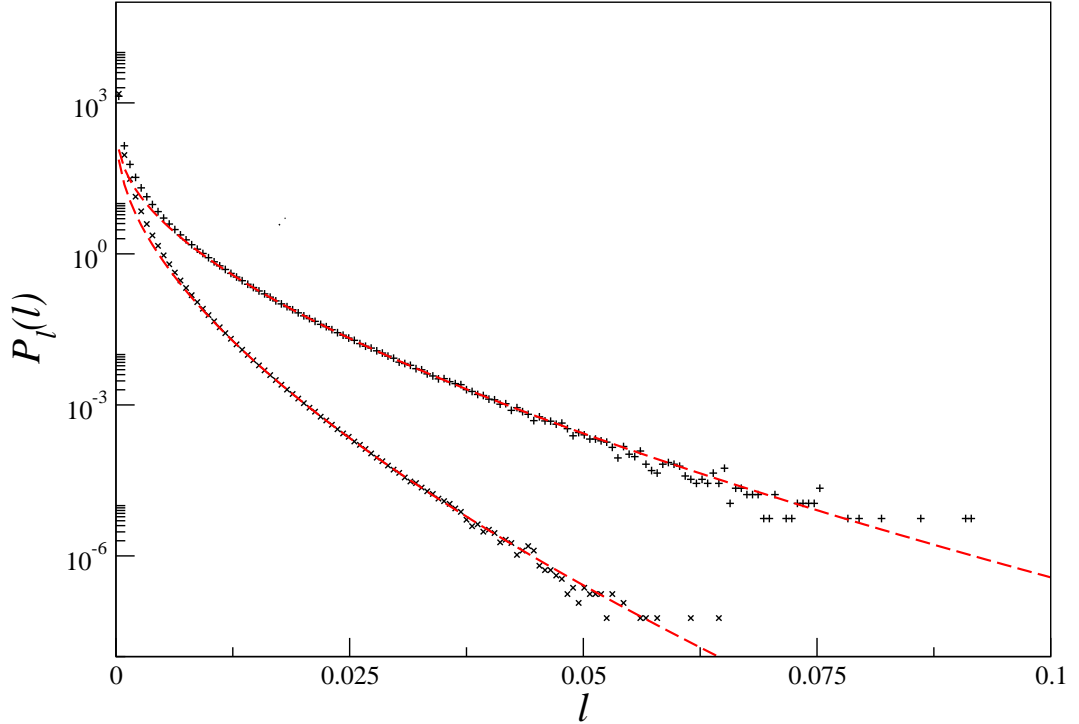


Fig. 4.10: Comparison between the free path distributions generated from the Random Force Model of packing fractions 0.353(plus) and 0.530 (cross), and the fit to equation 4.25 (dashed lines).

decades), or  $1.61 \pm 0.04$  (fitted over six decades), for packing fraction of 0.530. These values for  $D_f$  are very near to that measured for the equivalent structure factors where  $D_f$  is determined as  $1.66 \pm 0.09$  and  $1.60 \pm 0.03$  for the respective packing fractions.

Figure 4.10 show the free path distribution for the two packing fractions as data points. The dashed lines represent the best fit to equation 4.25 when  $D_f$  is chosen to be equal to 1.63. At large distance the fit and data converge over at least five decades, as expected. Therefore equation 4.25 is sufficient to describe the long distance tail of the free path distribution.

## 4.4 Summary

In this chapter we revisited a previously discussed question: what is the behaviour of the large-scale structure of the two-dimensional Random Force Model? We found that, for systems of sufficient size, the structure factor  $S(k)$ , at  $k$  within the dissipative regime, is always described by a power-law decay of the form  $S(k) = Ak^{-D_f}$ , where  $D_f$  is typically measured in the range 1.60 to 1.66. We find that the variation in value of  $D_f$  is very weak and not systematic suggesting that it can be treated as approximately constant within the accuracy of our results. This decaying power-law is the hallmark

of large-scale fractal structure, above that of the average behaviour, where no single characteristic length scale can be used to describe the structure. We argued that although the bulk of the system is distributed uniformly it is the fluctuations away from homogeneity, in the dilute regions of the system, that is of most interest where particles are found fractally arranged.

We next discussed the effect of the fractal structure on particle behaviour. We measured the distribution of free paths, where the free path of a particle was define as the displacement made by a particle between consecutive collisions. We found that for systems of sufficient size, where finite size effects can be ignored, that the long distance tail of the free path distribution is effected by the large-scale fractal structure of the system and calculated it to be of the form:

$$P_l(l) \simeq A_0 \exp(-Cl^{D_f-1}) l^{D_f-2},$$

using the theory of Isliker and Vlahos (2003) whereby fast particles are treated as ballistic while other particles make up the fractal environment.

### **Connecting the Structure to the Velocity**

An important feature of the asymptotic shape of structure (long distance) is that it remains unchanged with respect to dissipation and packing fraction once the system is large enough that finite size effects can be ignored. Similarly in the next chapter we find that for moderate to high dissipation the asymptotic shape of the velocity distribution of these systems also remain unchanged with respect to dissipation. This suggest that it is possible to relate the structural properties to the velocity statistics. The high velocity particles of the systems are a result of the coupling of the structural inhomogeneity of the system and the random force: Particles undergo an accelerating walk between collisions but require a large amount of room to reach high velocity. Each particle can be thought of as a single particle wandering through a fractal background environment of other particles.

In the next chapter we introduce a two-dimensional Single Particle Model, which we use to create a self-consistent theory, where the fractal behaviour of the structure determines the asymptotic behaviour of the velocity statistics. We use this new model to conclusively decide whether the velocity distribution is either non-universal with respect to dissipation or if it is actually a crossover function ranging from Gaussian, for low velocity, to a fixed determinable anomalous shape, for high velocity.

## Chapter 5

# Velocity Properties of a Two-dimensional Random Force Model

Amongst the literature there is much confusion about the shape of the velocity distribution for the multi-dimensional Random Force Model. This results from the fact that it is difficult to measure the high velocity behaviour of particles within the system to sufficient accuracy and the lack of an appropriate kinetic theory to describe these systems. This chapter is about the measurement of the velocity distribution and the development of a theory that incorporates the structural features of the system.

We describe the velocity distribution of the two-dimensional Random Force Model and precede by using the standard approaches, applied by other research groups, in an attempt to determine the high velocity tail of the distribution. The complete velocity distributions is not described by any previously used granular kinetic theory. We further show that, when the system is of moderate to high dissipation and of sufficient size, all velocity distributions can be described by a stretched-exponential of fixed exponent. We conjecture that other systems will also have velocity distributions of the same asymptotic limit if better statistics could be obtained.

However caution must be applied when reading these results because the standard methods have significant drawbacks that bias the calculated stretched-exponential shape of the velocity distribution. In the second section we show how the high velocity tail of the distribution is generated through coupling the systems structural and velocity properties. It is the fractal structure that determines the shape of the high velocity tail of velocity distribution.

Instead of considering all  $N$  particles, we concentrate on the motion of one particle in the fractal environment provided by the remainder. We call this the Single Particle Model. When the fractal dimension of the environment is  $D_f = 1.63 \pm 0.03$  then the high velocity tail of the velocity distribution is approximately exponential. These results are shown to be consistent with the data of the Random Force Model.

## 5.1 Observations using Standard Methods

It is widely held that the velocity distribution  $P(v)$ , where  $v$  denotes a component of velocity, of the two-dimensional Random Force Model represents a crossover function that is Gaussian for low velocities and anomalous for high velocities. There is good reason to assume that the distribution does behave in this way as there are two extreme types of particles: those that are strongly influenced by post-collision velocity and consequently are slow moving; those that are strongly influenced by the random force and are fast moving with near-ballistic trajectories. For high velocities the distribution is assumed to be a stretched-exponential, but its exact shape is still contested in the literature. A prominent view (Moon, Shattuck, and Swift 2001) is that the high velocity tail of the distribution of the Random Force Model obeys  $P(v) \simeq A \exp(-B|v|^{3/2})$  as described by the granular kinetic theory of van Noije and Ernst (1998). However van Noije and Ernst assume that the system is homogeneous which requires us to ignore the structural behaviour of these systems, in particular strong inhomogeneities in the form of clustering. Consequently the relevance of van Noije and Ernst theory has been put into doubt (van Zon and MacKintosh 2004).

### Simple Scaling Moments

One major difference between the one-dimensional and two-dimensional Random Force Model is the behaviour of the  $m^{\text{th}}$  order moments of velocity,  $\langle |v|^m \rangle$ . In the one-dimensional case we found that the moments of velocity did not have expected scaling behaviour suggested by Williams and MacKintosh (1996). We would now like to repeat the mean field approach of Williams and MacKintosh for the two-dimensional case.

This involves deriving the equation of state for the two-dimensional Random Force Model and follows identical steps taken in section 3.1.1. The only changes that occur are in the derivation of the rate of the average loss of energy, which requires the inclusion of the tangential coefficient of restitution as well as the normal coefficient of restitution, and in the derivation of the average distance between collision, which we will now

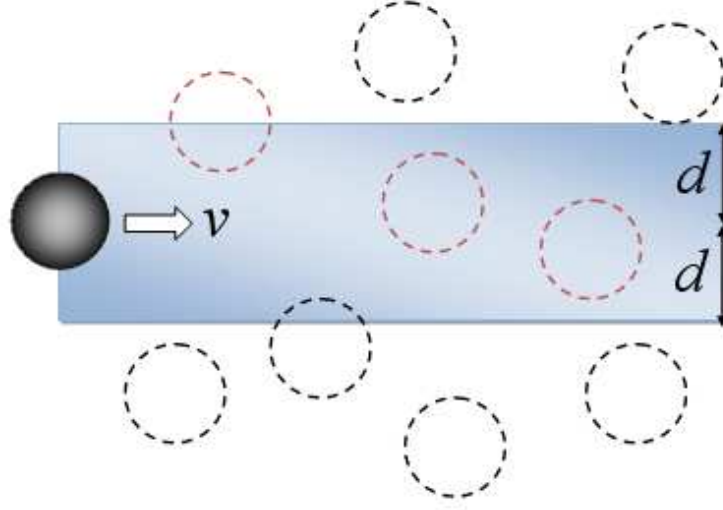


Fig. 5.1: A particle moving through the granular system. At any given time, only particles whose centre lies within the shaded rectangle have a chance of colliding with the particle.

describe. For a two dimensional system the average distance a particle travels before collision,  $l_0$ , is given by average separation of particles found along the path of a particle. Figure 5.1 shows a typical particle moving through the system.  $l_0$  is calculated as one over the product of the number density of the system,  $N/L^2$ , and the collision cross section  $2d$ , such that:

$$l_0 = \frac{L^2}{2dN} = \frac{\pi d}{8\phi}. \quad (5.1)$$

This leads to a equation of state for the two dimensional system of the form:

$$\langle |v| \rangle^3 = \frac{C_1}{\phi} \frac{Dd\pi}{M^2(2 - \varepsilon_n^2 - \varepsilon_t^2)}, \quad (5.2)$$

where  $\langle |v| \rangle$  is the mean velocity between collision and  $C_1$  is a numerical compensation constant used when assuming that  $\langle |v| \rangle^2 = C_1 \langle v^2 \rangle$ . We finally make the assumption that all the moments of the velocity scale in the same way so that the above expression can be written as  $\langle |v|^m \rangle^{3/m} \propto 1/\phi$ .

We now test this mean field theory prediction by measuring the moments of velocity for packing fractions ranging from very dilute  $\phi = 0.0014$  to very dense  $\phi = 0.84$ . In each case we keep the scale of the system fixed, with the system size either  $L = 0.2\text{m}$  or  $0.4\text{m}$ , and allow the population of particles to vary. Further increases in system size do not significantly change the findings. The dissipation of the system is chosen to be  $\varepsilon_n = \varepsilon_t = 0.1$ , such that any deviation from mean field approach is most strongly exhibited.

Figure 5.2 shows measurements of the 3rd, 6th, 9th and 12th moment of velocity as a function of packing fraction. For low packing fraction of less than 0.1 all measured

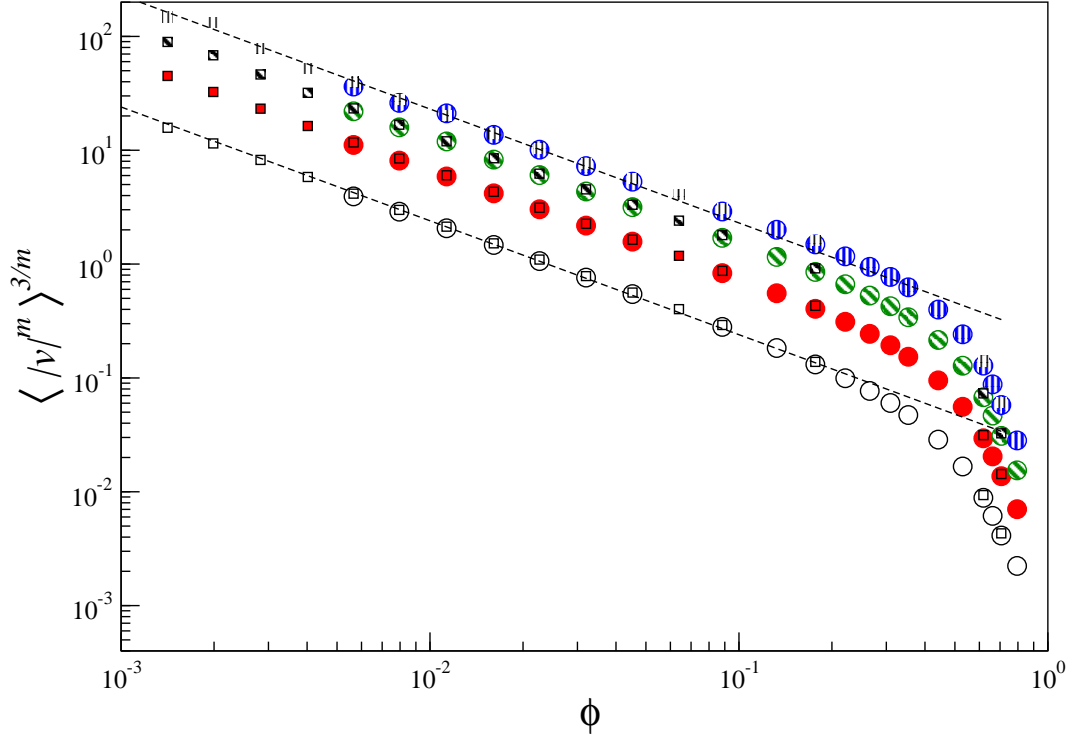


Fig. 5.2: The behaviour of the  $m^{\text{th}}$  order moment of velocity with respect to packing fraction,  $\phi$ . The different order moments are distinguished by different patterns and the figure shows the 3rd (unshaded) 6th (shaded), 9th (left slash lines) and 12th (vertical lines) moment of velocity whilst the different shapes demonstrate invariance towards system scale where  $L$  is either 0.2m (circle) or 0.4m (square). The dashed lines are power law fits of  $A/\phi$ .

orders of the moments of velocity obey the expected mean field prediction of:

$$\langle |v|^m \rangle^{3/m} \propto 1/\phi. \quad (5.3)$$

The low packing fraction systems exhibit this apparent simple scaling because these systems have velocity distributions dominated by the Gaussian peak such that the high velocity tail of the distribution occurs at very large velocity-scales.

For higher packing fractions the moments of the velocity distribution deviate away from the mean field prediction and a crossover in behaviour is observed. The moments of the velocity distribution must tend to zero as the system moves towards maximum packing and the particles become locked into place. Adjusting the size of the system does not significantly alter the measured value of the moments of the velocity distribution for a given packing fraction.

The complex nature of the moments of velocity, for moderate to high packing fraction, means that they do not provide good insight for understanding the behaviour of the velocity distribution. We are forced instead to study  $P(v)$  in its entirety.

### The Asymptotic Shape of the Velocity Distribution

The aim of this section is to determine the asymptotic shape of the velocity distribution using standard approaches to show that it is different to any shape previously suggested, particularly that proposed by van Noije and Ernst. We describe the shape of the velocity distributions and comment on the changing form as the coefficients of restitution or particle population is varied. Unlike previous studies we do not keep  $\varepsilon_t = 1.0$  and so are able to explore higher dissipative systems. The distribution of velocity is measured in simulation by methods described in appendix A. We demonstrate that asymptotic behaviour of the velocity distribution can be fitted with a stretched-exponential distribution of the form  $P(v) \sim \exp(-|v/v_0|^\alpha)$ , where the exponent  $\alpha$  is consistently much lower than that required for Maxwell-Boltzmann statistics,  $\alpha = 2$ . However we caution against taking too much from the exact value of  $\alpha$  measured as it is difficult to determine the correct asymptotic high velocity shape due to finite statistics and limitations of the fitting method and rather this value of  $\alpha$  should be viewed as an upper limit.

Nonetheless these methods of fitting are suitable to our needs and we vary the size of the system to show that changes in asymptotic shape due to packing fraction are removed when larger sized systems are studied. This leads us to the conclusion that the variations seen in high velocity shape due to packing fraction of fixed sized systems are only caused by finite size effects. Our investigation concludes by asking whether all these systems (regardless of dissipation extent) can be described by just one type of velocity distribution: a crossover distribution in which the behaviour crosses over from Gaussian for low velocities to anomalous with an exponent fixed in value for high velocities. This type of crossover distribution will be justified by theory later in this chapter.

#### 5.1.1 The Velocity Distribution for a Fixed System Size

We begin by discussing the general behaviour of the velocity distribution observed from the simulation of the two-dimensional Random Force Model. For simplicity we will consider only the case where the tangential coefficient of restitution equals that of the normal coefficient of restitution; in this case the fractional energy lost of each collision is the same regardless of orientation between the normal of the collision and the centre of velocity of the colliding particle pair.

**General Trend with Respect Dissipation**

We measure the velocity statistics for a range of dissipations. The density and size of the system are fixed at a moderate packing fraction of 0.530 and system size of  $L = 0.2\text{m}$ . Figure 5.3 shows the velocity probability distribution for a spectrum of coefficients of restitution ranging from  $\varepsilon_n = \varepsilon_t = 0.1$  to 0.9. The shown distribution  $P'(v)$  is a vertically scaled velocity distribution where the value at  $v = 1$  is the same as that measured for the velocity distribution of the system with dissipation  $\varepsilon_n = \varepsilon_t = 0.1$  (which we denote as  $P_0(v)$ ). We transform the measured velocity distribution ( $P(v)$ ) to  $P'(v)$  by using the map:

$$P(v) \mapsto P'(v) = P(v) \frac{P_0(1)}{P(1)}. \tag{5.4}$$

The vertical rescaling of the distributions is used to emphasise any similarity in shape within the asymptotic tails of the distributions. If the distributions have the same shape at  $v > 1$  then all points of the scaled distribution will collapse onto one curve.

As the coefficients of restitution raises from zero, shown in figure 5.3(a), the velocity distribution is increasingly dominated by the peak behaviour. Remarkably we find that the asymptotic tail of the velocity distributions for systems with dissipation of  $\varepsilon \lesssim 0.5$  collapse onto one curve in the described way. These distributions have the same asymptotic shape.

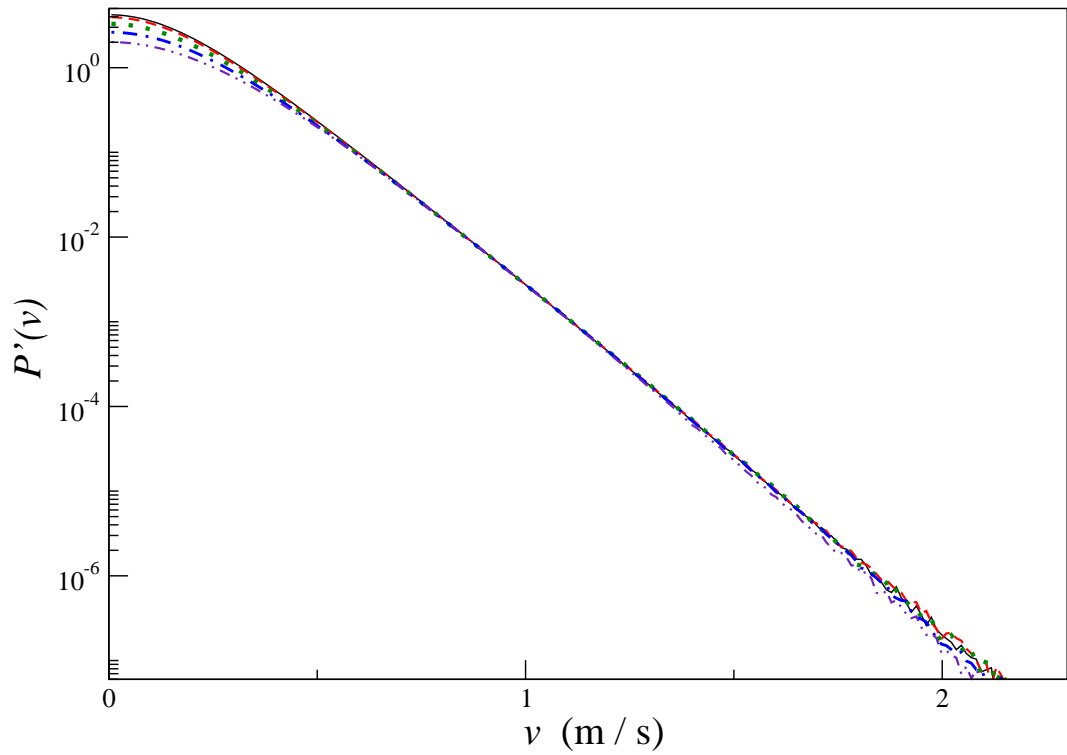
Physically the observation suggests that the fastest velocity particles have forgotten about the extent of dissipation of the system and consider any subsequent collision to be near-inelastic. Particles cluster in sufficient numbers that high velocity colliding particles lose most of their momentum and become strongly correlated with the cluster.

We conjecture that the velocity distributions of higher coefficients of restitution, shown in figure 5.3(b), have the same asymptotic shape but at probability densities beyond the measured range of the distributions, an idea explored further in section 5.1.3.

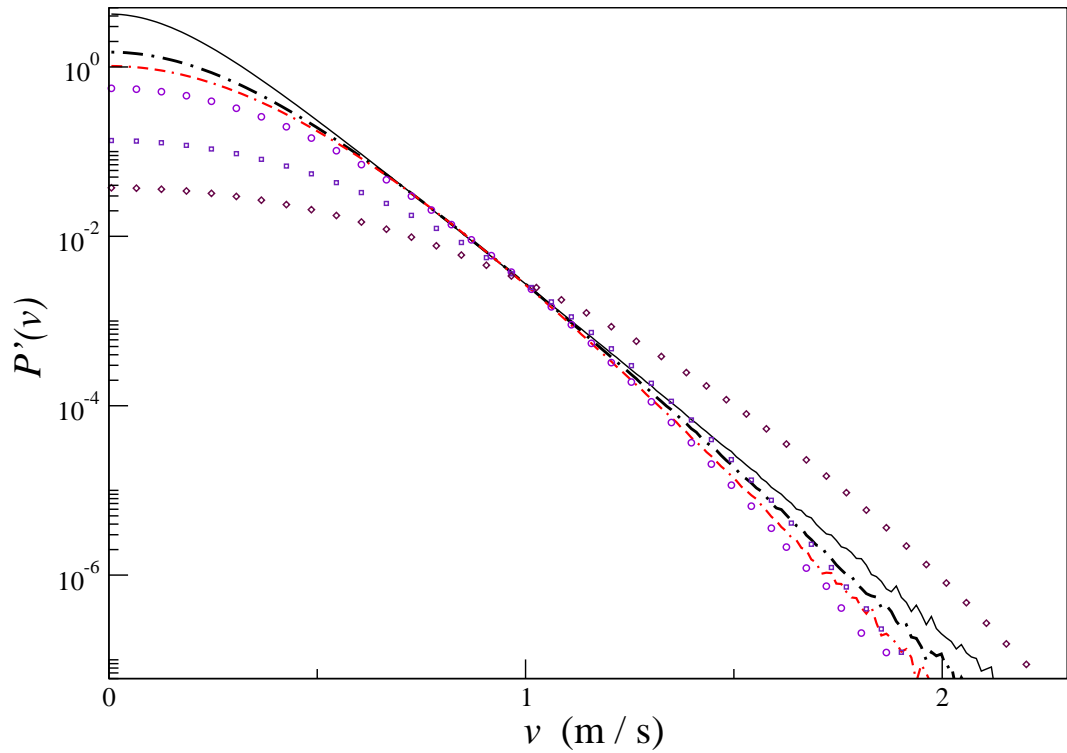
**General Trend with Respect to Population Number**

We measure the velocity statistics for a range of packing fractions. The dissipation is maximised by the use of low coefficients of restitution where  $\varepsilon_n = \varepsilon_t = 0.1$ . We vary the density of the system from a low packing fraction of  $\phi = 0.088$  up to a high packing fraction of 0.848 such that we crossover from systems of gaseous-like state to those that are crystalline. The system size is fixed at a width  $L = 0.2\text{m}$ .

Fig. 5.3: The vertically scaled velocity distribution for a system with  $L = 0.2, N = 3000$  such that the value at  $v = 1$  are the same. Each data set represents a particular coefficient of restitution.

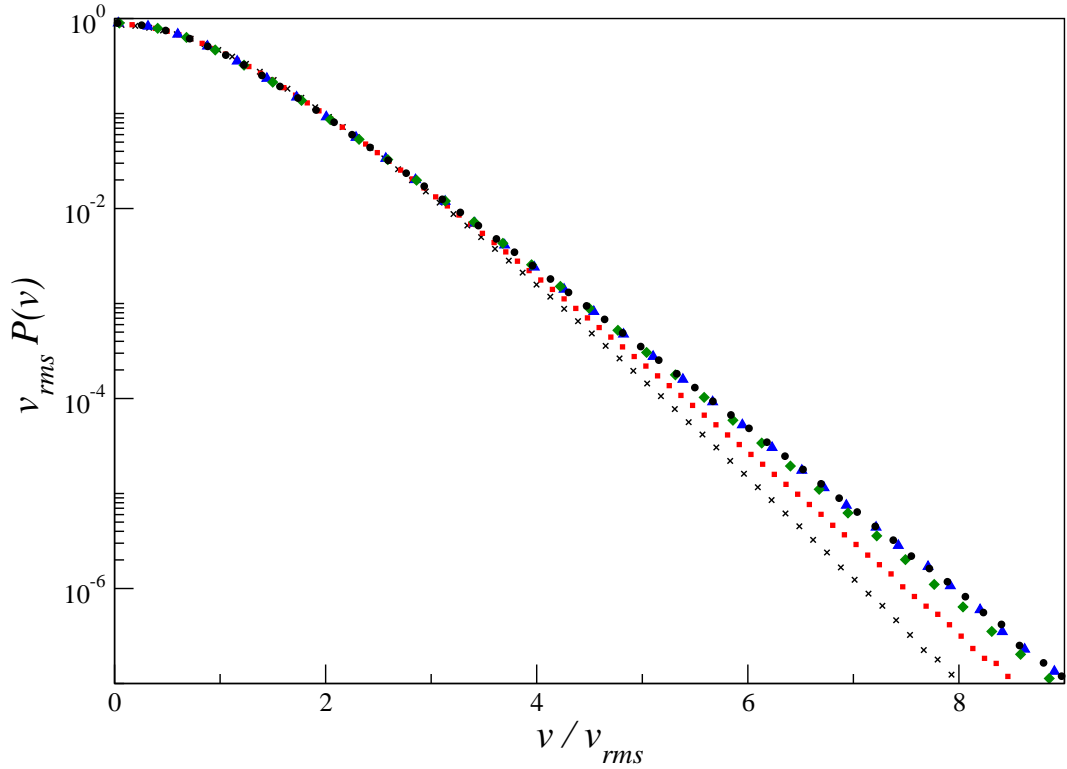


(a)  $\varepsilon_n = \varepsilon_t =$ : 0.1(solid line); 0.2(dashed line); 0.3(dotted line); 0.4(dot-dash line); and 0.5(dot-dot-dash line).

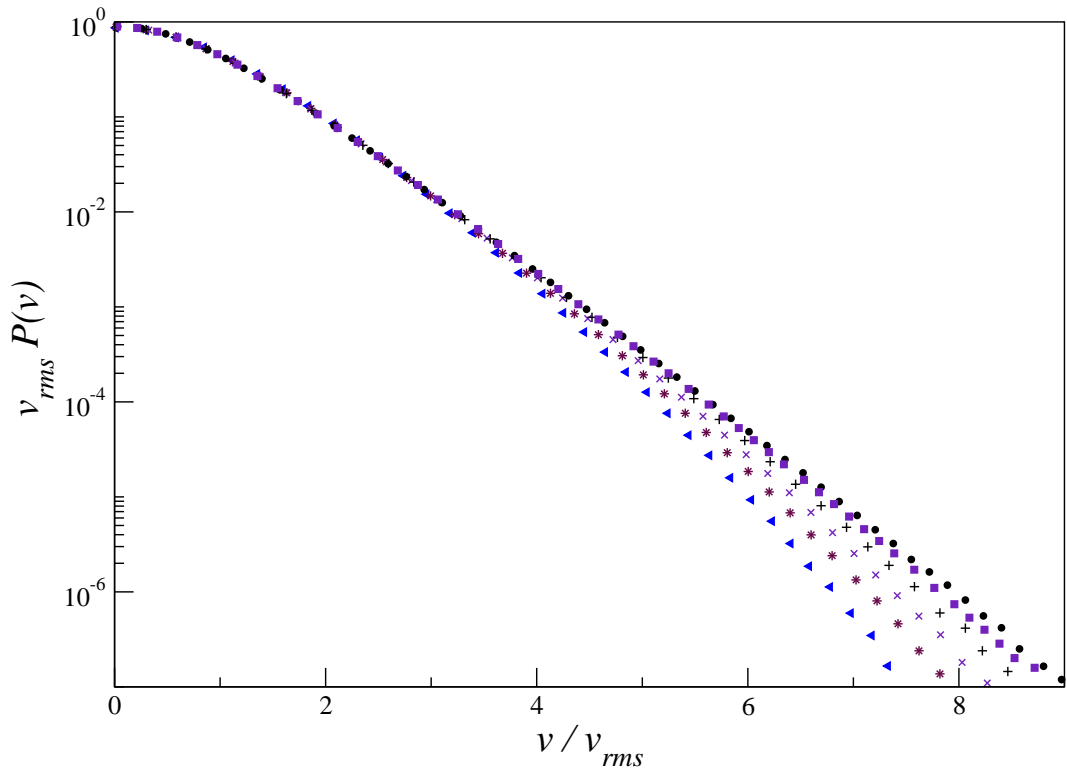


(b)  $\varepsilon_n = \varepsilon_t =$ : 0.1(solid line); 0.6(long dash-dot line); 0.7(dash-dash-dot line); 0.8(circle); 0.9(square) and 0.95(diamond).

Fig. 5.4: The velocity distribution for a system with  $L = 0.2, \varepsilon_n = \varepsilon_t = 0.1$ . Each data set represents a particular number of particles.



(a)  $N =$ : 4800(cross); 4500(square); 4000(diamond), 3500(up-triangle) and 3000(circle).



(b)  $N =$ : 3000(circle); 2500(square); 2000(plus), 1500(cross); 1000(star) and 500(left-triangle).

Figure 5.4(a) covers the velocity distributions for systems with high packing fraction that lie between  $\phi = 0.848$  and  $0.530$ . Figure 5.4(b) shows the velocity distributions for systems with low packing fraction that lie between  $\phi = 0.530$  and  $0.088$ .

As the density of the system increases the granular temperature decreases. The granular temperature reflects that time-scales between collision decreases in accordance with the packing fraction but the rate of energy injection remains static. We scale out the root mean square velocity from the velocity distributions to emphasize the change in shape of the statistics that is beyond that explained through the granular temperature. In all cases the slow moving particles, represented by the part of the velocity distribution where  $v/v_{rms} \lesssim 2$ , are dominated by the randomisation of velocities that occurs after collision and here  $P(v)$  is well described by a Gaussian distribution. At higher velocities the distribution becomes distinctly non-Gaussian, except at very high coefficients of restitution. Let us consider figures 5.4(a) and 5.4(b) in turn.

In figure 5.4(a) we decrease the packing fraction of the system from  $\phi = 0.848$  ( $N = 4800$ ) to  $\phi = 0.530$  ( $N = 3000$ ). Between a packing fraction of  $\phi = 0.530$  ( $N = 3000$ ) and  $\phi = 0.707$  ( $N = 4000$ ) there is little change in the distribution, signified by the collapse of these distributions onto one curve. These packing fractions are below the liquid to crystalline transition point of  $\phi_c \approx 0.719$ . For densities above  $\phi_c$  the distributions become less over populated with increased density, signified in the figure by the reducing width of these distributions as the number of particles increase. The interpretation is that particles become less able to move freely as the system becomes more crystalline.

In figure 5.4(b) we decrease the density of the system from  $0.530$  ( $N = 3000$ ) to  $\phi = 0.088$  ( $N = 500$ ). The high velocity tail of the velocity probability distribution becomes significantly less over populated as the density decreases, signified by the decrease in the width of the distribution with number of particles.

### **Simple Analysis of Asymptotic High Velocity Behaviour**

We now quantitatively describe the change in behaviour of the velocity statistics as either the number of particles or coefficient of restitution is varied. We assume that the high velocity behaviour of the particles can be described by a simple stretched-exponential with no other velocity factors such as power terms, of the form:

$$\lim_{v \rightarrow \infty} P(v) = A \exp(-B|v|^\alpha). \quad (5.5)$$

We use two-dimensional systems of fixed system size,  $L = 0.2\text{m}$  and dissipation such that  $\varepsilon_n = \varepsilon_t$ .

The velocity distributions are fitted by comparing the frequency distribution  $\mathcal{P}(v)$  (where the value is equal to the number of particles measured to have a velocity component of  $v$ ) to the fit  $\mathcal{P}_T(v) = A_0 \exp(-B_0|v|^\alpha)$ . We select the lowest three decades of data where  $\mathcal{P}(v) = X_i$  has a value between 50000 and 50 and assume the error in each point lies within  $\pm\sqrt{X_i}$  (except for those denoted with † where the error is taken as  $\pm 2\sqrt{X_i}$ ). We are specifically interested in the values that the exponent  $\alpha$  can take in the fit  $\mathcal{P}_T$  whilst agreeing with reasonable accuracy to the real velocity probability distribution. We use a chi-square fitting method to determine the best-fit of  $\mathcal{P}_T$  and accept values for  $\alpha$  if the reduced chi-square,  $\chi_r^2$ , is less than 1.2. In some respect this method gives an upper bound for the exponent  $\alpha$  as we cannot ensure that we are measuring the asymptotic tail of the velocity distribution nor does the error weighting guarantee the correct emphases placed on each data point as those with larger magnitude are assumed to have smaller error but those of smaller magnitude are nearer the true asymptotic limit.

The table below shows for a variety of systems the ranges of  $\alpha$  that are accepted through the above outlined method. The columns represent systems with fixed dissipation (where  $\varepsilon_n = \varepsilon_t \equiv \varepsilon$ ) whilst the row are for systems containing constant packing fractions.

$\phi$	$\varepsilon = 0.01$	$\varepsilon = 0.40$	$\varepsilon = 0.55$	$\varepsilon = 0.70$	$\varepsilon = 0.95$
0.088	$1.48 \pm 0.03$	$1.53 \pm 0.08$	$1.43 \pm 0.03$	$1.47 \pm 0.43\dagger$	$2.13 \pm 0.13$
0.177	$1.45 \pm 0.05$	$1.48 \pm 0.08$	$1.38 \pm 0.03$	$1.48 \pm 0.08$	$2.13 \pm 0.13$
0.265	$1.43 \pm 0.08$	$1.33 \pm 0.43\dagger$	$1.40 \pm 0.10$	$1.48 \pm 0.48\dagger$	$2.13 \pm 0.58\dagger$
0.353	$1.30 \pm 0.10$	$1.33 \pm 0.13$	$1.28 \pm 0.03$	$1.40 \pm 0.10$	$2.10 \pm 0.10$
0.442	$1.25 \pm 0.35\dagger$	$1.20 \pm 0.10$	$1.30 \pm 0.10$	$1.38 \pm 0.13$	$2.00 \pm 0.60\dagger$
0.530	<b><math>1.13 \pm 0.13</math></b>	<b><math>1.23 \pm 0.08</math></b>	<b><math>1.18 \pm 0.08</math></b>	$1.33 \pm 0.08$	$2.05 \pm 0.15$
0.619	<b><math>1.10 \pm 0.10</math></b>	<b><math>1.10 \pm 0.10</math></b>	<b><math>1.10 \pm 0.05</math></b>	$1.28 \pm 0.13$	$2.08 \pm 0.53\dagger$
0.707	<b><math>1.18 \pm 0.03</math></b>	<b><math>1.13 \pm 0.08</math></b>	<b><math>1.08 \pm 0.18</math></b>	$1.23 \pm 0.13$	$1.98 \pm 0.18$
0.795	<b><math>1.18 \pm 0.03</math></b>	<b><math>1.18 \pm 0.38\dagger</math></b>	<b><math>1.13 \pm 0.08</math></b>	$1.23 \pm 0.08$	$2.05 \pm 0.25$

Table 5.1: Measurement of the exponent  $\alpha$  for a wide range of systems spanning both packing fraction and dissipation. The system size is fixed at  $L = 0.2\text{m}$ .

The data in the above table is consistent with the observations described earlier

for variation of dissipation extent and particle number. From the table we conclude that there exist a region of moderate to high dissipations ( $\varepsilon < 0.6$ ) and moderate to high packing fractions ( $\phi \gtrsim 0.530$ ) in which the shape of the high velocity tail of  $P(v)$  and the value of exponent  $\alpha$  is approximately constant with no systematic variation in value, with upper limit of  $\alpha = 1.163 \pm 0.017$  obtained from the weighted average of bold data values. However this value depends on the simple form we have chosen for  $P(v)$  in equation 5.5 and the method of fitting.

In the following two sections we suggest that any variations in the apparent asymptotic shape of the velocity distribution are not real but instead are caused by two effects: first, variation due to density is caused by finite size effects that are more prevalent in dilute systems; second, variation due to dissipation is caused by the shifting value of a crossover velocity of the velocity distribution such that good approximation to the asymptotic limit requires higher velocities and lower probability scales with decreased dissipation.

### 5.1.2 System Size Dependence and Stability with Respect to Packing Fraction

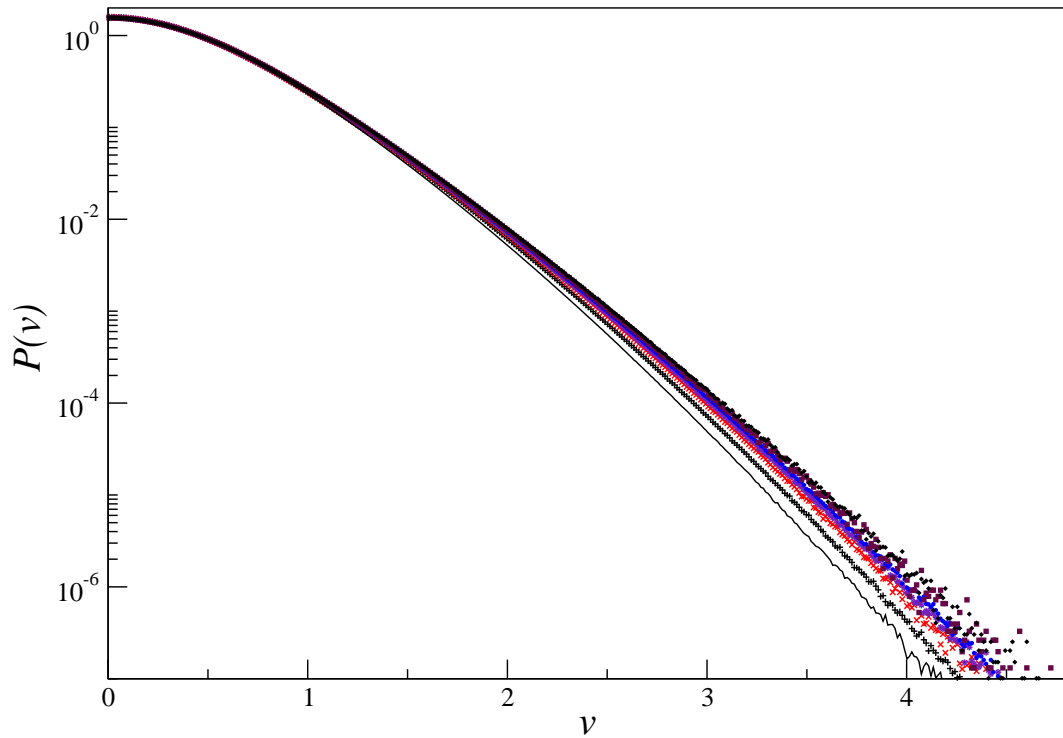
We now wish to understand what causes the variation of shape of the velocity distribution as the density is made more dilute. Is it because there is some inherent change in structure as particles become more gaseous-like with decreased density or is it simply due to finite size effects?

We measure the velocity statistics for a variety of system sizes whilst keeping the packing fraction and dissipation fixed. The system is kept in the high dissipation limit by choosing the coefficients of restitution to be  $\varepsilon_n = \varepsilon_t = 0.1$ . We choose packing fractions ranging between  $\phi = 0.088$  and  $0.619$  and scale up the system by enlarging the system size and particle numbers. We choose an initial system size of  $L = 0.1\text{m}$  with  $N$  particles and simulate subsequent systems by increasing the scale of the system by up to a factor of  $j$  times, such that  $j$  takes values 1,2,4,6, 8,12 or 16. The new systems have system length of  $jL$  and particle numbers of  $j^2N$ .

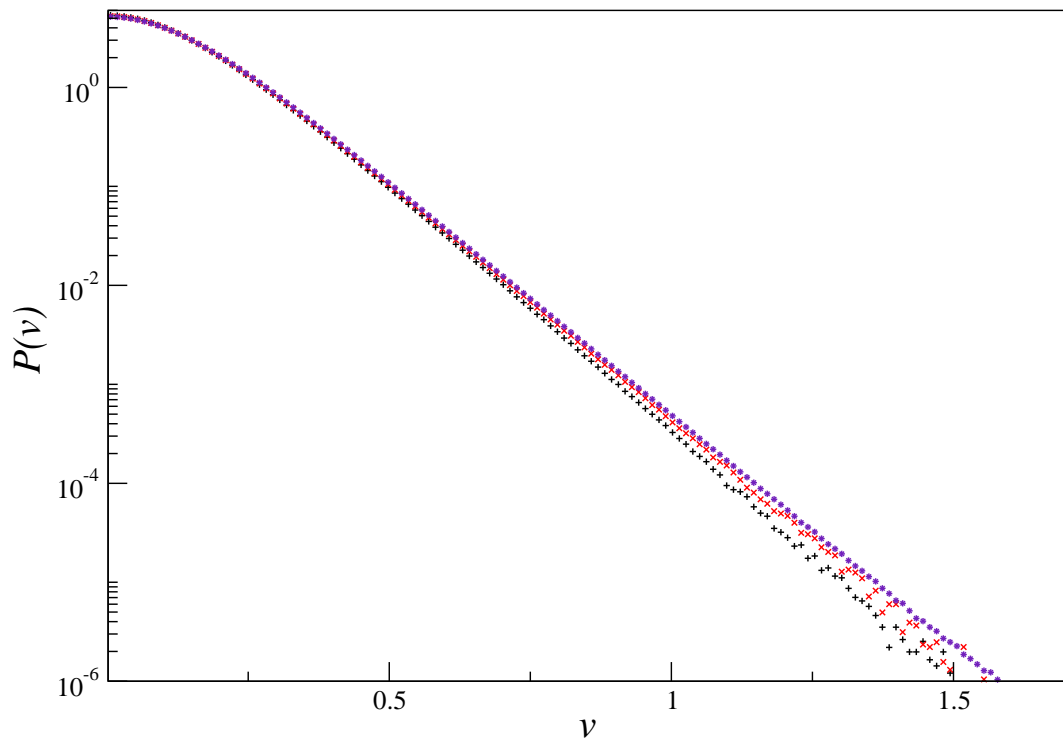
In a well-behaved system once the system is of sufficient size, finite size effects are irrelevant and the shape and magnitude of the velocity distribution remain unchanged with further increases in system size.

Figures 5.5(a) and 5.5(b) show the change in shape of the velocity statistics as the scale of the system is increased whilst the density remains fixed. From the figures it can

Fig. 5.5: The velocity distribution for a system with fixed density. The data sets are for combinations of particle number and system size



(a) The packing fraction is 0.088 and  $N = 125, L = 0.1\text{m}$  (line);  $N = 500, L = 0.2\text{m}$  (plus);  $N = 2000, L = 0.4\text{m}$  (cross);  $N = 4500, L = 0.6\text{m}$  (star);  $N = 8000, L = 0.8$  (circle);  $N = 18000, L = 1.2\text{m}$  (square) and  $N = 32000, L = 1.6\text{m}$  (diamond).



(b) The packing fraction is 0.619 and  $N = 3500, L = 0.2\text{m}$  (plus);  $N = 14000, L = 0.4\text{m}$  (cross) and  $N = 31500, L = 0.6\text{m}$  (star).

be seen that the asymptotic behaviour of velocity distribution becomes more over populated with increasing system size. As the system scale increases the difference between distributions becomes less pronounced. For example, when the system size is doubled from  $L = 0.1m$  to  $L = 0.2m$  there is a distinct change in the tail of the distribution. When the system is doubled from  $L = 0.4m$  to  $L = 0.8m$  the distinction between the two resultant velocity statistics is far weaker and the tails of the distributions are almost indistinguishable from one another. As a consequence the asymptotic behaviour of the velocity statistics is described by a stretched-exponential with exponent  $\alpha$  that reduces in value as the system becomes larger.

The table below demonstrates the above point for some of the more dilute systems considered. The values of  $\alpha$  are calculated by the same method as in section 5.1.1.

$\phi$	$L = 0.1$	$L = 0.2$	$L = 0.4$	$L = 0.8$
0.088	$1.40 \pm 0.05$	$1.53 \pm 0.08$	$1.38 \pm 0.03$	$1.33 \pm 0.08$
0.177	$1.50 \pm 0.10$	$1.45 \pm 0.05$	$1.33 \pm 0.08$	$1.23 \pm 0.03$
0.353	$1.40 \pm 0.10$	$1.30 \pm 0.10$	$1.27 \pm 0.08$	$1.13 \pm 0.03$
0.530	$1.13 \pm 0.18$	$1.10 \pm 0.15$	$1.05 \pm 0.10$	$1.13 \pm 0.03$

Table 5.2: Measurement of exponent  $\alpha$  for highly dissipative systems of four packing fractions and a range of system sizes.

The table demonstrates that as the system size increases the measured value of  $\alpha$  lowers towards that seen for higher densities and equivalent dissipation. No significant variation in  $\alpha$  with respect to system scale is observed for higher densities  $\phi \geq 0.530$  suggesting that a constant value (unchanged with higher sizes) is reached, which for these dissipation we estimated previously to have an upper-bound of value  $\alpha = 1.163 \pm 0.017$ .

These results suggest that the shape of the velocity statistics have two important properties: first, the change in asymptotic shape as the density becomes very dilute is due to a finite-size effect (probably caused by the fixed finite size of the particles) rather than structural changes in the system; second, for systems of sufficient size the exponent  $\alpha$  characterizing the high velocity tails of the distributions is a constant value for all packing fractions (beneath that of crystallisation).

### 5.1.3 A Crossover in Particle Behaviour and Stability with Respect to Dissipation

For the multi-dimensional Random Force Model the complete shape of the velocity distribution  $P(v)$  is often described to fit a crossover function where the low velocity particles obey Gaussian statistics and the high velocity particles are distributed by a stretched-exponential with an exponent  $\alpha$  much less than two (van Zon and MacKintosh 2004; Moon, Shattuck, and Swift 2001). The crossover velocity,  $v_c$ , defines the velocity scale at which the distribution is halfway from being Gaussian to being the anomalous high velocity tail.

In the published literature it is typically assumed that systems at moderate dissipation (where tangential dissipation is prohibited) have velocity distributions where the exponent  $\alpha$  agrees with the granular kinetic theory described in van Noije and Ernst (1998) such that  $\alpha = 1.5$ . However, it is not clear why the kinetic theory of should be valid in these systems. Instead, we propose that  $\alpha = 1.5$  is an anomaly of measurement brought on by finite statistics and the choice of moderate dissipation. By using Random Force Models comparable to previous studies, we show that with better statistics the asymptotic behaviour of the velocity distribution has an exponent  $\alpha$  which is much lower than 1.5. The above point is significant because it means that the variation of exponent  $\alpha$  with respect dissipation, seen in section 5.1.1, is caused by measuring over the non-asymptotic part of the distribution brought on by the distribution's high crossover velocity and an insufficient number of measured decades. The crossover velocity can be made more favourable through increasing the dissipation of the system, beyond that of any previous study and there by shifting  $v_c$  to smaller values. By doing so we find that the high velocity tail of the velocity distribution can be fitted by stretched-exponential with exponent much closer to 1.0 than 1.5 over a sizeable region. We suggest that for all dissipations using a value for  $\alpha$  such as 1.16 brings us nearer to the true exponent of the high velocity tail.

#### Determining the Asymptotic Behaviour

We plot the velocity statistics by the method employed in the published paper of Moon, Swift, and Swinney (2004) whereby  $-\ln(-\ln(P(v/v_{rms})/P(0)))$  is plotted against  $\ln(v/v_{rms})$  and compared with functions of the form:

$$f(v/v_{rms}) = -\alpha_T \ln(v/v_{rms}) + C. \quad (5.6)$$

The constant  $C$  is free to change while  $\alpha_T$  is predetermined and represents a proposed value for  $\alpha$  (not its actual value). In this section we choose  $\alpha_T$  to be either 2, 1.5 or 1.16. Again we caution against taking too much from the use of particular values of  $\alpha_T$  as dividing  $P(v)$  through by  $P(0)$  affects the apparent slope of the high velocity tail of  $P(v)$  shown in these plots. We will explain this effect more fully in the next section, but for now we shall use this method as it is a standard approach used in the literature.

When attempting to fit  $f(v/v_{rms})$ , with specific value of  $\alpha_T$ , three possible cases arise: the velocity distributions do converge to a stretch exponential of  $\alpha = \alpha_T$ , in which case the line of fit touch the distributions and continue to go through the data points as the velocity further increases; the velocity distributions are described by  $\alpha < \alpha_T$ , in which case the line of fit touches the data points at one point only and is considered to be tangent to the data; the velocity distributions are described by  $\alpha > \alpha_T$ , in which case there does not exist a line of fit which will coincide with the velocity data without crossing through.

### **The Asymptotic Behaviour of Systems with just Normal Dissipation**

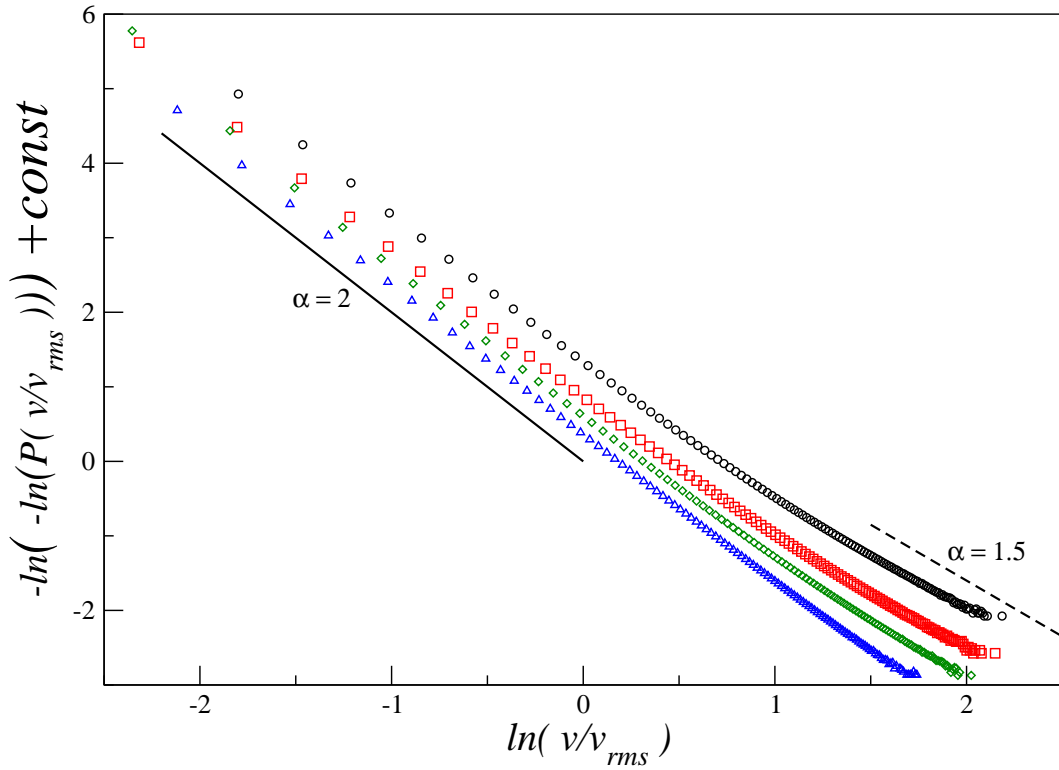
We first consider systems where only normal dissipation is present at collision. Our data is comparable with work published in previous papers. We vary the normal coefficient of restitution between 0.1 and 0.9. The tangential coefficient of restitution is kept fixed at 1. We choose a moderate packing fraction of  $\phi = 0.530$ , that is well away from being crystalline, and a system size such that  $L = 0.4\text{m}$  and  $N = 12000$ .

Figure 5.6 shows the obtained velocity distributions, where figure (a) displays the complete velocity statistics and figure (b) focusses on the high velocity tail. We attempt to fit the data with functions of the form  $f(v/v_{rms})$  such that  $\alpha_T$  is selected to be either  $\alpha_T = 2$  or  $\alpha_T = 1.5$ .

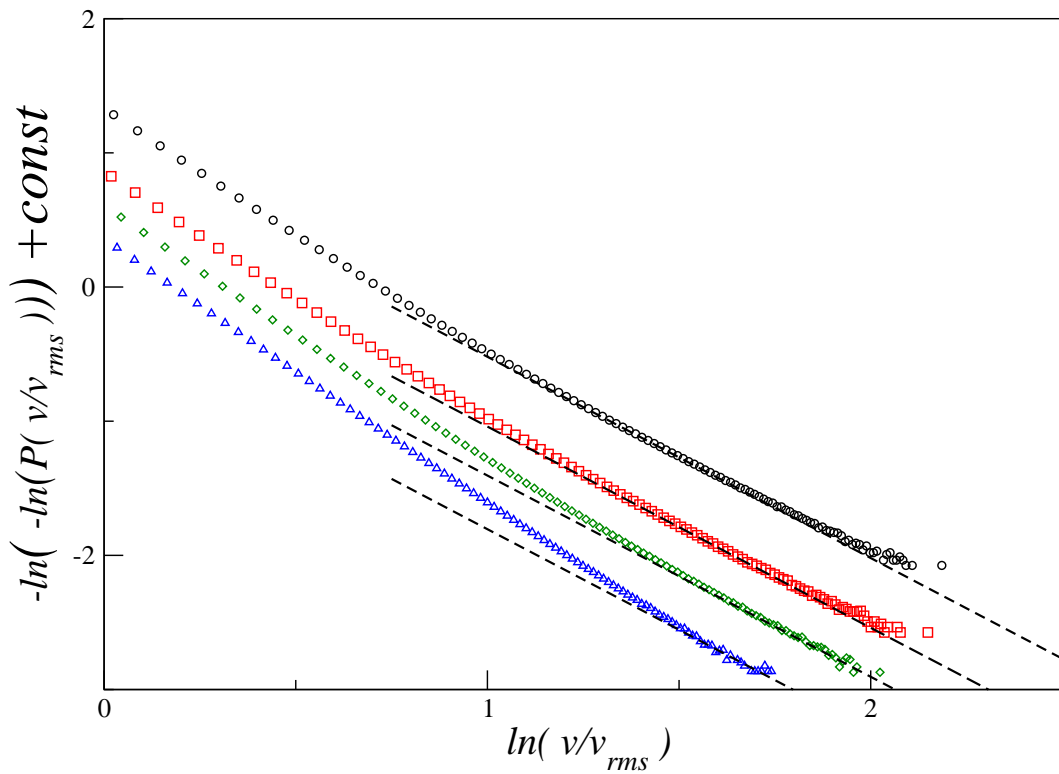
We find, in line with other works, that the low velocity region of all data sets, where  $v/v_{rms} \rightarrow 0$ , can be fitted by functions of  $f(v/v_{rms})$  with  $\alpha_T = 2$  and represent the Gaussian central peak of the velocity distribution. As the coefficient of restitution decreases less of the data can be fitted by a Gaussian curve, suggesting that the crossover velocity  $v_c$  shifts towards lower velocities with increasing dissipation.

The dashed lines on figure 5.6 represent functions of  $f(v/v_{rms})$  with  $\alpha_T = 1.5$  that are fitted such that they lie tangent to the data. The range of  $v$  that the dashed lines approximately fit the data is very small, typically over  $\Delta \ln(v/v_{rms}) \leq 1/4$ . Reducing the normal coefficient of restitution improves the fit by reducing the crossover velocity

Fig. 5.6: Crossover in behaviour of velocity distributions for a system with fixed packing fraction and tangential coefficient of restitution 1. The four data sets represent different extents of normal dissipation such that  $\varepsilon_n = 0.2$  (circle);  $\varepsilon_n = 0.4$  (square);  $\varepsilon_n = 0.6$  (diamond);  $\varepsilon_n = 0.8$  (up-triangle). The lines are linear fits of  $-2 \ln(v) + C$  (solid) and  $-1.5 \ln(v) + C$  (dot-dash).



(a) Complete distribution



(b) High velocity behaviour

to lower velocities. However, any agreement between the fit  $f(v/v_{rms})$  with  $\alpha_T = 1.5$  and the data are false and instead a better fit can be obtained by choosing a different value for exponent  $\alpha$ .

We illustrate the above point by focussing, in more detail, on the high velocity region of the data, where  $\ln(v/v_{rms}) > 1$ , as shown in figure 5.6(b). For high coefficient of restitution,  $\varepsilon_n = 0.8$ , the dashed line (representing the best fit for  $\alpha_T = 1.5$ ) only goes through the data points representing highest  $v/v_{rms}$ . Furthermore these points have largest error and are least reliable. An alternative fit, that would cover more of the data, would use  $f(v/v_{rms})$  with a exponent  $\alpha$  greater than 1.5. For low restitutions, such as  $\varepsilon_n = 0.2$  and  $\varepsilon_n = 0.4$ , the data can be argued to be systematically deviating above the dashed line, such that the relative difference between fit and data increases with  $v$ . In this case the fitting function,  $f(v/v_{rms})$  with  $\alpha_T = 1.5$ , is tangent to the data and suggests that a better value for exponent  $\alpha$  is slightly less than 1.5.

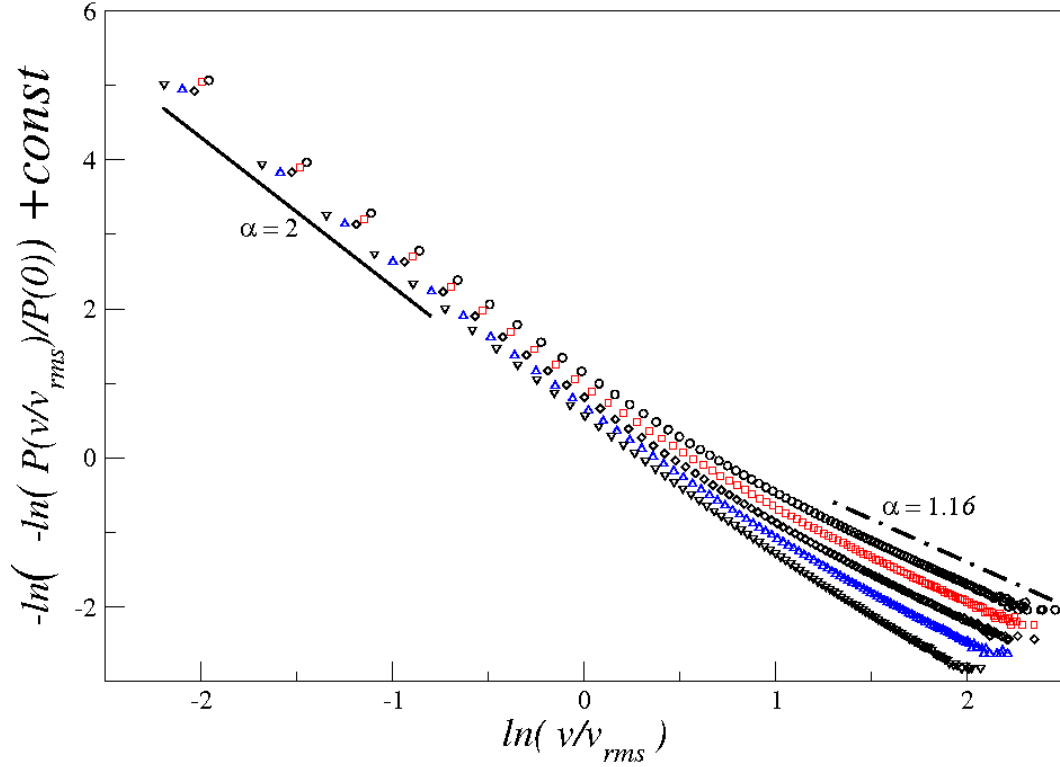
Both these observations hint that  $\alpha = 1.5$  does not describe the high velocity tail of  $P(v)$  and instead the velocity distribution is described by either a continuum of  $\alpha$  values that are dependent on density and coefficient of restitution, such that  $\alpha$  takes some value in the range  $2 > \alpha > 0$ ; or there is a single value for  $\alpha$  that is lower than 1.5. We would judge against the former possibility because the distributions shown here do not appear to have unchanging shape at large  $v$  and thus these high velocity tails are not in the asymptotic limit. Comparatively, it is the latter possibility that is more supported by our work, where for a range of coefficients of restitutions, packing fractions and large system sizes the exponent  $\alpha$  (as a result of  $D_f$  as will be shown later) was fixed with an upper-bound of value  $1.16 \pm 0.02$ . Nonetheless, to pursue this in more detail requires more of the high velocity tail of  $P(v)$  to be seen than can be currently obtained by these moderately dissipative systems.

### **The Asymptotic Behaviour of Systems with High Tangential Dissipation**

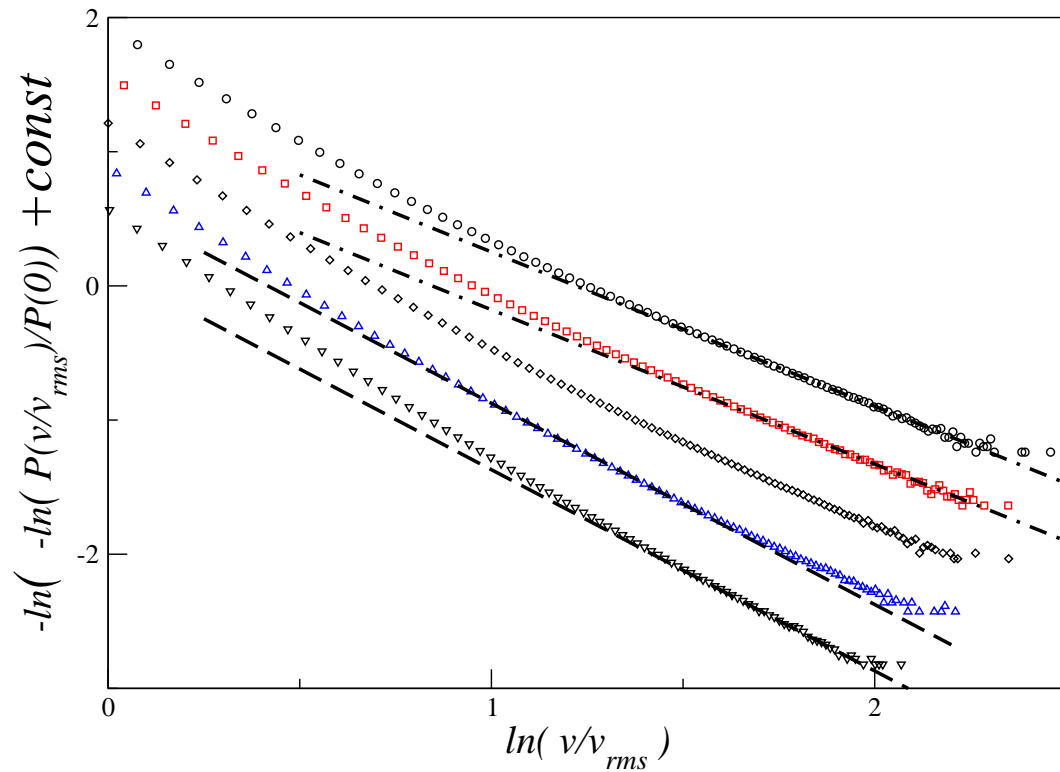
To increase the chance of seeing the asymptotic high velocity tail of  $P(v)$  the crossover velocity of the distribution needs to be as small as possible. We achieve this by either increasing the density of the system or increasing the dissipation of the system. Further dissipation of the system can only be induced by allowing tangential dissipation. Hence the tangential coefficient of restitution is minimised to  $\varepsilon_t = 0.1$  and again the normal coefficient of restitution is varied between 0.1 and 0.9.

Figure 5.7 shows the obtained velocity distributions. We fit the data sets with func-

Fig. 5.7: Crossover in behaviour of velocity distributions for a system with fixed packing fraction and tangential coefficient of restitution 0.1. The five data sets represent different extents of normal dissipation such that  $\varepsilon_n = 0.1$  (circle);  $\varepsilon_n = 0.3$  (square);  $\varepsilon_n = 0.5$  (diamond);  $\varepsilon_n = 0.7$  (up-triangle) and  $\varepsilon_n = 0.9$  (down-triangle). The lines are linear fits of  $-1.5 \ln(v) + C$  (dashed) and  $-1.16 \ln(v) + C$  (dot-dash).



(a) Complete distribution



(b) High velocity behaviour

tions of  $f(v/v_{rms})$  where either  $\alpha_T = 1.5$  (shown as dashed lines) or  $\alpha_T = 1.16$  (shown as dot-dashed line). Figure 5.7(a) shows the complete measured velocity distribution from peak to tail. At the peak the distribution behaves as a Gaussian with  $\alpha = 2$ . As the velocity increases, typically  $\ln(v/v_{rms}) \gtrsim 0$ , the measured exponent crosses over to anomalous and decreases in value. We propose that the asymptotic value of  $\alpha$  can be given by  $1.16 \pm 0.02$ .

Figure 5.7(b) shows the high velocity region of the velocity distribution. As the coefficient of restitution increases, the crossover velocity decreases towards zero and the range of  $v/v_{rms}$  over which functions of  $f(v/v_{rms})$  with  $\alpha_T = 1.16$  agrees with the data enlarges. In contrast, functions of  $f(v/v_{rms})$  with  $\alpha_T = 1.5$  form tangents to the velocity distribution and agreement becomes progressively worse with higher dissipation. The range of velocities over which  $\alpha_T = 1.5$  is a reasonable fit remains the same as seen with just normal dissipation but the fit can no longer be said to represent the asymptotic behaviour.

We conclude that the velocity distribution is well described by a crossover function which changes from Gaussian to anomalous with increasing velocity. The asymptotic behaviour is describe by a stretched-exponential with exponent much less than 1.5 and closer to  $1.16 \pm 0.02$ . However it is not clear whether this is an accurate value for the exponent.

#### 5.1.4 Brief Summary on the Velocity Distribution

Here is a brief summary of the velocity statistics of the two-dimensional model. The distribution of velocity  $P(v)$  is represented by a function which is Gaussian for low velocities and then crosses over to a stretched-exponential, with exponent  $\alpha$ , for high velocities. These distributions have a crossover velocity,  $v_c$  (the exact value of which is not calculated), that represents the point at which the distribution changes from one form to another. We find that there is no evidence to support the theory that the high velocity tail of  $P(v)$  is a stretched-exponential with exponent  $\alpha = 1.5$ . Instead we make two statements about the velocity distribution: for systems of sufficient size and packing fraction beneath crystallisation, the high velocity shape of  $P(v)$  is approximately packing fraction independent; for high dissipation all velocity distributions crossover to the same large  $v$  shape of a stretched-exponential, with exponent  $\alpha$  upper-bounded by  $1.16 \pm 0.02$ .

In general the crossover velocity  $v_c$  increases as the dissipation or packing fraction of

the system reduces. This is one reason why systems of low packing fraction exhibit an apparent simple scaling of the moments of the velocity distribution, rather than a more complicated scaling involving the two velocity-scales suggested by the crossover function. In these cases  $P(v)$  is dominated by the central Gaussian peak. The increasing of value of  $v_c$  also means that it becomes more difficult to study the asymptotic high velocity limit of the velocity distribution as lower probabilities must be measured. A physical interpretation is that, as the dissipation of the system decreases, particles need to travel faster before a collision in order for the collision to be treated as near-inelastic. Subsequently the chance of a particle doing so becomes less likely.

Lastly, we conjecture that systems of low dissipation also have distributions of velocity with asymptotically high velocity tails described by stretched-exponentials with  $\alpha \lesssim 1.16 \pm 0.02$ . However the crossover velocity of these distribution is too large to measure from simulation and the statement cannot be directly tested.

## 5.2 A Single Particle Model

In this section we use observations of a particle's motion between collisions to construct a single particle model. We demonstrate that the new model captures the behaviour of high velocity particles of the highly dissipative Random Force Model.

### 5.2.1 A Physical Basis

In the Random Force Model, the motion of a target particle is a series of accelerating walks separated by rapid loss of energy during interactions with other meandering particles, see figure 5.8(a). Each walk can be considered to be independent from the previous one as long as the background particles are not jammed and sufficient energy is damped out during collision so that there is little memory of its previous speed. Let us consider a particular walk of a particle which travels solely under the random force a distance  $l$  before the next collision. The distance  $l$  is called the particle's *free path*; the mean free path is the average distance a particles moves between collision. The free path is defined as the effective change in particle position between consecutive collisions:

$$l = |\mathbf{r}_i(\tau + t_0) - \mathbf{r}_i(t_0)|. \quad (5.7)$$

Here  $\mathbf{r}_i(t)$  is the particle's position at time  $t$ ,  $t_0$  is the initial time just after previous collision whilst  $\tau$  is the time between collision (sometimes referred to as the free time of the particle).

Diagram 5.8(b) is a pictorial representation of the particle's motion during the walk from one collision to the next. Each number represents a collision between the particle and another. Collision 1 is the previous collision of the particle whilst 2 and 3 represent possible locations, relative to 1, of the next collision. As the system is isotropic the next collision is equally likely to occur any where around the circumference of the marked circle. If a particle with a free path  $l$  is selected at random in the system then we know neither the net direction the particle travels before collision (demonstrate by the two possible collisions 2 and 3 in the figure) nor the specific path the particle takes getting from the initial to the next collision (two such allowed paths are shown in the figure).

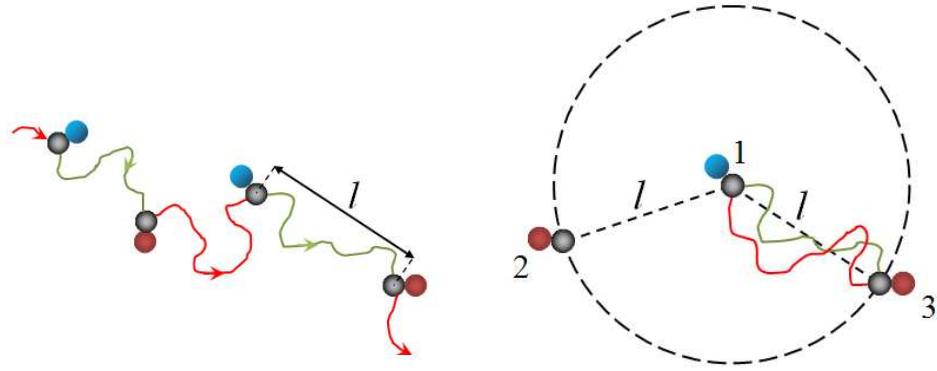
Such a representation of the particle's motion provides a basis for a single particle model. We describe a particle walking between two collisions, separated by a free path length of  $l$ , as a particle travelling within a circular region of radius  $l$  where the radial distance represents the free path length. During a single walk, the particle experiences a random force and moves from the centre until it reaches the boundary. The centre of the interval is the position of the previous collision; the boundary represents the next collision.

The behaviour of a complete system of many particle measured over a long time can also be thought of in terms of singular particles moving within circular regions. During the simulation, at some point, many particles travelled the the same free path length,  $l$ , between collisions. The statistic behaviour of these particles during this particular walk length, between collisions, is the same as the time average behaviour of a single particle travelling between two collisions of distance  $l$ . This is equivalent in our new model to the statistical behaviour of a particle travelling in any direction, without preference, within the circle of length  $l$ .

Thus the complete behaviour of all particles within a system of the two-dimensional Random Force Model can be represented by the average behaviour of particle travelling a distance  $l$  between centre and boundary of a circle *weighted* by the probability of a particle travelling that distance between a collision.

Hence we arrive at our Single Particle Model (SPM) representation of the Random Force Model. A single pseudo-particle is continually placed *at rest* in the centre of the circle. The circle is defined each time with a new radius  $l'$ . The particle moves under Gaussian noise until it reaches the boundary. The radius  $l'$  is chosen from the probability distribution of free paths which ensures the correct weighting of free paths.

Fig. 5.8: Developing a single particle model of the random force model.



(a) A pictorial demonstration of the motion of a particle between several collisions. The effective distance moved between collision is denoted the free path; a particular one of length  $l$  is shown.

(b) A particle moving between collisions with a free path of  $l$  can only exist (without having collided) within a circular region of radius  $l$  (assuming the velocity cannot change sign) centred on the previous collision.

This simple representation captures the physics of the high velocity particles driven solely by the random force. The main approximations used in the representation are that: the particle starts from rest each time; the particle's displacement cannot exceed that of  $l$  without collision; all possible paths inside the circle are valid. We considered the validity of these three assumptions in turn.

### Zero Initial Velocity

In the Random Force Model, a particle's initial velocity,  $v_0$ , can be neglected when its current velocity,  $v$ , can be treated as the result of interaction with the random force rather than collisions, such that  $v \gg v_0$ .

The distribution of post-collision velocity,  $P(v_0)$  is defined as the probability that a particle has a velocity  $v_0$  just *after* collision with another particle. When the post-collisional distribution,  $P(v_0)$ , and overall velocity probability distribution,  $P(v)$ , are comparable, in gradient, then significant contributions to the velocity statistics come from the initial velocity and the initial velocity cannot be assumed to be zero. The velocity probability distributions (with unscaled velocities) of post-collisional velocities and overall velocities are shown in figure 5.9, where (a) is for a highly dissipative system and (b) a low dissipation system.

In strongly dissipative systems a high proportion of a particle's incoming energy is removed during collision and thus the two velocity distributions are very dissimilar. In particular the post-collision velocity distribution is much narrower. Therefore the assumption of zero velocity is reasonable as long as we are interested in the high velocity tail.

In near-elastic systems, little of the particles momentum is lost through collision and thus the post-collision statistics become comparable with and mimics the overall velocity statistics across the range of measurable velocities. Therefore the assumption of zero initial velocity is poor and the Single Particle Model will not model the velocity statistics of Random Force Model.

### **Absorbent Boundaries**

A second approximation in the Single Particle Model is that the particle is stopped the *first* time it reaches a distance  $l$ .

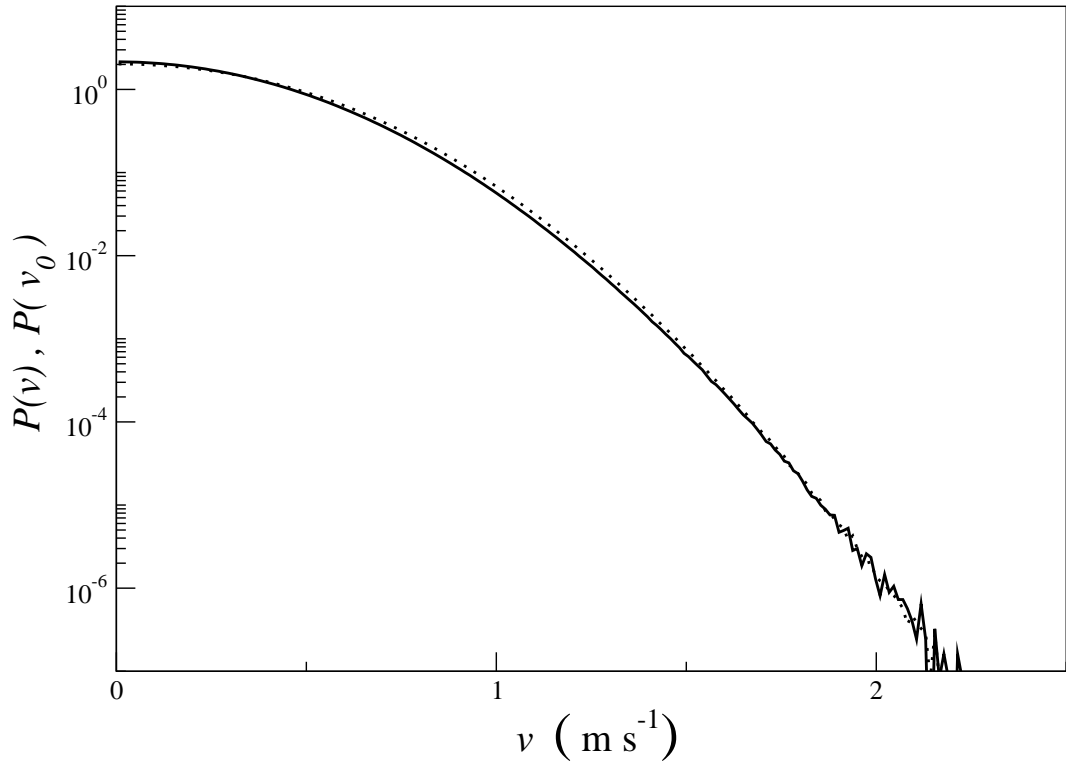
The statistical average velocity of a particle, started from rest at the origin, grows proportional to its distance, as  $l^{\frac{1}{3}}$ . The further a particle travels from the centre, the faster the average velocity. Hence the opportunity for the particle to reverse direction reduces with distance as it becomes more difficult to remove all the particle's momentum through the interaction between particle and the random force.

### **All Allowed Paths are Valid**

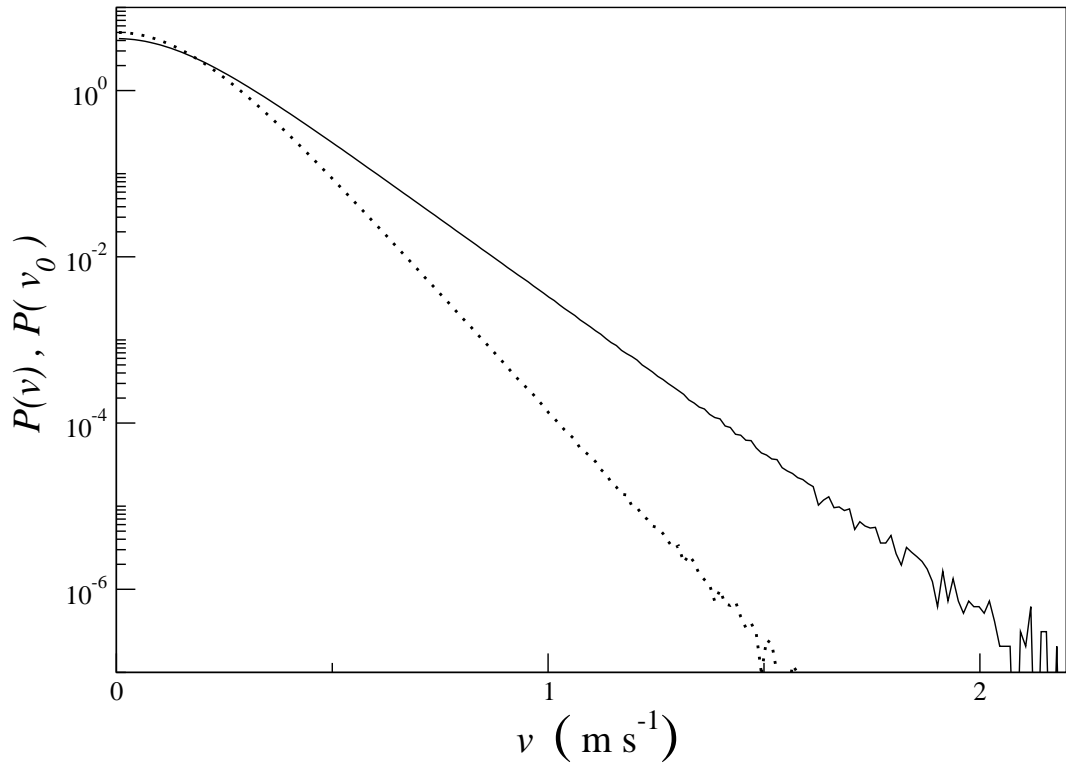
The Single Particle Model assumes that the particle will move along any path that stays within the boundary of the circle. In the real Random Force Model, when a particle moves between consecutive collisions, separated by a distance  $l$ , other non-interactive particles can lie within a distance  $l$  of the particle and not result in a collision. In particular, the position of the particle of previous collision starts next to that of the target particle.

In these cases it might be expected that for the Single Particle Model to work then certain paths of the particle through the circle must be discounted as they represent interactions with these other particles that are not allowed. However this is not the case, because these disallowed paths have already been accounted for through particles travelling within other circles of smaller radius than  $l$ . Also these circles are used to generate the time average behaviour of a particle travelling a distance  $l$  between

Fig. 5.9: The velocity distribution for a system of 12000 particles contained in a region with widths  $L = 0.4\text{m}$ . The solid lines show the full velocity distribution while the dots show the post-collisional velocity statistics, as described in the text.



(a) High dissipation,  $\varepsilon_n = \varepsilon_t = 0.1$



(b) Low dissipation,  $\varepsilon_n = \varepsilon_t = 0.9$

collision, not a particular case, and so there will always exist some occasion at which any particular path within the circle will become valid.

### 5.2.2 SPM Integral Identity

The velocity distribution of the particle in the Single Particle Model can be derived using Conditional Probability Theory. The distribution of free paths,  $P_l(l)$  (discussed in chapter four), describes the probability weightings that a particle has been displaced a distance  $l$  between successive collisions *upon* arrival at another collision. When a particle is travelling along a walk of length  $l$  the distribution of velocities,  $Q(v, l)$ , is given as the probability of a particle having a velocity  $v$  *knowing* that it is travelling a free path of length  $l$ .

The probability of a particle having a free path of length  $l$  *and* a velocity  $v$  (sometime before collision), denoted  $P(v, l)$ , is equal to the probability of having a velocity  $v$  when travelling a length  $l$  multiplied by the probability of travelling a free path of length  $l$ :

$$P(v, l) = Q(v, l)P_l(l). \tag{5.8}$$

The total probability that a particle has a velocity  $v$ , denoted  $P(v)$ , is simply the integral over all  $l$  of  $P(v, l)$ , whereby:

$$P(v) = \int_0^\infty P(v, l) dl. \tag{5.9}$$

By this process we derive the **SPM Integral Identity**:

$$P(v) = \int_0^\infty Q(v, l)P_l(l) dl, \tag{5.10}$$

which describes the velocity distribution obtained from the Single Particle Model.

### 5.2.3 Performing Numerical Simulations

We have performed computational simulations of the Single Particle Model so as to compare the generated velocity probability distribution with that obtained from the equivalent simulation of the Random Force Model. When the key assumptions of the Single Particle Model hold then the high energy particles of the Random Force system are described sufficiently.

A computer simulation of the Single Particle Model can be performed by programming the following routine.

Step one, a circular region is defined with absorbent boundaries at a radius  $l$ .

Step two, the radius is chosen by selecting a value of  $l$  from the distribution of free paths,  $P_l(l)$  (obtained earlier from simulation of the Random Force Model), using the Acceptance-Rejection Method (Abramowitz and Stegun 1965). Simply put, we generate two random numbers  $l$  and  $p$ , from uniform distributions, and accept  $l$  if  $p < P_l(l)$ .

Step three, a particle is placed at rest in the centre of the circular region. The particles position,  $\mathbf{r}$ , and velocity,  $\mathbf{v}$ , evolves with each time-step,  $\Delta t$ , using the 1st order algorithm:

$$\begin{aligned} \mathbf{r}_{t+\Delta t} &= \mathbf{r}_t + \mathbf{v}_t \Delta t, \\ \mathbf{v}_{t+\Delta t} &= \mathbf{v}_t + \frac{\mathbf{F} \Delta t}{M}. \end{aligned} \tag{5.11}$$

The force  $\mathbf{F}$  is the Gaussian random force calculated by the method described in equation 2.23.

Step four, the particle is allowed to move until the position satisfies  $|\mathbf{r}| > l$ , in which case the particle is assumed to have collided with the boundary.

Step five, the above routine is then repeated. The outline routine is repeated many times and the velocity distribution compiled by sampling uniformly in time.

We perform numerical simulations of the Single Particle Model for a variety of systems where the system size is of  $L = 0.6\text{m}$  and dissipation is  $\varepsilon_n = \varepsilon_t = 0.1$ . Figure 5.10 shows comparisons of the velocity distribution obtained from the Random Force Model and Single Particle Model. The solid lines represent the velocity statistics for the Random Force Model whilst the dashed lines are vertically scaled distributions of the Single Particle Model. The vertical scaling is required to compensate for the differences in shape for small velocities brought on by the Single Particle Model inadequacies in describing particles travelling a small free path. Agreement between the model and representation is remarkably good over many decades of  $P(v)$  which demonstrates that the Single Particle Model gets the high velocity behaviour of the particles correct. For low velocities the two distributions deviate: here the velocity distribution is strongly dependent on the distribution of post-collisional velocities.

It is expected that the Single Particle Model will fail to describe the observable behaviour of the Random Force Model for low dissipation systems because assumption of zero initial momentum after collision becomes poor.

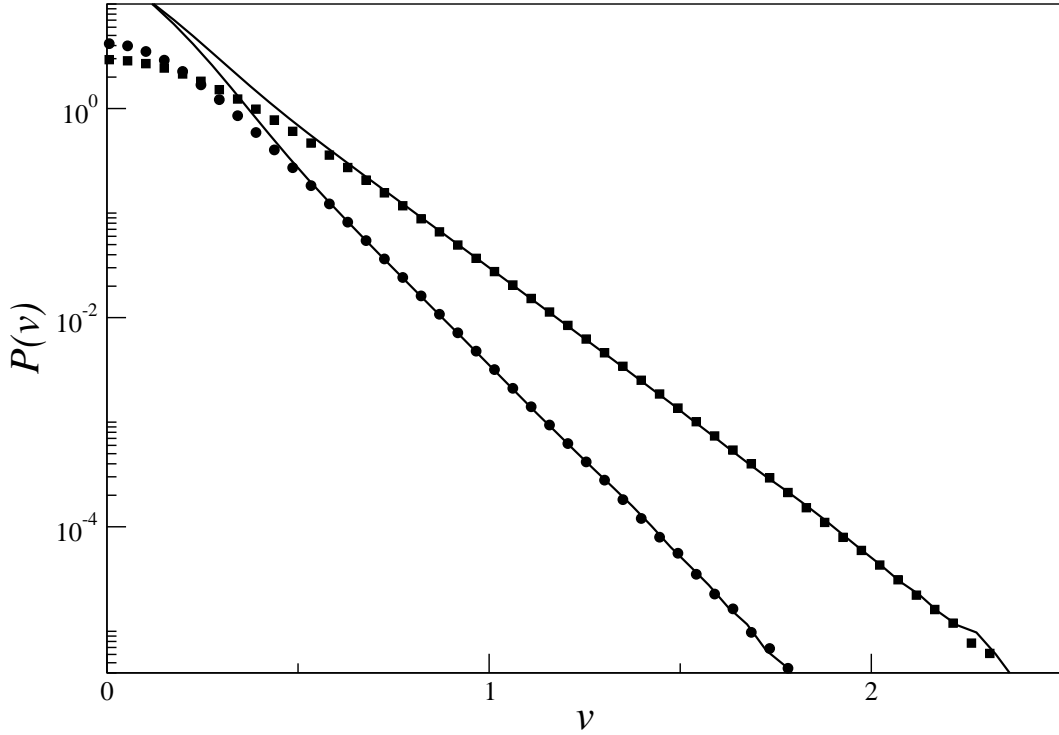


Fig. 5.10: Comparison between the velocity statistics generated from the highly dissipative two-dimensional random force model (data points) and the equivalent single particle model (solid line). The distributions demonstrate agreement across a range of densities for a system of size  $L = 0.6$  where the packing fraction (particle numbers) is either 0.530 (27000) 0.353 (18000), narrowest to broadest distribution respectively.

### 5.3 Self-Consistent Calculation of the Asymptotic Behaviour of the Velocity Distribution

In the previous section we demonstrated that the Single Particle Model does indeed capture the high velocity behaviour of particles within the Random Force Model. Now we aim to determine the specific shape of high velocity tail of the velocity statistics,  $P(v)$ , from knowledge of the structure's fractal dimension,  $D_f$ , and achieve this by solving the SPM Integral Identity, which was stated as:

$$P(v) = \int_0^\infty Q(v, l) P_l(l) dl.$$

In this expression the free path distribution,  $P_l(l)$ , contains all the information about the system's structure and its form was previously determined in chapter four. Thus all we require before solving SPM Integral Identity is to calculate the velocity distribution of a particle contain within a circular region of fixed radius  $l$ ,  $Q(v, l)$ , which we now proceed in doing.

### 5.3.1 A Single Particle in a Circular System of Fixed Radius $l$

Imagine a case where the only information we are given about a target particle's behaviour is that it will travel a distance  $l$  before colliding and starts at rest with no velocity. In such a case a particle can be thought of as being placed in the centre of a circle where the bounding circumference gives possible positions of the next collision. The statistical behaviour of the particle is determined by repetitively placing a particle into the middle of the circle and allowing the particle move, by picking up energy from the random force, until the boundary is met. The velocity distribution of a particle in this system is given by the probability density of the velocity of a particle conditional on the free path being a fixed length  $l$ ,  $Q(v, l)$ .

To obtain an estimate of the exact form of these probability distributions we simulate the system using computers. The routine used is the same as that described for the full Single Particle Model, in section 5.2.3, except that the boundary of the circle remains fixed at a predetermined radius of length  $l$ . The particle's velocity is sampled uniformly in time and a velocity probability density distribution  $Q(v, l)$  is obtained.

We simulate a particle moving in a circle of radius  $l = 0.0036\text{m}$ , the figure 5.11 shows the obtained velocity distribution  $Q(v, l)$  as a solid line. It is worth noting two features common to  $Q(v, l)$ : firstly  $Q(v, l)$  has a cusp at the origin because all walks of the particle (where a walk runs the duration between the time the particle initiates at the origin with zero velocity until it reaches a distance  $l$ ) start with the particle having zero velocity; secondly the shape of  $Q(v, l)$  is independent of  $l$  such that all distributions of  $Q(v, l)$  collapse by the rescaling of the velocity axis, using the map  $v \mapsto v/l^{\frac{1}{3}}$ .

We find that, for large  $v$ ,  $Q(v, l)$  of figure 5.11 can be fitted by the Gaussian,

$$\lim_{v \rightarrow \infty} Q(v, l) \approx A_1 \exp\left(-0.98 \left(\frac{M^2}{2Dl}\right)^{\frac{2}{3}} v^2\right), \quad (5.12)$$

which we show in the figure as a solid line.

### 5.3.2 Solving the SPM Integral Identity

We have now brought ourselves to a position in which we can calculate the high velocity tail of  $P(v)$  using the SPM Integral Identity.

#### Setting up the Integral

The velocity distribution,  $P(v)$ , can always be expressed in the form of a stretched-exponential multiplied by polynomial correctional terms,  $H(v)$ , such that the velocity

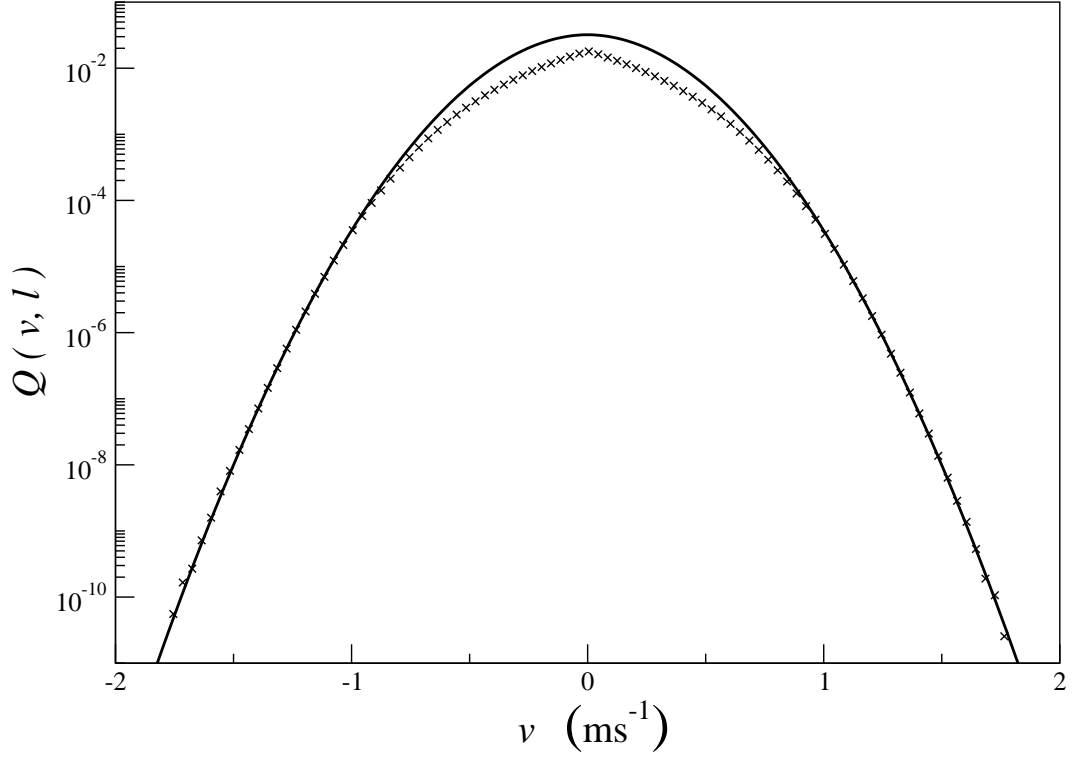


Fig. 5.11: The velocity statistics,  $Q(v, l)$ , of a particle when contained within a circle of radius  $l = 0.0036\text{m}$ , given by data points. An asymptotic fit of  $0.025 \exp(-6.56|v|^2)$  is shown as a solid line.

distribution is given as

$$P(v) \simeq H(v) \exp(-|v/v_A|^\alpha),$$

where  $\alpha$  is a fixed power exponent and  $v_A$  the scaling velocity associated with the high velocity tail. Alternatively,  $P(v)$  can be expressed in terms of  $Q(v, l)$  and  $P_l(l)$ , as was given by the SPM Integral Identity. By the substitution in expressions for  $Q(v, l)$  and  $P_l(l)$ , obtained in earlier sections, the SPM Integral Identity can be calculated approximately by using a steepest decent approach to solve the integral. Our choice of method of integration is only valid for high velocity and so we begin by writing out the large velocity approximate expressions for the components of the SPM Integral Identity. The free path distribution (derived in chapter four) is stated (for large  $l$ ) as

$$P_l(l) \simeq A_0 \beta l^{\beta-1} \exp(-Cl^\beta),$$

where  $\beta = D_f - 1$ ; and the distribution  $Q(v, l)$  is Gaussian of the form

$$Q(v, l) \simeq A_1 \exp\left(-Bv^2/l^{\frac{2}{3}}\right),$$

where  $B = 0.98(M^2/2D)^{\frac{2}{3}}$ . Using these two expressions we re-express the SPM Integral Identity as

$$H(v) \exp(-|v/v_A|^\alpha) = \int_0^\infty A_2 \beta l^{\beta-1} \exp\left(-Bv^2/l^{\frac{2}{3}}\right) \times \exp(-Cl^\beta) dl. \quad (5.13)$$

Here  $B, C$  are constants with respect to  $l$  and  $v$  where as  $A_2 = A_0 \times A_1$  is the normalisation constant. We next simplify the right-hand side of equation 5.13 through the substitution of  $y = l^\beta$ , with which  $dy = \beta l^{\beta-1} dl$ , such that:

$$H(v) \exp(-|v/v_A|^\alpha) = \int_0^\infty A_2 \exp(f(y)) dy, \quad (5.14)$$

where the function  $f(y)$  is defined as:

$$f(y) = -Bv^2/y^{\frac{2}{\gamma}} - Cy, \quad (5.15)$$

and  $\gamma = 3\beta$ . The remaining integral in equation 5.14 is still too difficult to calculate directly and so we instead reduce  $f(y)$  to a power-series where only the dominant leading terms of  $v$  need be considered.

We start by expressing  $f(y)$  in the form of a Taylor series about  $y = y_m$ , where  $f(y_m)$  is the maximum value of  $f(y)$ , such that:

$$f(y) = f(y_m) + \frac{1}{2}(y - y_m)^2 \left. \frac{d^2 f(y)}{dy^2} \right|_{y=y_m} + \frac{1}{6}(y - y_m)^3 \left. \frac{d^3 f(y)}{dy^3} \right|_{y=y_m} + \dots \quad (5.16)$$

This new expression for  $f(y)$  reduces the preceding complex expression down to a simpler power series of  $y$ , with each of the derivatives of  $f(y)$  evaluated at  $y = y_m$ , such that their dependence on  $y$  is removed.

Our next step is to calculate expressions for both  $y_m$  and the derivatives of  $f(y)$ , which we do so in the following few lines. The peak value of  $f(y)$  occurs when the first order derivative, with respect to  $y$ , equals zero with its second order derivative having value less than zero. The first order derivative of  $f(y)$ , with respects to  $y$ , is evaluated at  $y = y_m$  and given by the equality

$$f'(y_m) = \left. \frac{df}{dy} \right|_{y=y_m} = \frac{2}{\gamma} \times \frac{Bv^2}{y_m^{(2+\gamma)/\gamma}} - C \equiv 0. \quad (5.17)$$

Here we are using  $f'(y)$  as shorthand notation for the first derivative and subsequently will continue to use this type of notation for higher order derivatives. The expression implies that the value of  $y$  at which  $f(y)$  is maximised is given by:

$$y_m = \left[ \frac{2Fv^2}{\gamma} \right]^{\frac{\gamma}{\gamma+2}}, \quad (5.18)$$

where  $F = B/C$ .

Having obtained the identity of  $y_m$  we are now able to calculate the second derivative, which is found to be

$$\frac{d^2 f(y)}{dy^2} = -\frac{2}{\gamma} \times \frac{(\gamma + 2)}{\gamma} \times \frac{Bv^2}{y^{(2+2\gamma)/\gamma}}, \quad (5.19)$$

and evaluate  $f''(y)$  at  $y = y_m$  to obtain the expression

$$f''(y_m) = \left. \frac{d^2 f(y)}{dy^2} \right|_{y=y_m} = -A_3 v^{2 \times \left(1 - \frac{2+2\gamma}{2+\gamma}\right)}, \quad (5.20)$$

where  $A_3$  contains the remaining fixed terms of  $\gamma$ ,  $B$  and  $F$ . In fact higher order derivatives can also be expressed in this way and we find that for the  $n^{th}$  derivative of  $f(y)$ , evaluated at  $y = y_m$ , we arrive at:

$$f^{(n)}(y_m) = \left. \frac{d^n f(z)}{dz^n} \right|_{y=y_m} = A_{n+1} v^{2 \times \left(1 - \frac{2+n\gamma}{2+\gamma}\right)}, \quad (5.21)$$

where  $A_{n+1}$  contains the remaining fixed terms of  $\gamma$ ,  $B$  and  $F$ .

It is at this point that we refer back to the Taylor expansion of  $f(y)$  and relate the preceding expressions for  $f^{(n)}(y_m)$  to  $f(y)$  in order to simplify down the expansion to a few leading terms. For large velocity, when evaluated at  $y = y_m$  the magnitude of the  $n^{th}$  order derivative is very much smaller than the  $(n - 1)^{th}$  order derivative, in such a way that

$$|f''(y_m)| \gg |f^{(3)}(y_m)| \gg |f^{(4)}(y_m)| \gg \dots \gg |f^{(n)}(y_m)| \rightarrow 0. \quad (5.22)$$

As a consequence only the first leading power-term of  $v$  in the Taylor expansion of  $f(y)$ , expression 5.16, needs to be considered whereas other powers are neglected. Hence  $f(y)$  can simply be given as

$$f(y) \approx f(y_m) - \frac{A_3}{2} (y - y_m)^2 v^{2 \times \left(1 - \frac{2+2\gamma}{2+\gamma}\right)} + \mathbf{O} \left( v^{2 \times \left(1 - \frac{2+3\gamma}{2+\gamma}\right)} \right), \quad (5.23)$$

without too much loss in accuracy.

### Approximate Integration

We are now in a position to approximate the solution for  $P(v)$  from the SPM Integral Identity. Using the Taylor expansion of  $f(y)$  the equation 5.14 can be rewritten such that:

$$H(v) \exp(-|v/v_A|^\alpha) \approx A_2 \exp(f(y_m)) \int_0^\infty \exp((y - y_m)^2 f''(y_m)) dy. \quad (5.24)$$

We solve the above integral by substituting variables, using  $x = y - y_m$ , to leave the equality:

$$\lim_{v \rightarrow \infty} P(v) \approx \exp(f(y_m)) \int_{-y_m}^\infty \exp(f''(y_m) x^2) dx, \quad (5.25)$$

then, for very large  $v$ , the value of  $y_m$  can be treated as being very large and so the remaining integral approximates to the form of standard identity:

$$\int_{-\infty}^\infty \exp(-Ax^2) dx = \sqrt{\pi/A}.$$

Thus we finally obtain that the overall velocity distribution,  $P(v)$ , is given asymptotically by

$$\lim_{v \rightarrow \infty} P(v) \approx \exp(f(y_m)) \times \sqrt{-\pi/f''(y_m)}. \quad (5.26)$$

All that is left is to replace  $f(y_m)$  and  $f''(y_m)$  with the relevant expressions.

**The Dominant Exponential of  $P(v)$  and the Exponent  $\alpha - \beta$  Relation**

First, we ascertain the shape of the exponential part of  $P(v)$ , contained within the term  $\exp(f(y_m))$ . To do so we express the exponential terms of equation 5.14 by the following equality:

$$-\left|\frac{v}{v_A}\right|^\alpha \equiv -\left[B\left(\frac{\gamma}{2F}\right)^{\frac{2}{\gamma+2}} + C\left(\frac{2F}{\gamma}\right)^{\frac{\gamma}{\gamma+2}}\right] |v|^{\frac{2\gamma}{\gamma+2}}. \quad (5.27)$$

Thought this equality we not only are able to determine the exponent ( $\alpha$ ) of the stretched-exponential part of  $P(v)$  but also its quantitative shape (through calculating  $v_A$ ).

For the equality 5.27 to hold for all values of  $v$  the indexes of  $v$  must match and so the index  $\alpha$  equates to  $\gamma$  by the relation:  $\alpha = 2\gamma/(\gamma + 2)$ . Equivalently the relation can be written as

$$\alpha = \frac{6\beta}{3\beta + 2}, \quad (5.28)$$

which represents the possible allowed combinations for the indexes in the velocity and free path probability distributions. The relation 5.28 does not depend on constants  $B$ ,  $C$ .

From this exponent relation we can now predict the asymptotic shape of the velocity statistics of the two-dimensional Random Force Model. Previously, we have shown that the long distance tail of the free path distribution incorporates the system structure by taking the form:

$$P_l(l) \simeq A \exp(-Cl^{D_f-1}) l^{D_f-2},$$

where  $D_f$  is the fractal dimension found for  $S(k)$  in which  $D_f$  takes a value somewhere in the range  $1.63 \pm 0.03$ . Therefore, as the value of exponent  $\beta$  is by definition given by  $\beta = D_f - 1$ , we determine that the velocity distribution,  $P(v)$ , has a high velocity tail of the form of a stretched-exponential with exponent  $\alpha$  determined as:

$$\alpha = \frac{6\beta}{3\beta + 2} = \frac{6(D_f - 1)}{3D_f - 1} \approx \frac{3.78}{3.89} \approx 0.972 \pm 0.03. \quad (5.29)$$

This solution suggest that the high velocity tail is very close to being exponential.

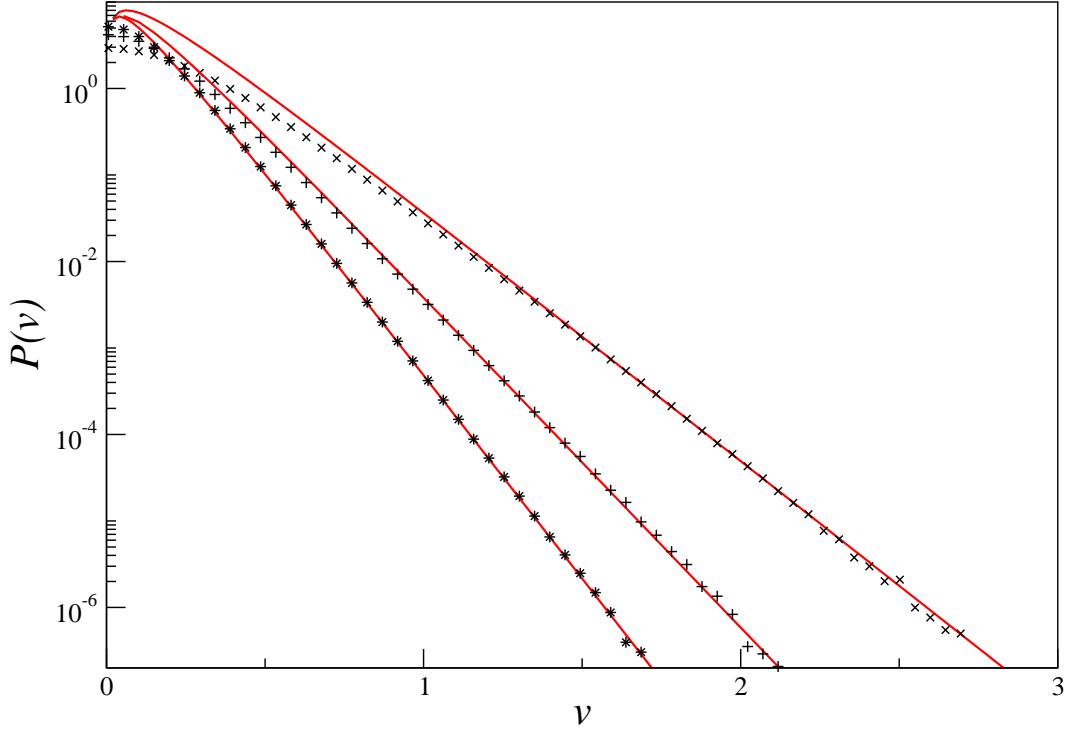


Fig. 5.12: Comparison of the velocity distributions given by data from the Random Force Model (data points) and the predicted asymptotic behaviour (line). Three highly dissipative systems ( $\varepsilon_n = \varepsilon_t = 0.1$ ) are shown with packing fractions of either  $\phi = 0.619$  (star),  $\phi = 0.530$  (plus) or  $\phi = 0.353$  (cross).

### Power-law Contribution and the Complete high Velocity Shape of $P(v)$

Having determined the dominant exponential term of  $P(v)$  we next ascertain the leading power contributions of  $v$  contained within  $H(v)$ . In expression 5.26  $H(v)$  was approximately given by  $\sqrt{-\pi/f''(y_m)}$ , with  $f''(y_m)$  defined in equation 5.20, it therefore follows that the leading term of  $H(v)$  is determined as:

$$H(v) \sim v^{\left(\frac{2+2\gamma}{2+\gamma}\right)-1}. \quad (5.30)$$

Again we can calculate an approximate magnitude of the power of  $H(v)$  by using a suitable value for  $\beta = D_f - 1$ , measured from simulation data of the Random Force Model, and hence we determine that the leading power for  $H(v)$  is given by  $H(v) \sim v^{0.49 \pm 0.02}$ .

The full asymptotic shape of the velocity distribution can hence be written as:

$$\lim_{|v| \rightarrow \infty} P(v) = A_0 \exp\left(-|v/v_A|^{\frac{6(D_f-1)}{3D_f-1}}\right) v^{\frac{3(D_f-1)}{3D_f-1}}. \quad (5.31)$$

### 5.3.3 Comparison with data from the Random Force Model

With this derived form for  $P(v)$  we are now in the position to test and confirm that this new theory not only predicts the correct high velocity shape but also determines the correct gradient.

We simulate three highly dissipative systems, each with system size of  $L = 0.6\text{m}$  and a packing fraction of either 0.353, 0.530 or 0.619. During the simulations we calculate the free path distribution and use this to estimate the value of the constant  $C$  by applying equation 5.3.2. We find that  $C$  approximately equals 78, 121 and 179 for the three respective systems. Our choice of particle mass ( $M$ ) and noise strength ( $D$ ) means that  $Q(v, l)$  is described for large  $v$  by  $\exp(-Bv^2/l^{\frac{2}{3}})$ , where  $B = 0.154$ . With these values for  $C$  and  $B$  we can obtain the value of  $v_A$ , which controls the gradient of the high velocity tail, using equation 5.27.  $v_A$  is determined to be either 7.21, 9.48 or 11.60 for the three respective systems. These values thus represent predictions for the shape of the high velocity tail of  $P(v)$ .

In figure 5.12 we illustrate the good agreement that can be achieved, for large velocities, between the predicted solution for  $P(v)$  and the real data obtained from simulation of the Random Force Model. The data can be seen to agree over at least four decades of data. As the packing fraction increases the agreement improves as the crossover velocity (between the low-velocity behaviour described by a Gaussian and the high velocity behaviour) in these distributions decreases towards zero and the high velocity tail begins at lower velocity-scales.

As the agreement between the prediction and simulation data is so good and visible at observable velocity scales this leads us to wonder why our direct measurements from the Random Force Model data using standard practices could not extract a value for exponent  $\alpha$  close to one. The predicted value of  $\alpha$  is significantly lower than the value of  $1.16 \pm 0.02$  measured directly from the velocity distribution of the Random Force Model. The discrepancy is due to the method of analysis used previously. Firstly, the previous method of curve fitting produces overestimates for the value of  $\alpha$  as it places more emphasis on higher parts of the distribution which are assumed to be more reliable which is not the case. Secondly, the plots of  $-\ln(-\ln(P(v/v_{rms})/P(0)))$  against  $\ln(v/v_{rms})$  are misleading because they assume that the amplitude of the asymptotic behaviour of  $P(v)$ ,  $A_0$ , is equal to  $P(0)$ . By using  $P(0)$  in these plots the central peak is determined as a Gaussian but the asymptotic shape becomes distorted. Instead to study asymptotic behaviour we must actually plot  $-\ln(-\ln(P(v/v_{rms})/A_0))$  against

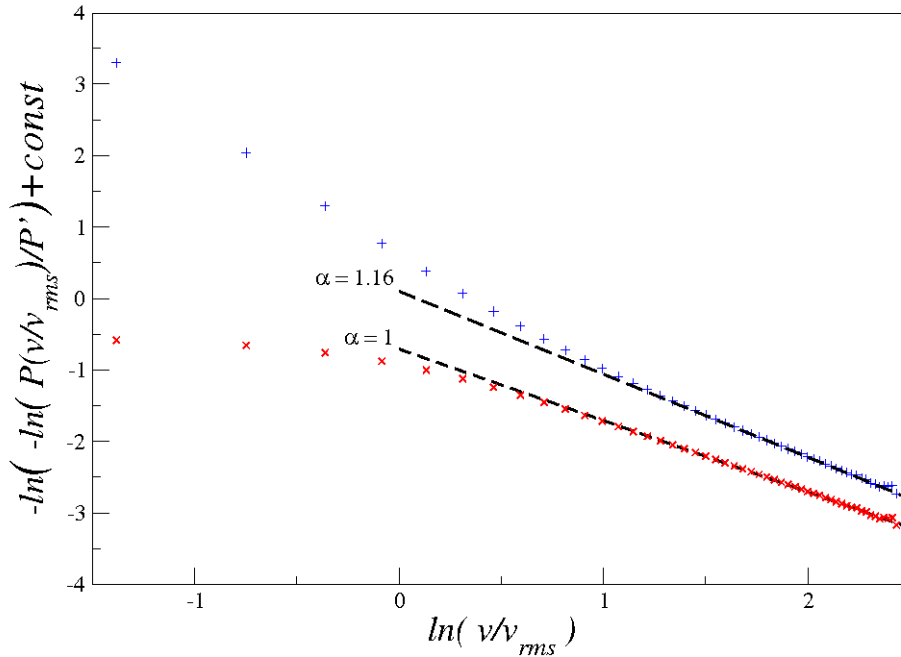


Fig. 5.13: Demonstration that asymptotic form of the velocity distribution predicted by Single Particle Model is consistent with data from the Random Force Model. We choose a high dissipation system of packing fraction  $\phi = 0.530$  and treat  $P'$  as equal to either  $P(0)$  (plus) or  $A_0$  (cross). The lines represent linear fits of  $-1.15 \ln(v) + \text{const.}$  (upper line) or  $-1.0 \ln(v) + \text{const.}$  (lower line).

$\ln(v/v_{rms})$  such that the asymptotic shape is determined correctly at the expense of distorting the low velocity Gaussian. This approach has a drawback as we first have to know the asymptotic shape of  $P(v)$  in order to know the value of  $A_0$  and hence we cannot and should not use these kinds of plots as a method to determine what the asymptotic shape of  $P(v)$  is.

To demonstrate the effect of the two different approaches we plot, in figure 5.13,  $-\ln(-\ln(P(v/v_{rms})/P'))$  against  $\ln(v/v_{rms})$  for a two-dimensional Random Force Model of packing fraction  $\phi = 0.530$ , where  $N = 27000$  and  $L = 0.6\text{m}$ , and the dissipation is  $\varepsilon_n = \varepsilon_t = 0.1$ . We either choose  $P'$  to be either  $P(0)$  taken from the maxima of the  $P(v)$  data or  $A_0$  calculated by fitting an exponential asymptotically to the data. We find that the value of  $A_0$  is between seven and eight times larger than  $P_0$ . The figure shows that by changing the value of  $P'$  from  $P(0)$  to  $A_0$  we lower the apparent value of exponent  $\alpha$  without causing the apparent shape of the large velocity behaviour to deviate from being stretched-exponential. Not only is the high velocity tail of the

velocity distribution fitted by a simple exponential ( $\alpha \simeq 1.00$ ), but also the range of high velocities for which it is a good fit is greater than the equivalent for a stretched-exponential with exponent  $\alpha = 1.16$ . Thus an exponential really does provide a better description for the true asymptotic shape of the velocity distribution as predicted by the Single Particle Model. Moreover, this diagram demonstrates how difficult it is to get a reliable, unbiased measurement of  $\alpha$  from the velocity distribution data alone.

### 5.3.4 Implications for lower Dissipation Systems

Having understood the behaviour of the highly dissipative systems we would now like to understand the behaviour of lower dissipative systems. The Single Particle Model tells us much more than the velocity distribution for the highly dissipative systems. In all systems the behaviour of the particles changes from having a low velocity that is influenced heavily by the memory of the previous collision to having a high velocity influenced solely by the random force. As the dissipation of the system decreases the velocity-scale at which a particle crosses over from one behaviour to the other rises and higher velocities are required before the particle is memoryless such that it acts as a particle in the Single Particle Model.

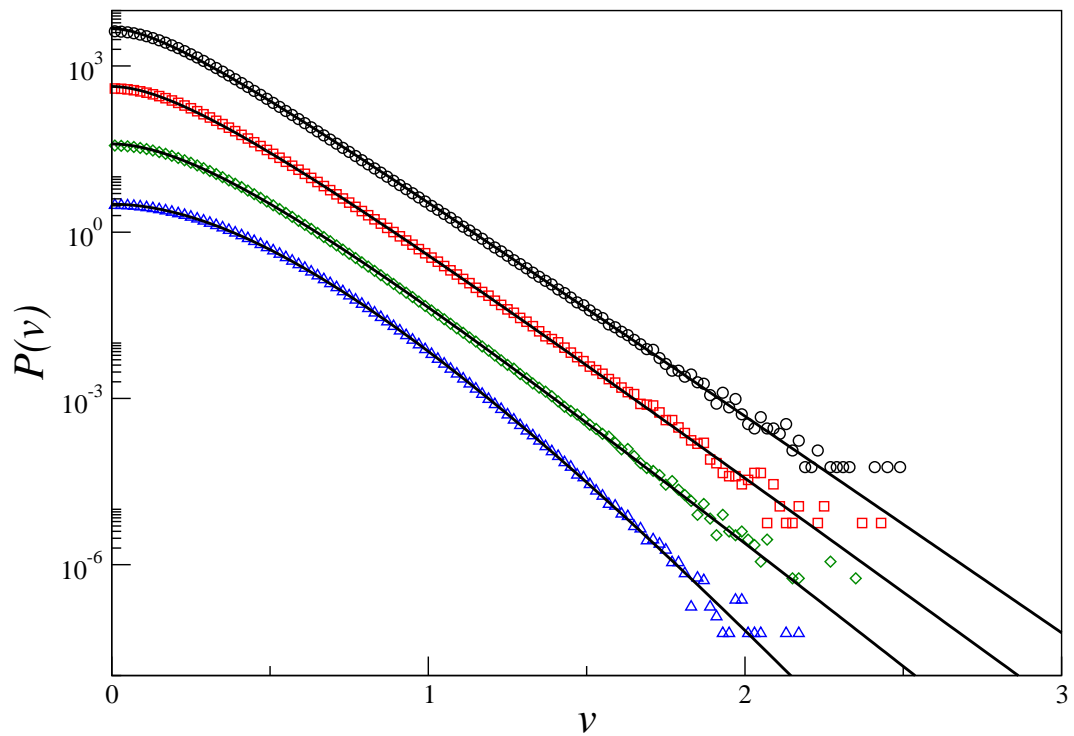
Given that the fractal dimension of the large scale structure of the Random Force Model is unchanged with variation of dissipation, the Single Particle Model would suggest that the asymptotic behaviour of the high velocity particles must be the same. Therefore the velocity distribution of Random Force Model for any dissipation must approximately tend to an exponential as  $v$  tends to infinity. Hence, let us propose that  $P(v)$  is given by a simple crossover function,  $P_0$ , which we define as

$$P_0(v) = D \exp\left(\frac{-(v/v_r)^2}{1 + |(v/v_c)|^{(2-\alpha)}}\right), \quad (5.32)$$

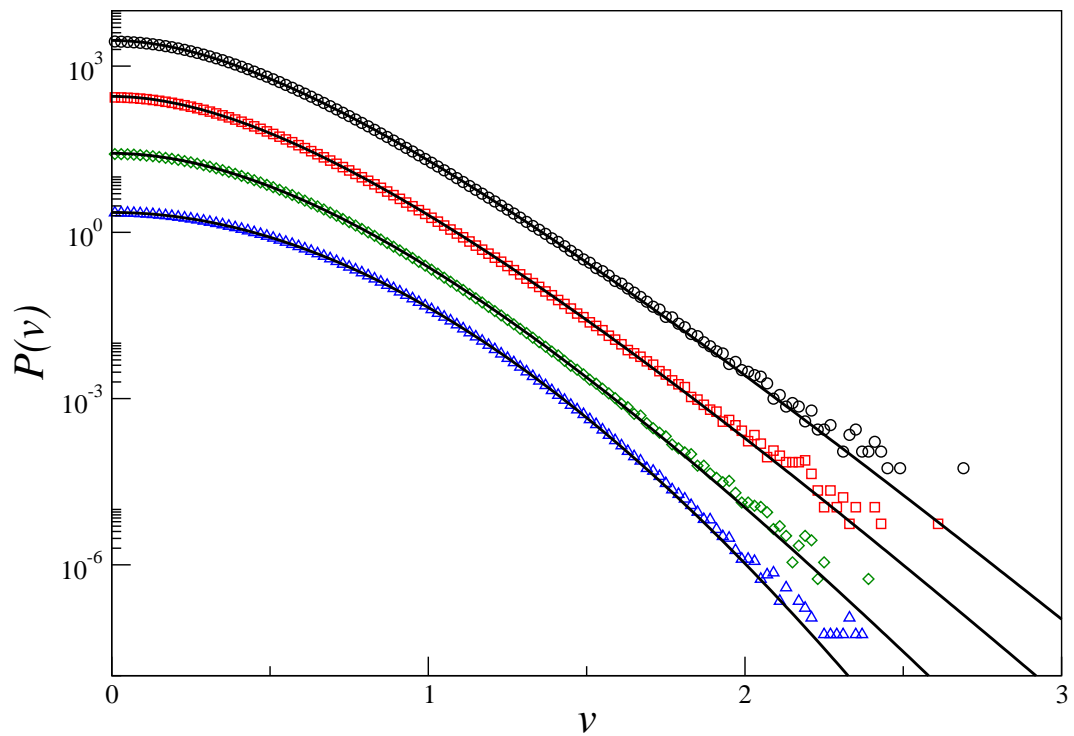
where  $\alpha$  is taken to be 1.00 for simplicity and the crossover velocity of the distribution is simply given by  $v_c$ . For low velocities the distribution is Gaussian with width determined by the velocity-scale  $v_r$ . For high velocities the distribution is exponential with width characterised by the velocity-scale  $v_A = (v_r)^2/v_c$ .

Figure 5.14(a) demonstrates that the velocity distribution of the highly dissipative Random Force Model, where tangential dissipation is maximised at 0.1, can be described by the crossover function  $P_0(v)$ .  $P_0(v)$  is obtained by best fitting to the data and a close fit is achieved for low velocity scales as well as for high velocity. Figure 5.14(a) also illustrates that as the dissipation of the system decreases the high velocity tail can superficially appear less exponential-like. This is because as the dissipation of

Fig. 5.14: Demonstration on scaled velocity distributions that the crossover function  $P_0(v)$  provides a good description for  $P(v)$ .



(a) Here the tangential coefficient of restitution is fixed at 0.1 where as the normal coefficient of restitution takes values of  $\epsilon_n =$ : 0.1(circle); 0.4(diamond); 0.6(square) and 0.9 (up-triangle). The lines are best fits for the crossover function described in the tables.



(b) Here the tangential coefficient of restitution is fixed at 1.0 where as the normal coefficient of restitution takes values of  $\epsilon_n =$ : 0.2(circle); 0.4(diamond); 0.6(square) and 0.8 (up-triangle). The lines are best fits for the crossover function described in the tables.

the system reduces, the crossover velocity,  $v_c$ , increases relative to the root mean square velocity of the velocity distribution, and hence the true asymptotic tail is pushed out towards higher velocity.

Using the measured fits of  $P_0(v)$  we can make specific predictions about the velocity scale and probability at which the velocity distribution crosses over from being Gaussian to asymptotic behaviour. The high velocity tail of the distribution will occur at velocity scales greater than the crossover velocity  $v_c$ . In order to see this high velocity tail in the data of  $P(v)$  we need to have data points with probability of value less than  $P(v_c) = P(0) \exp(-(v_c/v_r)^2/2)$ . The table below shows the values of  $v_c$  and  $v_r$  obtained by fitting the velocity distribution with  $P_0(v)$ . The table also calculates the relative number of decades required before the asymptotic behaviour of the distribution will start to be seen.

$\varepsilon_n, \varepsilon_t$	$v_r$	$v_c/v_r$	$P(v_c)/P(0)$
0.1, 0.1	0.168	1.524	0.313
0.2, 0.1	0.177	1.540	0.260
0.3, 0.1	0.186	1.743	0.219
0.4, 0.1	0.198	1.914	0.160
0.5, 0.1	0.213	2.141	0.101
0.6, 0.1	0.231	2.463	0.292
0.7, 0.1	0.253	2.927	0.0138
0.8, 0.1	0.282	3.784	$7.78 \times 10^{-4}$
0.9, 0.1	0.318	5.100	$2.24 \times 10^{-6}$

Table 5.3: The measurement of the value of the crossover velocity,  $v_c$  and the relative probability of this occurring by fitting  $P(v)$  of higher dissipation systems to a crossover distribution  $P_0(v)$ .

The table shows that for very high dissipation the high velocity tail is very long relative to the peak and the tail of the distribution begins less than one decade down from the peak of the distribution. Hence these distributions look very exponential like in the tails. It is only when the dissipation of the systems is very low (see lowest three entries in table) that the crossover velocity become large relative to the  $v_r$ , even though  $v_r$  has changed very little in value between  $\varepsilon_n = 0.1$  and  $\varepsilon_n = 0.9$ , with an increase of only approximately 1.5 times in value for  $v_r$  compared to approximately 5 times in value for  $v_c$ . Thus for these lower dissipation systems, the high velocity tail of  $P(v)$  will begin at least 4 decades beneath the peak. The apparent tail of the distribution

appears curved (see lowest data set in figure 5.14(a)) and stretched-exponential-like because we can only simulate between 6 to 8 decades of  $P(v)$ , in a reasonable amount of time. This results in at most two decades of visible high velocity tail compared to six decades of peak and crossover behaviour.

The situation worsens when studying moderate to low dissipative systems in which dissipation tangential to the collision is prevented ( $\varepsilon_t = 1.0$ ). Figure 5.14(b) illustrates that in these systems functions of  $P_0(v)$  can again be fitted to  $P(v)$  such that good agreement is obtained over the complete range of velocity scales. While the table below shows the corresponding values of  $v_r$  and  $v_c/v_r$  and  $P_0(v_c)/P(0)$  for these systems.

$\varepsilon_n, \varepsilon_t$	$v_r$	$v_c/v_r$	$P(v_c)/P(0)$
0.2, 1.0	0.337	3.877	$5.45 \times 10^{-4}$
0.3, 1.0	0.344	4.107	$2.17 \times 10^{-4}$
0.4, 1.0	0.352	4.469	$4.59 \times 10^{-5}$
0.5, 1.0	0.365	5.133	$1.90 \times 10^{-6}$
0.6, 1.0	0.389	6.469	$8.16 \times 10^{-10}$
0.7, 1.0	0.422	9.592	$\sim 10^{-20}$
0.8, 1.0	0.481	23.037	$\sim 10^{-115}$

Table 5.4: The measurement of the value of the crossover velocity,  $v_c$  and the relative probability of this occurring by fitting  $P(v)$  of lower dissipation systems to a crossover distribution  $P_0(v)$ .

Consequently in these cases, to have a good chance of seeing the high velocity tail fairly low values of normal coefficient of restitution must be chosen, whereby  $\varepsilon_n < 0.5$ . Once the dissipation of the system is significantly reduced and the coefficient of normal restitution has risen, to say  $\varepsilon_n \simeq 0.6$ , the high velocity tail of  $P(v)$  is hidden beneath probabilities that can be obtained through simulated data. It is thus not a surprise that these velocity distributions appear to be non-universal at such low dissipations, whereby the apparent high velocity tail is stretched-exponential with an exponent increasing towards two as dissipation continues to reduce.

## 5.4 Summary

We began this chapter by measuring the velocity distributions of the Random Force Model for a range of systems dissipation that included both normal and tangential coefficients of restitution. With the inclusion of the tangential coefficient of restitution

we have been able to raise the dissipation of the system to higher extents than has previous been studied. We showed that the velocity distribution could be described by a function that crossed over from being Gaussian distributed for low velocity, caused by the randomisation of momentum at collision; to non-Gaussian stretched-exponential behaviour for high velocity described by an exponent  $\alpha$ . Importantly we showed that the velocity distribution is not asymptotically described by  $P(v) = A \exp(-|v/v_0|^{1.5})$ . Instead the exponent of 1.5 is a fact of the finite accuracy.

These observations parallel those seen for a one-dimensional system. In both the one- and two-dimensional Random Force Model there exists a range of high dissipations where the distribution of velocity collapse onto one asymptotic shape.

The main purpose of the first section was to demonstrate how difficult it was to calculate a reliable estimate for the value of  $\alpha$  using standard methods. This results from the fact that we do not know how to correctly weight the errors of the distributions or how much of the high velocity tail of the distribution is visible. Therefore any estimate we derive for the value of  $\alpha$  is likely to be an overestimate of its true value. Hence it is difficult to state anything more than a qualitative description of the asymptotic shape of the velocity distribution.

We next provided a theory for the asymptotic shape of the velocity distribution for the two-dimensional Random Force Model by focussing on the motion of a single fast particle which we encapsulate in the description of the Single Particle Model. This Single Particle Model treats high velocity particles as singular particles driven by a random force through a fractal background environment until collision. Essential to the model are the assumptions that these particles: have zero velocity after collision; will collide when they first reach a distance of the free path length; can travel along any viable path. These assumptions only hold for the highest velocity particles where sufficient velocity is built up through successive interactions with the random force that their motion is effectively ballistic and their initial momentum, after previous collision, can be neglected.

The velocity distribution,  $P(v)$ , is calculated by solving the SPM Integral Identity:

$$P(v) = \int_0^\infty Q(v, l)P_l(l) dl,$$

where  $P_l(l)$  is the probability a particle travels a free path  $l$  between collision and  $Q(v, l)$  is the velocity distribution of a particle travelling a distance  $l$ . Through numerical simulation we have showed that the SPM Integral Identity well describes the high velocity tails of  $P(v)$  and we next derive the extreme asymptotic shape. The high

velocity tail of  $Q(v, l)$  is determined to be Gaussian whereas the long distance tail of the free path distribution is calculated using the theory of Isliker and Vlahos (2003) to be of the form:

$$P_l(l) \simeq A_0 \exp(-Cl^{D_f-1}) l^{D_f-2},$$

where  $D_f$  is the fractal dimension of the Random Force Model with a value that lies in the range of 1.60 to 1.66. Thus, we predict that the velocity distribution is described by a stretched-exponential with exponent  $\alpha = 6(D_f - 1)/(3D_f - 1)$ . This value of  $\alpha$  is very near unity such that the asymptotic shape of  $P(v)$  can be considered approximately exponential. Incidentally an exponential is also predicted from the Maxwell Model of the Boltzmann equation, but this is derived for different reasons.

We showed that  $P(v)$  is sufficiently described, over all  $v$ , by a crossover function that is Gaussian for low velocities and exponential for high velocities, even for low dissipation systems. Physically this distribution represents the change in behaviour that occurs from particles losing memory of previous collisions as momentum is picked up from the random force after a collision.

Significantly, the only value needed to be calculated from simulation is the fractal dimension  $D_f$ . Ideally we would like to predict  $D_f$  as well, enabling us to calculate the behaviour of the Random Force Model without performing any simulations. In the next chapter we propose that the fractal dimension  $D_f$  can be predicted using geometrical considerations. We are motivated by the one-dimensional model where we showed that there is some evidence that the system self-organises into a state of criticality. We now ask ourselves the question: can the two-dimensional Random Force Model do the same and what would this mean for the fractal dimension?

## Chapter 6

# Multiplicative Cascade Process and Fractal Structure

In this chapter we hypothesise a mechanism to generate fractal structure of the type observed for the two-dimensional Random Force Model. Using this mechanism we measure a fractal dimension,  $D_f$ , close to those obtained from our simulations of the Random Force Model.

### 6.1 Self-Similarity

At the end of the paper of Peng and Ohta (1998a) it was suggested that the two-dimensional Random Force Model might self-organise into a state of criticality. This was suggested as an explanation for why these systems showed neither a characteristic spatial-scale nor temporal-scale. From our studies, in chapter four, we confirmed that the structure factor,  $S(k)$ , has small  $k$  dependence that varies as a power-law. This power-law is a fractal feature of the system and implies that features of different length-scales show self-similarity towards one another. Therefore the system can rescale its lengths without affecting its large-scale structural behaviour, as occurs during the process of renormalisation. These arguments will only apply to the large-scale features of the system which are described by the power-law decay of  $S(k)$ . However, as the size of the system is increased towards infinite extent more of the system features are large-scale compared to the particle diameter and the system exhibit self-similarity over a larger range of length-scales.

When we discussed the one dimensional Random Force Model we suggested that the system had structure that was approximately renormalisable. We proceeded to perform

decimation on the particles during snap shots of a system with  $2N$  particles in which we removed every other particle from the system to leave only  $N$  particles. The remaining system had half as many particles and had statistical structure that was approximately similar to a  $N$  particle Random Force Model. This demonstrated that the structure of these systems were statistically self-similar.

The corresponding method for renormalising a two-dimensional system is called blocking. To demonstrate how this method works we use the example of the two-dimensional Ising model of a critical  $2N$  by  $2N$  spin lattice. Each lattice site is either occupied or not. The system is renormalised in the following way: first, the sites are grouped into squares of four; second, the total number of occupied sites in each group of four is counted; third, each square of four lattice points is reduced down to one lattice site, which takes position at the average position of the four replaced lattice points; fourth, the new site is chosen to be either occupied or not by using a majority rule in which it is occupied if most of the original four sites were also occupied. The result of the renormalisation is a  $N$  by  $N$  spin lattice with structural features that are self-similar to the original  $2N$  by  $2N$  system.

These ideas of renormalisation can be applied to the two-dimensional Random Force Model. In this case we split the system into  $2N$  by  $2N$  square boxes, of length  $L/2N$ . The occupancy of each box is equal to the number of particles found within. The centre of each box is equivalent to the lattice point described in the Ising model. The system is renormalised by the same process, as outlined above for the Ising model, except that instead of using a majority rule to determine the occupancy of a new box it is simply assigned to be the sum of the occupancies of the four boxes it replaced.

Formulating the system in this way leads us to consider that, if we can remove structural features by merging boxes, then it might be possible to do the reverse process and increase structure by breaking the boxes into smaller boxes. Imagine that we have a system of  $N$  particles. Initially all we know is that the particles are distributed somewhere in the square system and so we create a box spanning the whole system and give it an occupancy of  $N$ . The structure of the system is then generated by the following routine.

One, the box is broken into four smaller square boxes, each with a side length half that of the unbroken box. Two, we generate the occupancy of the four new boxes by randomly assigning an integer proportion of the occupancy of the original unbroken box to each. The total occupancy of the four new boxes equals that of the original

unbroken box. Three, we then repeat the above process by breaking up all the new boxes into four new boxes.

By repeatedly breaking the system into smaller boxes we obtain detail on the structure of the system at smaller length-scales.

This method for the generating the structure has one limitation: the system can only be broken down into smaller regions a finite number of times before each box has a maximum occupancy of one particle, which means that only structural features over a finite range of length-scales can be measured. An alternative method to particle occupancy of a box is to treat the occupancy of each box as the probability of finding a particle in that region. This has no effect on the generated macroscopic structural properties but will change the microscopic features seen.

## 6.2 The Multiplicative Cascade Process

In this section we aim to describe a method of breaking a system into parts, which we call the Multiplicative Cascade Process, in a way that captures the process outlined in the previous section. Multiplicative Cascade Processes have been used successfully to describe a variety of scientific systems, most notably that of turbulence (Kolmogorov 1941) and also in predicting the spatial distribution of rainfall (Over and Gupta 1996). The process can be thought of as determining the probability that each region of the system is occupied by a particle. The system is represented by an array of  $2^n$  by  $2^n$  square regions where  $n$  is an integer. Each square region is identified by being the  $(i + 1)^{th}$  across in the  $x$ -direction and  $(j + 1)^{th}$  down in the  $y$ -direction, where  $i$  and  $j$  take integer values between 0 and  $2^n - 1$ . The position of the centre of the square is given by the coordinates  $\mathbf{r}(n)_{i,j}$  where:

$$\mathbf{r}(n)_{i,j} = \frac{L}{2^n} \begin{bmatrix} i + 1/2 \\ j + 1/2 \end{bmatrix}. \quad (6.1)$$

The index  $n$  indicate the overall number of regions. Each region has an occupancy given by the probability,  $m_{i,j}(n)$ , which takes a value between 0 and 1.

### 6.2.1 Outline of the Method

The general routine for Multiplicative Cascade Processes is as follows. The system is consecutively broken into parts by progressing through a set number of levels. The zeroth level encompasses the complete system by a single square region of extent  $L$ ,

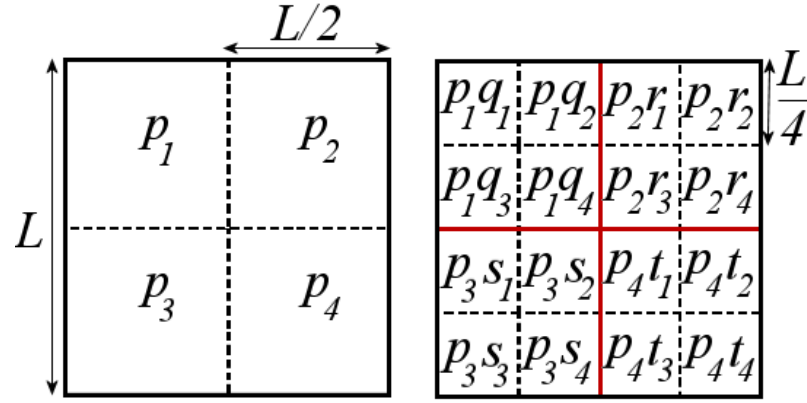


Fig. 6.1: The diagram shows the splitting of the system space into squares for the first two levels of the Multiplicative Cascade Process. The probability  $m_{i,j}(n)$  of each square is shown at the centre of each square as the product of random numbers. The symbols  $p_i$ ,  $r_i$  and  $s_i$  and  $t_i$  are random numbers that satisfy  $\sum_{i=1}^4 s_i = 1$ .

with centre position of  $\mathbf{r}_{0,0}(0) = L/2(1, 1)$ . On reaching the  $n^{th}$  level the system has fractured into  $4^n$  smaller squares with centre positions as given in equation 6.1. To progress from one level to the next, say from the  $n^{th}$  to the  $n + 1^{th}$  level, each and every square region of length  $L/2^n$  is broken up in to four smaller square sub-region of extents  $L/2^{n+1}$ . The probability  $m_{i,j}(n)$  of the original square region is shared amongst the four new square sub-regions without preference such that the sum of the four squares probabilities equals the original unbroken square's probability. The figure 6.1 demonstrates the Multiplicative Cascade Process that occurs when progressing from the first to the second level.

**Partitioning the probability  $m_{i,j}(n)$  into four**

There are many methods in which the probability of a square can be broken into four parts. We outline one particular method of ‘probability breaking’ which we shall call Uniformly breaking whilst Conserving Probability (UCP). At the  $n^{th}$  level each square is broken into four. The probability  $m_{i,j}(n)$  of the square is shared by the four replacement square by: first, generating four random numbers  $a_{2i+g,2j+h}$ , where  $g$  and  $h$  takes values 0 and 1, using a uniform distribution such that  $0 < a_{2i+g,2j+h} < 1$ ; then, calculating the new probabilities  $m_{2i+g,2j+h}(n + 1)$  of each replacement square using the expression:

$$m_{2i+g,2j+h}(n + 1) = m_{i,j}(n) \frac{a_{2i+g,2j+h}}{A_{2i,2j}} \quad g, h = 0, 1. \tag{6.2}$$

The term  $A_{i,j}$  normalises and correlates the four square sub-regions through:

$$A_{i,j} = a_{i,j} + a_{i+1,j} + a_{i,j+1} + a_{i+1,j+1}. \tag{6.3}$$

The inclusion of  $A_{i,j}$  ensures the conservation of probability between the  $n^{th}$  and  $(n + 1)^{th}$  level. This method maximises the randomness of the partitions at each stage of the process.

### Other Methods of Probability Breaking

For the purpose of comparison, we now briefly describe three alternative methods of ‘probability breaking’ which are related to UCP but differ when calculating the random numbers  $a_{i,j}$ ,  $a_{i+1,j}$ ,  $a_{i,j+1}$  and  $a_{i+1,j+1}$ .

In the first method we do not ensure probability conservation by replacing equation 6.3 with  $A_{i,j} = 1$ . We call this method UnonCP. In the second method, the probability of each square is shared into four by using a symmetrised method such that:

$$\begin{aligned} a_{i,j} &= a_{i+1,j+1} \\ a_{i+1,j} &= a_{i,j+1} \equiv 1 - a_{i,j}. \end{aligned} \tag{6.4}$$

For each square we only need to calculate the value of  $a_{i,j}$  to obtain the value of the three other random numbers. We choose  $a_{i,j}$  from a uniform distribution such that  $0 < a_{i,j} < 1/2$ . This method we call Symmetrised Cascade. The third method is given in the paper of Meakin (1987). Four numbers,  $p_1, p_2, p_3, p_4$ , are predetermined (such that the sum adds up to one) and simply randomly assigned once to the four random numbers  $a_{2i+g,2j+h}$ . These models have been used before to generate a fractal. We consider four possible Meakin models where the numbers,  $p_i$ , are defined in the table below:

Process	$p_1$	$p_2$	$p_3$	$p_4$
Meakin 1	0.001	0.15	0.32	0.53
Meakin 2	0.02	0.32	0.32	0.34
Meakin 3	0.18	0.21	0.29	0.31
Meakin 4	0.07	0.26	0.32	0.36

Table 6.1: A sample selection of the allowed choices for the set of numbers,  $p_i$ , that can be used when performing Meakin Model.

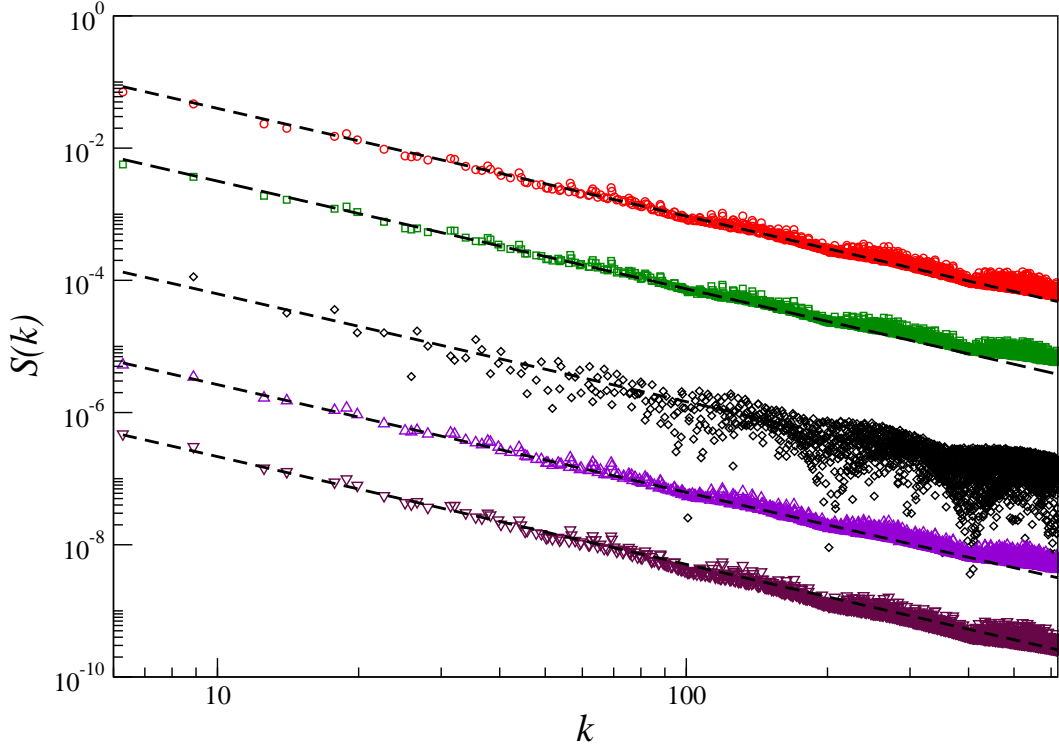


Fig. 6.2: The structure factor obtained for various Multiplicative Processes: UCP (circle); UnonCP (square); Symmetrised Cascade (diamond); Meakin 2 (up-triangle) and Meakin 4 (down-triangle). The dashed lines is a power-law fits of  $Ak^{-1.63}$ .

### 6.2.2 Comparison with data from the Random Force Model

The purpose of the following section is to demonstrate that Multiplicative Cascade Processes can produced geometric structures of the form seen in the two-dimensional Random Force Model. We define an equivalent measure to the structure factor and find that these functions are described by a power-law decay whereby the exponent  $-D_f$  can have the same value for a variety of different versions of the Multiplicative Cascade Process that is consistent with that seen for the Random Force Model.

The structure factor for the Multiplicative Cascade Process can be defined as:

$$S(\mathbf{k}) = \left\langle \sum_{i=1}^{2^n} \sum_{j=1}^{2^n} m_{i,j} \exp(i(\mathbf{k} \cdot \mathbf{r}_{i,j})) \times \sum_{i=1}^{2^n} \sum_{j=1}^{2^n} m_{i,j} \exp(-i(\mathbf{k} \cdot \mathbf{r}_{i,j})) \right\rangle, \quad (6.5)$$

where  $\mathbf{r}_{i,j}$  is the position of the centre of the square described earlier and  $\langle \cdot \rangle$  represents a configuration average. The angular average structure factor  $S(k)$  is calculated in the same way as for the Random Force Model.

We simulate the discussed Multiplicative Cascade Processes by breaking square regions into four until the eighth level is reached. In each case a system of length  $L = 1\text{m}$

is broken up into  $256 \times 256$  squares, each of length  $1/256 = 3.91 \times 10^{-3}$ m. This process of breaking the system is repeated for a large number of runs and a configuration average structure factor measured.

Figure 6.2 shows part of the structure factor obtained from different versions of the Multiplicative Cascade Process given in 6.2.1. These distributions are displayed vertically for clarity. The periodic features are due to the choice of square lattice and the number of levels used. Running the Process to higher levels reduces these features. In the figure we demonstrate, for a range of different variant of the Multiplicative Cascade Process using dashed-line fits of the form  $S(k) = Ak^{-1.63}$ , that it is possible to fit the generated structure factor with a power-law that has an exponent  $D_f$  of similar value, around 1.63.

Having shown it is possible to describe these structure factors with an exponent of fixed value we next more accurately determine  $D_f$  by fitting the structure factor to a power-law of the form  $S(k) = Ak^{-D_f}$  using a  $\chi^2$  fitting program. The following table shows the obtained measurements of the fractal dimension  $D_f$  for the different versions of the Multiplicative Cascade Process (except for Symmetrised Cascade which is difficult to accurately fit):

Process	$D_f$
UCP	$1.602 \pm 0.066$
UnonCP	$1.595 \pm 0.064$
Meakin 1	$1.287 \pm 0.084$
Meakin 2	$1.596 \pm 0.147$
Meakin 3	$1.828 \pm 0.233$
Meakin 4	$1.689 \pm 0.178$

Table 6.2: The measured values of the fractal dimension  $D_f$  for different Multiplicative Cascade Processes where  $S(k)$  is fitted by  $Ak^{-D_f}$ .

The quoted errors arise from the systematic effects shown in figure 6.2. Our calculation determines that both the UCP and UnonCP gives values for  $D_f$  that lie within the range 1.60 to 1.66 suggesting there is little difference between these two solutions. In contrast, the Meakin models appear to give very different answers but on closer examination we find that the Meakin models (that of 2, 3 and 4) can take a value within the range 1.60 to 1.66.

Significantly, it is only with Meakin 1 that the range 1.60 to 1.66 does not lie within

the allowed range of exponent  $D_f$ . This model is different from the others as the random number  $p_1$  is effectively zero and hence makes a case in point because once a square region has a probability ( $m_{i,j}$ ) of zero, then all subsequent divisions of the square will also have probability zero. Therefore square region with probability of zero are not structurally similar to other square regions in the system that have non-zero probability. In consequence Meakin 1 should be considered separate from the rest.

Finally, as these models generally allow  $D_f$  to be in the range 1.60 to 1.66 we speculate that this may mean that the value of  $D_f$  might be caused by the hierarchical nature of the Multiplicative Cascade Process. Although we concede that to explore this idea fully would require further work.

### 6.3 Summary

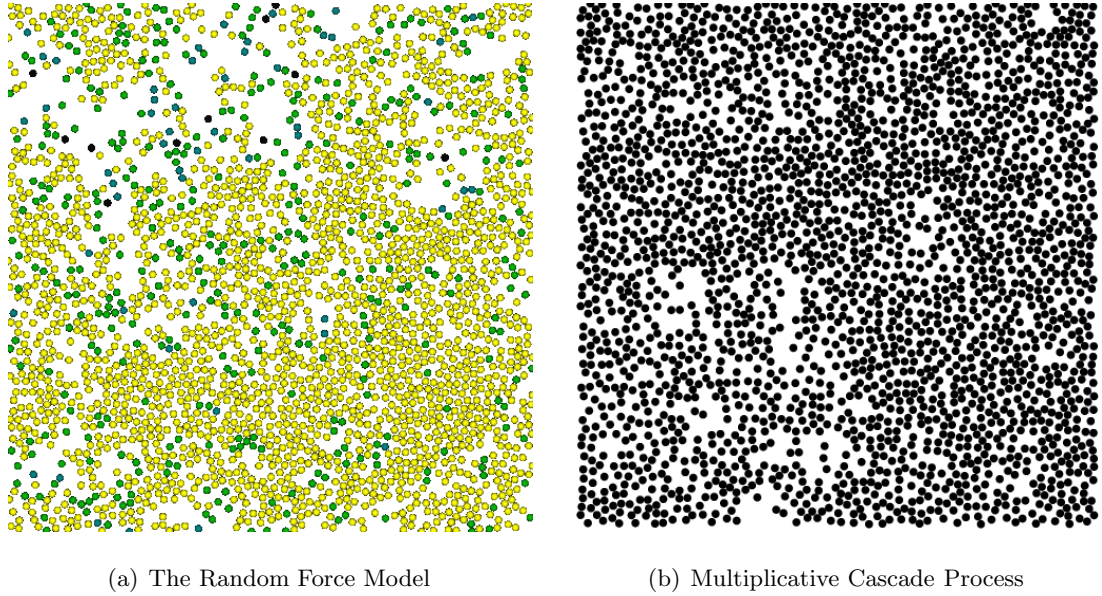
We suggested that the Random Force Model might represent an example of a system that self-organises into a state of criticality. If these systems are critical then the self-similarity of structural features allows the system to be renormalised into a smaller system without loss of generality.

The Multiplicative Cascade Process provides a reverse method to the process of renormalisation. A system is broken up into smaller parts by breaking each region into four equal subregions. The probability of a region is considered to be the fraction of total particles that lie within the region. The probability of the total region is shared between the four sub-regions. By repeating the described routines a smaller system can be subsequently broken up into smaller parts to restore the structure of a much larger system. Regions of high probability represent clustered particles while low probability regions are dilute regions.

We presented several possible routines to preform the ‘probability breaking’ in the Multiplicative Cascade Process, the most notable was called UCP where the routine outlined splitting the probability of a region into four random proportions and assigning to each sub-region. For those routines of the Multiplicative Cascade Processes that preserve self-similarity of the system we find the structure factor is a power-law decay which could be described using an exponent  $D_f$  that lies within the range 1.60 to 1.66.

We suggest that a routine similar to UCP provides a method worth further exploring in regards to describing the structure of the Random Force Model as it represents a Multiplicative Cascade Process which maximizes randomisation and avoids preselecting

Fig. 6.3: A comparison of structure produced by Random Force Model and Multiplicative Cascade Process for a system of  $\phi = 0.442$ ,  $N = 2500$  and dissipation  $\varepsilon_n = \varepsilon_t = 0.2$



particular values for the probabilities that would require further justification.

We end this chapter by showing that a Multiplicative Cascade Process can produce configurations of particles that look similar macroscopically to the snap-shots taken during simulation of the the Random Force Model. Microscopic features on scales smaller than a particle are not expected to be the same. First we simulate the two-dimensional Random Force Model for a system containing 2500 particles in a square box of lengths  $L = 0.2\text{m}$  and high dissipation of  $\varepsilon_n = \varepsilon_t = 0.2$ . A snap-shot is taken for the steady state system showing the configuration of particles at a moment in time and is displayed in the left-hand image of figure 6.3.

We next generate an equivalent system using the Multiplicative Cascade Process and breaking the system into square regions using the routines described for the UCP method. The system starts with lengths of  $L = 0.2\text{m}$  and broken into  $4^n$  of length  $l_n = L/2^n$  such that there are many more square regions than particles of the above Random Force Model. This produces a probability density field,  $m_{i,j}$ , across the system which we use to determine where particles are placed. Each particle is circular with a radius of  $r = 1.5\text{mm}$  and is placed such that it will not overlap another particle. We place particles one at a time by randomly selecting an  $x$  and  $y$  coordinate and generating a third random number  $p$ . We next determine which square region this corresponds to by finding the integer value of  $i$  and  $j$  that satisfies  $i - 0.5 < x/l_n < i + 0.5$  and  $j - 0.5 < y/l_n < j + 0.5$ . We accept the  $x$  and  $y$  coordinates as the particle's position if both  $p < m_{i,j}$  and another particle is not already occupying the spatial region.

Otherwise we generate new values for  $x$ ,  $y$  and  $p$  without placing the particle. We repeat the routine until 2500 particles are placed. The right-hand image of figure 6.3 show an example of the particle arrangement achievable by using the Multiplicative Cascade Process. From the figure we can see that the same type of open-spaces with few particles are present in the system produced by the Multiplicative Cascade Process as was seen in the Random Force Model.

## Chapter 7

# Concluding Remarks

The work presented in this thesis described a theoretical granular system called the Random Force Model. We aimed to show that these systems formed structures which consequently influenced the behaviour of the dynamics of particles within the system. In doing so we reinterpreted the properties of the Random Force Model and resolved two disagreements that lay amongst the published literature. Furthermore, we developed a new theory based around a single particle that incorporated the structure of the system. Importantly we tackled how the structure might arise using a hierarchical method. In this final chapter we review the material presented within the previous six chapters and discuss the general conclusions that we have formed about the Random Force Model. We finish the thesis by suggesting future research that might be useful and interesting to pursue on the back of the material described here.

### 7.1 Chapter Review

**Chapter one** provided an in-depth introduction into the topic of steady state non-equilibrium granular systems. We discussed that in most granular kinetic theories the granular system was assumed to be spatially homogeneous. One of the most widely quoted theories was that given by van Noije and Ernst (1998) in which the velocity distribution of individual particles,  $P(v)$ , was assumed to behave asymptotically as  $P(v) = A \exp(-B|v|^{3/2})$ . The problem with all these theories was their inconsistency with the weight of evidence, drawn from performed experiments and simulations, that granular media form structural features, caused by the slight tendency for granular particles to cluster.

We then introduced the Random Force Model. These theoretical systems were

thought to provide simple comparison with the granular kinetic theories. In the model a  $d$ -dimensional system of  $N$  identical particles were energised by the continual injection of random momentum on to each and every grain. Considering the apparent simplicity of the model it was perhaps intriguing that there remained no consensus, amongst the literature, on several key properties that dealt with velocity and structure of the system. This lack of consensus provided the motivation for this research.

**Chapter two** gave instructions into performing simple simulations of granular media. We outlined the computer algorithms, based around the methods of Molecular Dynamics, that would be used to model one and two dimensional systems. We concluded the chapter by utilising the simulation methods to model the one- and two-dimensional Random Force Model and showed that these systems relaxed into a steady state with a fixed granular temperature (on time-average).

**Chapter three** described the multi-scaling properties seen in simulations of the one-dimensional Random Force Model. These scaling properties were not predicted by the mean field theory given by Williams and MacKintosh (1996). Instead, we found that the moments of the velocity distribution could not be characterised by a single velocity-scale and therefore implied that the velocity distributions of systems for which all quantities, except particle number, were constant would not be rescale onto a single curve. Moreover, we found that for low coefficient of restitution, beneath 0.5, the granular temperature of the system was effectively independent of coefficient of restitution and described by  $\langle |v^2| \rangle \propto N^{-0.53}$ . Furthermore, it was found that the higher order moments of velocity also became independent of dissipation for a range of coefficient of restitution.

We next wanted to understand what caused this multi-scaling behaviour in the velocities. We believed that the structure of the system was responsible for these behaviours and demonstrated that the moments of separation distance between nearest neighbouring particles exhibited strong multi-scaling properties. Even systems with a high coefficient of restitution showed significant multi-scaling structure, where previously it had been quoted to be near-homogeneous. We next measured the complete distribution of nearest neighbour distances and found that for systems of high dissipation these could be identified with power-law functions of logarithmic distance. Such functions had no characteristic length scale and subsequently motivated us to treat the highly dissipative system with  $2N$  particles as approximately renormalisable to the

equivalent  $N$  particle system such that the second neighbour distribution for the  $2N$  particle system was similarly shaped to that of the nearest neighbour distribution for the  $N$  particle system.

This finally lead us to formulate a hierarchical method, which we called the multiplicative bisection process, in which the system arranged itself such that self-similar properties were exhibited. The multiplicative bisection process yielded a successful way to collapse the distribution of nearest neighbours and thus demonstrated the relevance of the process towards these highly dissipative systems.

**Chapter four** explored the structure factor in two dimensions. We found that the structure factor,  $S(k)$ , had a small  $k$  behaviour that was a power-law with an exponent that is typically in the range 1.60 to 1.66. The value of  $D_f$  remained largely unchanged with variation of dissipation or packing fraction as long as the system was of sufficient size. Instead, it was the region of  $k$ , within which  $S(k)$  fitted a power-law decay, that decreased with dissipation. In terms of the real-space arrangement of particles, the fractal features of  $S(k)$  described the anomalous behaviour of the locally dilute regions of the system, where particles arrange fractally such that the number of particles encountered within a growing area, around a fixed point, is less than that expected from mean field theory.

We next considered how the fractal structure affected the motion of individual particles and studied the distribution of free paths. We found that the long distance tail was dependent on the structure and was described by a power-law multiplied by a stretch-exponential predicted by modifying the theory given by Isliker and Vlahos (2003), where high velocity ballistic particles travelled until collision with the fractal background environment.

**In chapter five** we studied the velocity distribution,  $P(v)$ , and confirmed that it was well described by a crossover function in which for low velocities  $P(v)$  was Gaussian distributed and for high velocities  $P(v)$  was a stretched-exponential with exponent  $\alpha$ . Again, as with the structure, we found that, over a range of dissipations and packing fraction,  $\alpha$  roughly maintained a fixed value once the system was of sufficient size and we estimated that  $\alpha$  had value nearer to one than 1.5. Furthermore we conjecture that if better statistics could be obtained we would find that  $\alpha$  remains unchanged for all dissipations. This was based on the evidence in the available data that it was the crossover velocity,  $v_c$ , shifting to higher velocity scales rather than  $\alpha$  increasing in value

that caused the apparent non-universal behaviour in  $P(v)$  for low dissipation.

We next construct a Single Particle Model to self-consistently couple the structure of the two-dimensional system to the velocity distribution. We described the fastest particles of the system as singular particles that undergo a random acceleration in velocity during walks between collision. In contrast the remaining low velocity particles constituted a fractal background. The velocity distribution of the Random Force Model can be calculated using the free path distribution,  $P_l(l)$ , taken to be that predicted by Isliker and Vlahos (2003), and the velocity distribution of a particle that undergoes a walk of distance  $l$  between two collisions,  $Q(v, l)$ . The distribution  $Q(v, l)$  is numerically generated from simulation of a particle contained within a fixed radius disc and found to have a high velocity tail which approached Gaussian. By combining these two component distributions into the SPM Integral Identity we derived that the high velocity tail of the velocity distribution,  $P(v)$ , must tend to near-exponential with exponent  $\alpha$  related to the fractal dimension  $D_f$  by  $\alpha = 6(D_f - 1)/(3D_f - 1)$ . We had therefore pinned down the description of  $P(v)$  to a crossover function that changed from Gaussian to near-exponential as the velocity scale increases. We finally demonstrated that all velocity distributions, of the two-dimensional Random Force Model, regardless of dissipation, could be described by crossover functions of this form and deduced that the shape of  $P(v)$  could in fact be treated as universal. Significantly we stated that this universal asymptotic behaviour was not seen for systems with low dissipation because the crossover velocity was too large in value for the asymptotic behaviour of  $P(v)$  to be seen in the measurable data.

We have thus arrive at the following physical understanding. Particles that travel long distances between collision exhibit a crossover in behaviour as they move away from the previous collision. For small distances the particles initial velocity after collision has a notable influence over its behaviour. As the particle travels further from the previous collision the influence of the initial velocity is washed out by the momentum gained through successive interaction with the random force and the knowledge of the previous collision is lost. This process forms the basis of the two behaviours of the velocity statistics. For low velocity the distribution is dominated by the initial conditions of particles just after collision which is partly determined by the extent of dissipation. These particles only know about the local environment and hence structural considerations of the system are irrelevant. For high velocity the velocity distribution is determined by *memoryless* high velocity particles and hence the distributions shape

is not dependent on dissipation. Instead, these particles know about the wider environment and thus the large-scale structure of the system plays an important role in determining whether a particle can achieve a high velocity.

**Finally, in chapter six** we aimed to complete our theory for the two-dimensional Random Force Model by purposing a method for arranging particles in the system such that the fractal dimension,  $D_f$ , of the system's structure took a value near to one and two thirds. As with the one-dimensional Model, we explored the implications on the structure of the system of assuming that particles continually rearranged to remain in a state of criticality, as previously implied to occur in these system by Peng and Ohta (1998a). We presented a method for fracturing the system into small parts called the Multiplicative Cascade Process in which the system was successively broken into smaller parts by taking each region of the system and breaking it into four identically sized subregions, such that each new subregion took a proportion of the replaced regions probability. In these Processes the probability of each region referred to the likelihood of finding one of the system's particles there and structural self-similarity was induced into the system through the hierarchical structure such that the resultant structure factor had a power-law decay with an exponent consistent with  $D_f$ . This gave us optimism that an approach such as this could well provide the explanation for the structure of the Random Force Model.

## 7.2 Future Work

The Random Force Model provides a clear demonstration that the structure of the system is an important factor in determining the dynamics of the particles. Crucially structural features are present even in relatively low dissipative systems and hence this model provides a very relevant demonstration of the effects likely to be seen at the level of dissipation obtainable in real experimental systems. We now outline several extensions to the work covered in this thesis. These include further refinement of several aspects of the model and the generalisation of theory to more experimental systems.

Let us begin by first discussing some refinements on the Single Particle Model that could be explored in the process of more fully comprehending its importance. For example, we still do not know how to correctly treat slow moving particles. This may be improved by either replacing the assumption that particles have zero initial velocity after collision with a better approximation, such as choosing some non-zero velocity

picked from a distribution; or removing the assumption that particles will not reverse direction before collision, as slow moving particles move at a similar rate to those they collide with allowing them to be *caught* by the other particle. Another refinement would be to prove conclusively an analytic expression that the high velocity tail of the distribution  $Q(v,l)$  is Gaussian. A preliminary attempt was made in Appendix B, however it was found to be very difficult to obtain a simplified asymptotic expression even for the one-dimensional case.

A more important extension of the thesis's work will be to assert its importance on finite experimental systems. One of the closest experimental systems to the Random Force Model were those described by Reis, Ingale, and Shattuck (2006) whereby a quasi-two-dimensional system of particles, are shaken vertically between narrowly separated roughen base and smooth plate. It would be interesting to see how well our predictions compare with their data as it is uncertain whether more dominant forces such as drag friction play a role, which may change the system behaviour as is implied by Puglisi, Loreto, Marconi, and Vulpiani (1999).

In systems where particles are known to be affected by drag as well as the random force we would expect there to be competition on the particle's motion between the change in momentum generated by the random force and the loss of momentum through the drag. For very high velocity the drag term always dominates over the random force. In these types of systems there is clearly going to be a crossover in behaviour from that driven by the random noise to that governed by the drag friction. Thus we would expect that the velocity distribution of low packing fraction systems would visibly deviate away from work described in this thesis and tend towards the Gaussian predicted by Puglisi, Loreto, Marconi, and Vulpiani (1999). In contrast the higher packing fraction systems, in which there is generally insufficient space for particles to pick up sufficient momentum for drag to become the dominant force, should maintain the behaviour described in this thesis over the observable statistics. Ultimately the asymptotic high velocity behaviour of the statistics must be governed by the drag friction.

Finally it may of interest to further pursue the implications of treating these systems as a collection of self-organising particles that continually rearrange to maintain large-scale fractal structure. In this thesis we promoted the above idea by introducing Multiplicative Processes as a geometrical method to obtain the same type of fractal structural features. We proposed that methods that maximises the randomness of particle positioning within the hierarchical structure are likely to lead to the correct

structural features. However, currently it is difficult to refine further without developing precise physical arguments into why the system should organise in such a way.

## Appendix A

# Velocity Properties a One-dimensional Random Force Model

The dynamical behaviour of particles in the random force system describes how an individual particle progresses through the system. At any given moment a particle has a position and an instantaneous velocity (defined as the velocity of the particle at the moment in time). The random force interacts with the particle by accelerating the particle, changing its instantaneous velocity. Statistically over time all particles are indistinguishable as the system does not break into regions of unique behaviour. Hence we can describe the statistical behaviour of the particles motion by the instantaneous velocity probability distribution.

In this appendix: we describe how to measure the velocity distribution through simulation; we make general observation on the possible forms exhibited by the probability distribution of instantaneous velocity; we then attempt to describe the asymptotic behaviours of these distributions by use of standard techniques.

### A.1 Details of Technique used for Generating Velocity Distribution

The following material outlines techniques used to generate the probability density function of the velocity statistics of any particle in the system; methods for analysing the shape of such a distribution; and measurements of the moments associated with the distribution. Although this section has specifically described methods for obtaining

statistics on the velocity of a particle the same principles can be employed in the calculation of statistics of other quantities such as correlations between particles.

We assume that all particles in the system behave the same: There is no phase separation or unique behaviour associated with any particular region of the system. The Velocity distribution  $P(v)$ , is defined to be the probability density function of any particle in the system having an instantaneous velocity of magnitude  $v$ . Hence the probability a particle has a velocity between  $v_L$  and  $v_U$  is given by the integral:

$$P(v_L < v < v_U) = \int_{v_L}^{v_U} P(v) dv, \quad (\text{A.1})$$

and the distribution is normalised such that the total probability is 1:

$$\int_{-\infty}^{\infty} P(v) dv = 1. \quad (\text{A.2})$$

### **General Method for Calculating Distribution Through Simulation**

In simulations we calculate discrete approximations to the true probability density function. The distributions are calculated during the computer simulation through sampling of all particles uniformly at a constant rate, typically at a rate of once every  $1000\Delta t$  seconds (although the distribution should be invariant to the rate of sampling) and tabulating into a frequency distribution,  $\mathcal{P}(v)$ , the details of which are as follows: firstly the distribution is defined; secondly the statistics are generated and thirdly the associated errors are calculated and the distribution normalised.

Lets us begin by defining the discrete approximation of the velocity distribution. We identify the range of magnitudes of velocity,  $v$ , that we wish to consider  $v \in (v_{min}, v_{max})$  where the span is ensured to be sufficient such that the measured value of a particle velocity does not fall out side this range (the likelihood of a particle falling outside this range is so small that it is never seen over the times measured in the simulation). This region of velocities is further subdivided into  $N_{bin}$  regions with widths spanning,  $\Delta v$ , defined by  $\Delta v = (v_{max} - v_{min})/N_{bin}$ . Any sampled velocity that falls inside the  $j^{th}$  region is assumed to approximate the average value of the region  $V_j$  given by  $V_j = (j - \frac{1}{2}) \Delta v$  such that the sampled velocity become discretise with one of the following set of values  $V_1, V_2, \dots, V_{N_{bin}}$ .

We now outline the steps required to populate the statistics during simulation. Before sampling the probability density distribution  $\mathcal{P}(v)$  is assumed to be 0 over all  $v$ . Each time the  $i^{th}$  particle is sampled its instantaneous velocity  $v_i$  is mapped onto

the discrete set of velocities  $V_j$  where the specific  $j$  is determined by:

$$j = \frac{v_i - v_{min}}{\Delta v}. \quad (\text{A.3})$$

The value of the frequency distribution  $\mathcal{P}(v)$  at velocity  $v = V_j$  then increments by 1. The probability  $\mathcal{P}(V_i)$  is thus the number of times at which  $v$  was measured to be  $V_i$  and so the normalised probability distribution  $P(v)$  is obtained by dividing  $\mathcal{P}(v)$  by the total number of all possible measurements of  $v$ .

Having obtained measurements of the profile of the velocity probability distribution we now need an estimate of the errors associated with each data point. The exact errors on the distribution are unknown as change in velocities occur at random but for a large sample the variation of estimated values can be assumed to be normal distributed about the true value. Thus for an unnormalised velocity distribution where  $X_i$  is simply the number of particles sampled that have a velocity  $V_i$ , the error associated to the velocity is given as  $s\sqrt{X_i}$  such that:

$$\mathcal{P}(V_i) = X_i \pm s\sqrt{X_i}, \quad (\text{A.4})$$

where  $\sqrt{X_i}$  is the predicted standard error ( $\sigma$ ) and  $s = 1, 2, 3 \dots$  such that there is a 68% chance the true value of  $\mathcal{P}(V_i)$  lies within  $\pm\sigma$  of the measured value, 95% chance within  $\pm 2\sigma$  and 99% chance within  $\pm 3\sigma$ . The normalised probability distribution has probabilities:

$$P(V_i) = \frac{X_i}{N_s} \pm s \frac{\sqrt{X_i}}{N_s}, \quad (\text{A.5})$$

where  $N_s = \sum_{i=1}^{N_{bin}} X_i$  is the total number of particles sampled (over all times sampled) and  $N_{bin}$  is the number of discrete bins that span the velocity distribution. Equation A.5 can also be written in terms of the normalised probability  $x_i$  such that:

$$P(V_i) = x_i \pm s \sqrt{\frac{x_i}{N_s}}. \quad (\text{A.6})$$

For clarity errors are not shown in general on the probability distributions unless specifically used to perform a calculation or fit.

The precision of the distribution is affected in a number of ways including through the size of the bin-width and the length of simulated time sampled.

### **Specific Method Used in the 1D Random Force Model Simulation**

The details of the simulations are as follows.

Molecular dynamical simulations are carried out with a simulated 20 seconds being allowed to elapse before sampling. The velocity distribution is tabulated by taking

snapshots of the system at regular intervals, of frequency  $1/(1000\Delta t)$ , and recording the instantaneous velocities of the complete set of particles over a simulated time length of 2000 seconds.

The velocity distribution is compiled by accepting particle velocities where  $0 < |v| < 6\text{ms}^{-1}$  such that the distribution consists of 5000 regions each of bin-width  $\Delta v = 6/5000 = 1.2 \times 10^{-3}\text{ms}^{-1}$ .

The accuracy of the velocity distribution is further improved by re-running the simulation five times, each time using a different random seed value (to ensure unique initial conditions). The five obtained distributions are merged into one which is then renormalised such that  $\int_{v_{min}}^{v_{max}} P(v)dv = 1$ , where  $v_{min}, v_{max}$  are the maximum magnitude measured for the instantaneous velocity of a particle.

### **Fitting Curves to Measured Distributions**

Once we have obtained a velocity distribution we may wish to test a hypothesised fit. We fine tune the parameters of the fit by minimising the chi square value between the fit and measured data.

The chi-square measurement is calculated by the following method. Let  $O(V_i)$  be the actual measured value of  $P(V_i)$  obtained from simulation and  $s(V_i)$  the associated error. If  $p(v)$  is a hypothesised fit of  $P(v)$  with  $N_{par}$  parameters. Then the expected value of  $P(V_i)$  is given by  $E(V_i)$ . A measure for the goodness-of-fit is given by chi-square measurement,  $\chi^2$ :

$$\chi^2 = \sum_{i=1}^{N_{bin}} \left( \frac{O(V_i) - E(V_i)}{s(V_i)} \right)^2. \tag{A.7}$$

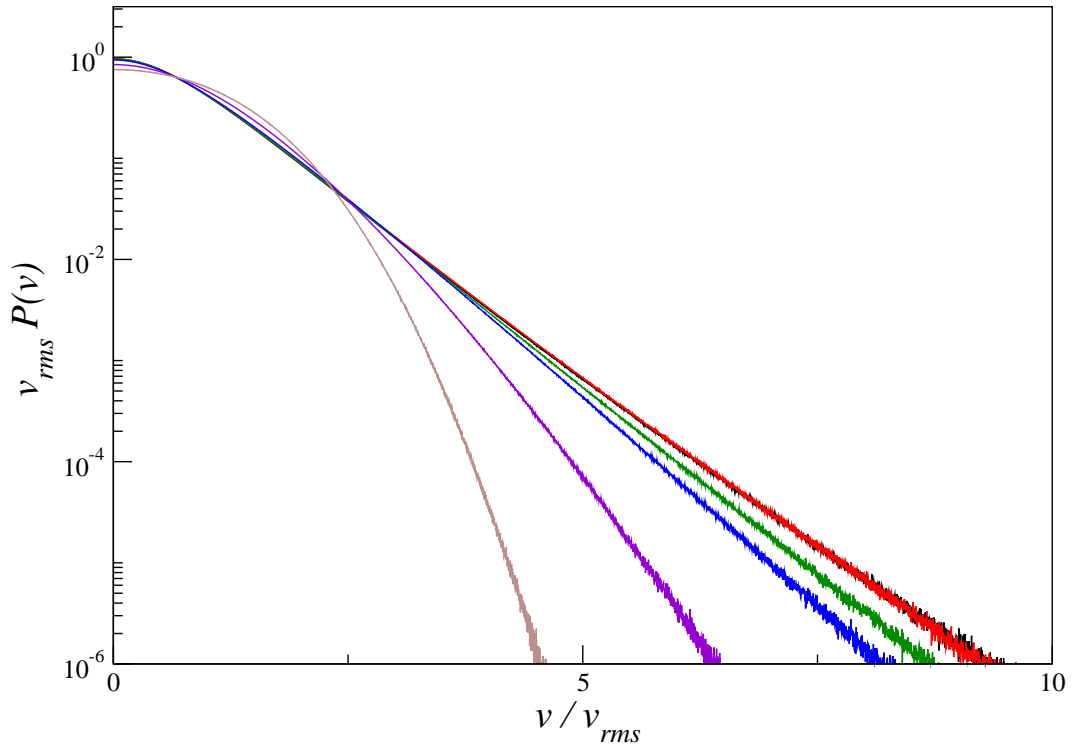
The function  $p(v)$  is a good fit to the data if the reduced chi-square,  $\chi_r^2 = \chi^2/(N_{bin} - N_{par})$  is close to 1.

An adaptive fitting method such as (William H. Press 1992) can be used to fine tune  $p(v)$  by varying the parameters to minimise  $\chi_r^2$  and allows us to judge the appropriateness of such a fit.

## **A.2 The Variation of Shape with Respect to Dissipation**

We show that the instantaneous velocity probability density takes a range of shapes that change depending on the amount of dissipation occurring in the system. We examine a typical set of systems where the number of particles is kept fixed whilst the extent of dissipation is varied from near-elastic to totally inelastic. We choose the particular set

Fig. A.1: The family of velocity probability density distributions for a system containing 1000 particles and the following coefficients of restitution (from outer to inner curve) 0.1; 0.37; 0.68; 0.8; 0.94 and 0.99.



of systems populated by 1000 particles, however we have seen through simulation that the exact number is irrelevant. The range of particles and coefficients of restitution have been chosen to coincide with the work done by Williams and MacKintosh (1996) and Puglisi *et al.* (1999), whilst heating (by the random force) during collision prevents the system from inelastically collapsing at the highest dissipations.

Figure A.1 shows a selection of solutions for the velocity probability density distribution of a system containing 1000 particles for various coefficients of restitution. We display the velocity probability density distributions on a linear-log plot shown in figure A.1. The data shown is more accurate than any previously shown research, with at least eight decades of the distribution achieved. Two points about the distributions should be emphasise: first, the breath of the distributions becomes narrower as the coefficient of restitution of the particles contained in the system increases, corresponding to a reduction in the granular temperature of the steady state system; second, the curvature of the distributions decreases with coefficient of restitution corresponding to a relative increase in probability of a particle having a high velocity (where  $v \gg v_{rms}$ ) compared to the root mean square velocity.

The velocity distributions of figure A.1, and the other families of systems with fixed

numbers of particles in the range considered, clearly show a trend towards a common form as the coefficient of restitution approaches 0. Indeed the transition of shape of the velocity probability density distribution with respect to coefficient of restitution becomes more subtle as the coefficient of restitution approaches 0, with the greatest difference in shape being between the velocity probability distributions of systems with near elastic collisions, as demonstrated by the distributions representing coefficients of restitution of 0.99, 0.94 and 0.8 in the figure A.1; whilst only minor changes occur between the distributions representing coefficients of restitution of 0.68 or less.

In the following section we study the behaviour as the velocity becomes asymptotic ( $|v| \rightarrow \infty$ ).

### A.3 Measuring the Observable High Velocity Behaviour

We compare the asymptotic behaviour of the velocity statistics to the established idea that these distributions asymptotically behave as stretched exponential. Here we describe the methods used to fit velocity distributions, then we analyse the results and lastly discuss the major limitations of using these methods.

Let us assume that the high velocity behaviour of the particles can be described by a stretch exponential of the form:

$$\lim_{v \rightarrow \infty} P(v) = A \exp(-B|v|^\alpha), \tag{A.8}$$

where  $A$ ,  $B$  and exponent  $\alpha$  are constants dependent on the properties of the system.

Fitting the velocity distributions of the Random Force Model to that of a stretch exponential has an appeal because of two features: first, the family of distributions becomes more overpopulated at large velocities as the exponent  $\alpha$  is decreased from  $\alpha = 2$  (Gaussian) towards 0; second, if a set of systems are described by a distribution with fixed exponent  $\alpha$  then the distributions will collapse onto a single curve by the linear rescaling of the velocity axis through the map of  $v \mapsto v/v_0$  where  $v_0$  is a constant scaling velocity.

#### Fitting the Distribution to a Stretch Exponential

We fit the velocity distributions by comparing the frequency distribution  $\mathcal{P}(v)$  to the fit  $\mathcal{P}_T(v) = A_0 \exp(-B_0|v|^\alpha)$ . Let us assume that the lowest few decades of the visible distribution mimic the asymptotic behaviour of the complete distribution whereby

measurement was made over an infinite time period. We select the lowest two decades of data where  $\mathcal{P}(v)$  has a value between 5000 and 50 and assume the error in each point lies within  $\pm\sqrt{X_i}$ . We ignore  $\mathcal{P}(v) < 50$  because we assume the error in these data points to be too large for the data to be meaningful. We choose a chi-square fitting method to determine the best-fit of  $\mathcal{P}_T(v)$  and accept values for  $\alpha$  if the reduced chi-square,  $\chi_r^2$ , between  $\mathcal{P}_T(v)$  and  $\mathcal{P}(v)$  is less than 1.2 (or 1.3 in the case of †).

The table below shows ranges of  $\alpha$  that are accepted through the above outlined method for a variety of systems. The columns represent systems with fixed dissipation whilst the row are for systems containing constant number of particles.

$N$	$\varepsilon = 0.1$	$\varepsilon = 0.37$	$\varepsilon = 0.68$	$\varepsilon = 0.80$	$\varepsilon = 0.94$	$\varepsilon = 0.99$
398	$0.98 \pm 0.23$	$1.08 \pm 0.23$	$1.10 \pm 0.25$	$1.23 \pm 0.23$	$1.60 \pm 0.35$	$2.10 \pm 0.05\dagger$
631	$1.08 \pm 0.23$	$1.08 \pm 0.23$	$1.05 \pm 0.20$	$1.20 \pm 0.25$	$1.53 \pm 0.33$	$2.13 \pm 0.18$
1000	$0.88 \pm 0.28$	$0.98 \pm 0.23$	$1.05 \pm 0.25$	$1.08 \pm 0.28$	$1.35 \pm 0.35$	$2.10 \pm 0.45$
1585	$0.98 \pm 0.23$	$0.95 \pm 0.20$	$0.95 \pm 0.20$	$1.08 \pm 0.28$	$1.38 \pm 0.43$	$2.18 \pm 0.53$
2512	$0.93 \pm 0.23$	$0.88 \pm 0.12$	$0.88 \pm 0.33$	$1.05 \pm 0.35$	$1.28 \pm 0.33$	$2.15 \pm 0.40$
3981	$0.75 \pm 0.25$	$0.98 \pm 0.28$	$0.88 \pm 0.33$	$1.15 \pm 0.40$	$1.33 \pm 0.48$	$1.88 \pm 0.68$

Table A.1: Measurement of exponent  $\alpha$  for a wide range of systems.

The table demonstrates that, the value of exponent  $\alpha$  is increased by either decreasing dissipation or the number of particles in the system. The increase in power exponent  $\alpha$  corresponds to the high velocity tails of the distributions becoming less over-populated (when compared to a Gaussian).

We now ask: are these distributions consistent with current suggested granular kinetic theory? The table of measured  $\alpha$  for the probability density function obtained from the Random Force Model are compared against three asymptotic analytical stretched-exponential solutions suggested, from kinetic theories, namely:

$\alpha = 1$ , the Laplace distribution;

$\alpha = 1.5$ , suggested by Ernst;

and  $\alpha = 2$ , the Gaussian distribution.

The Laplace solution is consistent with the data for a broad range of systems, where particles have moderate to high dissipation of a coefficient of restitution approximately between 0.1 and 0.8. In contrast the remain two suggested solutions, derived by Ernst and Maxwell-Boltzmann’s Gaussian distribution, do not span many dissipation extents

and could even be described as coincidental. A Gaussian distribution might be expected to be applicable for low dissipation systems, where particles behave near-elastically, and is found to be a viable option for the asymptotic tail of the velocity distribution of a system with coefficient of restitution 0.99. However even small reductions in coefficient of restitution reduces  $\alpha$  significantly from two. Similarly the Ernst derived solution only provides a reasonable fit for systems with coefficients of restitution of around 0.94 and in some respects can be considered insignificant as there must exist a distribution of  $\alpha \approx 1.5$  if  $\alpha$  decays with increasing dissipation between two and one.

An interpretation of these observations is that for systems with coefficients of restitution less than 0.9 it is inappropriate to take a homogeneous approach and instead an approach that accounts for the spatial clustering of the system should be used.

**Limitations in Using the Fitting Method**

Finally we discuss some of the limitations of curve fitting the data to stretch exponentials. It is clear from the table of results that it is difficult to narrow down the possible values of  $\alpha$ . Indeed in some cases the variation in exponent  $\alpha$  of viable stretched exponentials is comparable to  $\alpha$ .

To demonstrate the above point we take the system of  $N = 1585$  and  $\varepsilon = 0.1$ . The figure A.2 shows the frequency distribution as points and the following fits for  $\mathcal{P}_T(v)$ :  
 $(17.9 \pm .3) \times 10^8 \exp(-7.220 \pm .008|v|^{0.75})$  which fits the data with a  $\chi_r^2=1.16$ .  
 $(50.3 \pm .6) \times 10^6 \exp(-4.305 \pm .005|v|)$  which fits the data with a  $\chi_r^2=1.05$ .  
 $(84.5 \pm .8) \times 10^8 \exp(-2.986 \pm .003|v|^{1.20})$  which fits the data with a  $\chi_r^2=1.20$ .

These distributions represent best fits for the two extreme allowed values of  $\alpha$  and also a intermediate value ( $\alpha = 1$ ) around the middle of the range.

It is difficult to distinguish which of the solutions agrees better with the real data over the fitting range shown, given by data pointed that lies between the two dotted lines. It is possible to narrow down the range of values of  $\alpha$  by including further data from outside the fitting region. However using higher magnitude data ( $\mathcal{P}(v) > 5000$ ) risks including more of the the distributions peak behaviour which may vastly differ from the asymptotic limit and using lower order data ( $50 < \mathcal{P}(v) < 1$ ) has scatter (due to finite sampling) that becomes so large that any one of these three fits can be still considered to be a good fit.

A further consideration is that, because the velocity probability distribution may only fit asymptotically to a stretch exponential, the precision (the order of magnitude

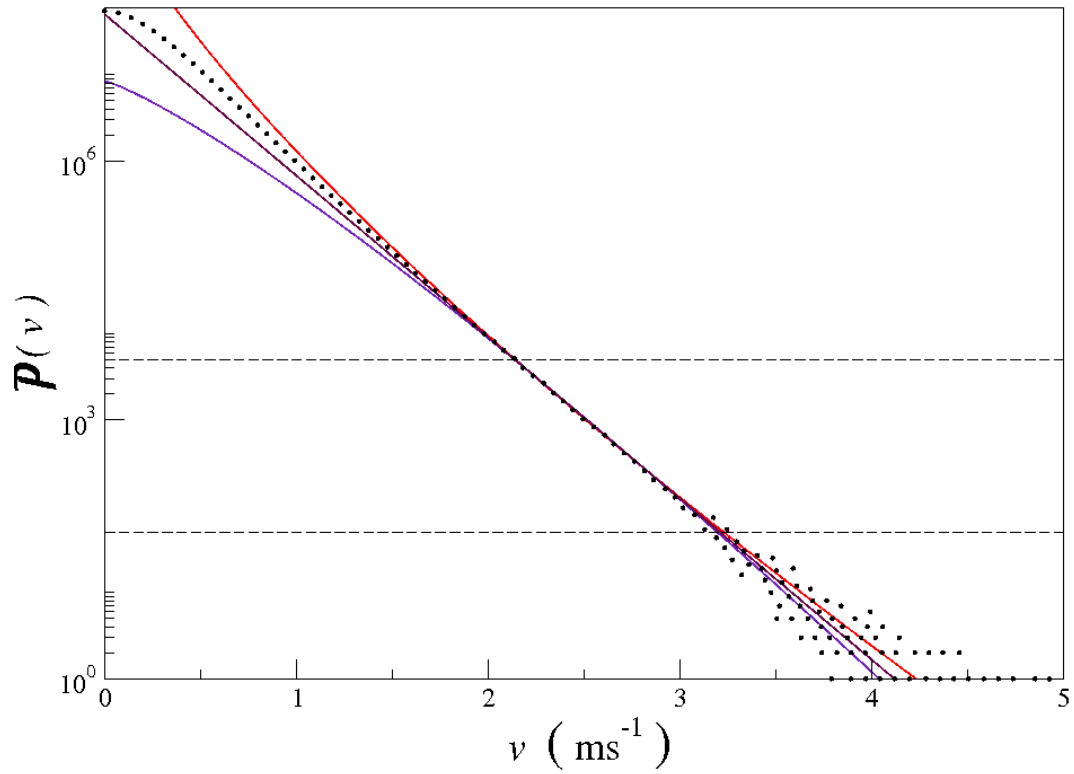


Fig. A.2: The velocity distribution for a system with  $N = 1585$ ,  $\varepsilon = 0.1$  is curve-fitted between the two dashed line and the solid lines represent three appropriate stretch exponentials (described in main text).

available) of the data or the range of the distribution considered will affect the obtained result by changing the measured value of the parameters obtained in curve fitting. The significance being that the measured value of  $\alpha$  is more likely to be too large than too small.

## Appendix B

# A Single Particle in a One-dimensional Interval

In appendix B we describe the behaviour of a single particle in a one-dimensional interval with fixed absorbent boundaries at  $x = 0$  and  $L$ . The particle is released at rest with a uniform random initial position. This system is different to that used in the Single Particle Model where particles are placed in the centre of the interval. However this toy model might provide a way to analytically calculate the asymptotic shape of the probability distribution  $Q(v, l)$ .

### B.1 Solving the Fokker-Planck Equation

Let us consider the following one-dimensional Fokker-Planck equation which describes a succession of isolated particles with velocity  $v$  and position  $x$  governed by the wave function  $P(x, v)$  that are injected uniformly across the system at a rate  $R$  with an initial velocity  $v_0$ .

$$v \frac{\partial P(x, v)}{\partial x} - \frac{\partial^2 P(x, v)}{\partial v^2} = R\delta(v - v_0). \quad (\text{B.1})$$

The Fokker-Planck equation is further constrained by three relevant properties:

Property I is that there exist a pair of finitely separated boundaries, at positions  $x = 0$  and  $x = L$ , that are absorbent such that  $P(L, v < 0) = P(0, v > 0)$ ;

Property II is that the system is invariant of direction such that there is a reflective symmetry in  $P(x, v)$  of  $P(x, v) = P(L - x, -v)$ ;

Property III is that the particles start from rest so that  $v_0 \rightarrow 0^+$ .

To obtain the solution to the wave function  $P(x, v)$  governed by the above Fokker-Planck equation we are going to follow the same methods as employed in the papers by

Burkhardt, Franklin, and Gawronski (2000) and Masoliver and Porra (1996). In these papers the solution is obtained by using the following steps: first Laplace transform (with respect to  $x$ ) the above Fokker-Planck equation to obtain a differential equation in terms of  $Q(s, v)$  where  $Q(s, v)$  is the Laplace transform of  $P(x, v)$ ; then solve the resulting differential equation for  $Q(s, v)$ ; next take the inverse Laplace transform of the obtained solution  $Q(s, v)$  to give the solution for  $P(x, v)$ ; finally obtain an explicit solution for the wave function  $P(x, v)$ . The advantage of Laplace transforming the Fokker-Planck equation is that the new equation contains only differentials in  $v$  rather than both  $x$  and  $v$ , as was found in the original Fokker-Planck equation.

Let us now work through the four stages to obtain the solution for  $P(x, v)$ . The Fokker-Planck equation (B.1) can be considered to be made of three components;  $P(x, v)$ ;  $\partial P/\partial x$ ; and  $R\delta(v - v_0)$ . To calculate the Laplace transform of the Fokker-Planck equation consider each of its component in turn: The first transforms to,

$$\mathcal{L}\{P(x, v)\} = Q(s, v) = \int_0^\infty \exp(-sx)P(x, v)dx; \quad (\text{B.2})$$

the second to,

$$\begin{aligned} \mathcal{L}\left\{\frac{\partial P}{\partial x}\right\} &= \int_0^\infty \exp(-sx)\frac{\partial P}{\partial x}dx \\ &= P \exp(-sx)|_{x=0}^\infty + sQ(s, v) \\ &= -P(0, v) + sQ(s, v); \end{aligned} \quad (\text{B.3})$$

and the third to,

$$\begin{aligned} \mathcal{L}\{R\delta(v - v_0)\} &= R \int_0^\infty \exp(-sx)\delta(v - v_0)dx \\ &= R\delta(v - v_0) \left[ \frac{-\exp(-sx)}{s} \right]_{x=0}^\infty \\ &= R \frac{\delta(v - v_0)}{s}. \end{aligned} \quad (\text{B.4})$$

Thus our Fokker-Planck equation B.1 is Laplace transformed to:

$$vsQ - \frac{\partial^2 Q}{\partial v^2} = R \frac{\delta(v - v_0)}{s} + P(0, v)v. \quad (\text{B.5})$$

If we consider only positive velocities, such that  $v > 0$ , we can neglect the second term by applying the condition (Property I) that the systems boundaries are absorbent, implying  $P(0, v) = 0$  if  $v > 0$ , and the solution to equation B.5 can be written as

(Abramowitz and Stegun 1965):

$$\begin{aligned}
 Q(s, v) &= W(s)\text{Ai}(s^{\frac{1}{3}}v) \\
 &+ R\pi s^{-\frac{4}{3}}\text{Bi}(s^{\frac{1}{3}}v) \int_v^\infty du \text{Ai}(s^{\frac{1}{3}}u)\delta(u - v_0) \\
 &+ R\pi s^{-\frac{4}{3}}\text{Ai}(s^{\frac{1}{3}}v) \int_0^v du \text{Ai}(s^{\frac{1}{3}}u)\delta(u - v_0),
 \end{aligned} \tag{B.6}$$

where  $W(s)$  is an arbitrary weight function and  $\text{Ai}(s)$ ,  $\text{Bi}(s)$  are Airy functions of  $s$ .

The weight function can be replaced with an expression in terms of  $Q(s, v)$  by differentiating equation B.7 with respect to  $v$  and evaluating at  $v = 0$ :

$$\left. \frac{\partial Q(s, v)}{\partial v} \right|_{v=0} = s^{\frac{1}{3}}W(s)\text{Ai}'(0) + R\pi s^{-1} \left( \text{Bi}'(0)\text{Ai}(s^{\frac{1}{3}}v_0)\Theta(v_0) \right), \tag{B.7}$$

and hence the weight function is expressed as:

$$W(s) = \frac{s^{-\frac{1}{3}}}{\text{Ai}'(0)} \frac{\partial Q(s, v)}{\partial v} - R\pi s^{-\frac{4}{3}} \frac{\text{Bi}'(0)}{\text{Ai}'(0)} \text{Ai}(s^{\frac{1}{3}}v_0), \tag{B.8}$$

whilst the solution of  $Q(s, v)$ , stated in equation B.7 is described as:

$$\begin{aligned}
 Q(s, v) &= s^{-\frac{1}{3}} \frac{\text{Ai}(s^{\frac{1}{3}}v)}{\text{Ai}'(0)} \left[ \frac{\partial Q(s, 0)}{\partial v} \right] \\
 &- R\pi s^{-\frac{4}{3}} \frac{\text{Bi}'(0)}{\text{Ai}'(0)} \text{Ai}(s^{\frac{1}{3}}v)\text{Ai}(s^{\frac{1}{3}}v_0) \\
 &+ R\pi s^{-\frac{4}{3}} \text{Bi}(s^{\frac{1}{3}}v)\text{Ai}(s^{\frac{1}{3}}v_0)\Theta(v_0 - v) \\
 &+ R\pi s^{-\frac{4}{3}} \text{Ai}(s^{\frac{1}{3}}v)\text{Bi}(s^{\frac{1}{3}}v_0)\Theta(v - v_0).
 \end{aligned} \tag{B.9}$$

To obtain the solution for  $P(x, v)$  we inverse Laplace transform the above expression of  $Q(s, v)$  (as suggested by equation B.2) which requires the use of the Convolution theorem of Laplace transformations:

$$\mathcal{L}\{u(x) * f(x)\} = \mathcal{L} \int_0^x u(y)f(x-y)dy = \mathcal{L}\{u(x)\}\mathcal{L}\{f(x)\},$$

in particular that of

$$\mathcal{L}\left\{f(x) * \frac{dP(x, 0)}{dv}\right\} = \mathcal{L} \int_0^x f(x-y) \frac{dP(y, 0)}{dv} dy = \mathcal{L}\{f(x)\} \frac{dQ(s, 0)}{dv}, \tag{B.10}$$

and

$$\mathcal{L}\{1 * u(x)\} = \mathcal{L} \int_0^x u(x-y)dy = \frac{1}{s} \mathcal{L}\{u(x)\}. \tag{B.11}$$

The function  $f(x)$  required is defined in equation B.9 where  $\mathcal{L}\{f(x)\}$  is  $s^{-\frac{1}{3}}\text{Ai}(s^{\frac{1}{3}}v)$  and the inverse Laplace transform is calculated by the following:

$$f(x) = \mathcal{L}^{-1}\left\{s^{-\frac{1}{3}}\text{Ai}(s^{\frac{1}{3}}v)\right\} = (2 \times 3^{\frac{1}{6}}\pi)^{-1} x^{-\frac{2}{3}} \exp\left(-\frac{v^3}{9x}\right),$$

whilst  $u(x)$  takes the functions defined in equation B.9 as either

$\mathcal{L}\{u_1(x)\} = s^{-\frac{1}{3}}\text{Ai}(s^{\frac{1}{3}}v)\text{Ai}(s^{\frac{1}{3}}v_0)$  or  $\mathcal{L}\{u_2(x)\} = s^{-\frac{1}{3}}\text{Ai}(s^{\frac{1}{3}}v)\text{Bi}(s^{\frac{1}{3}}v_0)$  such that:

$$u_1(x) = \mathcal{L}^{-1} \left\{ s^{-\frac{1}{3}} \text{Ai}(s^{\frac{1}{3}}v) \text{Ai}(s^{\frac{1}{3}}v_0) \right\} = (2 \times 3^{\frac{3}{2}}\pi)^{-1} x^{-1} (vv_0)^{\frac{1}{2}} \exp\left(-\frac{v^3 + v_0^3}{9x}\right) \times \left[ I_{-\frac{1}{3}}\left(\frac{2(vv_0)^{\frac{3}{2}}}{9x}\right) - I_{\frac{1}{3}}\left(\frac{2(vv_0)^{\frac{3}{2}}}{9x}\right) \right],$$

or

$$u_2(x) = \mathcal{L}^{-1} \left\{ s^{-\frac{1}{3}} \text{Ai}(s^{\frac{1}{3}}v) \text{Bi}(s^{\frac{1}{3}}v_0) \right\} = (6\pi)^{-1} x^{-1} (vv_0)^{\frac{1}{2}} \exp\left(-\frac{v^3 + v_0^3}{9x}\right) \times \left[ I_{-\frac{1}{3}}\left(\frac{2(vv_0)^{\frac{3}{2}}}{9x}\right) + I_{\frac{1}{3}}\left(\frac{2(vv_0)^{\frac{3}{2}}}{9x}\right) \right],$$

where the Airy's functions  $\text{Ai}(z)$  and  $\text{Bi}(z)$  can be expressed in terms of Bessel functions  $I_\nu(z)$  such that

$$\text{Ai}(z) = \frac{1}{3}\sqrt{z} \left[ I_{-\frac{1}{3}}\left(\frac{2}{3}z^{\frac{3}{2}}\right) - I_{\frac{1}{3}}\left(\frac{2}{3}z^{\frac{3}{2}}\right) \right], \quad (\text{B.12})$$

and

$$\text{Bi}(z) = \sqrt{\frac{z}{3}} \left[ I_{-\frac{1}{3}}\left(\frac{2}{3}z^{\frac{3}{2}}\right) + I_{\frac{1}{3}}\left(\frac{2}{3}z^{\frac{3}{2}}\right) \right]. \quad (\text{B.13})$$

Collating the above set of information together and removing the Airy derivatives, via  $\text{Ai}'(0) = -3^{-\frac{1}{2}}\text{Bi}'(0) = -3^{-\frac{1}{3}}\Gamma\left(\frac{1}{3}\right)^{-1}$  (where  $\Gamma(z)$  is a Gamma function) gives us the full solution for  $P(x, u)$ :

$$\begin{aligned} P(x, v) &= -\frac{3^{\frac{1}{3}}\Gamma\left(\frac{1}{3}\right)}{2 \cdot 3^{\frac{1}{6}}\pi} \int_0^x \frac{dy}{(x-y)^{\frac{2}{3}}} \exp\left(-\frac{v^3}{9(x-y)}\right) \frac{\partial P(y, 0)}{\partial v} \\ &+ \frac{R}{6} \int_0^x dy y^{-1} (vv_0)^{\frac{1}{2}} \exp\left(-\frac{v^3 + v_0^3}{9y}\right) \left[ I_{-\frac{1}{3}}\left(\frac{2(vv_0)^{\frac{3}{2}}}{9y}\right) - I_{\frac{1}{3}}\left(\frac{2(vv_0)^{\frac{3}{2}}}{9y}\right) \right] \\ &+ \frac{R}{6} \int_0^x dy y^{-1} (vv_0)^{\frac{1}{2}} \exp\left(-\frac{v^3 + v_0^3}{9y}\right) \left[ I_{-\frac{1}{3}}\left(\frac{2(vv_0)^{\frac{3}{2}}}{9y}\right) + I_{\frac{1}{3}}\left(\frac{2(vv_0)^{\frac{3}{2}}}{9y}\right) \right]. \end{aligned} \quad (\text{B.14})$$

The latter two integrals are the of the same form and thus equation B.14 simplifies to:

$$\begin{aligned} P(x, v) &= -\frac{3^{-\frac{1}{2}}\Gamma\left(\frac{1}{3}\right)}{2\pi} \int_0^x \frac{dy}{(x-y)^{\frac{2}{3}}} \exp\left(-\frac{v^3}{9(x-y)}\right) \frac{\partial P(y, 0)}{\partial v} \\ &+ \frac{2R}{6} \int_0^x dy y^{-1} (vv_0)^{\frac{1}{2}} \exp\left(-\frac{v^3 + v_0^3}{9y}\right) I_{-\frac{1}{3}}\left(\frac{2(vv_0)^{\frac{3}{2}}}{9y}\right). \end{aligned} \quad (\text{B.15})$$

To progress any further towards an explicit solution for  $P(x, v)$  we need to substitute out the derivative  $\partial P(y, 0)/\partial v$  and to do that we consider the case where the velocity is zero. The equation B.15 can be expressed in the following way when  $v = 0$ :

$$\begin{aligned} P(x, 0) &= -\frac{3^{\frac{1}{2}}\Gamma\left(\frac{1}{3}\right)}{2\pi} \int_0^x \frac{dy}{(x-y)^{\frac{2}{3}}} \frac{\partial P(y, 0)}{\partial v} \\ &+ \frac{R}{3} \int_0^x dy y^{-1} (vv_0)^{\frac{1}{2}} \exp\left(-\frac{v_0^3}{9y}\right) \Gamma\left(\frac{2}{3}\right)^{-1} (vv_0)^{-\frac{1}{2}} (9y)^{\frac{1}{3}}, \end{aligned} \quad (\text{B.16})$$

where we replace  $I_\nu(z)$  by  $I_\nu(z) \approx \Gamma(\nu + 1)^{-1}(z/2)^\nu$  as  $z \rightarrow 0$ .

The above expression (equation B.16) still contains  $P(x, 0)$  and its derivative  $\partial P(x, 0)/\partial v$ ; however  $P(x, 0)$  can be eliminated by using Property II of the constraints and the resulting expression further simplified by nullifying the initial velocity,  $v_0$  by invoking Property III to leave the following expression:

$$0 \equiv P(x, 0) - P(L - x, 0) = -\frac{3^{\frac{1}{2}}\Gamma\left(\frac{1}{3}\right)}{2\pi} \int_0^L \frac{dy}{|x - y|^{\frac{2}{3}}} \frac{\partial P(y, 0)}{\partial v} + \frac{R}{\Gamma\left(\frac{2}{3}\right)} \left( \int_0^x dy y^{-\frac{2}{3}} - \int_0^{L-x} dy y^{-\frac{2}{3}} \right). \quad (\text{B.17})$$

A rearrangement of equation B.17 can be expressed as:

$$\int_0^L \frac{dy}{|x - y|^{\frac{2}{3}}} \frac{\partial P(y, 0)}{\partial v} = 3R \left[ x^{\frac{1}{3}} - (L - x)^{\frac{1}{3}} \right]. \quad (\text{B.18})$$

To solve B.18 for  $\partial P(y, 0)/\partial v$  we will first consider instead the Fromholm Integral equation as stated in (Burkhardt, Franklin, and Gawronski 2000):

$$\int_0^1 dy \frac{R(y, u)}{|x - y|^{\frac{2}{3}}} = F(x, u). \quad (\text{B.19})$$

The difference between  $F(x, u)$  and  $F(1 - x, u)$  can be described as:

$$\int_0^1 dy \frac{R(y, u) - R(1 - y, u)}{|x - y|^{\frac{2}{3}}} = F(x, u) - F(1 - x, u) \quad (\text{B.20})$$

and has a known solution to  $R(y, u)$  of:

$$R(x, u) = -3^{-\frac{1}{2}}\Gamma\left(\frac{1}{3}\right)^{-1} \Gamma\left(\frac{5}{6}\right)^{-2} x^{-\frac{1}{6}} \frac{d}{dx} \times \int_x^1 dy \frac{y^{\frac{1}{3}}}{(y - x)^{\frac{1}{6}}} \frac{d}{dy} \int_0^y dz \frac{F(z, u)}{z^{\frac{1}{6}}(y - z)^{\frac{1}{6}}}. \quad (\text{B.21})$$

Consider the case where  $F(x, u)$  takes the form:

$$F(x, u) = 3Rx^{\frac{1}{3}} \quad (\text{B.22})$$

We can express equation B.21 as two integrals  $I_I$  and  $I_{II}$  such that  $R(x, u) = A(x) \frac{d}{dx} I_{II}$  and  $I_{II} = \int dy B(y) \frac{d}{dy} I_I$ , where  $A(y), B(y)$  are functions of  $y$ . The solution of  $R(x, u)$  is obtained by evaluating  $I_I$ , then using the result to calculate  $I_{II}$  and finally differentiating  $I_{II}$ .

Let us first consider the calculation of  $I_I$ :

$$I_I := \int_0^y \frac{F(z, u)}{z^{\frac{1}{6}}(y-z)^{\frac{1}{6}}} dz. \quad (\text{B.23})$$

In general, equations of this form are solved by the identity

$$\int_0^t z^{\mu-1}(t-z)^{\nu-1} dz = t^{\mu+\nu-1} \text{B}(\mu, \nu),$$

where  $\text{B}(\mu, \nu)$  is a Beta function.

Hence the integral  $I_I$  is solved by the following: replace  $F(z, u)$  with that of equation B.22; use a change of variable  $z = yz'$  and implement the above identity.

$$\begin{aligned} I_I &:= 3R \int_0^y \frac{z^{\frac{1}{6}}}{(y-z)^{\frac{1}{6}}} dz \\ &= 3R \int_0^1 \frac{(yz')^{\frac{1}{6}}}{y^{\frac{1}{6}}(1-z')^{\frac{1}{6}}} y dz' \\ &= 3R y \int_0^1 \frac{z^{\frac{1}{6}}}{(1-z)^{\frac{1}{6}}} dz \\ &= 3R y \text{B}\left(\frac{7}{6}, \frac{5}{6}\right). \end{aligned} \quad (\text{B.24})$$

The second integral,  $I_{II}$ , is defined as:

$$I_{II} := \int_x^1 dy \frac{y^{\frac{1}{3}}}{(y-x)^{\frac{1}{6}}} \frac{d}{dy} I_I = 3R \text{B}\left(\frac{7}{6}, \frac{5}{6}\right) \int_x^1 dy \frac{y^{\frac{1}{3}}}{(y-x)^{\frac{1}{6}}}. \quad (\text{B.25})$$

To solve integral  $I_{II}$  a change of variables is applied three times in the following order;  $z = y - x$ ,  $z' = z/(1-x)$  and  $z'' = 1 - z$ :

$$\begin{aligned} I_{II} &:= 3R \text{B}\left(\frac{7}{6}, \frac{5}{6}\right) \int_0^{1-x} \frac{(z+x)^{\frac{1}{3}}}{z^{\frac{1}{6}}} dz \\ &= 3R \text{B}\left(\frac{7}{6}, \frac{5}{6}\right) (1-x)^{\frac{5}{6}} \int_0^1 \frac{[(1-x)z' + x]^{\frac{1}{3}}}{(z')^{\frac{1}{6}}} dz' \\ &= 3R \text{B}\left(\frac{7}{6}, \frac{5}{6}\right) (1-x)^{\frac{5}{6}} \int_0^1 \frac{[(1-x)(1-z'') + x]^{\frac{1}{3}}}{(1-z'')^{\frac{1}{6}}} dz'' \\ &= 3R \text{B}\left(\frac{7}{6}, \frac{5}{6}\right) (1-x)^{\frac{5}{6}} \int_0^1 [1 - (1-x)z]^{\frac{1}{3}} (1-z)^{-\frac{1}{6}} dz. \end{aligned} \quad (\text{B.26})$$

The process of reparametrizing Integral  $I_{II}$  has left it in the form of the following Hypergeometric identity:

$${}_2F_1(a, b; c; x) = \frac{\Gamma(c)}{\Gamma(b)\Gamma(c-b)} \int_0^1 t^{b-1}(1-t)^{c-b-1}(1-tx)^{-a} dt,$$

where  $c > b > 0$  and thus  $I_{II}$  can be evaluated as:

$$I_{II} := 3R \text{B}\left(\frac{7}{6}, \frac{5}{6}\right) (1-x)^{\frac{5}{6}} \frac{\Gamma(1)\Gamma(\frac{5}{6})}{\Gamma(\frac{11}{6})} {}_2F_1\left(-\frac{1}{3}, 1; \frac{11}{6}; 1-x\right). \quad (\text{B.27})$$

We have now reached a state where  $R(x, u)$  can be calculated using:

$$R(x, u) = -3^{-\frac{1}{2}} \Gamma\left(\frac{1}{3}\right)^{-1} \Gamma\left(\frac{5}{6}\right)^{-2} x^{-\frac{1}{6}} \frac{d}{dx} I_{II}. \quad (\text{B.28})$$

The derivative of  $I_{II}$  can be calculated using the following generalised identity of hypergeometric functions (Masoliver and Porra 1996)

$$\frac{d}{dx} [x^c {}_2F_1(a, b; c+1; x)] = cx^{c-1} {}_2F_1(a, b; c; x),$$

which implies that equation B.28 becomes the expression:

$$\begin{aligned} R(x, u) &= \frac{3^{-\frac{1}{2}} \times 5}{2} R \left[ \Gamma\left(\frac{1}{3}\right) \Gamma\left(\frac{5}{6}\right) \Gamma\left(\frac{11}{6}\right) \right]^{-1} \text{B}\left(\frac{7}{6}, \frac{5}{6}\right) \\ &\times [x(1-x)]^{-\frac{1}{6}} {}_2F_1\left(-\frac{1}{3}, 1; \frac{5}{6}; 1-x\right). \end{aligned} \quad (\text{B.29})$$

Let us now relate the above solution of  $R(x, u)$  back to the problem set out in B.18. Choosing  $F(x, u)$  to have the form stated in equation B.22 has the benefit that the equation B.20 can be considered to be the generalised form of equation B.18 when we equate

$$\frac{\partial P(y', 0)}{\partial v} = R(y', u) - R(1-y', u) \quad (\text{B.30})$$

and use a rescaled length dimension such that  $y' = y/L$ . Thus the result of equation B.29 implies that:

$$\begin{aligned} \frac{\partial P(y, 0)}{\partial v} &= \frac{3^{-\frac{1}{2}} \times 5}{2} R \left[ \Gamma\left(\frac{1}{3}\right) \Gamma\left(\frac{5}{6}\right) \Gamma\left(\frac{11}{6}\right) \right]^{-1} \text{B}\left(\frac{7}{6}, \frac{5}{6}\right) \left[\frac{y}{L}\left(1-\frac{y}{L}\right)\right]^{-\frac{1}{6}} \\ &\times \left[ {}_2F_1\left(-\frac{1}{3}, 1; \frac{5}{6}; 1-\frac{y}{L}\right) - {}_2F_1\left(-\frac{1}{3}, 1; \frac{5}{6}; \frac{y}{L}\right) \right]. \end{aligned} \quad (\text{B.31})$$

The power of obtaining the above result is that we can now describe the rate expression  $P(x, v)$  set out in equation B.15 without referring to  $P(x, v)$  explicitly and hence the solution becomes a regular integral of the form:

$$\begin{aligned} P(x, v) &= \frac{R}{\Gamma\left(\frac{2}{3}\right)} \left[ -\frac{\Gamma\left(\frac{1}{6}\right)}{2\sqrt{3}\Gamma\left(\frac{1}{3}\right)\Gamma\left(\frac{5}{6}\right)} \int_0^x dy \frac{\exp\left(-\frac{v^3}{9(x-y)}\right)}{(x-y)^{\frac{2}{3}}} \left[\frac{y}{L}\left(1-\frac{y}{L}\right)\right]^{-\frac{1}{6}} \right. \\ &\times \left[ {}_2F_1\left(-\frac{1}{3}, 1; \frac{5}{6}; 1-\frac{y}{L}\right) - {}_2F_1\left(-\frac{1}{3}, 1; \frac{5}{6}; \frac{y}{L}\right) \right] \\ &\left. + \int_0^x dy y^{-\frac{2}{3}} \exp\left(-\frac{v^3}{9y}\right) \right]. \end{aligned} \quad (\text{B.32})$$

Equation B.32 is difficult to solve exactly due to the nature of the hypergeometric functions so further calculation of the above form is done by numerical integration.

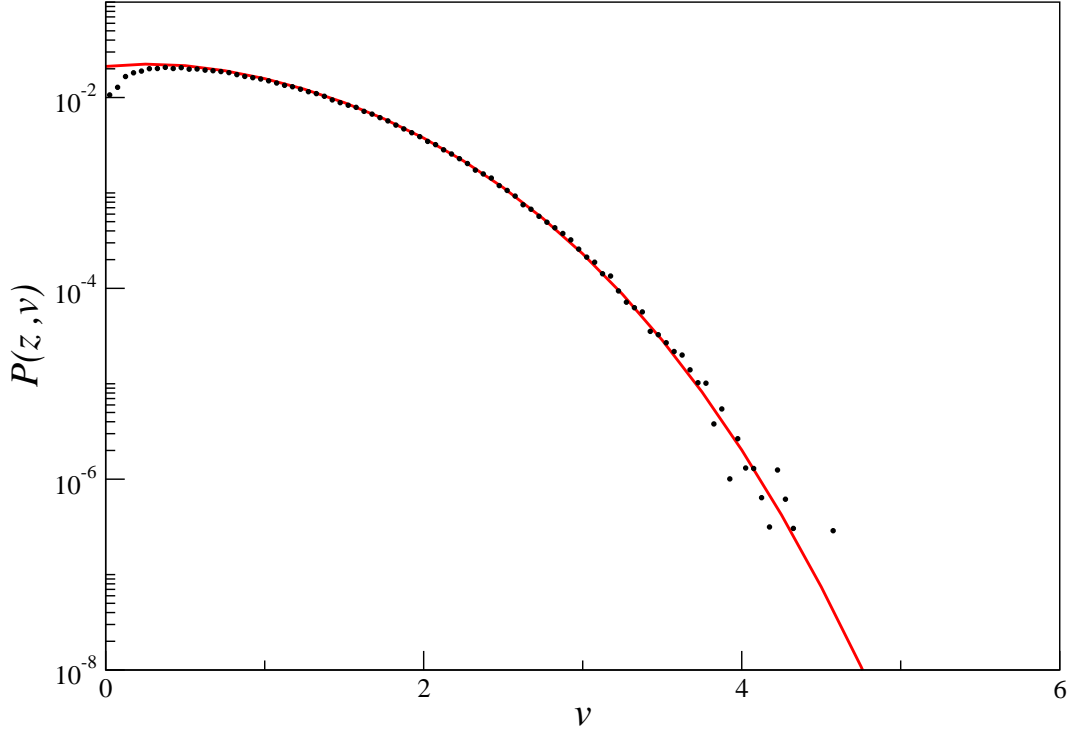


Fig. B.1: Comparison of numerical simulation data (circular points) with analytical solution (solid line) for rate of particles arriving with a given velocity at the right-hand side boundary ( $x = L$ ) of a one-dimensional system with particle uniformly distributed at rest each time it reaches a boundary. For simplicity the mass, separation and noise strength are set to unit.

## B.2 What is the form of $Q(v, l)$ ?

Can we use this solution for  $P(x, v)$  to further derive the form of the  $Q(v, l)$  distribution? First, we demonstrate that the equation B.32 provides correct solution for these systems. We numerically integrate equation B.32 by using a method such as QNG non-adaptive Gauss-Kronrod integration (William H. Press 1992) to obtain  $P(x, v)$ . We also calculate  $P(x, v)$  directly from simulation using a system with a noise strength of  $D/M^2 = 1$  and a system width of  $L = 1$ . The distribution of arriving velocities at right-hand boundary ( $x = L$ ) is calculate and then divided by the velocity to obtain the probability density. The two solutions for  $P(x, v)$ , at  $x = L$ , are shown in figure B.1 where the line represents the numerical integration and the points the simulation data. Both solutions agree until small velocities where numerical instabilities affect the results.

We now attempt to calculate the velocity probability distribution of a free path  $l$  (where  $L = 2l$ ),  $Q(v, l)$ , which is is defined by the integral:

$$Q(v, l) = \int_0^{2l} P(x, v) dx. \quad (\text{B.33})$$

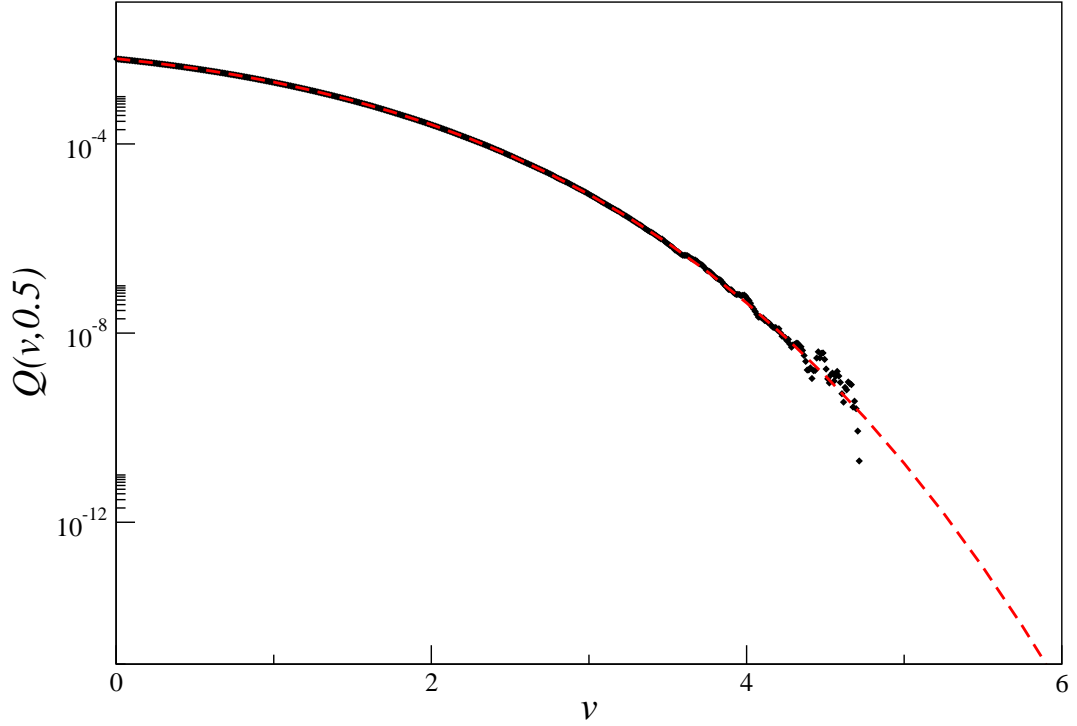


Fig. B.2: Comparison of numerical simulation data (circular points) with analytical solution (solid line) for the probability that a particle has a velocity  $v$  in one-dimensional system where the particle uniformly distributed at rest each time it reaches a boundary. For simplicity the mass, separation and noise strength are set to unit.

Using equation B.32  $Q(v, l)$  is expressed as:

$$Q(v, L) = \frac{R}{\Gamma\left(\frac{2}{3}\right)} \int_0^L dy A(y) \int_0^{L-y} dz \frac{\exp\left(-\frac{v^3}{9(z)}\right)}{(z)^{\frac{2}{3}}}, \quad (\text{B.34})$$

where the function  $A(y)$  contains all the remaining non-exponential components of the form:

$$A(y) = 1 - \frac{\Gamma\left(\frac{1}{6}\right)}{2\sqrt{3}\Gamma\left(\frac{1}{3}\right)\Gamma\left(\frac{5}{6}\right)} \left[\frac{y}{L}\left(1 - \frac{y}{L}\right)\right]^{-\frac{1}{6}} \\ \times \left[ {}_2F_1\left(-\frac{1}{3}, 1; \frac{5}{6}; 1 - \frac{y}{L}\right) - {}_2F_1\left(-\frac{1}{3}, 1; \frac{5}{6}; \frac{y}{L}\right) \right]$$

We perform both a numerical integration and computer simulation and find that the two solutions of  $Q(v, l)$  agree as shown in figure B.2.

# Bibliography

- Abramowitz, M. and I. A. Stegun (1965). *Handbook of Mathematical Functions*. New York: Dover.
- Allen, M. P. and D. J. Tildesley (1987). *Computer Simulation of Liquids*. Oxford: Oxford University Press.
- Aranson, I. S. and L. S. Tsimring (2006). Patterns and collective behavior in granular media: Theoretical concepts. *Rev. Mod. Phys.* 78, 641.
- Barrat, A., T. Biben, Z. Rácz, E. Trizac, and F. van Wijland (2002). On the velocity distributions of the one-dimensional inelastic gas. *J. Phys. A* 35, 463.
- Barrat, A. and E. Trizac (2003). Random inelasticity and velocity fluctuations in driven granular gas. *Eur. Phys. J. E* 11, 99.
- Barrat, A., E. Trizac, and M. H. Ernst (2005). Granular gases: dynamics and collective effects. *J. Phys. Condens. Matter*. 17, S2429.
- Baxter, G. W. and J. S. Olafsen (2003). Kinetics - gaussian statistics in granular gases. *Nature* 425, 680.
- Ben-Naim, E., S. Y. Chen, G. D. Doolen, and S. Redner (1999). Shocklike dynamics of inelastic gas. *Phys. Rev. Letts* 83, 4069.
- Ben-Naim, E. and P. L. Krapivsky (2000). Multiscaling in inelastic collisions. *Phys. Rev. E* 61, R5.
- Ben-Naim, E., B. Machta, and J. Machta (2005). Power-law velocity distributions in granular gases. *Phys. Rev. E* 72, 21302.
- Blair, D. L. and A. Kudrolli (2001). Velocity correlations in dense granular gases. *Phys. Rev. E* 64, 050301.
- Blair, D. L. and A. Kudrolli (2003). Collision statistics of driven granular materials. *Phys. Rev. E* 67, 041301.

- Bray, D. J., M. R. Swift, and P. J. King (2007). Velocity statistics in dissipative, dense granular media. *Phys. Rev. E* 75, 062301.
- Brilliantov, N. V. and T. Pöschel (2004). *Kinetic theory of granular gases*. Oxford: Oxford University Press.
- Burkhardt, T. W., J. Franklin, and R. R. Gawronski (2000). Statistics of a confined, randomly accelerated particle with inelastic boundary collisions. *Phys. Rev. E* 61, 2376.
- Chaikin, P. M. and T. C. Lubensky (1995). *Principles of Condensed Matter Physics*. Cambridge: Cambridge University Press.
- Herrmann, H. J. and S. Luding (1998). Modeling granular media on the computer. *Continuum Mech. Thermodyn.* 10, 189–231.
- Herrmann, H. J., S. Luding, and R. Cafiero (2001). Dynamics of granular systems. *Physica A* 295, 93.
- Huan, C., X. Yang, D. Candela, R. W. Mair, and R. L. Walsworth (2004). Nmr experiments on a three-dimensional vibrofluidized granular medium. *Phys. Rev. E* 69, 041302.
- Isliker, H. and L. Vlahos (2003). Random Walk Through Fractal Environments. *Physical review E* 67, 026413.
- Jaeger, H. M., S. R. Nagel, and R. P. Behringer (1996). Granular solids, liquids, and gases. *Rev. Mod. Phys.* 68, 1259.
- Kawarada, A. and H. Hayakawa (2004). Non-gaussian velocity distribution function in a vibrating granular bed. *J. Phys. Soc. Japan* 73, 2037.
- Kohlstedt, K., A. Snezhko, M. V. Sapozhnikov, I. S. Aranson, J. S. Olafsen, and E. Ben-Naim (2005). Velocity distributions of granular gases with drag and with long-range interactions. *Phys. Rev. Lett.* 95, 068001.
- Kolmogorov, A. N. (1941). The local structure of turbulence in incompressible viscous fluid for very large Reynold's numbers. *Comptes rendus (Doklady) de l'Académie des Sciences de l'U.R.S.S.* 30, 301.
- Krapivsky, P. L. and S. N. Majumdar (2000). Traveling waves, front selectiob, and exact nontrivial exponents. *Phys. Rev. Letts* 85, 5492.
- Kudrolli, A. (2004). Size separation in vibrated granular matter. *Rep. Prog. Phys.* 67, 209–247.

- Lätzel, M., S. Luding, H. J. Herrmann, D. W. Howell, and R. P. Behringer (2003). Comparing simulation and experiment of a 2d granular couette shear device. *Eur. Phys. J. E* 11, 325.
- Losert, W., D. G. W. Cooper, J. Delour, A. Kudrolli, and J. P. Gollub (1999). Velocity statistics in excited granular media. *Chaos* 9 3, 682.
- Lubachevsky, B. D. (1991). How to simulate billiards and similar systems. *J. of Comp. Phys.* 94, 255.
- Masoliver, J. and J. M. Porra (1996). Exact solution to the exit-time problem for an undamped free particle driven by gaussian white noise. *Phys. Rev. E* 53, 2243.
- McNamara, S. and W. R. Young (1992). Inelastic collapse and clumping in a one-dimensional granular medium. *Phys. Fluids A* 4, 496.
- McNamara, S. and W. R. Young (1994). Inelastic collapse in two dimensions. *Phys. Rev. E* 50, R28.
- Meakin, P. (1987). Diffusion-limited aggregation on multifractal lattices: A model for fluid-fluid displacement in porous media. *Phys. Rev. A* 36, 2833.
- Moka, S. and P. R. Nott (2005). Statistics of particle velocities in dense granular flows. *Phys. Rev. Lett.* 95, 068003.
- Moon, S. J., M. D. Shattuck, and J. B. Swift (2001). Velocity distributions and correlations in homogeneously heated granular media. *Phys. Rev. E* 64, 031303.
- Moon, S. J., J. B. Swift, and H. L. Swinney (2004). Steady-state velocity distributions of an oscillated granular gas. *Phys. Rev. E* 69, 011301.
- Olafsen, J. S. and J. S. Urbach (1998). Clustering, order, and collapse in driven granular monolayer. *Phys. Rev. Letts.* 81, 4369.
- Over, T. M. and V. K. Gupta (1996). A space-time theory of mesoscale rainfall using random cascades. *J. Geophys. Res.* 101, 319.
- Peng, G. and T. Ohta (1998a). Scaling and correlations in heated granular materials. *J. Phys. Soc. Japan* 67, 2561–2564.
- Peng, G. and T. Ohta (1998b). Steady state properties of a driven granular medium. *Phys. Rev. E* 58, 4737.
- Puglisi, A., A. Baldassarri, and V. Loreto (2002). Fluctuation-dissipation relations in driven granular gases. *Phys. Rev. E* 66, 061305.

- Puglisi, A., V. Loreto, U. M. B. Marconi, A. Petri, and V. Vulpiani (1998). Clustering and non-gaussian behavior in granular matter. *Phys. Rev. Lett.* *81*, 3848.
- Puglisi, A., V. Loreto, U. M. B. Marconi, and A. Vulpiani (1999). Kinetic approach to granular gases. *Phys. Rev. E* *59*, 5582.
- Redner, S. (1990). Random multiplicative processes: An elementary tutorial. *Am. J. Phys.* *58*, 267.
- Reis, P. M., R. A. Ingale, and M. D. Shattuck (2006). Crystallization of a quasi-two-dimensional granular fluid. *Phys. Rev. Letts.* *96*, 258001.
- Reis, P. M., R. A. Ingale, and M. D. Shattuck (2007a). Caging dynamics in a granular fluid. *Phys. Rev. Letts.* *98*, 188301.
- Reis, P. M., R. A. Ingale, and M. D. Shattuck (2007b). Forcing independent velocity distributions in experimental granular fluid. *Phys. Rev. E* *75*, 051311.
- Rouyer, G. F. and N. Menon (2000). Velocity fluctuations in homogeneous 2d granular gas in steady state. *Phys. Rev. Lett.* *85*, 3676.
- Schöllmann, S. (1999). Simulation of a two-dimensional shear cell. *Phys. Rev. E* *59*, 889.
- Shattuck, M. D., R. A. Ingale, and P. M. Reis (2009). Granular thermodynamics. In *Powders and grains 2009, Proceedings of the 6th International Conference on Micromechanics of Granular Media*, Melville, New York, pp. 43.
- Sibuya, M. and Y. Itoh (1987). Random sequential bisection and its associated binary tree. *Ann. Inst. Stat. Math* *39*, 69.
- Sornette, D. (1998). Multiplicative processes and power laws. *Physical Review E* *57*(4), 4811.
- Swift, M. R., M. Boamfá, S. J. Cornell, and A. Maritan (1998). Scale invariant correlations in a driven dissipative gas. *Phys. Rev. Letts.* *80*, 4410.
- van Noije, T. P. C., M. E. Ernst, E. Trizac, and I. Pagonabarraga (1999). Randomly driven granular fluids: Large-scale structure. *Phys. Rev. E* *59*, 4326.
- van Noije, T. P. C. and M. H. Ernst (1998). Velocity distributions in homogeneous granular fluids: the free and the heated case. *Granular Matter* *1*, 57.
- van Zon, J. S. and F. C. MacKintosh (2004). Velocity distributions in dissipative granular gases. *Phys. Rev. Letts.* *93*, 038001.

- van Zon, J. S. and F. C. MacKintosh (2005). Velocity distributions in dilute granular systems. *Phys. Rev. E* 72, 051301.
- Verlet, L. (1967). Computer experiments on classical fluids .i. thermodynamical properties of lennard-jones molecules. *Phys. Rev.* 159, 98.
- Warr, S., J. M. Huntley, and G. T. H. Jacques (1995). Fluidization of a two-dimensional granular system: Experimental study and scaling behavior. *Phys. Rev. E* 52, 5583.
- William H. Press, Saul A. Teukolsky, W. T. V. (1992). *Numerical Recipes in C: The Art of Scientific Computing* ,2nd ed. Cambridge University Press.
- Williams, D. R. M. and F. C. MacKintosh (1996). Driven granular media in one dimension: Correlations and equation of state. *Phys. Rev. E* 54, R9.
- Williams, J. C. (1976). Continuous mixing of solids, a review. *Powder Technol.* 15, 237.
- Yeomans, J. M. (1992). *Statistical Mechanics of Phase Transitions*. Oxford University Press.
- Zaccarelli, E., I. Saika-Voivod, S. Buldyrev, A. J. Moreno, P. Tartaglia, and F. Sciortino (2006). Gel to glass transition in simulation of a valence-limited colloidal system. *J. Chem. Phys.* 124, 123908.